

P-231

# BICONIC CARGO RETURN VEHICLE WITH AN ADVANCED RECOVERY SYSTEM

Department of Aerospace Engineering & Mechanics  
University of Minnesota  
Minneapolis, MN

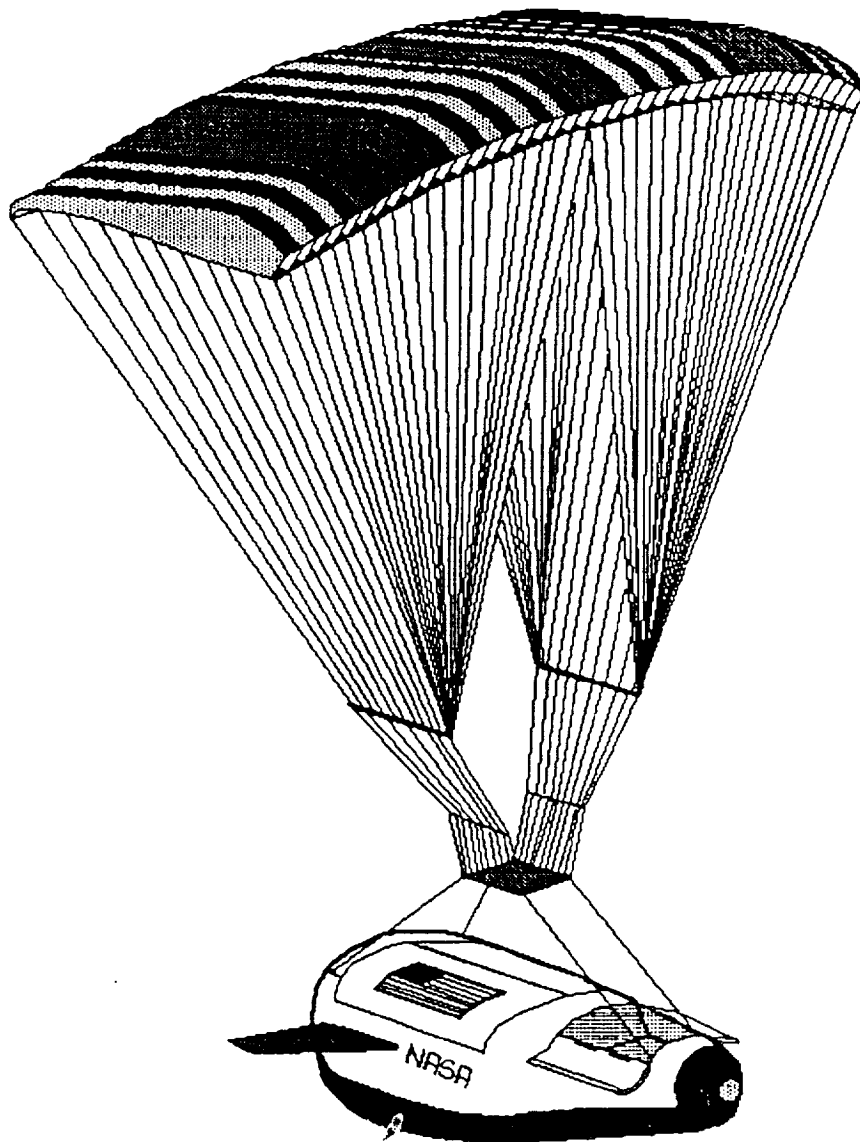
## VOLUME I -- CONCEPTUAL DESIGN

June 2, 1990

N90-26052

(NASA-CR-185920) BICONIC CARGO RETURN  
VEHICLE WITH AN ADVANCED RECOVERY SYSTEM.  
VOLUME I: CONCEPTUAL DESIGN NASA/USRA  
Advanced Design Project (Minnesota Univ.)  
231 P

Unclas  
CSCL 22B 63/18  
0395014



NASA/USRA Advanced Design Project

**BICONIC CARGO RETURN VEHICLE WITH AN  
ADVANCED RECOVERY SYSTEM**

By the

AEM 5331 Class of 1990

The Department of Aerospace Engineering and Mechanics  
University of Minnesota

June 2, 1990

In fulfillment of:

The NASA/USRA Advanced Design Project

# CLASS ORGANIZATION

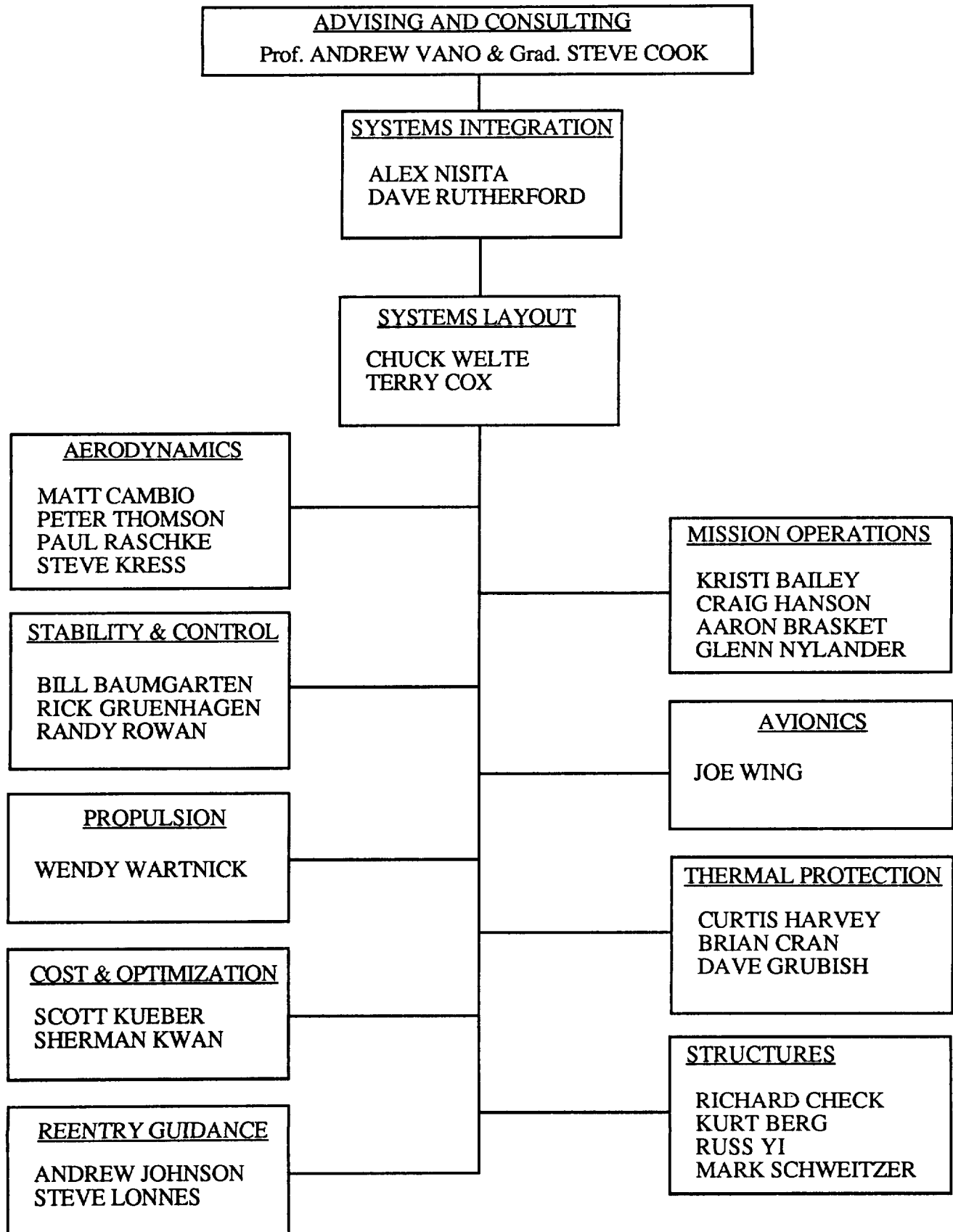


# **TABLE OF CONTENTS**

---

	<b>Page</b>
<b>List of Acronyms</b>	<b>v</b>
<b>List of Figures</b>	<b>vii</b>
<b>List of Tables</b>	<b>xiii</b>
<b>Executive Summary</b>	<b>xiv</b>
<b>1.0 Introduction</b>	<b>1</b>
<b>2.0 Mission Operations</b>	<b>3</b>
2.1 Introduction	3
2.2 Mission Profile	3
2.2.1 Launch	4
2.2.2 Separation Maneuver/Insertion Orbit	7
2.2.3 Phasing	7
2.2.4 SSF Rendezvous	7
2.2.5 Proximity Zone Operations (non-OMV)	8
2.2.6 Proximity Zone Operations (OMV)	8
2.2.7 Phase with Landing Site/Deorbit Burn	8
2.3 Alternate Scenarios and Contingency Plans	10
2.3.1 Abort Options	10
2.3.2 Alternate Landing Sites	11
2.3.3 Contingency Plans	11
2.4 Ground Operations	12
2.4.1 Delivery	12
2.4.2 Navigation	16
2.4.3 Return	19
2.4.4 Post Flight	19
2.5 Payload Bay	20
2.5.1 Door and Bay Placement Options	20
2.5.2 PLog/UnPLog	21
2.5.3 Payload Hold-down Methods	21
2.5.4 Stabilized Payload Deployment System	26
2.5.5 Cameras	27
2.5.6 SSF/CRV Proximity Operations	27
2.6 SSF/CRV Proximity Operations	27

<b>3.0</b>	<b>Systems Layout</b>	<b>39</b>
<b>4.0</b>	<b>Reentry Aerodynamics</b>	<b>43</b>
4.1	Introduction	43
4.2	Validation of Aero-Prediction Code	43
4.3	Body Optimization	46
4.4	Aerodynamics of Final Design	48
4.5	Drogue Decelerator	50
4.5.1	Requirements for the Drogue Decelerator	50
4.5.2	Drogue Decelerator Types	51
4.5.3	Drogue Decelerator Design	52
4.5.4	Drogue Decelerator Performance	53
4.5.5	Drogue Decelerator Deployment System	54
4.6	Advanced Recovery Systems	55
4.6.1	Configuration	55
4.6.2	Deployment	58
4.6.3	Reefing	59
4.6.4	Aerodynamic Characteristics	61
4.6.5	Performance	62
<b>5.0</b>	<b>Stability and Control</b>	<b>66</b>
5.1	Introduction	66
5.2	Biconic CRV Control	66
5.2.1	Horizontal Fins	66
5.2.2	RCS System	68
5.3	Stability Characteristics of the CRV	69
5.3.1	Static Stability	69
5.3.2	Longitudinal Stability	71
5.3.3	Lateral Analysis	74
5.3.4	Automatic Flight Control System	76
5.4	On-Orbit Control	78
5.4.1	Pitch Control	78
5.4.2	Roll/Yaw Control	79
5.5	C.G. and Moment of Inertia	80
5.6	Advanced Recovery System	83
5.6.1	Drogue Chute	83
5.6.2	Control System	84
5.6.3	ARS Stability	87
<b>6.0</b>	<b>Avionics and Power</b>	<b>88</b>
6.1	Introduction	88
6.1.1	Definition of Avionics Systems	88
6.1.2	Definition of Power Subsystems	88

6.2	Avionics Equipment List	88
6.3	Storage of Avionics Equipment	90
6.4	Choice of Power Supply System	93
6.4.1	Power Supply Cooling System	93
6.5	Effect of On-Orbit Times on Power Consumption	93
6.6	In Atmosphere Power Supply	95
6.6.1	Boost Stage Power Supply	95
<b>7.0</b>	<b>Thermal Analysis and Control</b>	<b>96</b>
7.1	Introduction	96
7.2	Avionics Cooling Design	96
7.3	Cargo Bay Heating Loads and Protection	103
7.4	Trajectory Heating Analysis	107
7.5	Control Surface Heating	107
7.6	Materials and Weights	108
7.7	Attachment Methods	113
7.8	Structure Type	115
7.8.1	Hot Structure	115
7.8.2	Warm Structure	116
7.9	Seals	116
7.9.1	Landing Gear Door Seals	116
7.9.2	Cargo Bay Door Seals	118
7.9.3	ARS Bay Doors	119
7.10	Space Debris	122
7.10.1	Meteoroid Analysis	122
7.10.2	Space Debris Shielding	122
7.10.3	Recommendation	124
7.11	Costs and Repairs	124
<b>8.0</b>	<b>Propulsion</b>	<b>125</b>
8.1	Introduction	125
8.2	Launch Configuration	125
8.3	The Orbital Maneuvering System (OMS)	129
8.3.1	The OMS Engine	129
8.3.2	The OMS Propellant Tanks	129
8.3.3	OMS Pressurant	131
8.4	The Reaction Control System (RCS)	131
8.4.1	Non-Command Control Zone RCS System	131
8.4.2	The Command Control Zone RCS System	132
8.5	CRV Pressurant Systems (Forward and Aft)	133
<b>9.0</b>	<b>Reentry Guidance</b>	<b>135</b>
9.1	Introduction	135

9.2.3	Final Footprint	139
9.3	Reentry Profile	140
9.3.1	Integrated Mission Program	141
9.4	Final Trajectory	141
9.5	Guidance System	147
9.6	Guidance Mission Profile	150
<b>10.0</b>	<b>Structural Analysis</b>	<b>155</b>
10.0	Introduction	155
10.1	CRV Fuselage Support Structure Layout	155
10.2	Fin Structure	161
10.3	Payload Bay	161
10.4	Payload Bay Support Structure	163
10.5	Materials	164
10.6	Outer Skin	168
10.7	Landing Gear System	175
10.7.1	Landing Gear Locations	176
10.7.2	Landing Geometry and Load Distributions	178
10.8	Engine Mount Design	180
10.8.1	OMS Engine Attachment	180
10.8.2	Removable Nozzle Ring	182
10.9	Advanced Recovery System	184
10.9.1	Drogue Parachute Compartment	184
10.9.2	Ram Air Parafoil Storage Compartment	187
10.9.3	ARS Attachment Cables	189
10.9.4	Parafoil and Attachment Lines	191
<b>11.0</b>	<b>Optimization and Costs</b>	<b>199</b>
11.1	Introduction	199
11.2	Optimization of Ground Facilities	199
11.2.1	Number of Missions Per Year	199
11.2.2	Use of Current vs New Facilities	200
11.2.3	Transportation from Landing Site	200
11.3	Future Optimization Tasks	201
11.3.1	Amount of Cargo	201
11.3.2	Fleet Size	201
11.3.3	Cost of a CRV	202
<b>12.0</b>	<b>Conclusion</b>	<b>203</b>
<b>13.0</b>	<b>References</b>	<b>205</b>

## **LIST OF ACRONYMS**

---

AA	Accelerometer Assy.
ARS	Advanced Recovery System
CCZ	Command and Control Zone
CRV	Cargo Return Vehicle
DBIA	Data Bus Isolation Amp
EVA	Extra Vehicular Activity
FRCI	Fibrous Refractory Composite Insulation
GPC	General Purpose Computer
GPS	Global Positioning System
HABP	Supersonic/Hypersonic Arbitrary Body Program
IMP	Integrated Mission Program
IMU	Inertial Measuring Unit
LEO	Low Earth Orbit
LH2	Liquid Hydrogen
LI 2200	Lockheed Insulation 2200
LINS	Laser Interval Navigation System
LM	Logistics Module
LO2	Liquid Oxygen
LPS	Launch Processing System
LRB	Liquid Rocket Booster
MBS	Mobile Remote Servicer Base System
MDM	Multiplexer
MEC	Master Event Controller
MECO	Main Engine Cut Off
MN	Modified Newtonian Method
MNPM	Modified Newtonian and Prandtl Meyer Method
MSC	Mobile Servicing Center
MSS	Mobile Servicing System
MT	Mobile Transporter
MTU	Master Timing Unit
OMS	Orbital Maneuvering System
OMV	Orbital Maneuvering Vehicle
PLOG	Pressurized Logistics Module
RAP	Ram-Air Parafoil
RCS	Reaction Control System
RGA	Rate Gyro Assy.
RJD	Reaction Jet Diver
RMS	Remote Manipulator System
SBT	S-Band Transponder

SC	Signal Conditioners
SDPS	Space Debris Protection System
SIP	Strain Isolator Pad
SPDM	Special Purpose Dextrous Manipulator
SPDS	Stabilized Payload Deployment System
SRS	Secondary Recovery System
SSF	Space Station Freedom
SSRMS	Space Station Remote Manipulator System
STME	Space Transportation Main Engine
TABI	Tailorable Advanced Blanket Insulation
TACAN	Tactical Air Navigation Units
TB	Timer Buffer
TDRSS	Tracking and Data Relay Satellite System
TPDM	Three Point Docking Mechanism
TPS	Thermal Protection System
UPLOG	Unpressurized Logistics Module
UNPLOG	Unpressurized Logistics Module
VDU	Van Dyke Unified Method

# **LIST OF FIGURES**

---

<b><u>Number</u></b>	<b><u>Title</u></b>	<b><u>Page</u></b>
<b>Introduction</b>		
Figure 1.1	Space Station Freedom	1
<b>Mission Operations</b>		
Figure 2.1	Hohmann Transfer	4
Figure 2.2	Inclination Correction Burn	5
Figure 2.3	Orbits at 28.5 deg. Inclination	5
Figure 2.4	Orbital Phase Time	6
Figure 2.5	Orbital Phase Time II	6
Figure 2.6	CRV Relative Position	9
Figure 2.7	Mission Profile	9
Figure 2.8	Data Summary	10
Figure 2.9	Phase Correction Burn	11
Figure 2.10	Ground Processing Scenario	14
Figure 2.11	CRV Maintenance Timeline	15
Figure 2.12	CRV Processing Timeline	17
Figure 2.13	Tracking and Data Relay Satellite System	18
Figure 2.14	PLOG with Trunnions	22
Figure 2.15	UPLOG in Cargo Bay	23
Figure 2.16	PLOG in Cargo Bay	24
Figure 2.17	Longeron Latch	24
Figure 2.18	Keel Latch	25
Figure 2.19	Latch Positions	25
Figure 2.20	SPDS Configuration	26
Figure 2.21	SPDS Deployment	27
Figure 2.22	Space Station Freedom	30
Figure 2.23	Vertical Docking - Side View	31
Figure 2.24	Horizontal Docking - Side View	32
Figure 2.25	Vertical Docking - Top View	33
Figure 2.26	Rotating Fore Cone Mechanism	34
Figure 2.27	Mobile Servicing Center	37
Figure 2.28	Orbital Maneuvering Vehicle	38
<b>Systems Layout</b>		

Figure 3.1	CRV Dimensions-Side View	39
Figure 3.2	CRV Dimensions-Top View	40
Figure 3.3	CRV Dimensions-Front View	40
Figure 3.4	Systems Layout-Top View/Layer #1	41
Figure 3.5	Systems Layout-Top View/Layer #2	41
Figure 3.6	Systems Layout-Bottom View	42
Figure 3.7	Systems Layout Dimensions-Side View	42

## **Aerodynamics**

Figure 4.1	Baseline Configuration	43
Figure 4.2	Lift to Drag Ratio of Baseline	45
Figure 4.3	Pitching Moment coefficient of Baseline	45
Figure 4.4	Baseline with 25 Degree Boat Tail	46
Figure 4.5	Shortened Baseline with 4 foot Nose Radius	47
Figure 4.6	Final Body Configuration	47
Figure 4.7	L/D of Final Configuration	48
Figure 4.8	$C_{m_a}$ of Final Configuration	48
Figure 4.9	Final Configuration with 25 Degree Sweep	49
Figure 4.10	Effect of Horizontal Fins on $C_{m_a}$	49
Figure 4.11	Construction of Drogue Parachute	52
Figure 4.12	Altitude vs. Velocity of CRV with Deployed Drogue Chute	53
Figure 4.13	Dynamic Pressure vs. Altitude of CRV with Deployed Drogue Chute	54
Figure 4.14	Parafoil Configuration	56
Figure 4.15	Clark - Y - 17 Airfoil	57
Figure 4.16	Anhedral	58
Figure 4.17	Trailing Edge Deflection	59
Figure 4.18	Parafoil Midspan Reefing	60
Figure 4.19	Flare Maneuver	63
Figure 4.20	Parafoil Loads	64
Figure 4.21	Range of Parafoil	65

## **Stability and Control**

Figure 5.1	Horizontal Fins	67
Figure 5.2	Horizontal Fins with Rudders Deployed	67
Figure 5.3	Fin Planform	68

Figure 5.4	Fin Cross-Section	68
Figure 5.5	Elevator Deflection vs. Trim Angle of Attack	69
Figure 5.6	Cm vs. Alpha	70
Figure 5.7	Cl (rolling) vs. Beta	71
Figure 5.8	Cl (yaw) vs. Beta	71
Figure 5.9	Phugoid Mode - Period	72
Figure 5.10	Phugoid Mode - Time to Half	72
Figure 5.11	Short Period Mode - Period	73
Figure 5.12	Short Period Mode - Time to Half	73
Figure 5.13	Rolling Mode - Time to Half	74
Figure 5.14	Spiral Mode - Time to Half	75
Figure 5.15	Dutch Roll - Period	75
Figure 5.16	Dutch Roll - Time to Half	76
Figure 5.17	Yaw Damper System for Automatic Flight Control System	77
Figure 5.18	Pitch Control Block Diagram	78
Figure 5.19	Roll/Yaw Control Block Diagram	79
Figure 5.20	Axes Rotation Orientation	81
Figure 5.21	Flight Envelope	83
Figure 5.22	Side View of Control system	85
Figure 5.23	Trailing Edge Detail	86
Figure 5.24	Load Bar Detail	86

## **Avionics and Power**

Figure 6.1	Location of Avionics Components	90
Figure 6.2	Avionics Shelf	91
Figure 6.3	Upper Shelf	92
Figure 6.4	Lower Shelf	92
Figure 6.5	Arrangements of Components on Control Buses	94

## **Thermal Protection Systems**

Figure 7.1	Avionics Cooling (0-20 minutes into 24 hr Mission)	98
Figure 7.2	Avionics Cooling (20 min - 2 hours into 24 hr Mission)	99
Figure 7.3	Avionics Cooling (2 hr - 22 hours into 24 hr Mission)	100
Figure 7.4	Avionics Cooling (22 hr - 23 hours 40 minutes into 24 hr Mission)	101

Figure 7.5	Avionics Cooling (23 hr 40 min - Touchdown for 24 hr Mission)	102
Figure 7.6	Negligible Heat Transfer Assumptions	104
Figure 7.7	PLOG/UNPLOG Heating rates	105
Figure 7.8	Time vs. Temperature	108
Figure 7.9	Material Placement	110
Figure 7.10	Materials and Attachments	111
Figure 7.11	ARS Cable Attachment	112
Figure 7.12	ARS Cable Attachment Section A-A	112
Figure 7.13	ARS Cable Attachment Section B-B	112
Figure 7.14	TPS Grid System of Attachment	114
Figure 7.15	Tile Bap Placement	115
Figure 7.16	Landing Gear Door Seals	117
Figure 7.17	Landing Gear Door Seal	118
Figure 7.18	Payload Bay/Docking Ring Bay/ARS Bay Seals	119
Figure 7.19	Cargo Bay/Docking ring Bay Seals	120
Figure 7.20	ARS Seal	121
Figure 7.21	Space Debris Density	123
Figure 7.22	Space Debris 'Bumper'	123

## **Propulsion**

Figure 8.1	Launch Configuration	126
Figure 8.2	Launch Sequence	127
Figure 8.3	Space Transportation Main Engine Specifics	128
Figure 8.4	STME Performance	128
Figure 8.5	The OMS Engine	130
Figure 8.6	OMS Propellant Tank Data	130
Figure 8.7	The Non-CCZ RCS Engine	131
Figure 8.8	Non-CCZ Propellant Data	132
Figure 8.9	CCZ RCS Engine	132
Figure 8.10	CCZ RCS Forward Propellant Tank	133
Figure 8.11	CCZ RCS Aft Tank	133
Figure 8.12	CRV Pressurant System	134

## **Reentry Guidance**

Figure 9.1	Landing Sites	136
Figure 9.2	CRV Footprint	140

Figure 9.3	Altitude Versus Time for Final Trajectory	144
Figure 9.4	Angle of Attack Versus Time for Final Trajectory	144
Figure 9.5	Acceleration Versus Time With Drogue Chute	145
Figure 9.6	Acceleration Versus Time Without Drogue Chute	145
Figure 9.7	Velocity Versus Altitude With Drogue Parachute	146
Figure 9.8	Velocity Versus Altitude Without Drogue Parachute	146
Figure 9.9	Biconic CRV Functional Diagram	148
Figure 9.10	Mission Profile From Launch To SSF Docking	151
Figure 9.11	Reentry Mission Profile	153

## Structures

Figure 10.1	Support Structure Skeleton	157
Figure 10.2	Structural Detail	159
Figure 10.3	Structural Cross-Sections	160
Figure 10.4	Fin Structure	162
Figure 10.5	Payload Bay (Front View)	163
Figure 10.6	Front View of Payload bay Support Structure	165
Figure 10.7	Side View of Payload Bay Support Structure	166
Figure 10.8	Effect of Temperature on Tensile Ultimate/Yield for Aluminum 2219	167
Figure 10.9	Honeycomb Sandwich Construction	169
Figure 10.10	Fabricated Honeycomb Sandwich Panels	170
Figure 10.11	Outer Skin	172
Figure 10.12	Notch in Shell for ARS Cables	173
Figure 10.13	Example Panel for Front, Mid, and Aft Cones	174
Figure 10.14	Panel Attachment methods	175
Figure 10.15	Side View of CRV with Landing Gear	177
Figure 10.16	Frontal Cut Out View of Two Main Gears	177
Figure 10.17	Structural View from Rear of CRV	181

Figure 10.18	OMS Engine Attachment	182
Figure 10.19	Removable Nozzle Ring	183
Figure 10.20	Side View of Ring and Support Arm	183
Figure 10.21	Advanced Recovery System Configuration	185
Figure 10.22	Drogue Parachute Compartment Placement	186
Figure 10.23	Dimensions of Drogue Parachute Compartment	187
Figure 10.24	Placement of ARS Compartment	188
Figure 10.25	Dimensions of ARS Compartment Bay	188
Figure 10.26	Placement of Aft ARS Attachment Cables	189
Figure 10.27	Deployed ARS Attachment Cable Configuration	190
Figure 10.28	Aft Cable Attachment	190
Figure 10.29	Attachment Cable Platform	191
Figure 10.30	Parafoil Reefing Stages	193
Figure 10.31	ARS Layout and Dimensions	194
Figure 10.32	First stages of Reefing (11 Cells Open)	195
Figure 10.33	Second Stage of Reefing (10 additional Cells Open)	196
Figure 10.34	Third Stage of Reefing (30 Additional Cells Open)	197

# **LIST OF TABLES**

---

<b><u>Number</u></b>	<b><u>Title</u></b>	<b><u>Page</u></b>
<b>Aerodynamics</b>		
Table 4.1	Decelerator Characteristics	51
Table 4.2	Deployment and Reefing Data	61
Table 4.3	Aerodynamic Characteristics	62
Table 4.4	Trajectory Points	62
<b>Stability &amp; Control</b>		
Table 5.1	C.G. Calculation, 59ft. - Fully Loaded	82
<b>Thermal Analysis &amp; Control</b>		
Table 7.1	Material Properties and Weights	110
<b>Reentry Guidance</b>		
Table 9.1	Crossrange Requirements	137
Table 9.2	Footprint Equations	138
Table 9.3	Symbol Definitions	138
Table 9.4	Vehicle Model for <u>Footprint</u>	139
Table 9.5	Footprint Characteristics	139
<b>Structures</b>		
Table 10.1	Structural Layout Data	158
Table 10.2	Properties of Aluminum 2219	166
Table 10.3	Honeycomb vs. Single Ply	171
Table 10.4	Properties of 3/8" HRH-327	171
Table 10.5	Properties of Nylon and Kevlar Cable	192

# **EXECUTIVE SUMMARY**

---

This volume presents the conceptual design of the biconic CRV. The CRV will be able to meet all of the SSF's resupply needs. Worth note is the absence of a backup recovery chute in case of ARS failure. The high reliability of ram-air parachutes does not warrant the penalty weight that such a system would create on successful missions. The CRV will launch vertically integrated with an LRB vehicle and meets all NASA restrictions on fuel type for all phases of the mission. Because of the downscaled OMV program, the CRV has been designed to be able to transfer cargo by docking directly to the Space Station Freedom as well as with OMV assistance. The CRV will cover enough crossrange to reach its primary landing site, Edwards Airforce Base, and all secondary landing sites with the exception of one orbit. Transportation back to KSC will be via the Boeing Super Guppy. Due to difficulties with man-rating the CRV, it will not be used in a CERV role. Following is a brief summary of the CRV's specifications:

- Bent axis biconic with a ram air inflated parafoil ARS
  - Δ (L/D)<sub>Hyper</sub> = 1.5
  - Δ (L/D)<sub>Subsonic</sub> = 3.8 -ARS
  - Δ Weight *Unloaded* = 34,061lbs
  - Δ Cargo Cap. = 40 Klb
  - Δ Crossrange ≈ 700 n.mi.

- The Advanced Recovery System
  - Δ Planform Area = 22,250 ft<sup>2</sup> (250 ft X 89 ft)
  - Δ Deployed at 10,000 ft altitude
  - Δ Midspan reefing in three stages
- Vehicle dimensions
  - Δ Length = 59 ft
  - Δ Radius<sub>nose</sub> = 7.7 ft
  - Δ Diameter<sub>max</sub> = 19.5 ft
- Supersonic reentry control via tail mounted adjustable deflection fins, with folding winglets
- The CRV will be capable of docking directly to the SSF as well as being OMV compatible
  - Δ Mission time with OMV = 19.85-76.85 hrs
  - Δ Mission time non-OMV = 18.35-75.35 hrs
- Propulsion
  - Δ Top mounted launch on dual booster/single core LRBs
  - Δ Orbit insertion at 50 n.mi. X 100 n.mi. @ 28.5°
  - Δ Three OMS engines
    - √ LH<sub>2</sub>/LO<sub>2</sub> propellant and oxidizer
    - √ Weight = 86.65 lbs (each)
    - √ I<sub>sp, vac.</sub> = 414.4 sec
    - √ Thrust<sub>vac.</sub> = 1600 lbf
  - Δ The RCS system uses LH<sub>2</sub>/LO<sub>2</sub> outside of the CCZ and GN<sub>2</sub> inside, as specified by SSF requirements
- Transportation of the CRV back to KSC will be via the Boeing Super Guppy
- CRV turnaround time is 66 days



# 1.0 INTRODUCTION

---

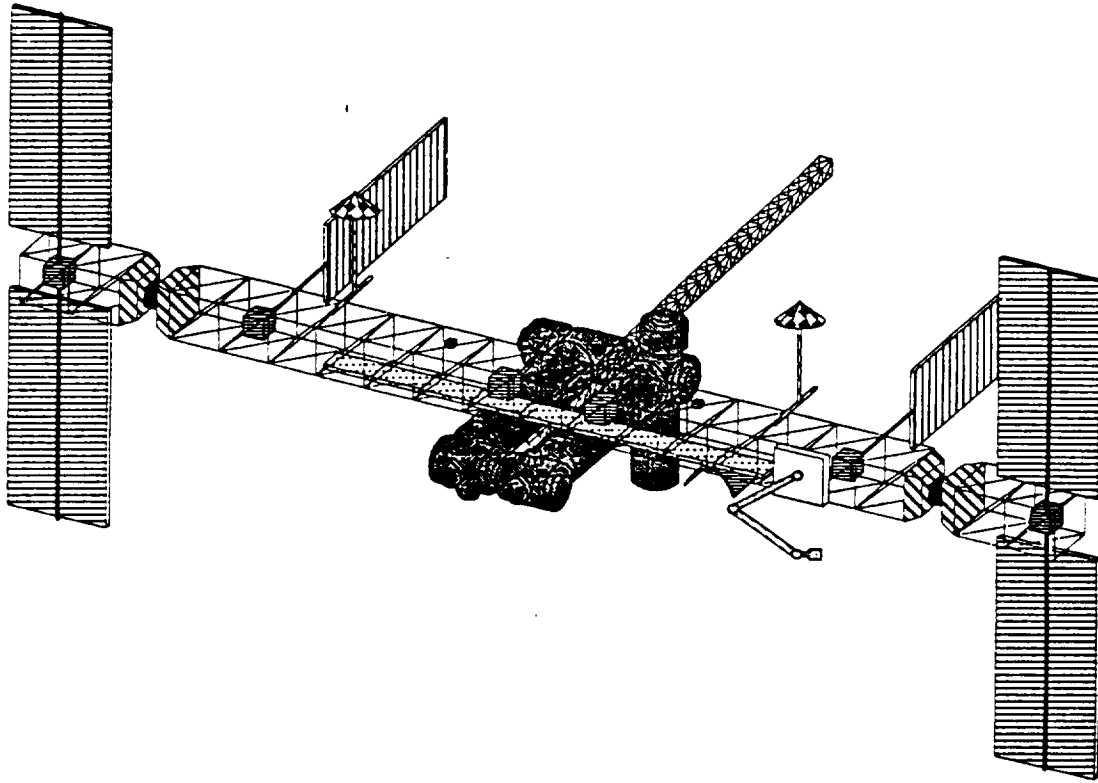


Figure 1.1 Space Station Freedom

Between the years 2000 and 2010, the Space Station Freedom (SSF) is projected to be fully operational. At that time, astronauts will begin to live and work on the station for extended periods of time. Since they will be in space, all their basic needs such as food, water, oxygen, etc., will have to be brought to them. When putting anything into space, the main factor is weight. NASA estimates the required annual cargo weight needed by the Space Station to be 214,000 lbs.

Currently, the only feasible way to resupply the station continually is the Space Shuttle fleet. According to NASA, due to a very burdened schedule, the Space Shuttle will only be able to make five resupply flights per year. This translates into a total yearly upcargo of 178,785 lbs annually, well short of the 214,000 lbs needed by the SSF. These figures are also not taking into consideration the possibility of a mission postponement or cancellation due to

weather, equipment malfunction, or any other external force that may inhibit the flight. Obviously, the astronauts on board the SSF can not wait for the necessary food and oxygen. This creates a major problem for NASA.

This report proposes a solution to this problem; a Cargo Return Vehicle (CRV).

As a basic starting point in this design, several requirements and assumptions were set for the design team members. They are as follows :

1. The CRV will be in operation between the years 2000 and 2020.
2. The Orbital Maneuvering Vehicle (OMV) may or may not be in operation.
3. The CRV will be unmanned.
4. Space Shuttle attachment methods will be used.
5. An existing booster takes the CRV to a 50x100 nmi orbit.
6. The CRV will have a dry land recovery.
7. The CRV will have an upcargo capability of 40,000 lbs.
8. The CRV will have both docking and OMV cargo exchange capability.
9. A Ram-Air parafoil (RAP) will be used as an advanced recovery system.
10. Edwards Airforce Base is initially the primary landing site.

## **2.0 MISSION OPERATIONS**

---

### **2.1 Introduction**

The Mission Operations portion of this report covers the mission profile, space station proximity procedures, and ground operations and facilities. The Cargo Return Vehicle's (CRV) purpose is to supply the Space Station Freedom (SSF) with needed materials. Supplies will be delivered to the SSF in standardized logistic modules. There are two different logistic modules, one each for pressurized and unpressurized cargo. These logistic modules will be referred to as PLOG's and UPLOG's throughout this report.

Cargo transfer between the CRV and the SSF will either take place by direct docking or with the assistance of an Orbital Maneuvering Vehicle (OMV). At this time, the status of the OMV is uncertain. Because of this, methods are developed for both OMV assisted and direct docking cargo transfer.

### **2.2 Mission Profile**

The nominal mission scenario for the CRV is a rendezvous and cargo exchange with the SSF. The SSF is in a 220 n.mi. circular orbit at an inclination of 28.5 degrees to the equator. Launch takes place from Kennedy Space Center which is at 28.5 degrees north latitude. Options are given for both OMV and non-OMV cargo transfer.

A number of assumptions were used in our calculations. One, the orbital mechanics are modeled as a standard two-body problem with the center of the Earth as the attractive center. All perturbing forces, such as from the moon or atmospheric drag, are ignored. In addition, velocity changes are modeled as instantaneous and referred to as  $\Delta V$ 's. This is a valid assumption even for vehicles with relatively low thrust to weight ratios as the burn times are small compared with the duration of the maneuvers.

In designing the mission schedule, there are two main parameters to be investigated: mission time and fuel consumption. Fuel consumption is directly related to the total  $\Delta V$  required for maneuvers. Because maneuver times are small in general compared with the phasing and cargo transfer times, minimizing  $\Delta V$ 's takes preference whenever possible. For example, Hohmann transfers are used for most orbital maneuvers. A Hohmann transfer is an elliptical orbit that intersects two circular orbits

tangentially. The Hohmann transfer is the minimum energy method but also requires the longest time of flight (see Figure 2.1). Each stage of the mission profile is detailed below. A graphical representation of the mission profile and a summary of the data are given in figures 2.7 and 2.8 following the individual descriptions.

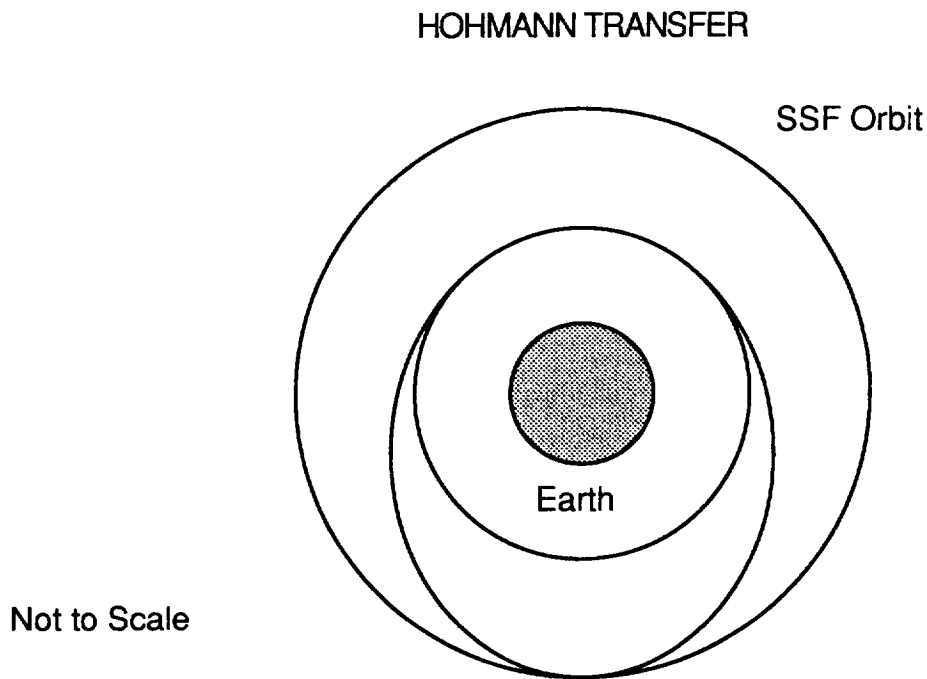


Figure 2.1 Hohmann Transfer

### 2.2.1 Launch

There is only one opportunity per day to launch the CRV into the orbital plane of the SSF. Any other launch time requires an out-of-plane maneuver to reach the rendezvous orbit. Out-of-plane maneuvers are prohibitive in terms of fuel expenditure (figure 2.2). A change in inclination of one degree requires a  $\Delta V$  roughly equal to our deorbit burn. Figure 2.3 shows two different orbital planes at 28.5 degree inclination with a nodal displacement of 180 degrees. To correct for a nodal displacement is difficult. Preliminary estimates showed that our RCS jets would change this nodal displacement at a negligible rate and using our main engines would cost too much fuel.

### INCLINATION CORRECTION BURN

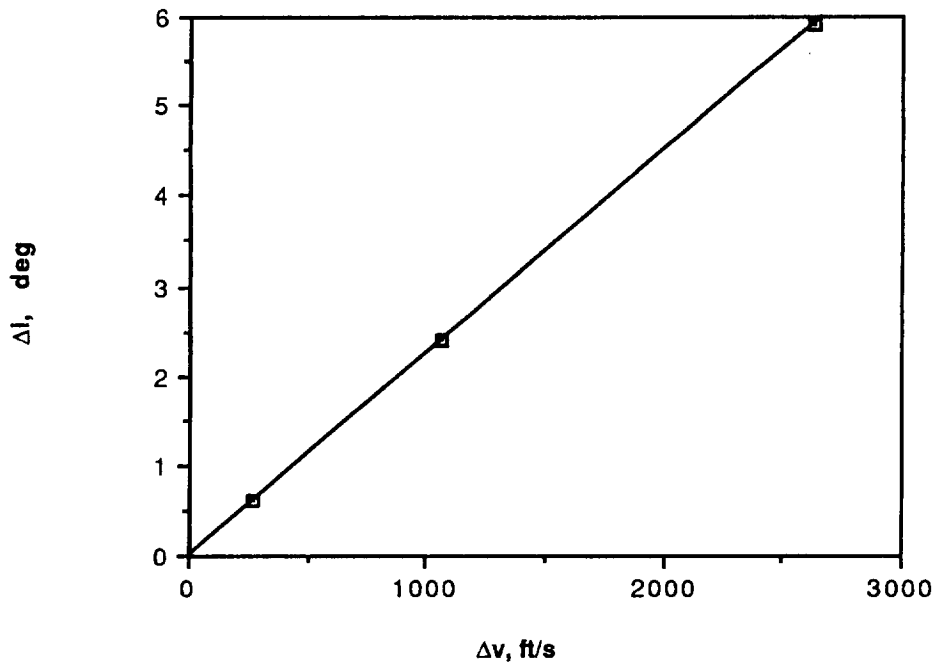


Figure 2.2 Inclination Correction Burn

### ORBITS AT 28.5 DEGREE INCLINATION

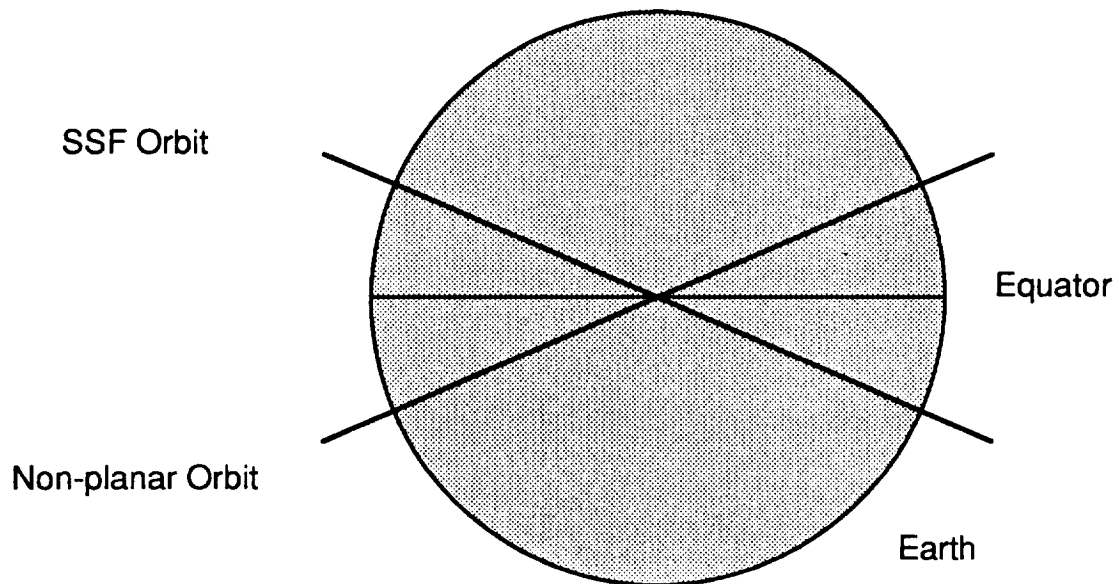


Figure 2.3 Orbits at 28.5° Inclination

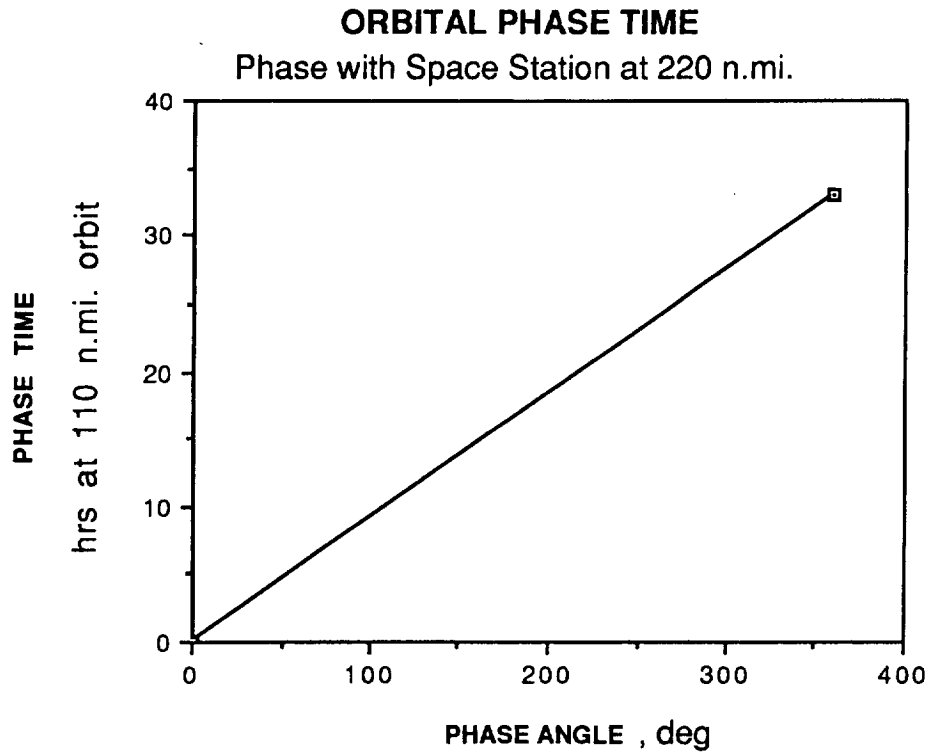


Figure 2.4 Orbital Phase Time

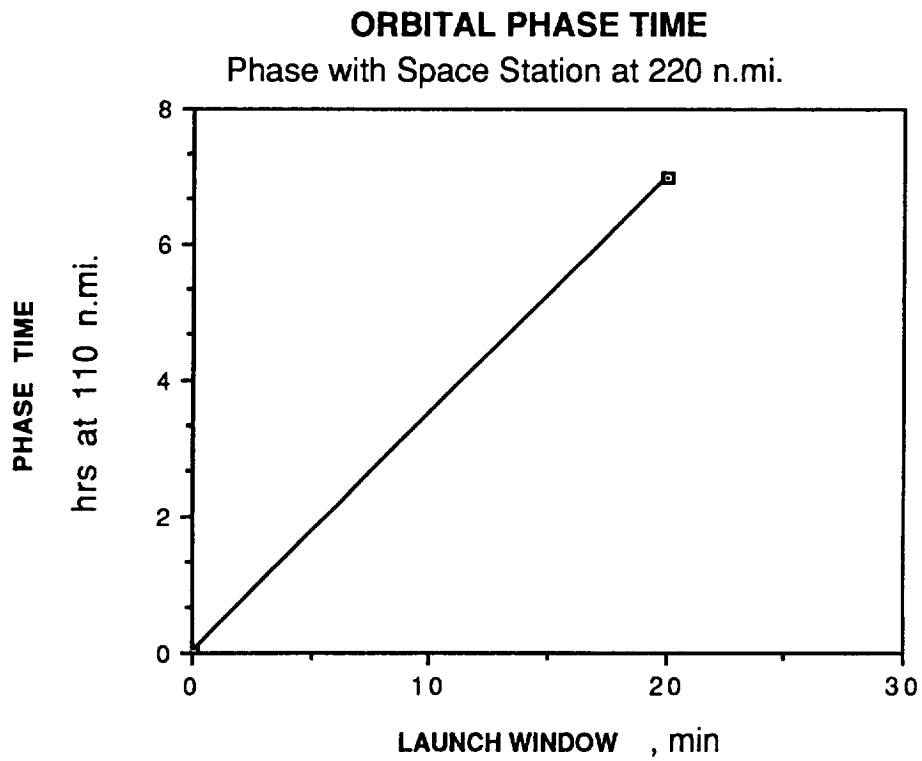


Figure 2.5 Orbital Phase Time II

This launch opportunity of once per day ignores phasing considerations however. As shown in figure 2.4, there is a phasing time between the CRV and the SSF. This cycle is at a minimum every fourth day or 62 orbits as determined by the period of the SSF orbit. This phasing period is increased from the minimum time if the launch opportunity is missed by a small amount. Figure 2.5 shows the launch window and associated phasing time. In this situation, the out-of-plane error is assumed to be either small or correctable.

### **2.2.2 Separation Maneuver/Insertion Orbit**

The launch system places the CRV into a 50 x 100 n.mi. elliptical orbit. At which point, the CRV separates from the booster. The Propulsion Group has examined the separation in more detail. The CRV continues in this orbit until apogee where it performs a Hohmann transfer orbit to reach the 110 n.mi. circular phasing orbit. Two  $\Delta v$ 's are required. One, at the apogee altitude of 100 n.mi. to initiate the Hohmann transfer. The other at 110 n.mi. to circularize the orbit. The magnitudes of each burn are 100 and 20 ft/s respectively.

### **2.2.3 Phasing**

The CRV phases with the SSF in a 110 n.mi. circular orbit. The angular displacement between the CRV at this altitude and the SSF at 220 n.mi. is 10.9 degrees per hour. Figure 4 shows this relationship. The maximum phasing delay would be 33 hours and would correspond to a 360 degree phase. Careful planning would avoid a delay of this magnitude.

### **2.2.4 SSF Rendezvous**

A Hohmann transfer is used to bring the CRV from the 110 to a 210 n.mi. circular orbit. Each  $\Delta V$  in this maneuver is 180 ft/s. One to initiate the transfer, the other to re-circularize the orbit at 210 n.mi.

The CRV enters the 210 n.mi. orbit approximately five degrees behind the SSF rendezvous point. The CRV gains on the SSF in the lower orbit and phases with the rendezvous zone in approximately five hours. During this period, any necessary corrections to the orbit prior to rendezvous can be made. When the phase difference is made up, the CRV performs another Hohmann transfer to reach the rendezvous zone, 20 n.mi. behind the SSF and coplanar. The Hohmann transfer to reach this point consists of 2  $\Delta V$ 's of magnitude 20 ft/s.

### **2.2.5 Proximity Zone Operations (non-OMV)**

Without the use of the OMV for cargo transfer, the CRV must dock to the SSF. Maneuvering the CRV from the rendezvous zone to the SSF must be done carefully. Proximity maneuvers are modeled as a perturbation from the circular orbit of the SSF. This results in a linear approximation of the equations of motion or Euler-Hill equations. Figure 6 shows the relative position of the CRV to the SSF during approach. Because these approximations are linear, the total  $\Delta V$  required to dock with the SSF can be split up into any number of steps. The total  $\Delta V$  required is 14.5 ft/s. This amount is split up into three jumps to limit the approach speed, 7.25, 4.85 and 2.4 ft/s.

With the distance traveled in each jump being one half, one third and one sixth of the total distance. Each jump takes half an orbit to complete and essentially is an approximate Hohmann Transfer. We are re-circularizing after each jump so the total  $\Delta V$  is actually 29 ft/s to approach the SSF. Re-circularizing has the advantage of allowing for corrections upon approach. It has the disadvantage of doubling the amount of fuel used in the proximity zone. This creates problems for space station operations. Once the CRV is adjacent to the SSF, cargo transfer takes six hours. Maneuvering to the departure zone is a mirror image of rendezvous. Total  $\Delta V$  expenditure within proximity zone is 58 ft/s. Total elapsed time, 10.5 hours.

### **2.2.6 Proximity Zone Operations (OMV)**

With an OMV for cargo transfer, the CRV never enters the control zone. The CRV performs a repositioning maneuver when cargo transfer is complete. This maneuver can be modeled as a Hohmann transfer. The CRV initiates a Hohmann transfer to bring itself back down to the 210 n.mi. orbit. Instead of completing the transfer however, the CRV continues and completes one orbit. This has the affect of repositioning the CRV 20 n.mi ahead of the SSF at the departure zone. The position of the CRV relative to the SSF is shown in Figure 2.6. Proximity operations with the OMV is estimated to take 12 hours and the repositioning maneuver requires two  $\Delta V$ 's of 20 ft/s each.

### **2.2.7 Phase with Landing Site/Deorbit Burn**

The CRV waits at the departure zone until it phases with the landing site. The primary landing site is Edwards Air Force Base. The wait required can be up to 24 hours. At all times however, there is a potential landing site within one orbit's range. Alternate landing sites are discussed in more detail under contingency plans.

The CRV deorbits with a single  $\Delta V$  upon completion of the phase delay. The deorbit maneuver is detailed in the Reentry Group's section. The magnitude of the deorbit burn is 317 ft/s. This is greater than the  $\Delta V$  required for a tangential reentry. The CRV enters the atmosphere with a flight path angle of 1 degree at 400,000 ft.

### CRV Proximity Operations Profiles From SSF Perspective

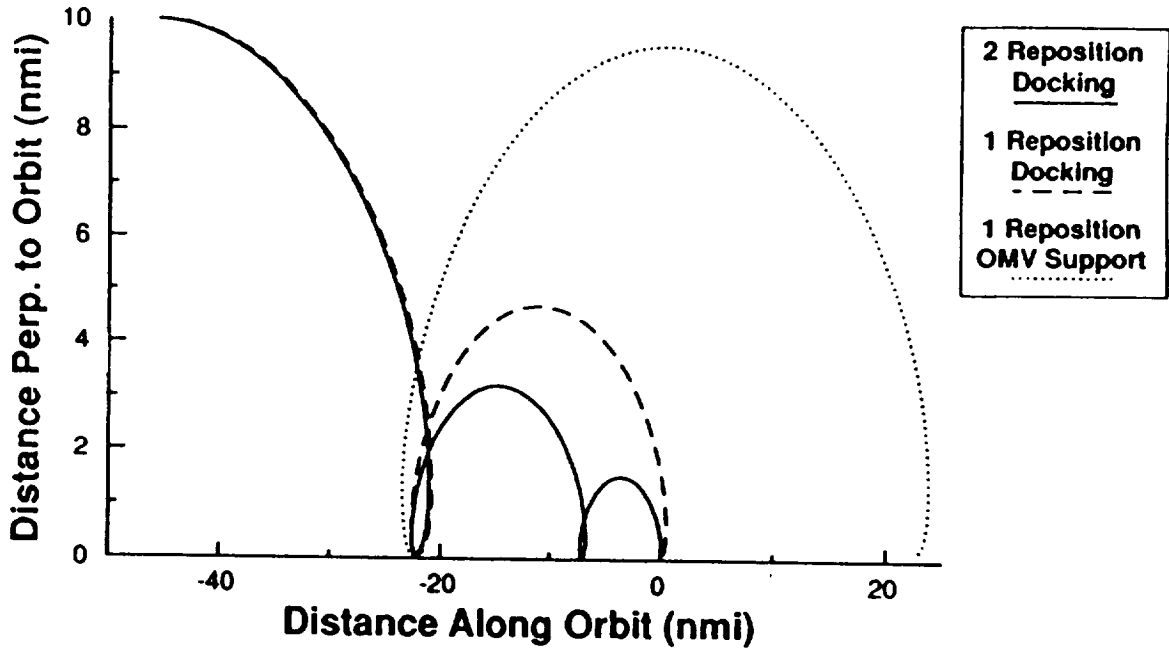


Figure 2.6 CRV Relative Position

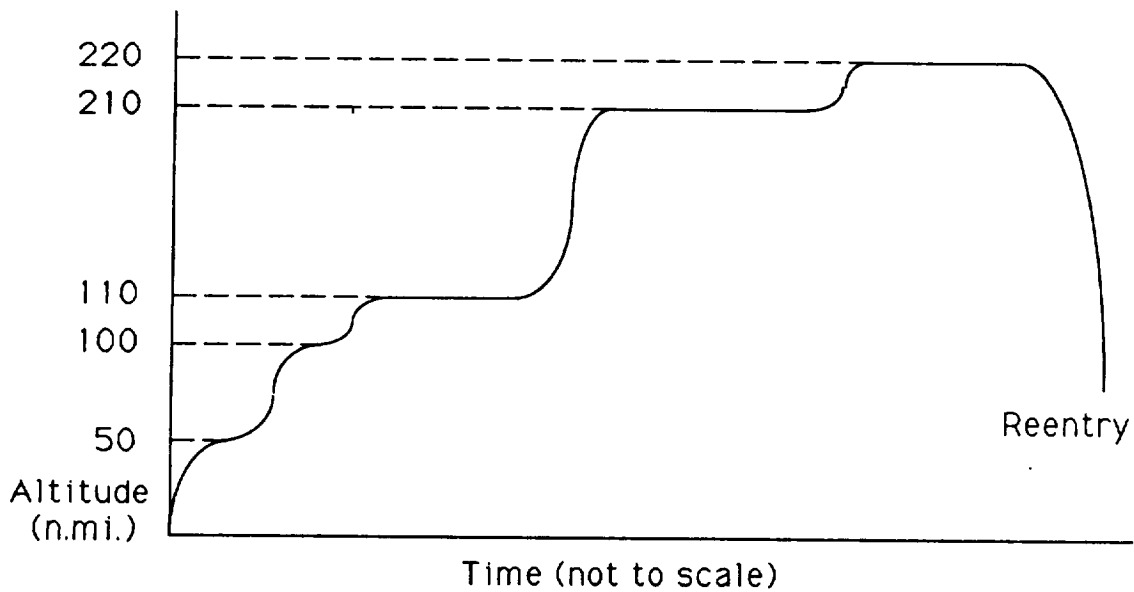


Figure 2.7 Mission Profile

## DATA SUMMARY

<u>Maneuver</u>	<u><math>\Delta V</math> (ft/s)</u>	<u>Mission Time (hr)</u>
50x100 - 110 Transfer	100	.737
110 Circularization Burn	20	-
110 Phasing	-	0 - 33
110 - 210 Transfer	180	.754
210 Circularization Burn	180	-
210 Phasing	-	5
210 - 220 Transfer	20	.771
220 Circularization Burn	20	-
Proximity Maneuvers (non-OMV)	58	10.5
Proximity Maneuvers (OMV)	40	12
220 Deorbit Burn	317	.585
<hr/>		
<b>Total</b>	<b>(non-OMV)</b>	<b>895</b>
	<b>(OMV)</b>	<b>877</b>
		<b>18.35 - 75.35</b>
		<b>19.85 - 76.85</b>

Figure 2.8 Data Summary

### 2.3 Alternate Scenarios and Contingency Plans

This section details events not included in a nominal mission scenario, including emergency situations.

#### **2.3.1 Abort Options**

Abort options during launch are limited for a number of reasons. One, the recovery system can not be counted upon to assist descent. In addition, for most of the launch period the CRV is over the Atlantic Ocean and would be unable to reach a landing site. There is a brief window where aborting to Dakar, Africa is an option but once again deployment of the recovery system poses an obstacle. The recovery system is designed to operate at a certain altitude and flight speed. Using the recovery system in an emergency role over the entire possible range of flight conditions and vehicle orientations would be risky at best. Abort to orbit using the CRV's engines is the best alternative but is not possible over the entire launch phase. Once orbit has been reached, there is a potential landing site within range on every orbit except one (see Table 3.1). Until the abort to orbit point is reached, the only abort option would be a parachute recovery system equipped with pontoons. Due to weight considerations, this is not possible in the present configuration.

### 2.3.2 Alternate Landing Sites

There is a potential landing site within the cross range of the CRV on every orbit except one. These potential landing sites include Kennedy Space Center, Hawaii, Guam and Dakar. The CRV has enough power reserves to stay in orbit for at least one extra pass at the primary site making the use of an alternate landing site unlikely and the lack of a landing site on one orbit reasonable .

### 2.3.3 Contingency Plans

For on orbit operations, contingency plans have been developed should any maneuver not be completed on schedule. This might be a result of navigation, engine or system failure. Only one maneuver requires a significant correction. The 110 - 210 n.mi. Hohmann transfer is timed to position the CRV a set phase distance behind the Space Station Freedom, SSF. If this maneuver is performed one orbit late, the CRV finds itself at a phase relationship of 5.84 degrees ahead of the SSF instead of 5 degrees behind. Figure 2.9 shows the  $\Delta V$  required to correct the phase angle. Other maneuver errors are resolved by either waiting for the phase difference to correct itself or by small perturbation methods.

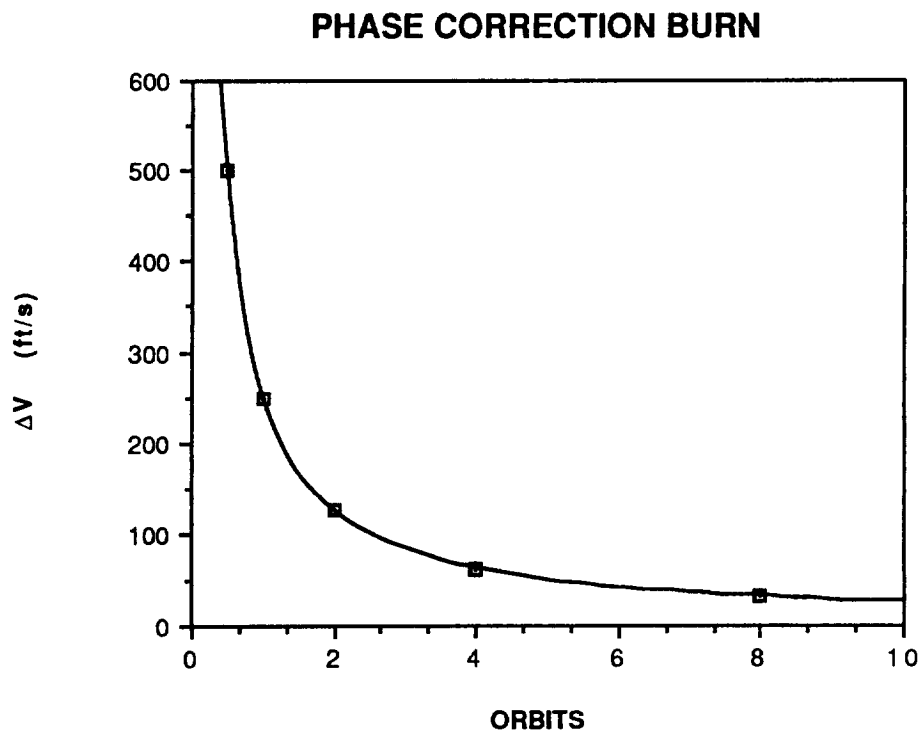


Figure 2.9 Phase Correction Burn

## **2.4 Ground Operations**

### **2.4.1 Delivery**

- Prelaunch CRV and payload processing--The launch of the CRV is broken down into processing and transporting to the pad. These will be described below as well as some of the ground facilities needed to support the CRV and its mission to the space station and back. A ground processing scenario for the CRV is given in Figure 2.10 .
  
- CRV processing--The CRV will be processed in the horizontal processing facility. In this facility, examination of the CRV for any damage from the last flight is conducted and testing of all the systems will be performed in preparation for the next flight. The Advanced Recovery System will be packed and readied for deployment on the next mission. It is suspected that a separate facility specifically for ARS repair and packing may be needed to be built due to its large size. Other systems which will be checked and/or serviced in the processing facilities include:
  - Internal power systems
  - OMS/RCS
  - Electrical systems
  - Data Management systems
  - Avionics (all nav aids and cameras)
  - Cooling systems
  - Landing gear
  - Thermal protection system
  - Structural leak test
  - Control surface systems

Aside from these specific system checks, the general condition of the CRV is observed and any necessary repairs made. Any major modifications needed to be made to the CRV will be completed in the Modification and Refurbishment facility. A preliminary CRV maintenance timeline is shown in Figure 2.11 on the following page. After the CRV has been checked out, the payload (pressurized and unpressurized logistics modules) will be loaded and all the payload related systems (cooling, SPDS, etc.) checked and security of the logistics modules ensured. Also, the related CRV docking mechanism is checked for operability. After the CRV is determined to be mission ready, it is transported to the Vehicle Assembly facility.

- Propulsion systems processing--The CRV's three external Liquid Rocket Boosters, LRB's, are processed in the Booster Processing facility. The LRB's are not reusable so they will be shipped from

the manufacturer and sent directly to the Booster Processing facility. Here, the LRB's are completely prepared for the next flight. All instrumentation and electronics as well as its thrust vector control system are tested and modified, if needed. After the completely assembled and processed LRB's are prepared, all three will be transported to the Vertical Assembly building for integration with the CRV.

- Payload processing--The Pressurized, PLOG, and Unpressurized, UPLOG's, logistics modules are processed in the Payload Processing facility. Supplies needed by the space station are packed into the logistics modules and secured for the flight. Once the logistics modules are packed, they are sealed and sent to the Horizontal Processing facility to be loaded into the cargo bay of the CRV.
- Vertical assembly--At the Vertical Assembly facility, the CRV with the payload in its cargo bay and the three LRB's are assembled in a vertical position using large lifting devices. The entire vehicle will rest on a mobile launch platform which will be designed specifically for the CRV configuration. When the assembly is completed and checked, the crawler transporter, a huge mobile platform, moves under the mobile launch platform and moves the assembly out to the launch pad.

Launch Pad--Once on the launch pad, the three LRB's and the CRV's propulsion system are purged and filled with liquid propellant from large storage tanks designed specifically for its contents. The propellant is fed through transfer lines to the launch structure which is connected to the vehicle. The Fixed Service Structure provides access to the vehicle in the event of a repairable malfunction before launch. There are several access panels on the CRV for the avionics systems, Advanced Recovery System, internal tanks and other systems which could be repaired on the pad without taking the vehicle off the launch pad.

A weather protection system is incorporated on the pad which could shield the vehicle from wind blown debris or extreme weather conditions. The system incorporates metal doors and inflatable seals as well as the structure's Rotating Service Structure, used primarily for the space shuttle, which surrounds the vehicle. The Fixed Service Structure also has a tall lightning mast on its top in case of lightning storms (reference 2.3). The pad the CRV will use is the same pad as the shuttle uses in order to save money.

# GROUND PROCESSING SCENARIO

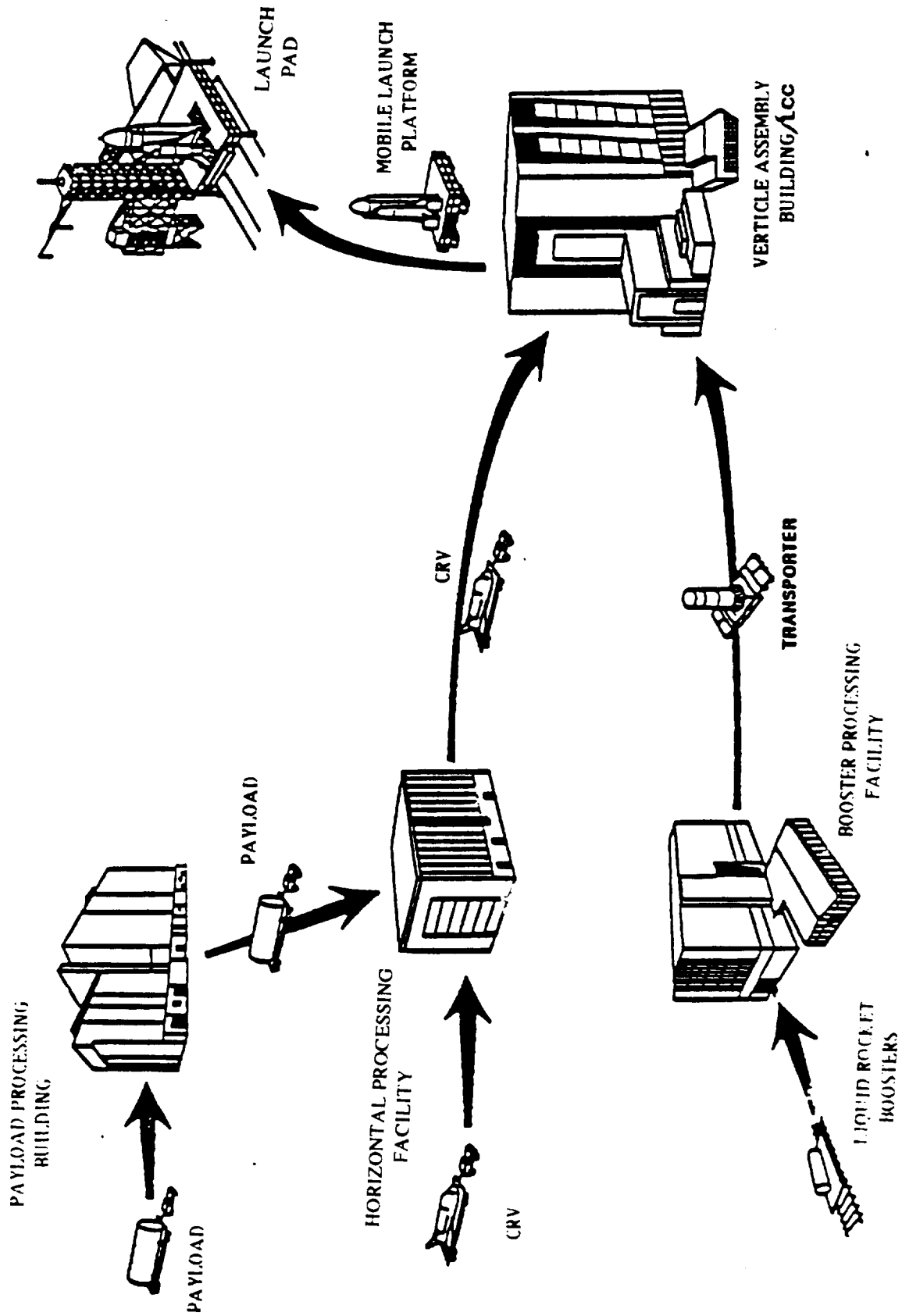


Figure 2.10 Ground Processing Scenario

# CRV MAINTENANCE TIMELINE (PRELIMINARY)

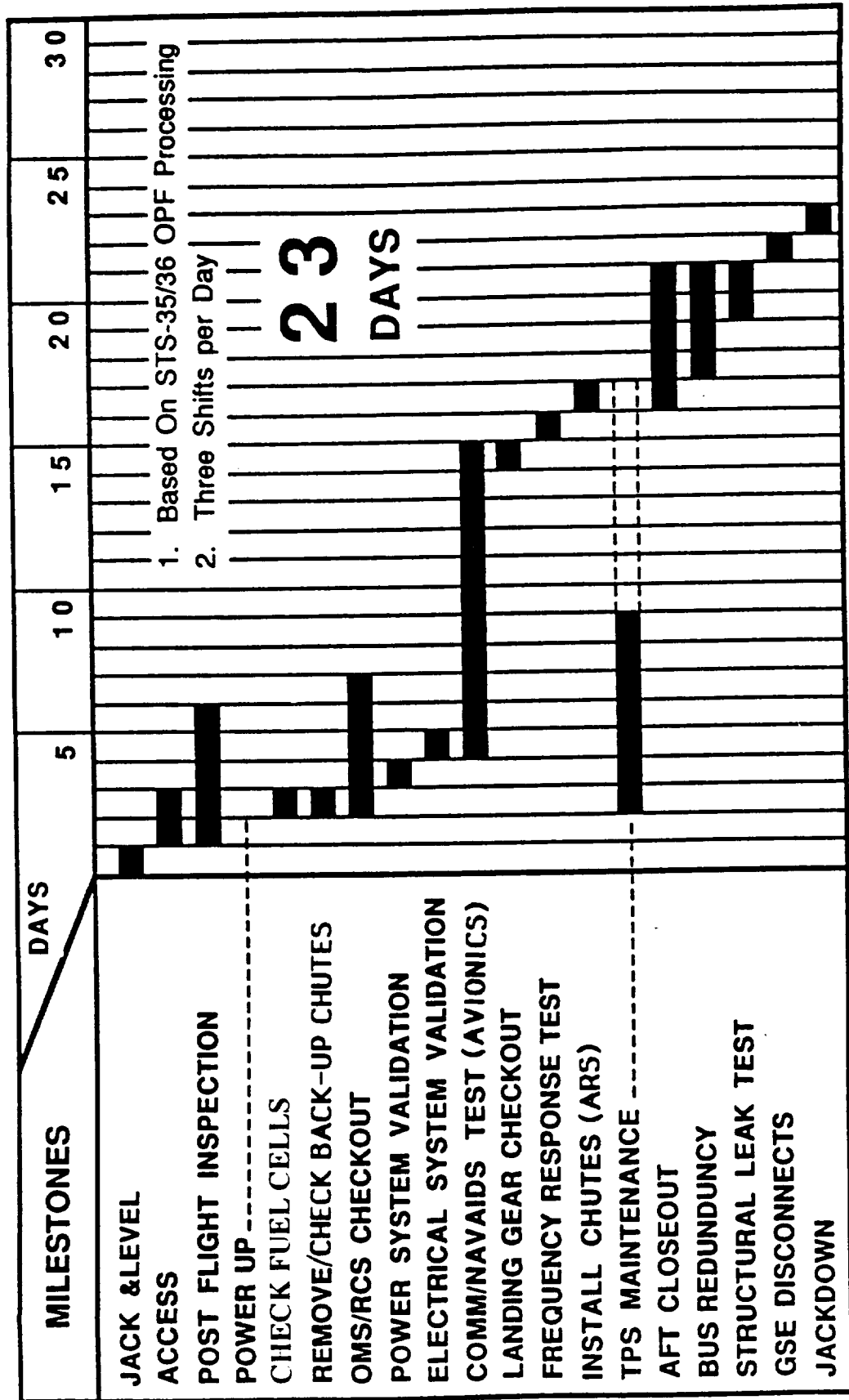


Figure 2.11 CRV Maintenance Timeline

- Launch Control Center--The Launch Control Center contains firing rooms each equipped with a "Launch Processing system" which monitors and controls the activity of the CRV from the assembly, to checkout, and launch. The Launch Processing System, LPS, greatly reduces the amount of time and personnel required for launch of the CRV which will be a benefit when short turnaround times are required.

The LPS consists of the central data subsystem and the checkout , control and monitor subsystem. From the time the CRV enters the CRV processing facility, a firing room is assigned to it including the LPS which controls all the assembly and checkout steps. All activities are reported to the LPS right up to launch. The LPS is connected to dozens of computer consoles in the firing rooms which show conditions that need to be evaluated by an engineer. In many cases the LPS will automatically correct the condition by performing safing operations. The LPS carries the CRV right up to launch and after all the connections are disconnected, fires the engines (reference 2.6).

The CRV turnaround time is 66 days and about a week more for transport from other landing sites (reference 2.1). A timeline is given for the prelaunch activities in Figure 2.12.

#### **2.4.2 Navigation**

- Ground based navigational aids and Control Center--Throughout the mission, the CRV is monitored and controlled by ground based control centers. Launch Control, as mentioned above, is responsible for all ground and launch activities and until about ten seconds into flight. The CRV is then controlled by Mission Control Center. Mission Control assumes responsibility of the CRV until it enters the Command and Control Zone, CCZ, of the space station. At this point, the CRV is directly controlled by the space station crew for docking, unloading, and departing the CCZ after which it is taken over by Mission Control to landing. The control centers will incorporate ground stations (the NASA ground terminal at the White Sands Missile Range, for example) to receive signals sent via the Tracking and Data Relay Satellite System. An illustration of TDRSS system interaction is given in Figure 2.13. Most ground stations needed are already existing and in operation due to the shuttle program. These ground facilities can easily be used with the CRV and therefore no new facilities will be needed.

# CRV PROCESSING TIMELINE

(PRELIMINARY)

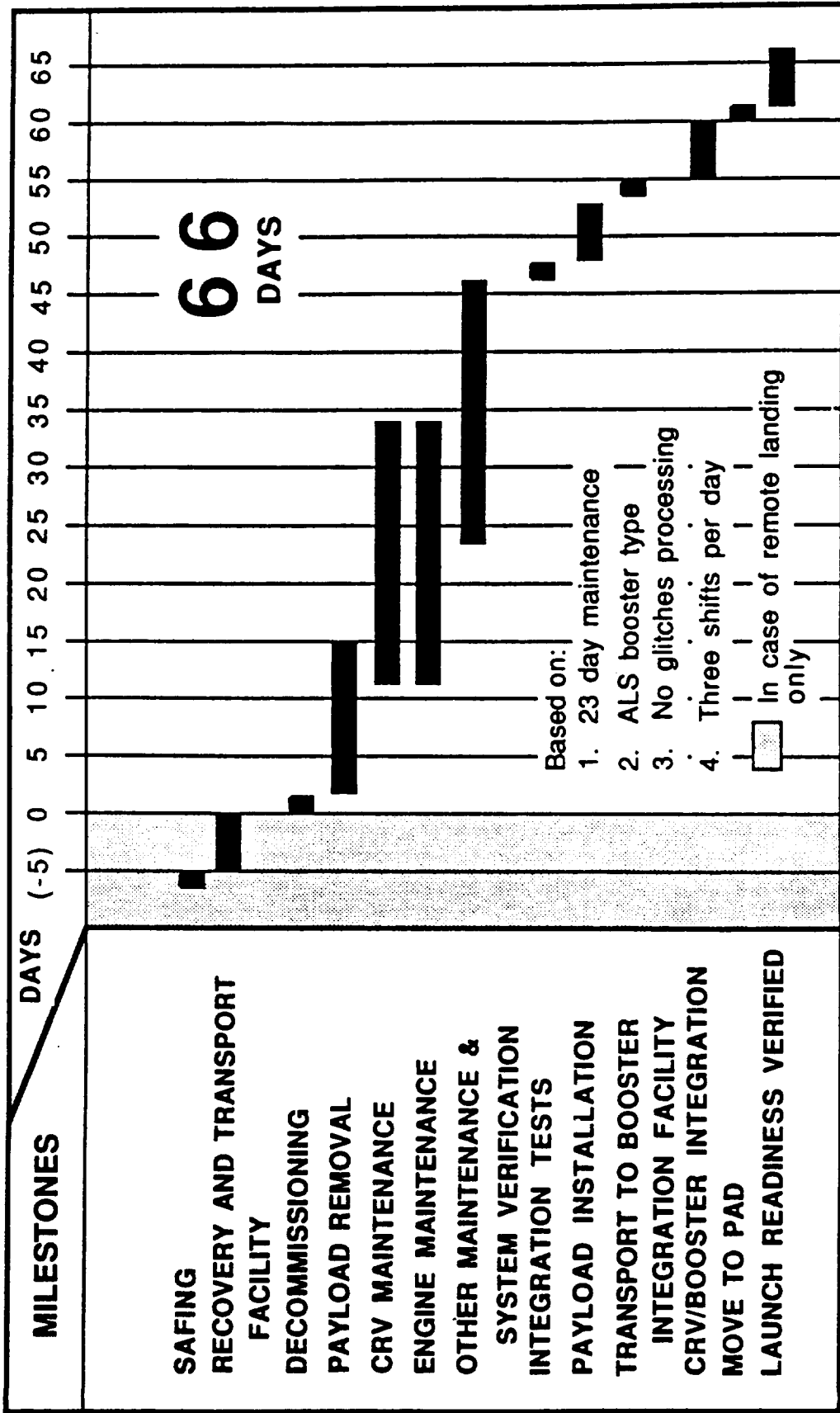


Figure 2.12 CRV Processing Timeline

- Ground based navigational facilities--Upon decent and landing, the CRV will rely on several ground base navigational facilities to provide it with the information necessary to guide it in for a successful landing. TACAN (Tactical Air Navigation) consists of several ground stations which send signals picked up by the CRV and give distance and bearing to the station. The Microwave Scanning Beam Landing System (MSBLS) provides elevations and azimuth from the ground station and guides the CRV in to landing. Radar altimeters provide altitude of the vehicle above the ground by transmitted and returned signals. Again, these systems are currently used by the space shuttle and can be easily used by the CRV.

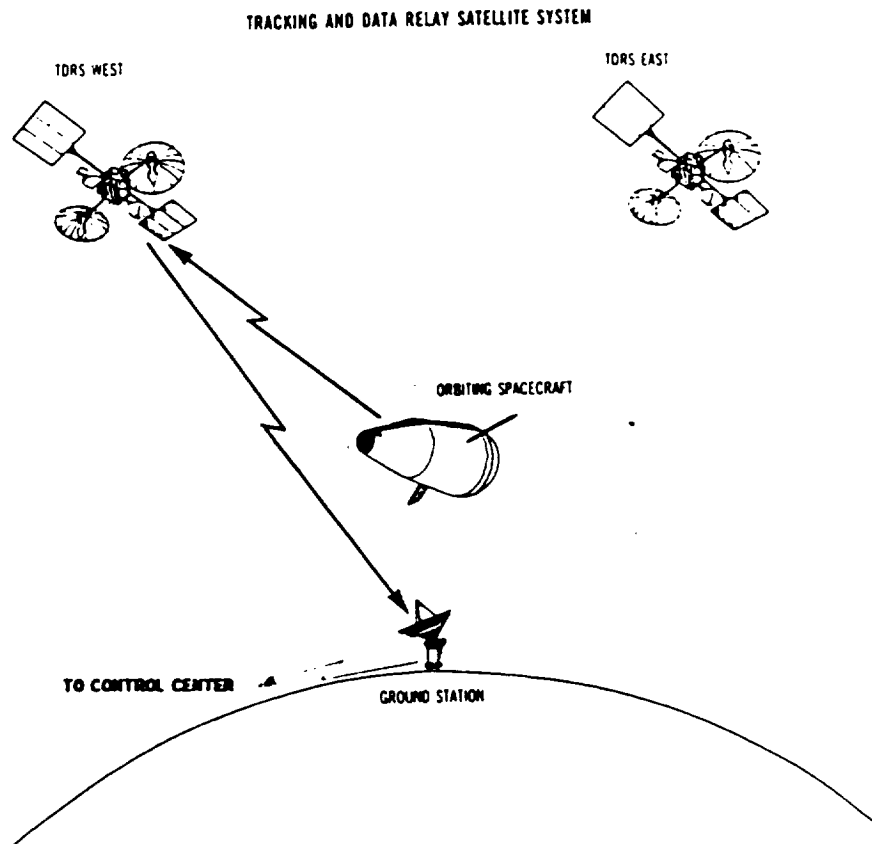


Figure 2.13 Tracking and Data Relay Satellite System

### **2.4.3 Return**

After the CRV performs its deorbit burn, it enters the atmosphere at -1 degree flight path angle and 26 degree angle of attack. In a constant 40 degree bank, the CRV varies its angle of attack up to 64 degrees and back down to 26 degrees as its flight path angle is decreased to approximately -14 degrees and velocity decreases to 6200 m/s at an altitude of 69,000 feet. At this point, the drogue chute is deployed. Maintaining the bank angle, the CRV slows to 230 ft/sec and the flight path decreases to -80 degrees at 10,000 feet altitude at which point the Advanced Recovery System is deployed.

The drogue chute will be deployed to slow and stabilize the CRV in preparation for the ARS deployment. At 10,000 feet, the Advanced Recovery System is deployed. The ARS will be reefed in several stages and disreefed periodically to an altitude of 7,000 feet where it will be completely filled. At this point, the drogue chute will be jettisoned to allow the CRV to be more maneuverable. The CRV will then fly steady state until the vicinity of the landing site. Similar to the shuttle, the CRV will make a course for the runway. The CRV flares at 60 feet until touchdown at a velocity of 5 ft/s vertical. After touch down, the CRV will roll to a stop in less than 10,000 feet, enabling it to land at various runways at Edwards AFB or KSC as well as many alternate landing sites at Hawaii, Guam, or Dakar.

### **2.4.4 Post Flight**

When the CRV comes to rest on the runway, crews meet it in specially designed vehicles and check for potentially inflammable vapors and lethal gases leaking from the engines. Fire equipment is positioned in event of an explosion or fire. Once deemed safe, coolant umbilical access vehicles are connected to the CRV and provide cooling of the electrical equipment and other areas of the CRV to remove residual explosive or toxic fumes. After the CRV is cooled and all systems are safe, the CRV is towed to a reception facility and readied for transport in NASA's Super Guppy aircraft.

The Super Guppy is a converted Boeing plane used to carry large rocket sections and various shuttle components (Ref. 2.3). The Super Guppy has a 25 ft. 6 in. x 25 ft. 1 in. compartment that is tapered to a length of 111 ft. 6 in. (Ref. 2.2). The Super Guppy has a maximum payload weight of 54,000 pounds which is quite adequate for the dry weight of the CRV. Due to the size of the aircraft, the CRV's stabilizing fins must be removed before transfer. The aircraft has a hinging fore section which will allow the CRV to be placed in it using a rising hydraulic trailer. The CRV will then be flown to

Kennedy Space Center to begin checkout or repairs for the next mission.

## **2.5 Payload Bay**

The CRV's most important function is to take cargo up to the space station and bring used materials back down to Earth. This makes the design and placement of the cargo bay key to the whole CRV design. The final design and placement of the bay corresponds to the final CRV design.

### **2.5.1 Door and Bay Placement Options**

The Advanced Recovery System that was planned for use would have required a 60 foot storage compartment placed along the center on top of the CRV. This would have made placement of the cargo bay doors on top in a normal position impossible. To deal with this problem, four options were proposed:

- OPTION 1: Top placement, either double or single door using Stabilized Payload Deployment System (SPDS) for cargo deployment if necessary. the bay would be placed parallel to the top of the CRV in the aft cone section. However, this option would not be feasible with the rigid wing ARS that was originally chosen.
- OPTION 2: Side placement with a single door using SPDS to rotate payload out of cargo bay. The major problem with this option would be the thermal heating experienced by the seal on the doors and how to fit the TPS around it. There would also be the problem of how to ensure a tight seal on the door.
- OPTION 3: A rear cargo door that would be accomplished by placing all of the propulsion devices in a small rear section and then opening this section up to expose the module and exchange it using the station's robot arm or the OMV. The module would be loaded like a flashlight battery into the cargo bay. Access to the module after the CRV is on the launch pad would be limited depending on the type of launch configuration used.
- OPTION 4: This option uses the same idea as option 3, but instead of the rear opening up, the nose section would. All of the avionics and electrical equipment would have to be positioned so that it was all in the section that opens up or in the rear of the CRV, behind the payload bay entirely. The major problem would be the heating effects on the nose cone during re-entry. Access would again be limited to cargo after it is loaded.

After much debate between the Aerodynamics, Structures, and Mission Operations groups, it was decided the best solution for everyone would be to change the Advanced Recovery System to the ram-air parafoil. This would make the OPTION 1 possible and alleviate the problems that the other three options created.

### **2.5.2 PLOG/UPLOG**

As it stands right now, the main function of the CRV is to re-supply the space station. The cargo bay has been designed with this purpose in mind, but allowing room for other payload to be transferred so the CRV can be more versatile and not just one payload specific. The longeron and keel bridges have holes along them that let a number of different combinations of cargo be attached. The bay is 15 feet in diameter which is concurrent with the Shuttle-C and Space Shuttle payload bays. The PLOG and the UPLOG have been designed with trunnions to be compatible with the longeron and keel latches to secure cargo in the bay, shown in Figure 2.14. With the length of the cargo bay set at 25 feet, there are two possible configurations to transport the station's required payloads.

The first configuration has two unpressurized logistics modules positioned in the bay as shown in Figure 2.15. This will be a maximum of 36,800 pounds of cargo up. As shown in the figure, they are positioned one foot apart and two feet from the rear of the bay to allow for ample clearance from the cameras and for removal from the bay. The UPLOG carries four subcarriers: fluids subcarrier, dry cargo subcarrier, Hydrazene subcarrier, and bi-propellant subcarrier.

The second configuration allows only one pressurized module to be taken up or down from the station. When the PLOG is being delivered to the station it will weigh a maximum of 40,000 pounds. These are scheduled to be exchanged every 90 days for re-supply. They transport needed hardware and consumables to the space station crew. It will also contain the numerous experiments to be performed in space. The position of the PLOG in the bay is shown in Figure 2.16. The PLOG is 1.5 feet from the rear of the bay to allow for clearance when the PLOG is being exchanged and for the cameras. The PLOG has been designed with a grapple fixture for use with the station's RMS for exchanging modules once the CRV is docked at the space station.

### 2.5.3 Payload Hold-down Methods

The two types of latches chosen to secure the payload in the bay are the longeron and the keel latch. The latch assemblies are electromechanical devices that interface with payloads and latch them into position in the payload bay (reference 2.10). The assembly

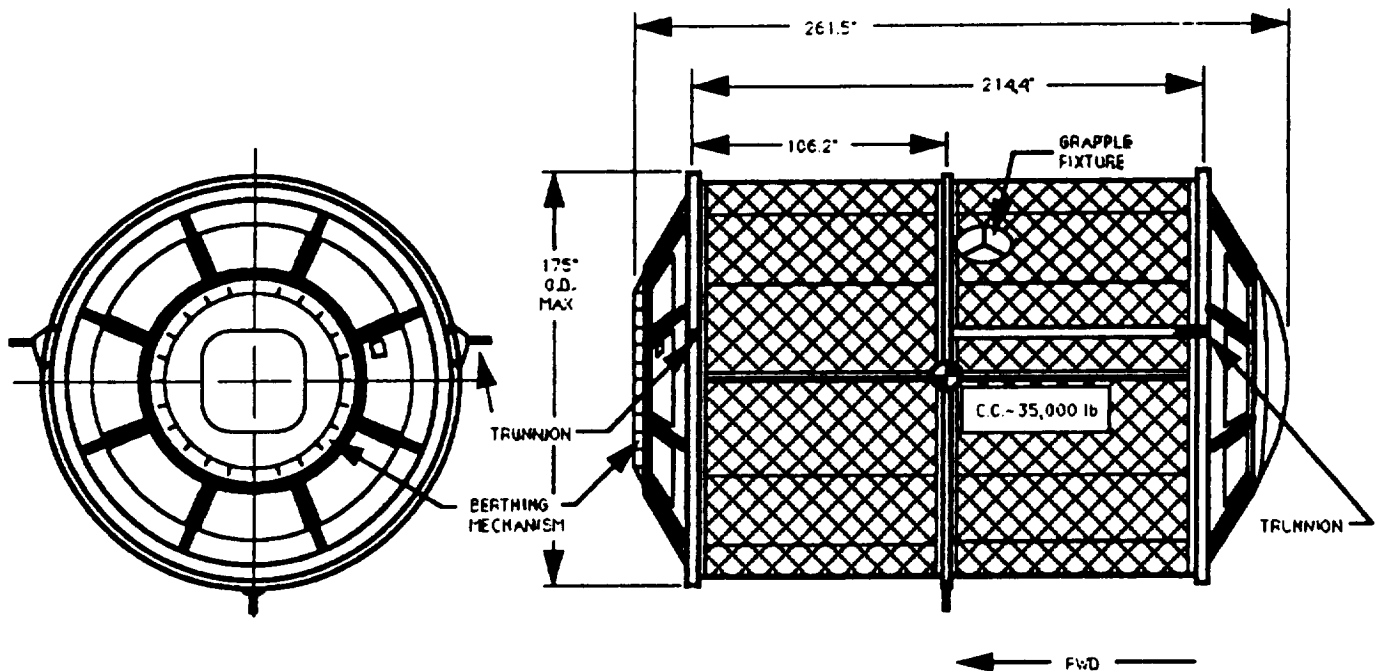


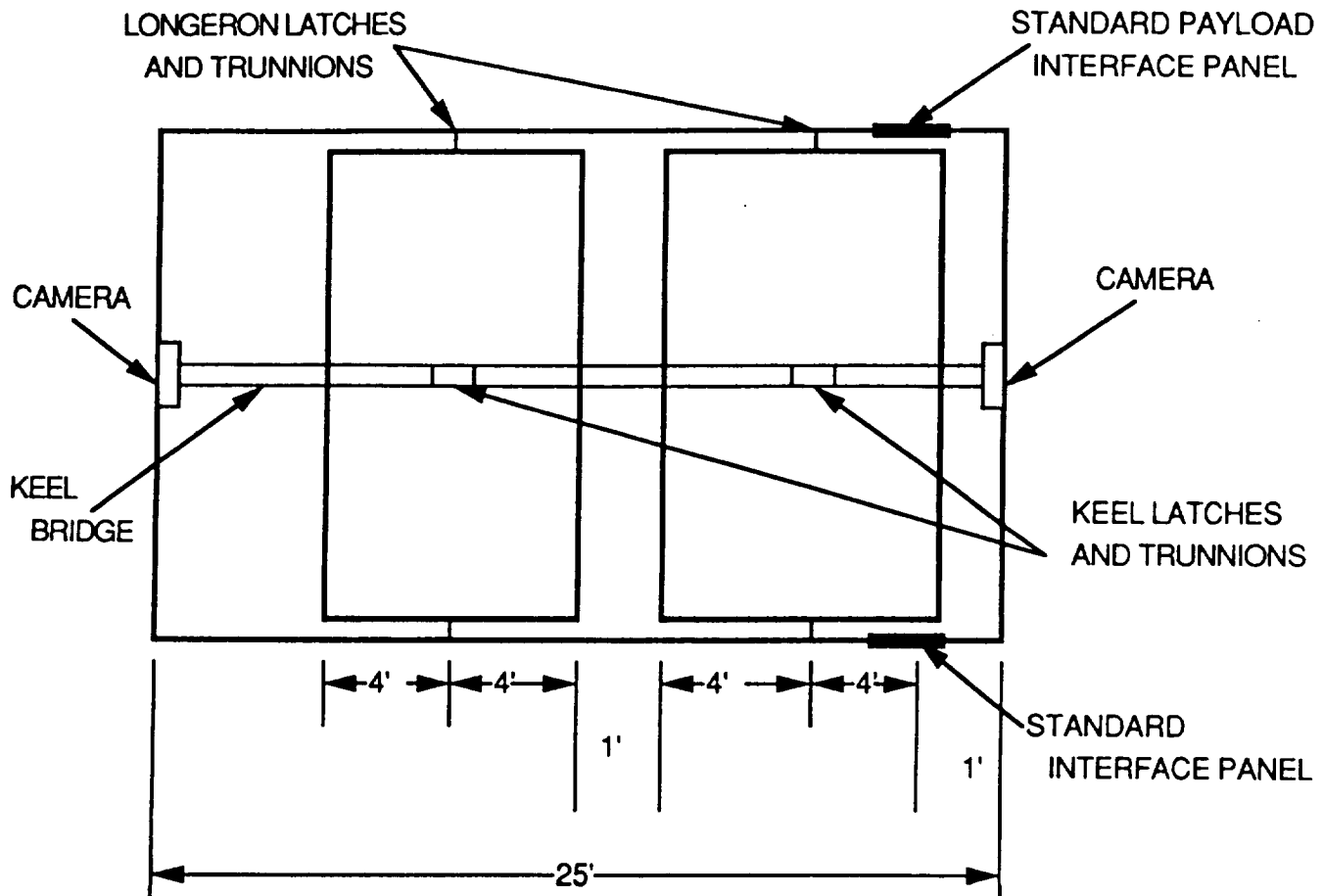
Figure 2.14 PLOG with Trunnions

consists of the latch, drive motors, differential-drive gear box, and limit switches. Each assembly contains two 115 volt three-phase, 400 hertz motors. The limit switches and mechanical stops are used to fix latch travel limits. Each limit switch is associated with a drive motor and sense end-of-travel of the latch, remove power from the drive motors, and provide a latch position indication signal to the control panel. Two additional limit switches sense the position of the payload trunnion and provide a ready-to-latch signal when the trunnion is properly positioned in the latch.

The longeron latch, shown in Figure 2.17, will be used to restrain the cargo in the X and Z directions with the axes defined as shown in the figure. The latch can attach to the CRV along the longeron bridge on the side in the bay at numerous points. The actuation time for this latch is 30 seconds for dual motors and takes twice as long with one motor failed (Ref. 2.10). It also has the feature of a manual override mechanism which uses EVA to manually bypass the normal drive train to open or close the latch in case of failure.

The keel latch, shown in Figure 2.18, is used to relieve the cargo in the Z direction reacting to Y loads. It fits at attachment points along the keel bridge that runs along the center of the bottom of the cargo bay. Each logistics module is designed with one keel trunnion along the line of its center of gravity in the Z direction, so only one keel latch is needed for each module.

The attachment points for these latches in the bay are shown in Figure 2.19. It shows each latch position for both configurations that were discussed previously.



TOP VIEW WITH TWO UNPLOG'S INSIDE BAY  
Figure 2.15 UPLOG in Cargo Bay

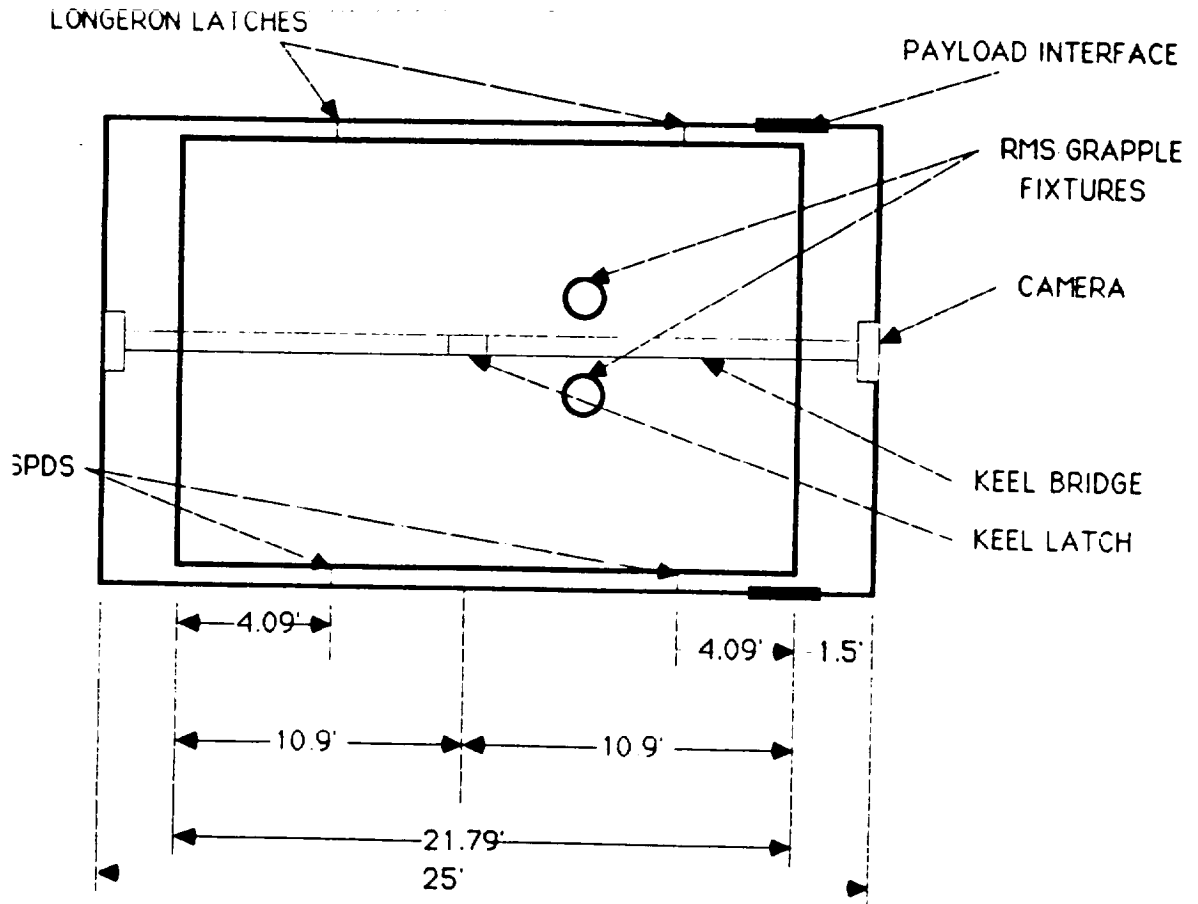


Figure 2.16 PLOG in Cargo Bay

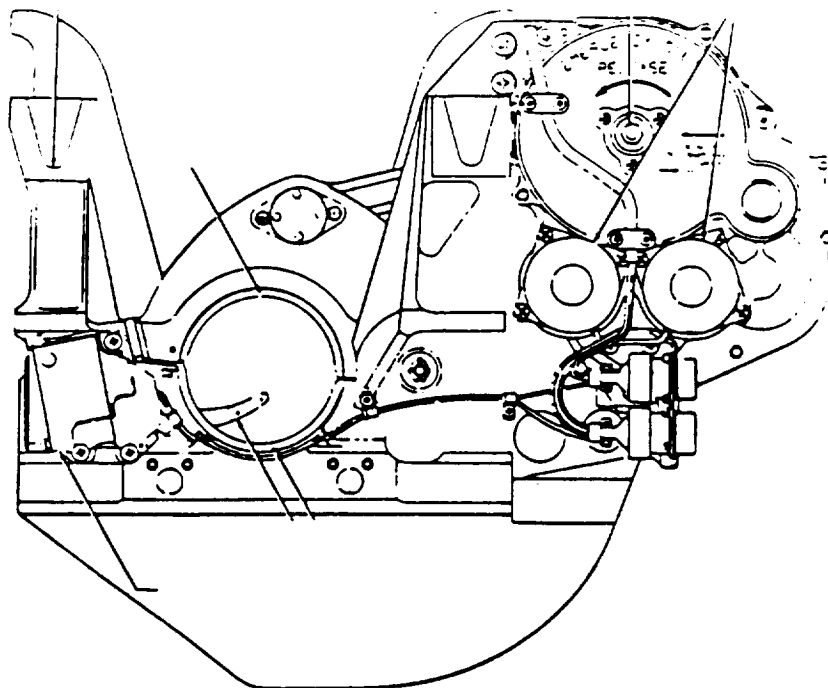


Figure 2.17 Longeron Latch

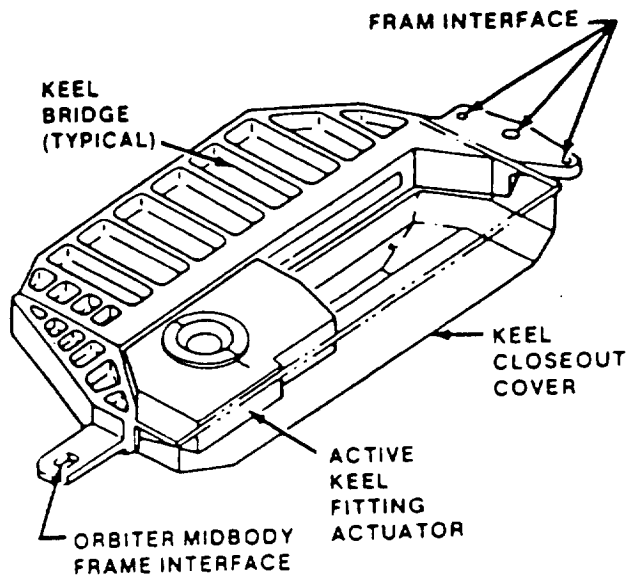


Figure 2.18 Keel Latch

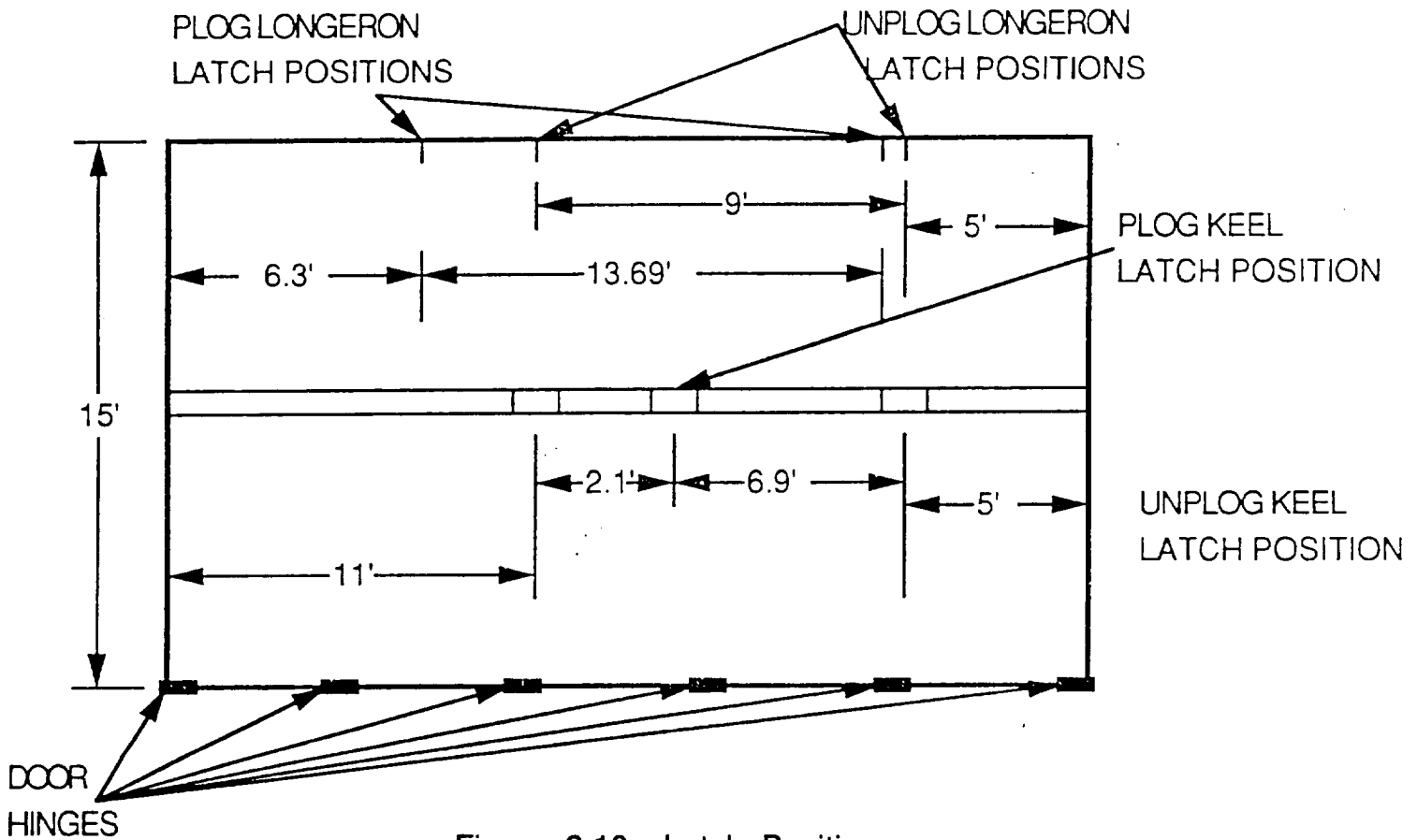


Figure 2.19 Latch Positions

## 2.5.4 Stabilized Payload Deployment System

On one side of the bay, along the longeron bridge will be points for Stabilized Payload Deployment System, SPDS, attachment. SPDS is used to rotate payload out of the cargo bay away from the CRV and aid in the cargo transfer scenario when the OMV is used to remove the cargo and transfer it to the station instead of the CRV directly docking to the station. Since it is not known at this time what the status of the OMV is or will be in the future, both options must be considered as possibilities. Also, depending on the extent of movement and maneuverability of the space station's SSRMS, the SPDS might be able to rotate the payload out of the bay and into position to be within reach of the arm.

The system consists of a dual-pedestal configuration, with one set being used only as a backup in case the primary pedestal malfunctions. The setup is shown in Figure 2.20. It works in conjunction with the payload retention latches and imparts a small velocity of up to 0.10 feet/second on the payload. The complete system weighs 180 pounds. It is 18x16x8 inches per pedestal.

Deployment on payload consists of three phases:

1. Payload is translated up (+Z direction) and outboard relative to the payload bay longeron to reposition the payload keel trunnion clear of the keel latch.
2. The payload is rotated over the side of the cargo bay to the desired orientation.
3. The payload is released at a low separation velocity.

This sequence is shown in Figure 2.21. The time for payload deployment takes approximately 22 minutes to complete (reference 2.8).

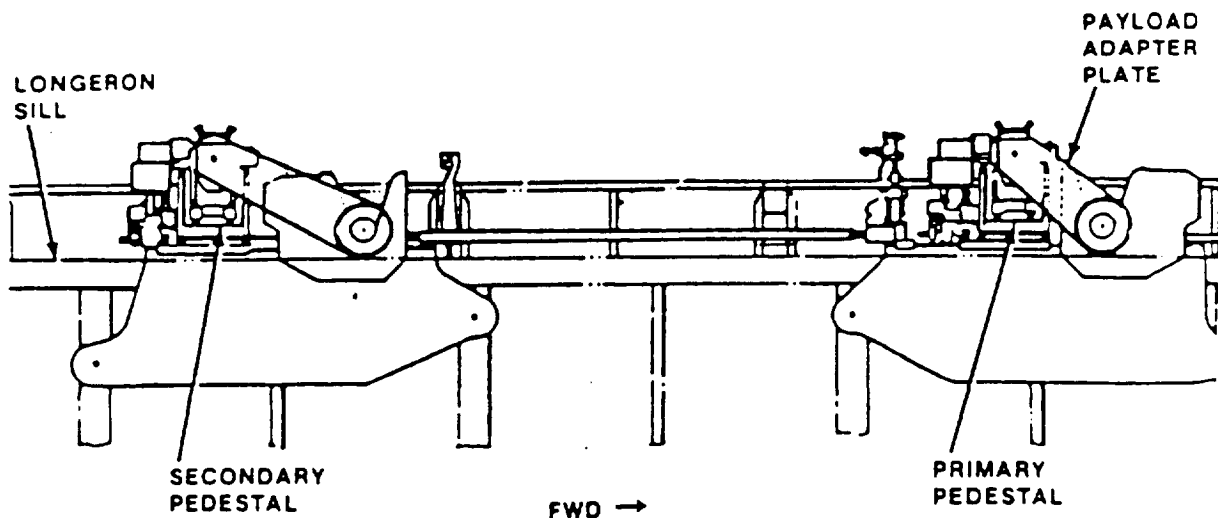


Figure 2.20 SPDS Configuration

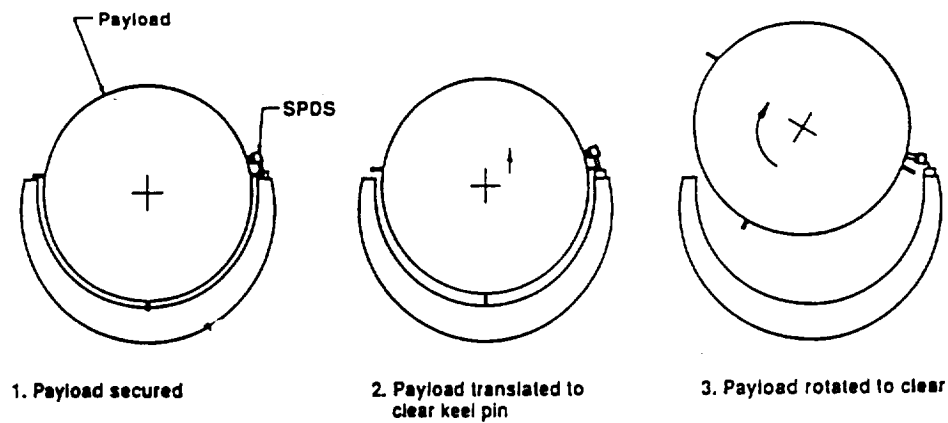


Figure 2.21 SPDS Deployment

### 2.5.5 Cameras

Two closed circuit TV cameras, one at each end of the bay, will aid in payload exchange since the vehicle is unmanned. There is a NASA requirement that EVA cannot be required to complete the mission, so secure payload attachment and release will have to be done remotely from inside the station through the use of the cameras and the limit switch signal lights. Also, if there is a malfunction in the switch, the cameras will be able to show if the latch is open or closed and if EVA is required to remedy the situation. This way a possible unnecessary EVA can be avoided.

### 2.5.6 Payload Service Interface Panel

There is one payload interface panel on each side of the bay to provide electrical power for the payload. They provide an interface for data management. These are standard payload interface service panels that were used on the Shuttle-C.

## 2.6 SSF/CRV Proximity Operations

Two primary missions were studied involving CRV/SSF proximity operations. The first, which is the nominal mission, has the CRV approach and dock to the station without requiring OMV assistance. The OMV is an unmanned, remote controlled "tugboat" capable of transporting cargo in the Space Station vicinity. Payload exchange occurs using the Mobile Servicing System (MSS). The CRV then separates and deorbits under ground control. If the CRV is unable to enter the Command and Control Zone (CCZ) or dock to the station, the mission will follow a contingency plan. In this case, the OMV is used to exchange cargo, making two trips to the CRV. The CRV deorbits itself under ground control after

the exchange. Inside the CCZ, the CRV must meet these, among other less profound, requirements :

- EVA shall not be required to exchange logistics elements, but it shall be capable of assisting SSF external robotic systems as a backup.
- Self propelled SSF elements and free flyer aircraft within the CCZ shall utilize a global positioning system receiver/processor for state vector computation.
- All vehicles within 1 km. (.54 n.mi..) of the SSF shall be equipped with visual ranging cues (markings/targets of known dimension) visible to the SSF crew along the elements normal approach path. (Vehicle structure may satisfy this requirement, depending on its geometry and body shape.
- These vehicles shall also provide for crew visibility (i.e.flood-lights or running lights for nighttime visibility).
- An arriving logistics element shall be attached and activated prior to deactivation and removal of the returning logistics element.
- Final approaches to the SSF shall be from the plus or minus V-bar direction.
- Only one free-flier at a time shall be scheduled to be within the CCZ.
- Unmanned vehicles within the CCZ shall be controlled by the SSF crew.

The above requirements were found in reference 2.12.

- The Mobile Servicing Center will be used to transfer the logistics elements during resupply activities. (reference 2.13)
- OMV rendezvous and docking with another vehicle will nominally occur outside the CCZ under ground control. (reference 2.13)

In the nominal mission, the CRV phases and circularizes into a 220x220 n.mi.. orbit at the edge of the CCZ, about 20 n.mi.. from the station. Under control of the SSF crew, it moves to the station using an cold gas thrusters in maneuvers taking one and one-half orbits to complete. During these maneuvers, the docking mechanism moves into its docking position. The CRV's cold gas thrusters are used in berthing operations; the RCS thrusters must be inhibited during this period. Docking will nominally occur at the front of the station. (Figure 2.22)

Payload exchange will occur with the use of the Mobile Servicing System, which is primarily made up of a Mobile Transporter (MT) to move it along the transverse boom; the Mobile Remote Servicer Base System (MBS); the Space Station Remote Manipulator System (SSRMS), consisting of a robotic arm; and a removable Special Purpose Dextrous Manipulator (SPDM), two highly movable robotic "fingers" that attach to the end of the arm (reference 2.14).

It has been stated that the SSRMS with the SPDM attached will be used to dock the Space Shuttle to the station's port. (reference 15) It is unclear whether or not the CRV is capable of using this method, as the Space Shuttle may also use its own robotic arm to interface with the SPDM and dock to the station. If an RMS system (i.e. robotic arm) is required on the docking vehicle, then the CRV would not use this method, but rather use its cold gas thrusters only. The SSRMS by itself is long enough to aid in the docking procedure, however.

Requirements of the docking mechanism include the capability to physically support the CRV, interface CRV monitoring with SSF systems, and compact enough so as not to adversely scar the vehicle. Considerations for location of the mechanism include vehicle approach to SSF, location of CRV propulsion and pressurized tanks relative to populated areas of SSF, and positioning of the payload within reach of SSRMS so a logistics module can be moved into place without moving the MSC.

Docking the CRV requires that approximately ten feet of space exist between the fore end of the payload and the center axis of the docking port to allow adequate clearance between the docking node and the removed payload. If a "straight" docking mechanism was used, it would therefore have to be placed in front of the cargo bay, in the fore cone. Figure 2.23 is a vertical view; Figure 2.24 is a horizontal view. Figure 2.25 is a top view of the system in Figure 2.23.

The cargo would be within reach of the SSRMS whether it is deployed from its bay using an SPDS (33.2 ft. reach, vertical dock), or not. (SSRMS work envelope radius = 46.65 feet) If the docking mechanism had to be placed within a non-extended cargo bay (25 feet long), not only would it have to fit in a space considerably less than three feet wide, it would also have to include an extendable end mechanism to reach out over the fore cone of the CRV to provide the required clearance and not increase SSRMS stretch. This is a rather complex system and may not easily meet the physical support requirement.

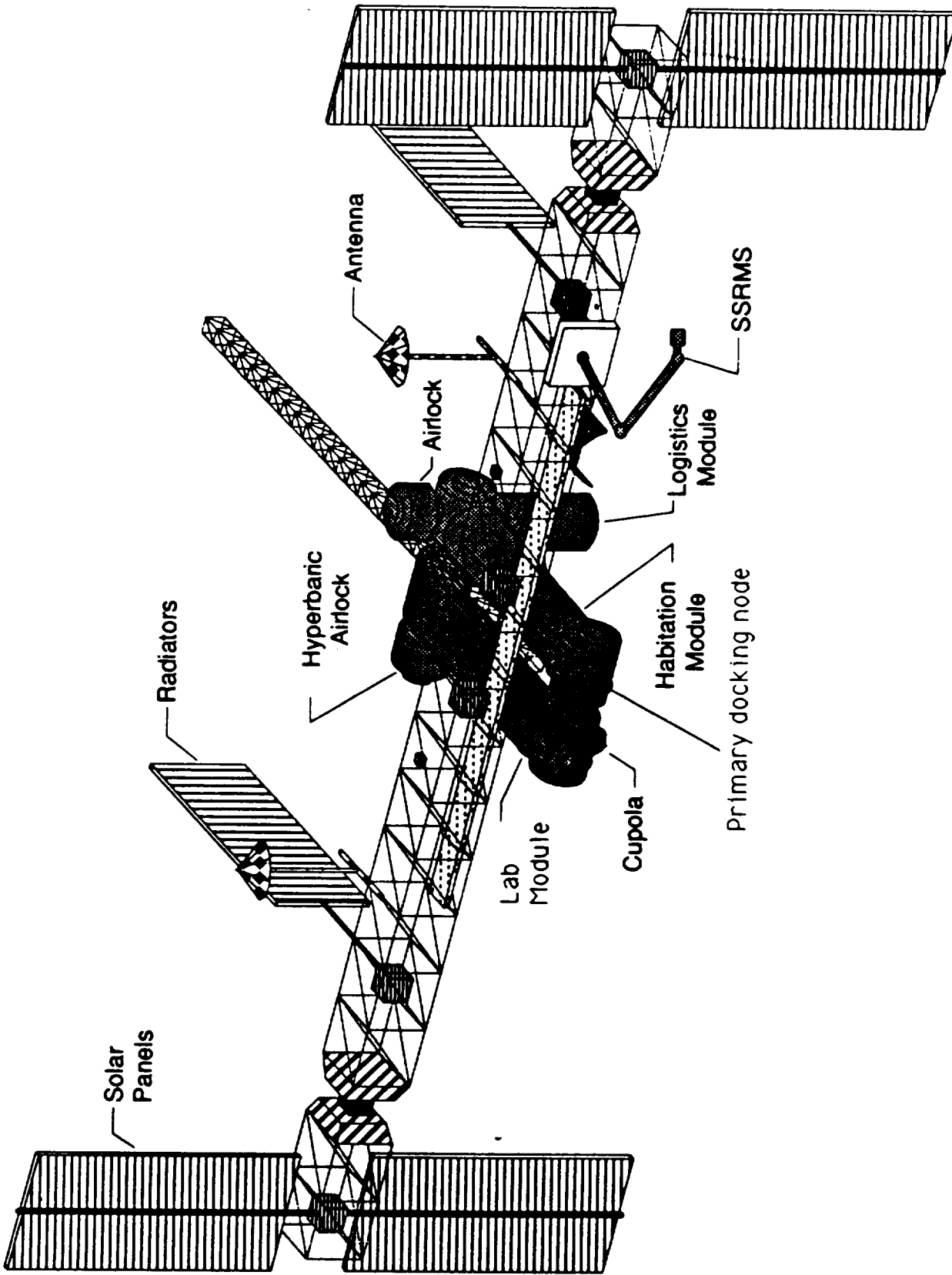


Figure 2.22 Space Station Freedom

# VERTICAL DOCKING -- SIDE VIEW

## FORE CONE MECHANISM

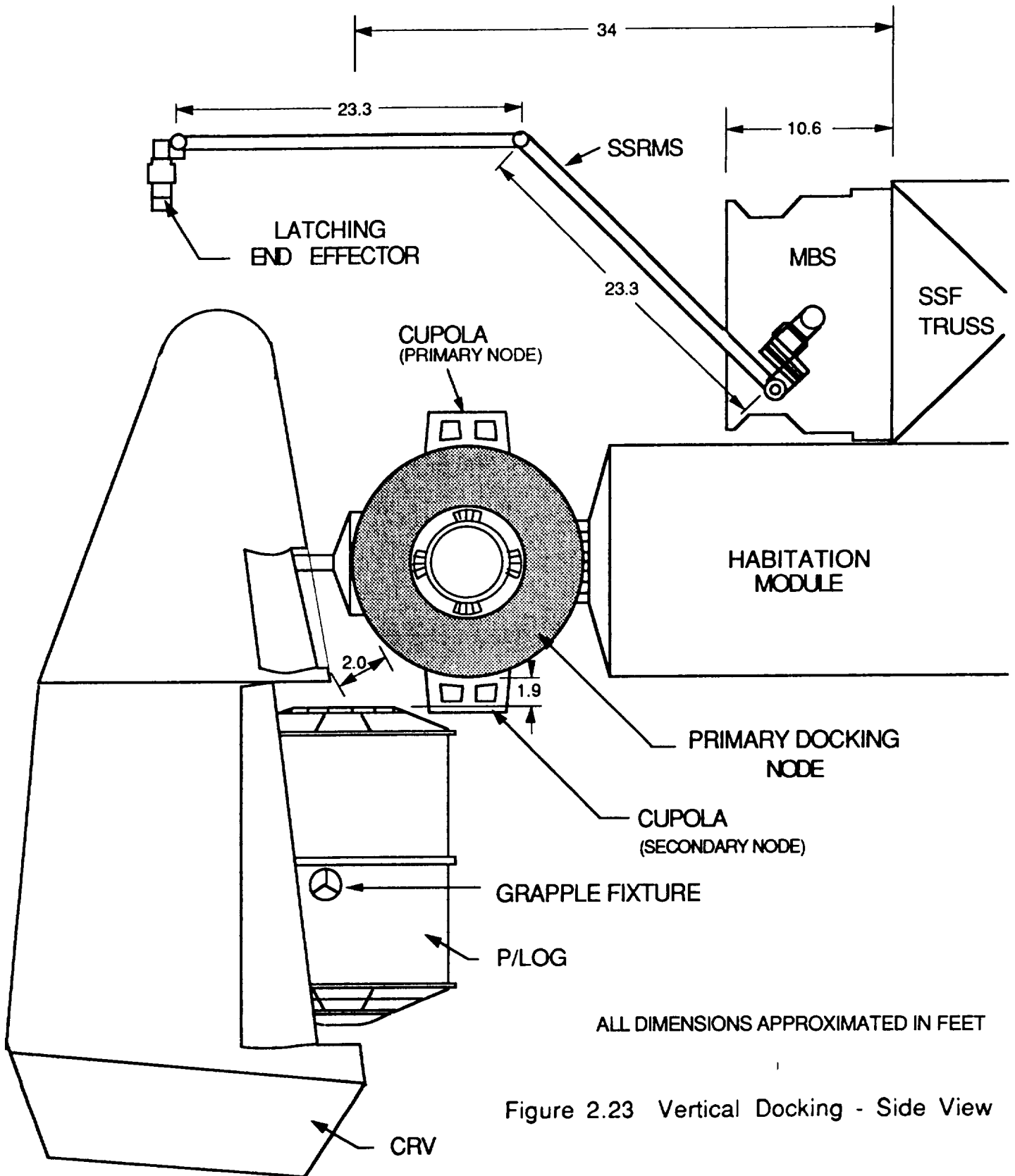
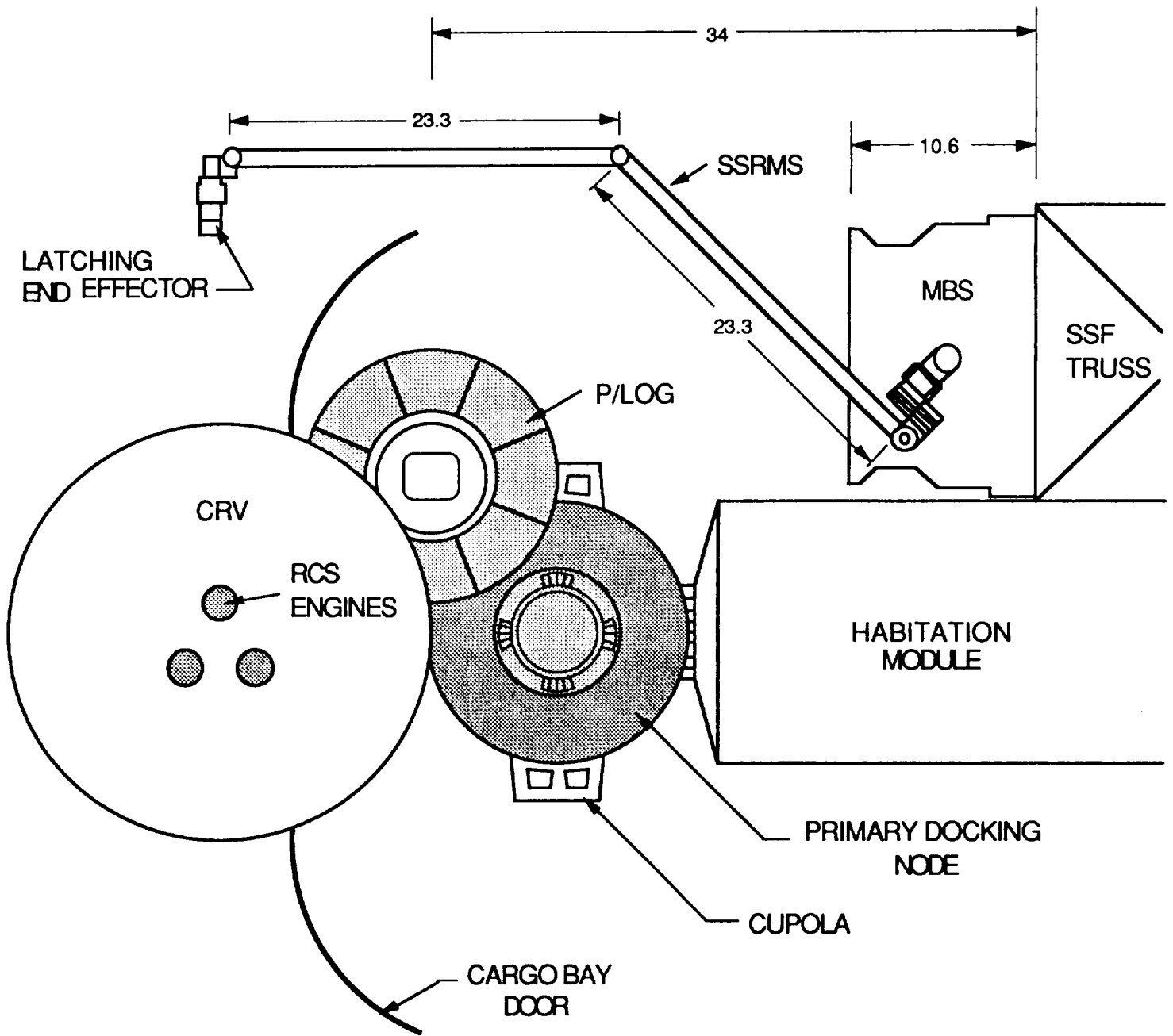


Figure 2.23 Vertical Docking - Side View

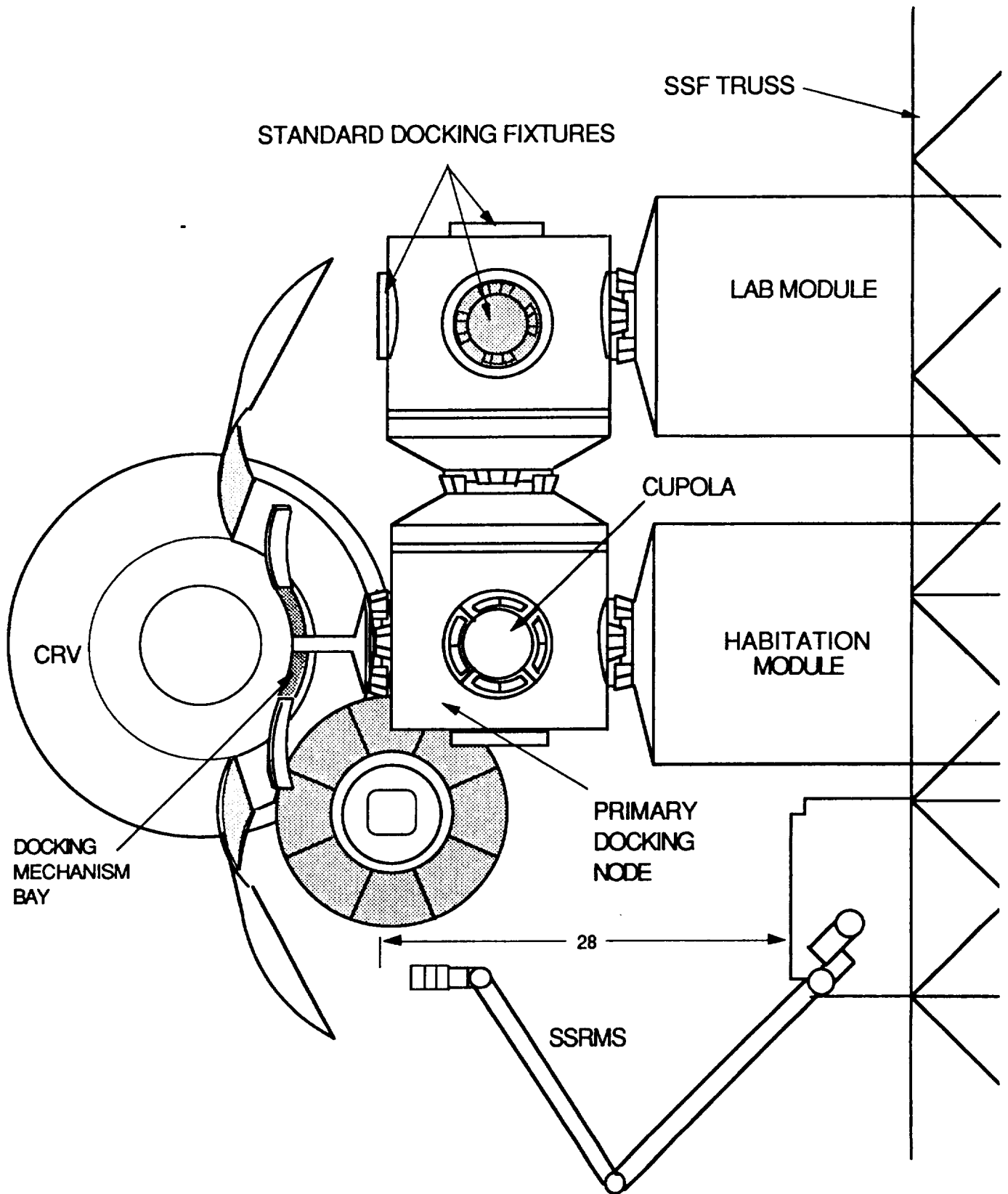
# HORIZONTAL DOCKING -- SIDE VIEW FORE CONE MECHANISM



ALL DIMENSIONS APPROXIMATED IN FEET

Figure 2.24 Horizontal Docking - Side View

# VERTICAL DOCKING -- TOP VIEW FORE CONE MECHANISM

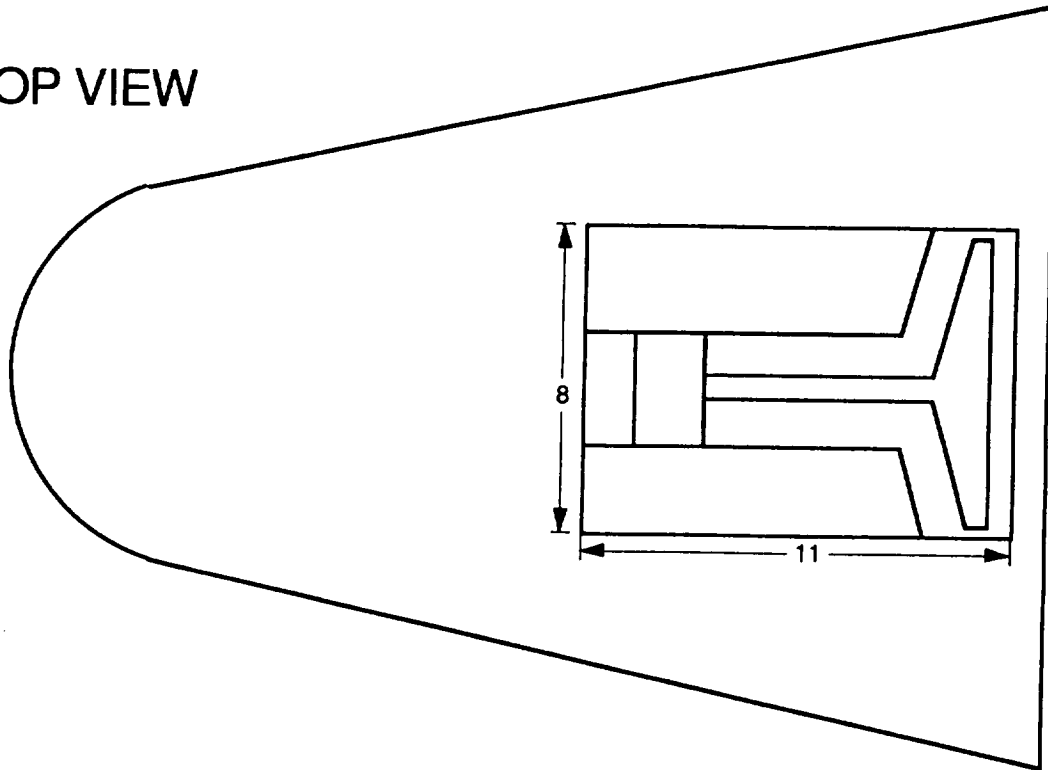


ALL DIMENSIONS APPROXIMATED IN FEET

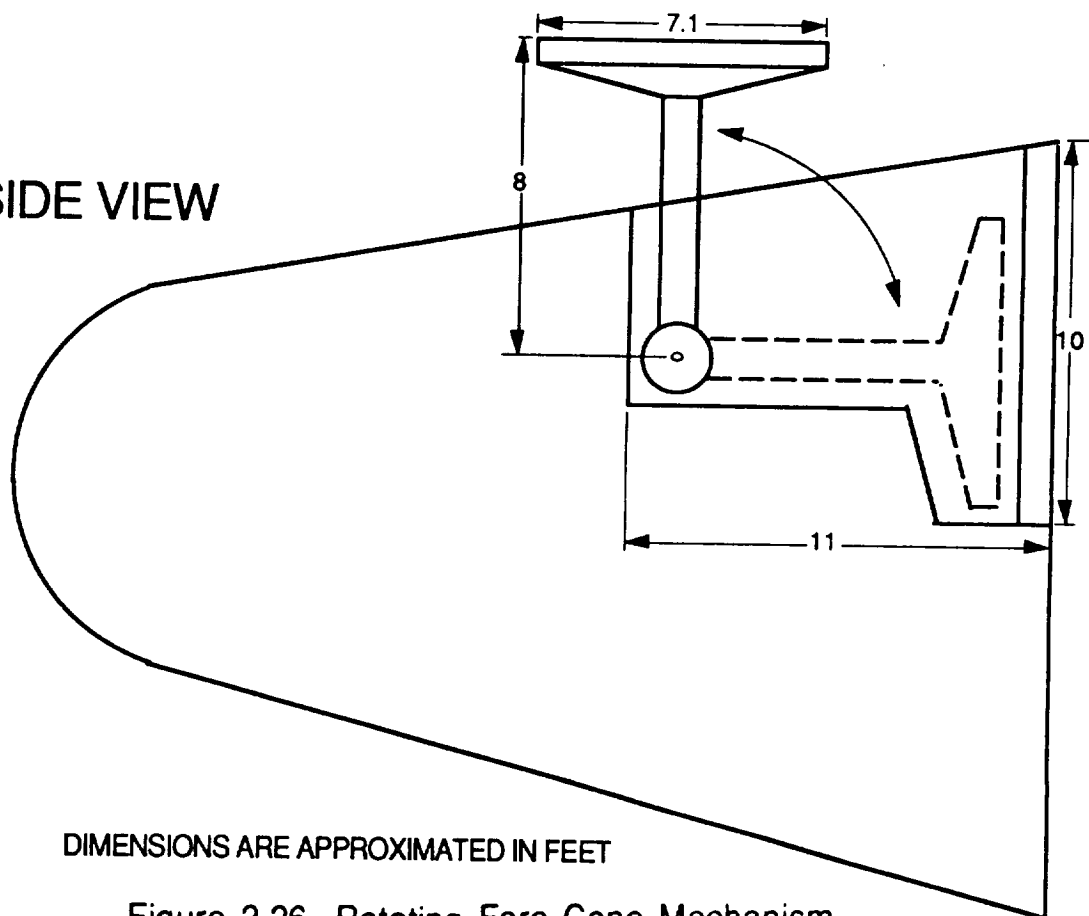
Figure 2.25 Vertical Docking - Top View

# ROTATING FORE CONE MECHANISM

TOP VIEW



SIDE VIEW



DIMENSIONS ARE APPROXIMATED IN FEET

Figure 2.26 Rotating Fore Cone Mechanism

If the docking mechanism was "straight" and had to be placed in the cargo bay, it would be required to extend at least eleven feet out of the bay to provide the necessary clearance. This would also increase the required stretch of the SSRMS to roughly 38 feet with a vertical dock. Docking horizontally with this method would require a reach of about 30 feet. Stability and physical support concerns may also arise because of the mechanism's length (approx. 27 ft., although over half that length would be supported by the cargo bay wall).

If a docking device could be designed compact enough, the fore cone would be an ideal location for placement. One of the concepts studied for placement in the fore cone employed a telescoping mechanism, hydraulically "lifting" the berthing assembly out of the CRV from its own bay. Unfortunately, this method occupied an excessively large volume since the 7.13 ft. diameter berthing mechanism had to be stored over five feet below the bay doors.

A second concept was relatively simple and compact, Figure 2.26. In this design, the mechanism stores sideways and rotates upward to its docking position; it could be made hydraulic or mechanical with great reliability because of its simplicity. Its volumetric requirements minimally displace existing components in the fore cone. Side and top views are shown in Figures 2.24 and 2.25.

Advantages to this system:

- Provides adequate clearance between cargo and docking node
- Positions cargo well within reach of SSRMS (23.4 ft., horiz. dock)
- Provides physical support

Disadvantages:

- Concern might arise about position of pressurized and propulsion tanks relative to SSF crew if horizontally docked.
- Requires its own "cargo doors"

The cargo doors will open, exposing the payload, when berthing to the station is complete. The on-board SPDS rotates the cargo out of the bay.

Cargo exchange will take place with the use of the MSS.(Figure 2.27) The SSRMS will extend and the latching end effector will attach to a compatible interface on the cargo. (It is unclear if the PLOG grapple mechanism is compatible with the latching end effector. Since the MSS is required to have the capability of moving logistics modules, it can probably be safely assumed that it is compatible.)

The SPDS-deployed cargo is detached, moved to the open LM port, and berthed adjacent to the existing logistics module. After the new module

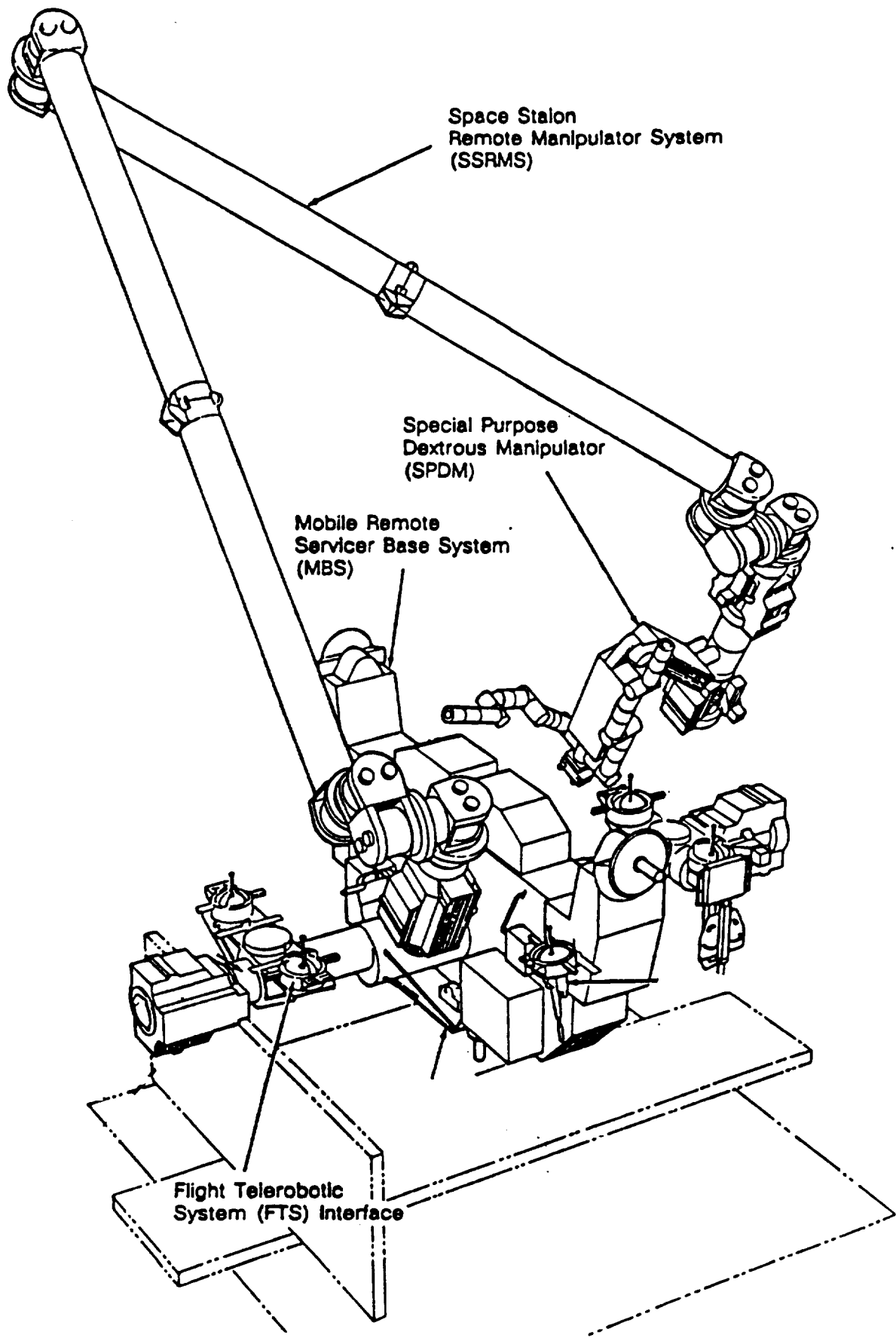
is attached and activated, the old LM is detached from the station and is re-berthed on the CRV's SPDS, which proceeds to secure it in the cargo bay. The CRV is docked to the station during these operations for approximately six hours, tapping the station's power through umbilical attachments in the docking mechanism. The vehicle separates and moves away from the station using its cold gas thrusters. (The baseline MSS capability of aiding in this maneuver is unclear).

In a reversal from its approach maneuvers, over a period of an orbit and one-half, the CRV moves to the edge of the CCZ where control is taken over by ground. The vehicle moves to its departure point where the deorbit maneuver takes place. The approximate mission time is roughly 10.6 hours for the nominal mission from the time it enters the CCZ to the time it leaves the CCZ.

In contingency operations, where the CRV cannot dock to the station, the vehicle remains outside of the CCZ throughout the entire mission, relying on the OMV (Fig. 2.28) with its GN2 cold gas thrusters and PM when away from station to make the cargo exchange. In this mission, the OMV is required to make two round trips to the CRV: the first trip retrieves the new module and attaches it to the SSF, the second brings the old module to the CRV where SPDS reattaches and secures the cargo. While inside the Command and Control Zone, it is controlled by the station crew; while in docking operations at the CRV, it is under control of the ground.

The OMV will use a Three Point Docking Mechanism (TPDM) to dock to the LM, but will require an adapter attachment for compatibility with the grapple mechanism on the logistics module. Use of the MSS to dock the module to the station will not be necessary, as the OMV is fully capable of maneuvering the cargo into position with the aid of its video cameras and visual contact from the SSF crew. While the OMV returns to the station, the CRV moves to its deorbit position.

To briefly summarize, in the nominal mission profile, the CRV approaches the station and docks under control by the SSF crew. The docking mechanism used is stowed in a compartment just ahead of the cargo bay and will rotate into position for docking. While docked, it taps the station for power and cargo exchange takes place with the use of the MSS. After securing the "new" cargo, the CRV detaches from the station, still under crew control and approaches the departure point where deorbit maneuvers occur. In the contingency mission profile, dual OMV trips and the use of a docking adapter are required while transporting the LM.



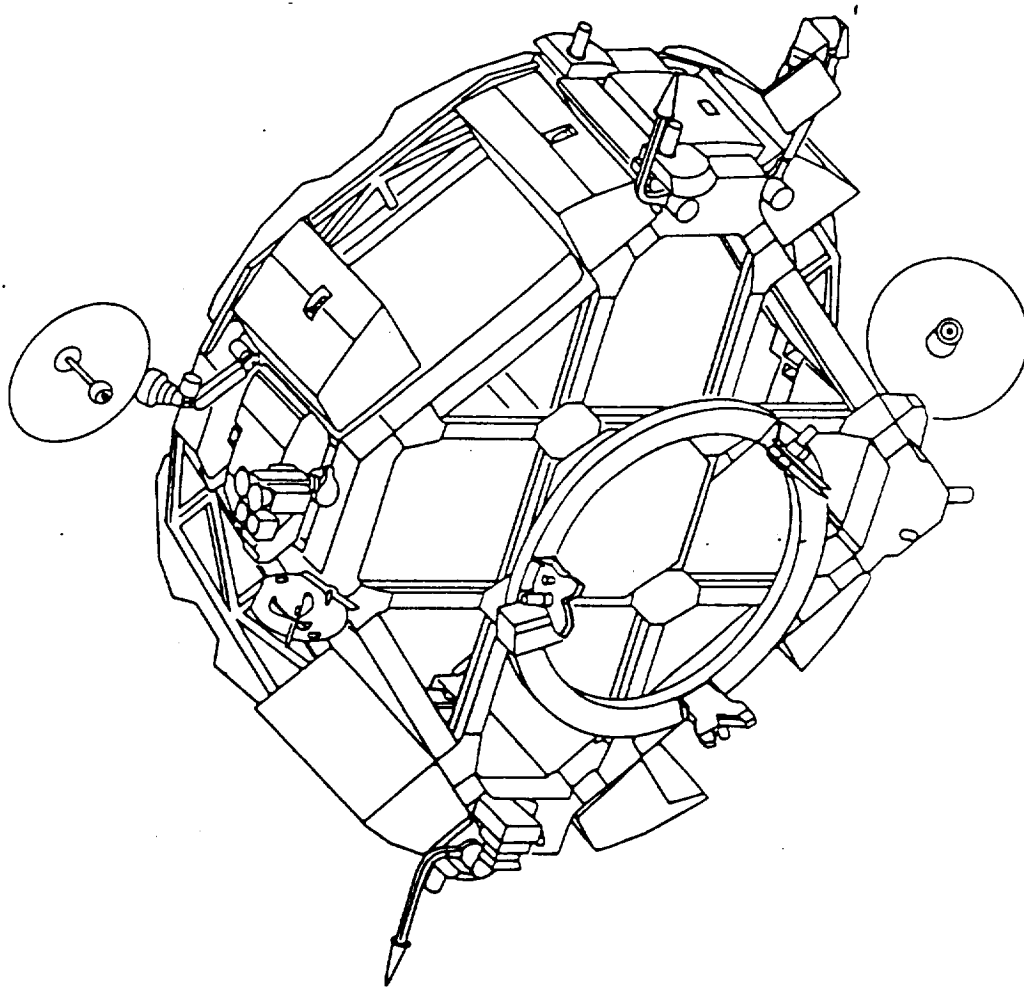
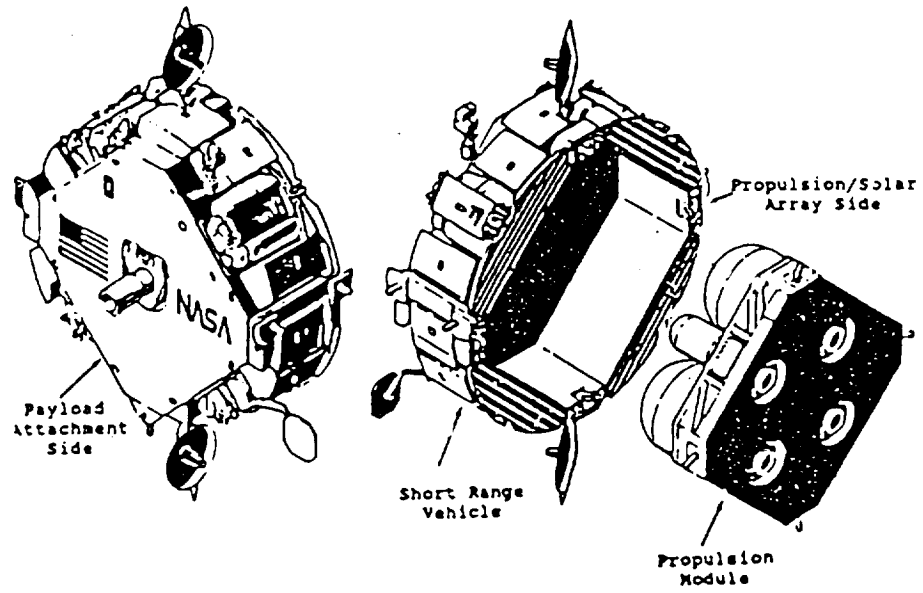
Space Station  
Remote Manipulator System  
(SSRMS)

Special Purpose  
Dexterous Manipulator  
(SPDM)

Mobile Remote  
Servicer Base System  
(MBS)

Flight Telerobotic  
System (FTS) Interface

Figure 2.27 Mobile Servicing Center



OMV with TPDM mounted on standoff structure

Figure 2.28 Orbital Maneuvering Vehicle

### 3.0 SYSTEMS LAYOUT

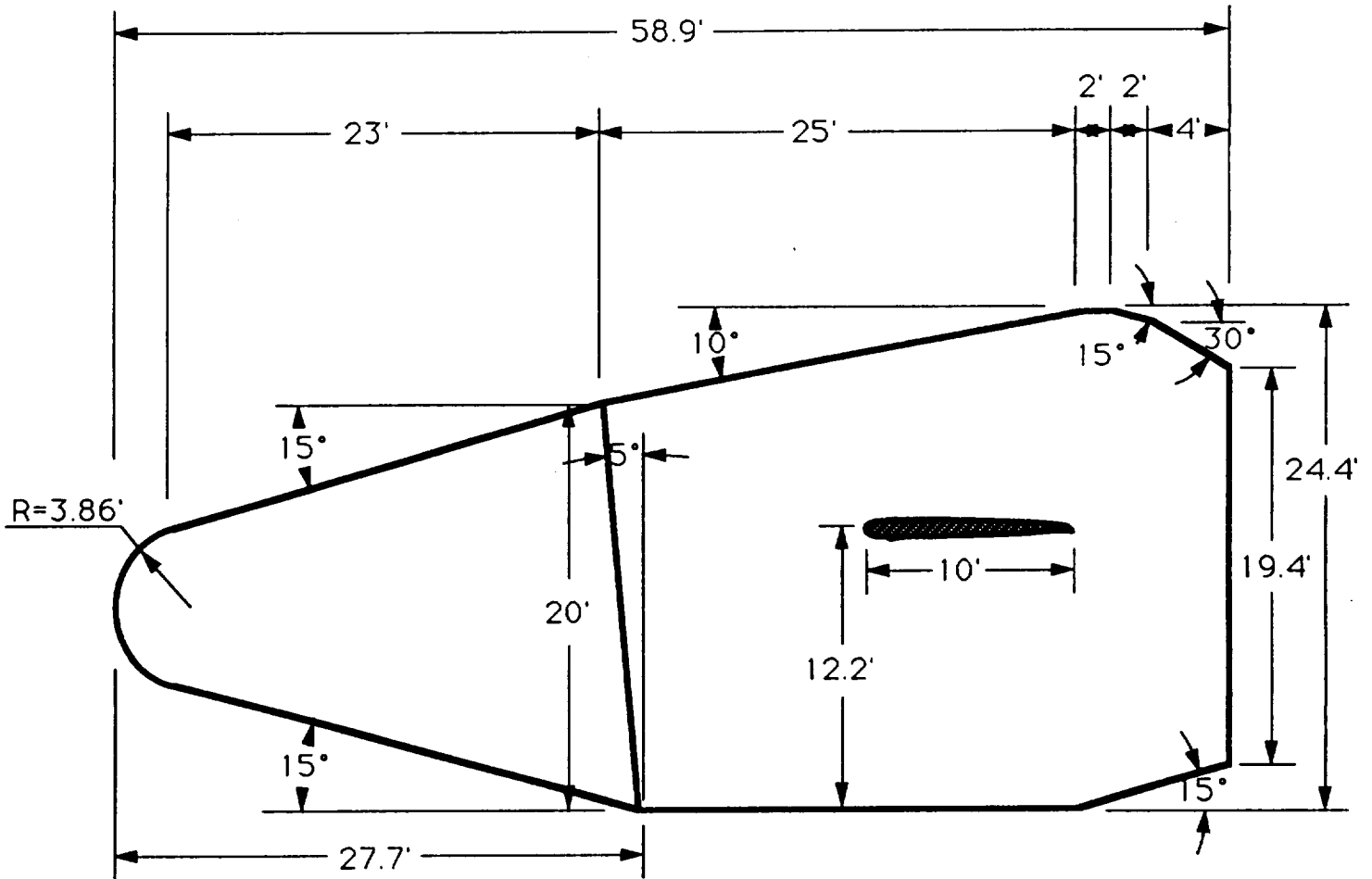
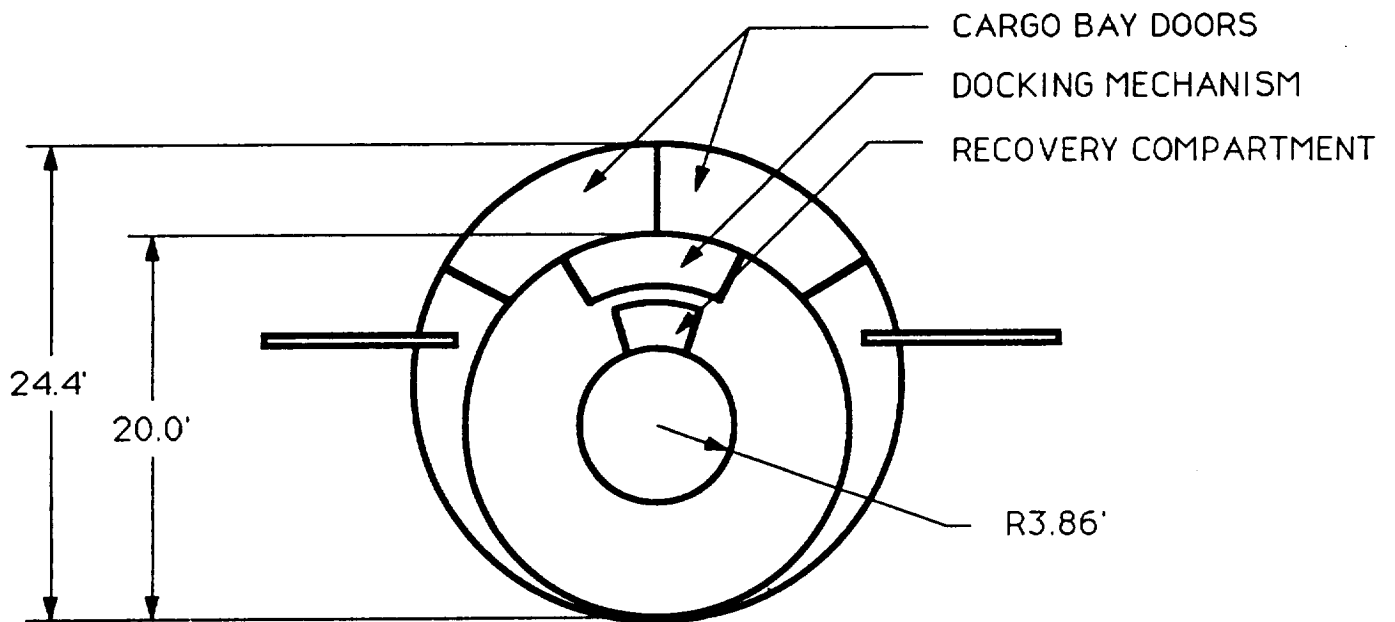
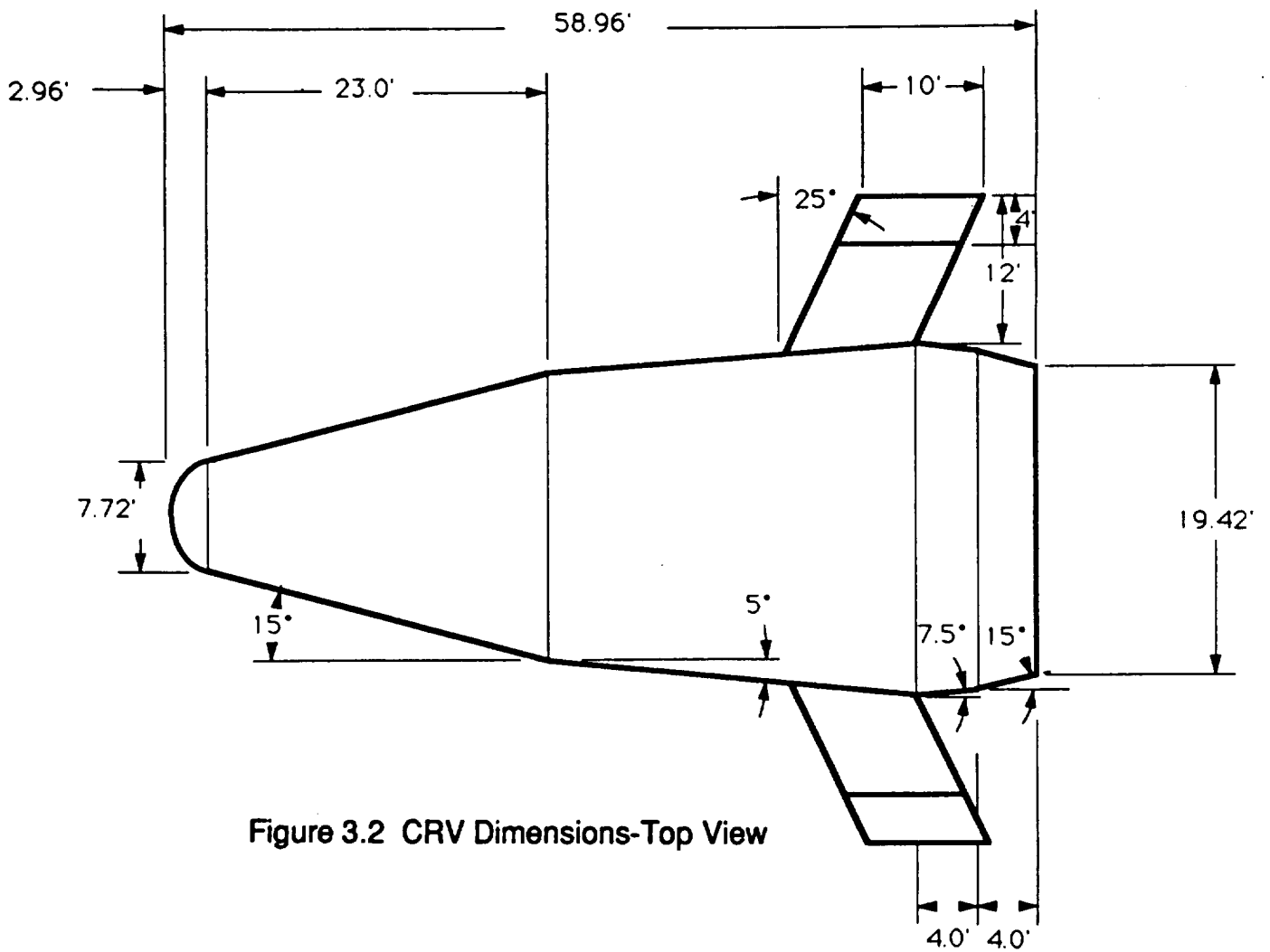


Figure 3.1 CRV Dimensions-Side View



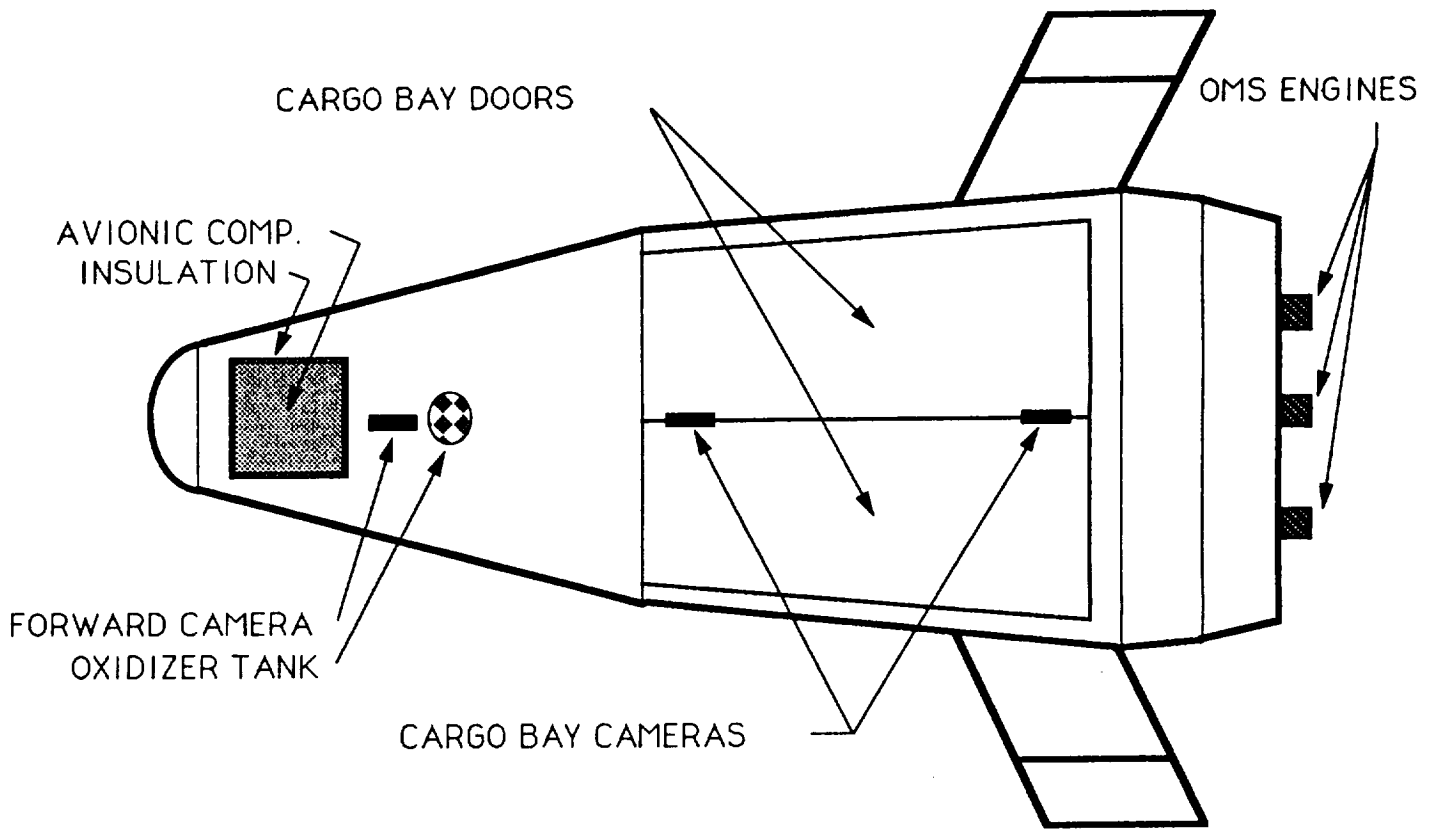


Figure 3.4 Systems Layout-Top View/Layer#1

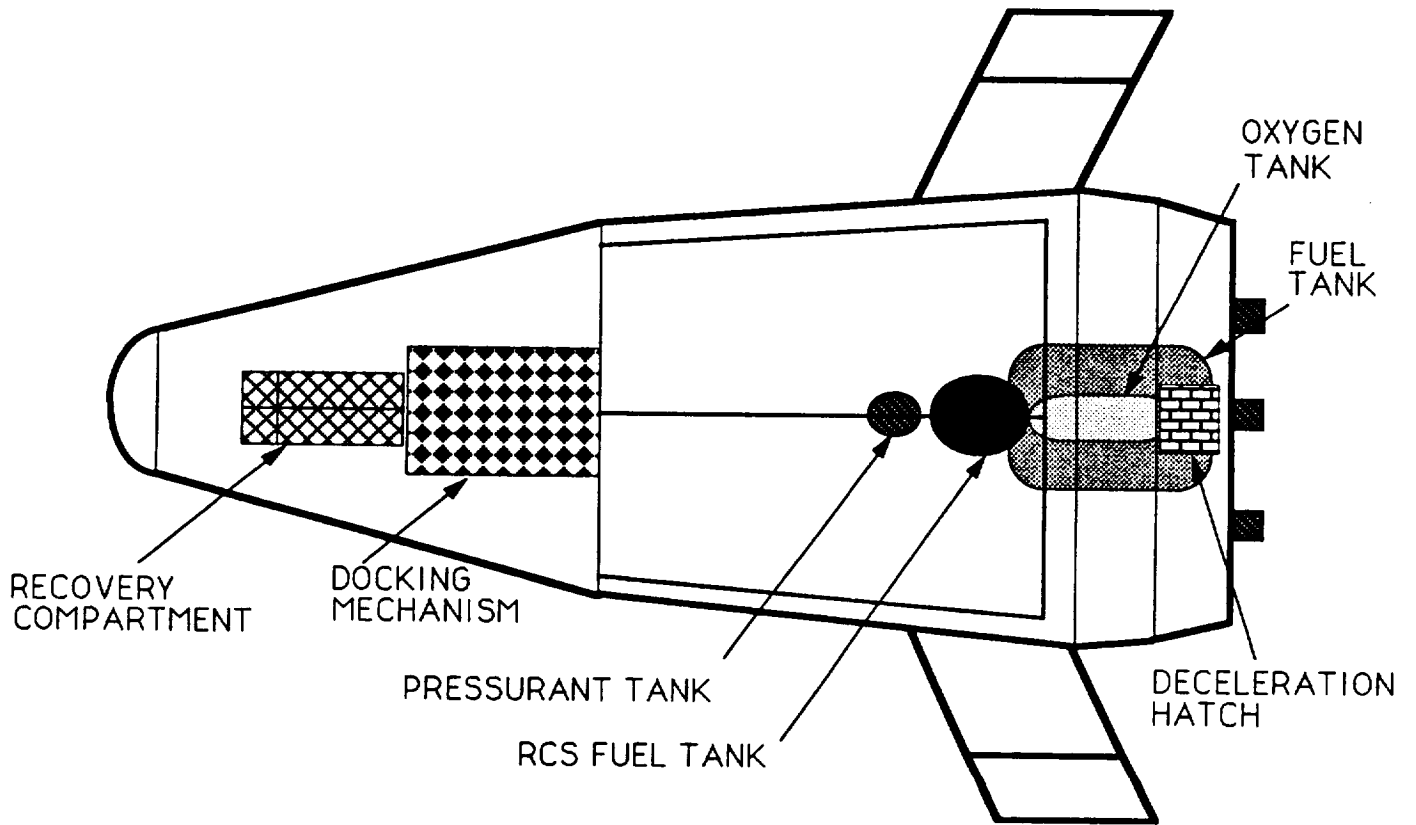


Figure 3.5 Systems Layout-Top View/Layer #2

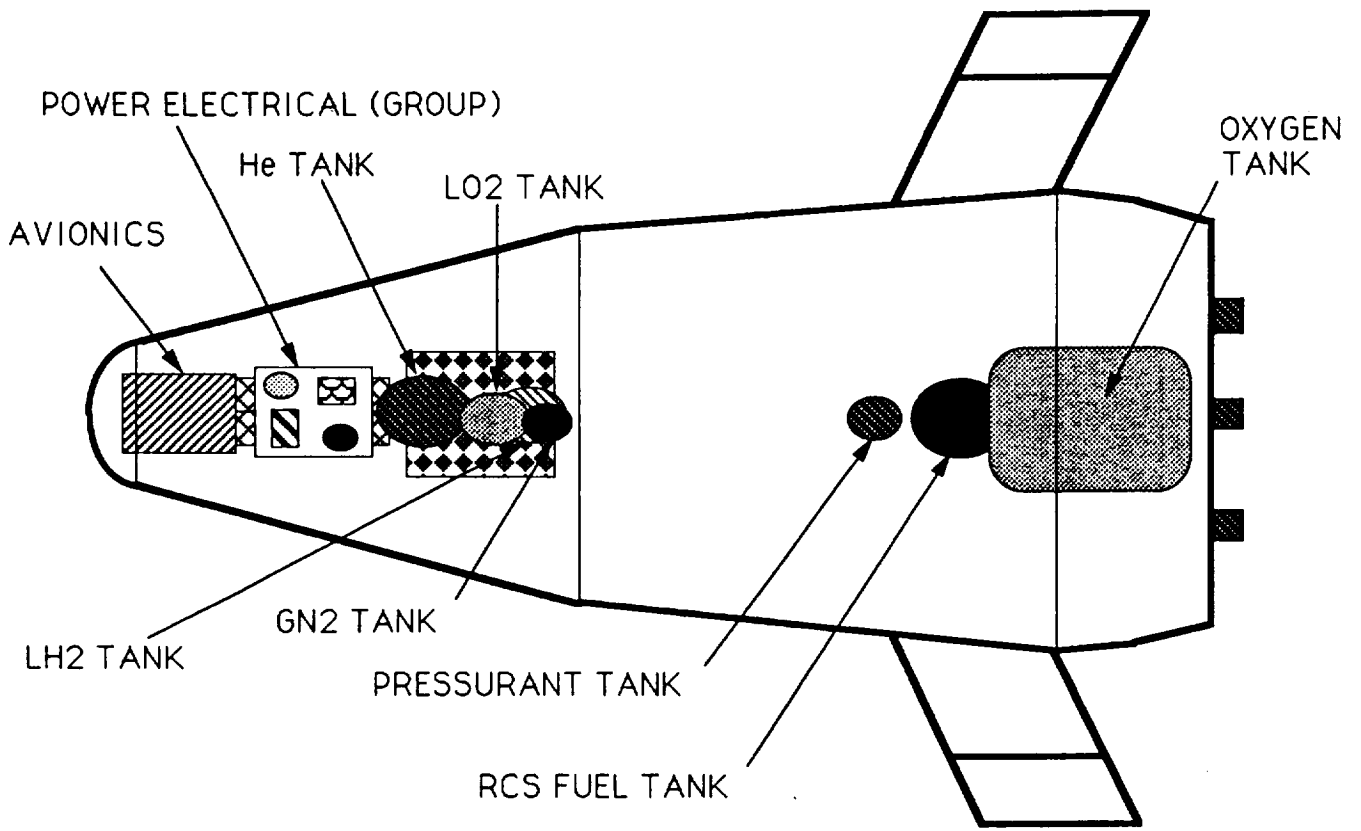


Figure 3.6 Systems Layout-Bottom View

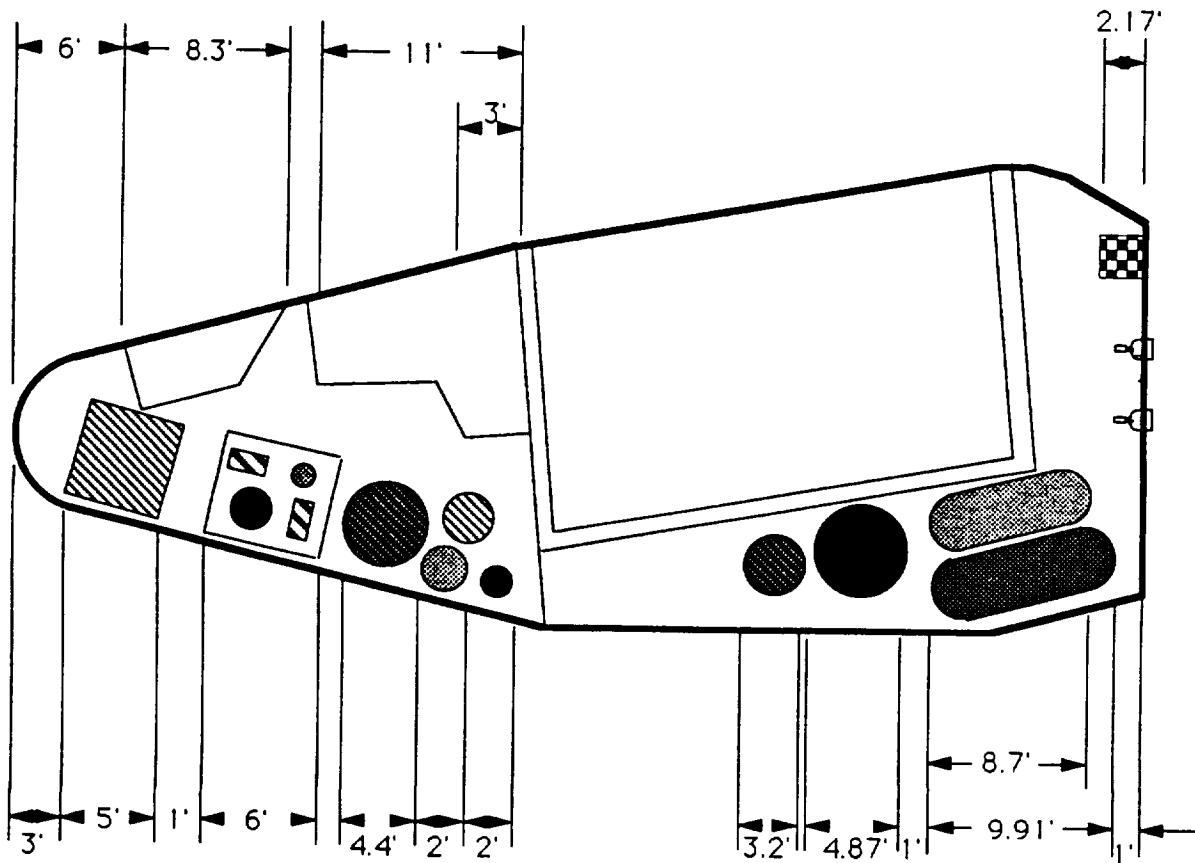


Figure 3.7 Systems Layout Dimensions-Side View

## 4.0 REENTRY AERODYNAMICS

### 4.1 Introduction

The reentry aerodynamic group was divided in two separate design groups: 1.) body configuration design and 2.) advanced recovery systems (ARS). Each group had separate goals and requirements to meet. The body configuration group had three objectives. The first objective was to find a method of predicting pressure distributions that agree well with wind tunnel data. The second objective was to redesign the baseline configuration such that a greater volumetric efficiency was achieved. And finally, the third objective was to complete a full aerodynamic analysis of the Cargo Return Vehicles final design. The ARS group was mainly concerned with examining different feasible recovery systems, and predicting their aerodynamic characteristics. Preliminary design proposals were concentrated specifically on the ram-air parafoil due to recommendations from the structures group, which will be explained in more detail in Section 10.0. A preliminary aerodynamic analysis was conducted to predict aerodynamic coefficients and performance.

### 4.2 Validation of Aero-Prediction Code

A baseline configuration, for the biconic cargo return vehicle (CRV), was derived from a aerobraking, aerocapture body intended to be used for planetary missions. The baseline design from ref. 1 was a  $12.84^\circ/7^\circ$  biconic configuration with a  $7^\circ$  bend of the axis (see Fig. 4.1), and all other dimensions were functions of the nose radius.

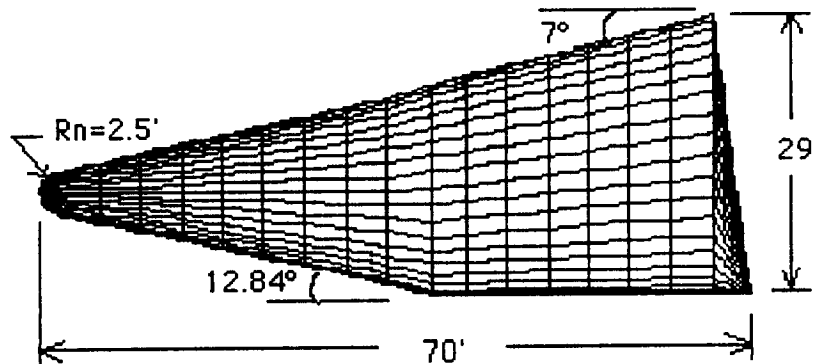


Figure 4.1: Baseline Configuration

The body was selected because there was substantial aerodynamic data available from wind tunnel tests. Although the body satisfied the aerodynamic requirements of the mission, the vehicle was volumetrically inefficient. Therefore, it was required that the body be modified in order to efficiently house all operating systems.

In designing the cargo return vehicle (CRV), it was important to understand how a single modification would effect the aerodynamic performance of the vehicle. The Supersonic/Hypersonic Arbitrary Body Program (HABP) was used to do the aerodynamic analysis of the bent biconic CRV. Reference (4.4) covers this program thoroughly. This particular aero-prediction code has several methods that can be used to calculate the pressure distributions around the vehicle. It was important to find the method that best agreed with actual wind data, and use that method to redesign the baseline configuration.

Three methods were chosen for the analysis of the baseline configuration: 1.) the Modified Newtonian Method (ref. 4.3), 2.) the Van Dyke Unified Method (ref. 4.2), and 3.) the Modified Newtonian and Prandtl/Meyer Method (ref. 4.2). The Modified Newtonian and Van Dyke Unified methods are suggested to be used for slender pointed bodies and the Prandtl/Meyer method is mainly used for blunt bodies.

In comparing the results from the three pressure methods with the wind tunnel data, it was found that all three methods exhibited little effect of mach number on aerodynamic characteristics. The Modified Newtonian and Van Dyke Unified methods gave good results for lift to drag ratios (L/D) with a maximum error of 15% and 5% respectively, where as the Prandtl/Meyer method gave a 30% error in maximum L/D and 20% error in the angle of attack that it occurred as shown in Fig. 4.2.

All methods gave good predictions of the pitching moment coefficient slope ( $Cm_a$ ), but all methods failed to predict accurate trim angle of attack (see Fig. 4.3). The Modified Newtonian and Prandtl/Meyer methods predicted values with 70% error and the Van Dyke Unified method with 100% error.

Of the three methods examined, the Modified Newtonian method was chosen as the method which agrees most favorably with the wind tunnel data. It predicts accurate values for L/D and gives the best

prediction for trim angles of attack. Another advantage of using this method is that aerodynamic characteristics are not effected by mach numbers greater than five (ref. 4.2). Some disadvantages in using this method are, there must be some error estimation in the trim angles of attack and values of  $C_{pmax}$  must be calculated for mach numbers lower than five.

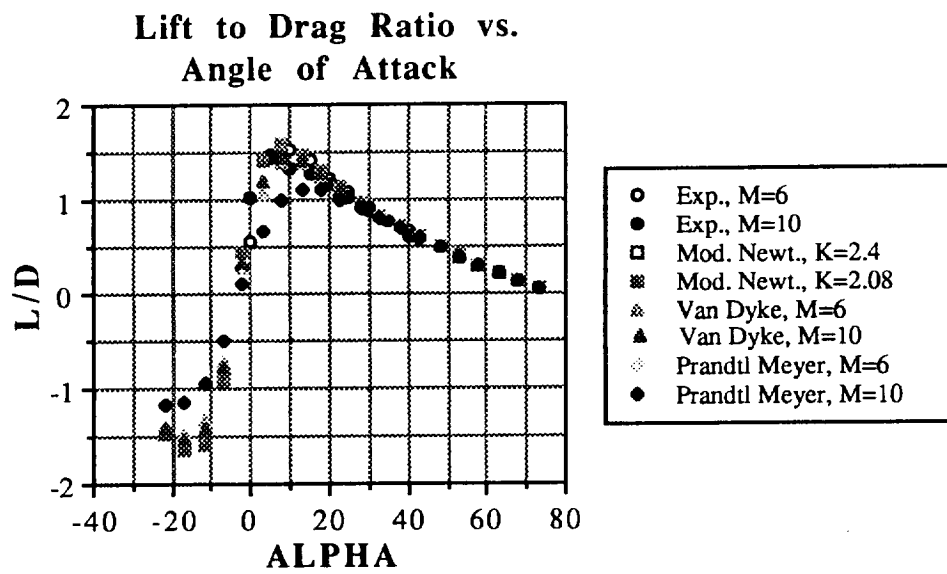


Figure 4.2 Lift to Drag Ratio of Baseline

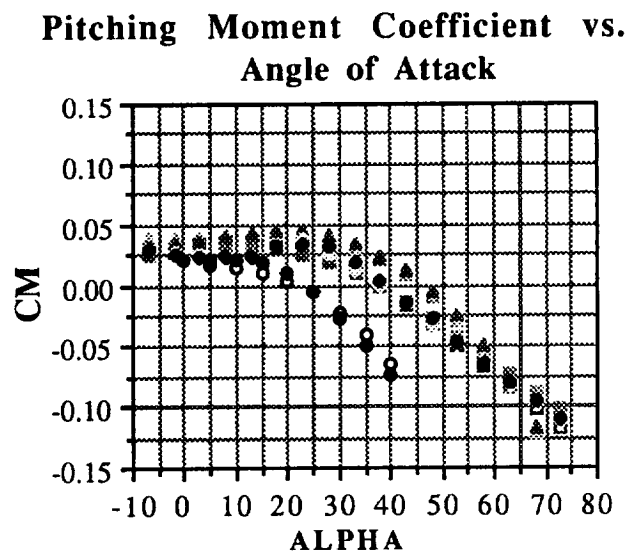


Figure 4.3 Pitching Moment Coefficient of Baseline

### 4.3 Body Optimization

The purpose of design optimization was to ensure optimal design for the entire mission. This included making changes to suit the mission requirements and to accommodate the requirements of other areas of the project. It was through this process that the final design was chosen.

The first modification of the baseline design was the implementation of a boat tail (see Fig. 4.4). This was done to increase performance of the vehicle, by reducing drag, in the subsonic range. However, it was not possible to analyze the effects of the boat tail in the subsonic regime, because of a lack of computational abilities. The boat tail will also provided increased ground clearance during the landing phase, in which a large angle of attack is required.

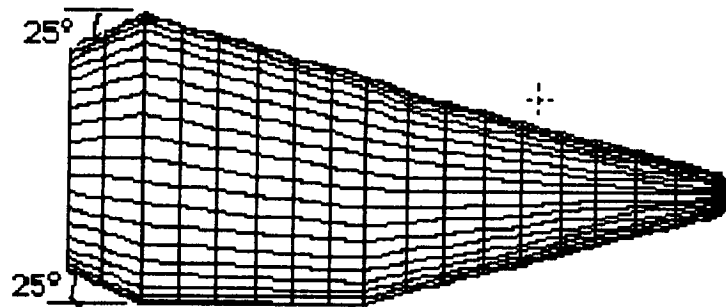


Figure 4.4 Baseline with 25° Boat Tail

The boat tail was found to slightly lower the maximum L/D from 1.6 to 1.5 of the baseline vehicle in the hypersonic regime at an angle of attack of 15°. The vehicle was also found to be unstable in pitch direction below 30° angle of attack, due to the reduced aft area.

The next modification was an increase in nose radius. There were two reasons for this: 1.) more compact vehicle and 2.) reduction of aeroheating. The boat tail was left off for the HABP run in order to understand the full effects of the blunt nose (see Fig. 4.5). The blunt nose decreased the L/D of the vehicle to a maximum 1.2, but did not effect the stability of the vehicle.

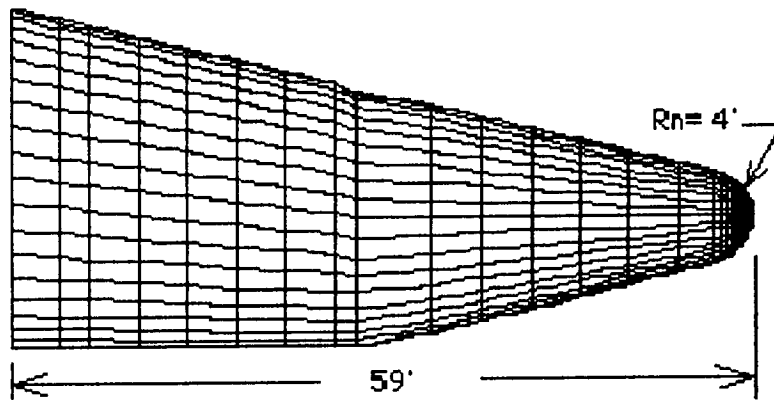


Figure 4.5 Shortened Baseline with 4' Nose Radius

The final design of the CRV was a culmination of geometry modifications due to performance requirements and the input of the other disciplines specifying various system requirements. The bend of the cones axis was reduced to five degrees, and the half cone angles of the fore and aft cones were now changed to  $15^\circ$  and  $5^\circ$  respectively (see Fig. 4.6).

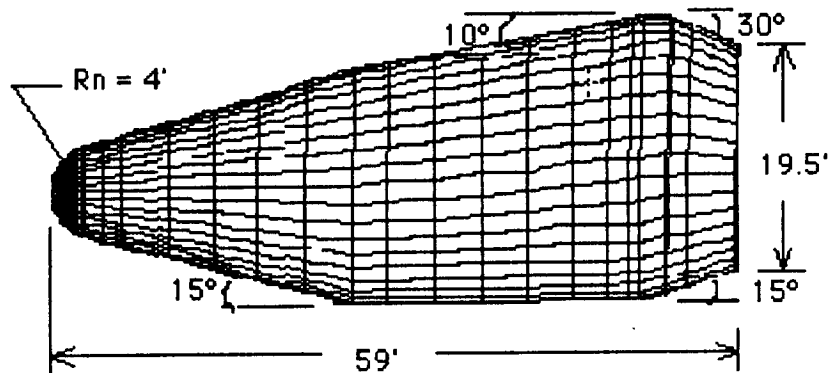


Figure 4.6 Final Body Configuration

This final configuration has a maximum L/D of 1.1 at  $20^\circ$  angle of attack, which fulfills mission requirements. However, it is very unstable in the pitch direction under an angle of attack of  $40^\circ$ . To remedy this problem, stabilizing fins have been added to the aft cone.

#### 4.4 Aerodynamics of Final Design

The aerodynamic analysis of the final design has been made for Mach numbers greater than five. This has been done because at about Mach five, a hypersonic decelerator will be deployed and will contribute significantly to the aerodynamic characteristics of the vehicle. Therefore, because the Modified Newtonian method will be used, the aerodynamic characteristics will not change. After running HABP for a value of correction factor  $K = 2.4$  the following results were obtained. The value for  $L/D_{max}$  was 1.1 and occurred at an angle of attack ( $\alpha$ ) of  $20^\circ$ . The vehicle could sustain an  $L/D > 0.8$ , which is the missions minimum requirement, for  $4^\circ < \alpha < 40^\circ$  (see Fig. 4.7). The  $C_{m_a}$  curve was found to be unstable for an  $\alpha < 40^\circ$  and trimmed at  $\alpha = 80^\circ$ . An error estimation was made for the HABP data, which consisted of taking the difference in the wind tunnel and HABP data, at each angle of attack, and dividing by the wind tunnel data at the same angle of attack. If the error estimated from the baseline configuration is taken into consideration, the vehicle could be stable for  $\alpha > 25^\circ$  and trim at  $\alpha = 60^\circ$  (see Fig. 4.8).

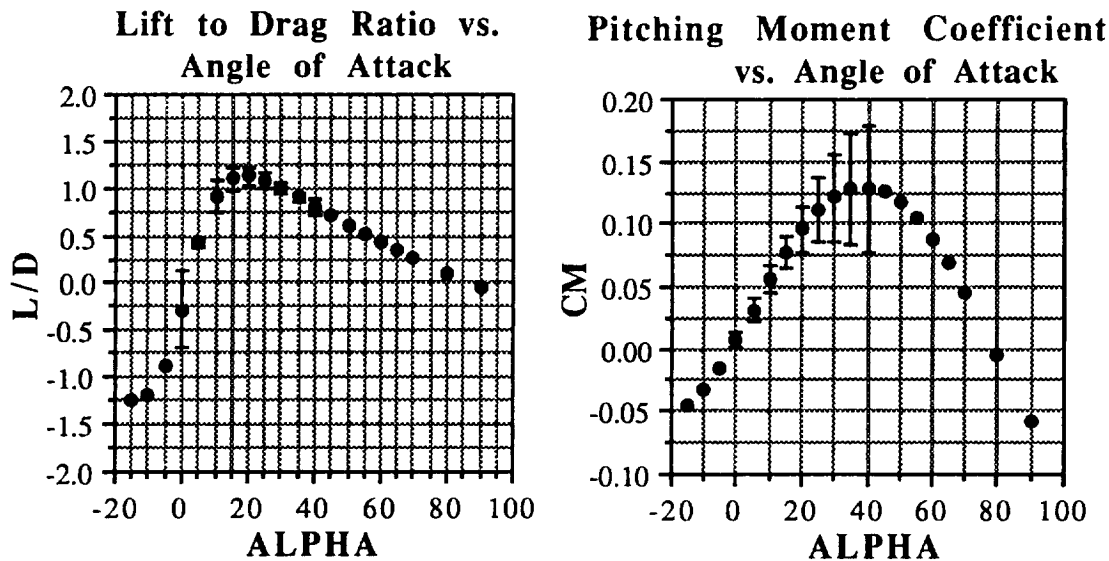


Figure 4.7 and 4.8  $L/D$  and  $C_{m_a}$  of Final Configuration

Because this configuration does not exhibit good longitudinal stability it was necessary to apply some sort of stabilizing fin. Therefore, a horizontal stabilizer was developed to resolve this problem. Figure 4.9 shows the final configuration with the new stabilizers.

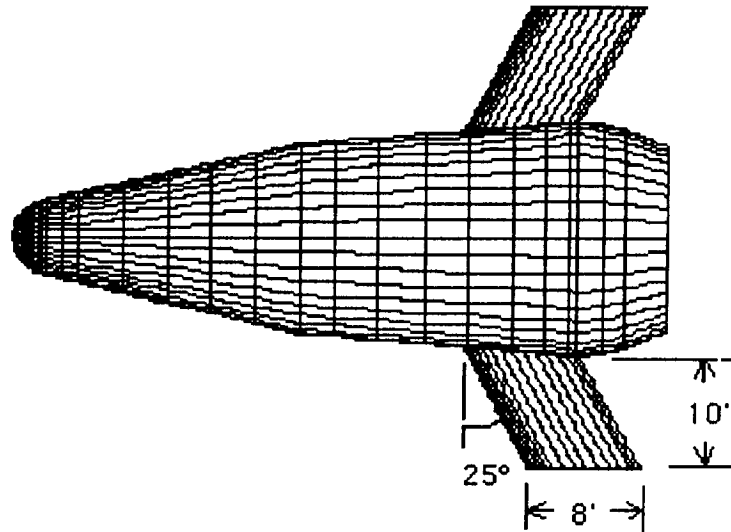


Figure 4.9 Final Configuration with 25° swept fins of Aspect Ratio of 1.25

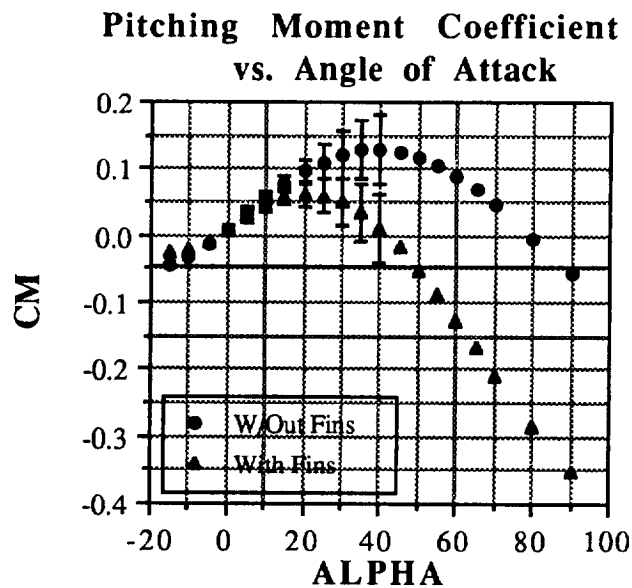


Figure 4.10 Effect of Stabilizing Fins on  $C_{m\alpha}$

The effect of the stabilizers on the  $C_{m\alpha}$  are shown in Figure 4.10. The trim alpha with zero deflection has been reduced to 42° and the vehicle is now stable for alpha > 15°. If the error estimations are taken into account, the trim angle of attack may be reduced to 35°. With the proper deflections the vehicle has been found to trim for 20° < alpha < 60°. A complete analysis of the effect of the

stabilizing fins on the aerodynamic characteristics is shown in Stability and Control section(5.0). It should be mentioned that the vehicle does exhibit lateral stability but is not directionally stable for yaw angles less than 30°. This characteristic is not uncommon for lifting bodies with no vertical tail. To correct this instability, HABP runs were made with the outer 1/3 of the horizontal fins deflected up at 90°. By doing this the  $C_{n\beta}$  curve had a slope of zero from angles of attack ranging from 0° to 5°.

In conclusion, the final CRV configuration can now more adequately fulfil the requirements of the proposed mission. The vehicle has been altered to have a greater volumetric efficiency which will give the required aerodynamic performance while efficiently housing all subsystems. The vehicle can achieve the minimum required L/D of 0.8 for  $4^\circ < \alpha < 40^\circ$ . The vehicle is stable in the pitch and roll modes, but experiences an instability in the yaw mode. The vehicle will employ deflectable wing tips as an additional control surface and a flight control system to combat this instability. Section 5.0 on Stability and Control will go into greater depth on the stability characteristics of the CRV.

#### **4.5 Drogue Decelerator**

In order for the Advanced Recovery System (ARS) to experience the required dynamic pressure of under 50 lb/ft<sup>2</sup>, at an altitude of 10,000 ft, it will be necessary to deploy a drogue decelerator.

##### **4.5.1 Requirements for the Drogue Decelerator**

The requirements for the drogue decelerator for the Biconic CRV were:

1. Decelerate the Biconic CRV so that its dynamic pressure at an altitude 10,000 ft was less than 50 lb/ft<sup>2</sup> (a velocity of under 238 ft/s).
2. Have G-loads of under 4.0g in the horizontal x-direction, the maximum allowed by the logistics modules.
3. Be effective during ARS deployment to stabilize the CRV if necessary.

#### 4.5.2 Drogue Decelerator Types

The possible decelerators available for use with the Biconic CRV were: conical ribbon parachute, hemispherical ribbon (hemisflow) parachute, glide surface parachute and a ballute. Table 4.1 shows the Mach ranges over which the decelerators are effective and their drag and opening force coefficients (the opening force coefficient is the ratio opening force over the steady state drag of the decelerator, (ref. 4.5).

<b>TYPE</b>	<b>MACH RANGE</b>	<b>C<sub>D</sub></b>	<b>C<sub>X</sub></b>
CONICAL RIBBON	0.1-2.0	0.50-0.55	1.05-1.30
HEMISPHERICAL RIBBON	1.0-3.0	0.30-0.46	1.00-1.30
GLIDE SURFACE	0.1-1.15	0.28-0.42	1.05
BALLUTE	0.8-4.0	0.51-1.20	1.20

Table 4.1 Decelerator Characteristics

The decelerator allows deceleration of the CRV through the transonic range. The conical ribbon parachute and the glide surface parachutes are effective during the conditions of ARS deployment ( $M = 0.22$ ). Of these two, the conical ribbon parachute was chosen because it had the higher drag coefficient of 0.50 - 0.55 compared to 0.28 - 0.42. The conical ribbon parachute did have a slightly higher open force coefficient of 1.05 - 1.30 compared to 1.05 for the glide surface parachute. The conical ribbon parachute does however decelerate the vehicle over a wide range of velocities providing a condition of small steady state drag.

### 4.5.3 Drogue Decelerator Design

Using the reentry and trajectory analysis program IMP, and the parachute trajectory program Trajectory Application, which was developed at the University of Minnesota, a drogue decelerator was designed.

DIAMETER, $D_c$	60 FT	
VENT DIAMETER, $D_v$	2 FT	
LINE LENGTH, $l_e$	60 FT	
NO. OF GORES	40	
COMPONENT	MATERIAL	WEIGHT (LBS)
HORIZONTAL RIBBONS	MIL-T-5608 E VI	181.21
SUSPENSION LINES	MIL-T-5608 E III	37.27
RADIAL TAPES	MIL-T-5608 E III	18.02
TOTAL		236.0

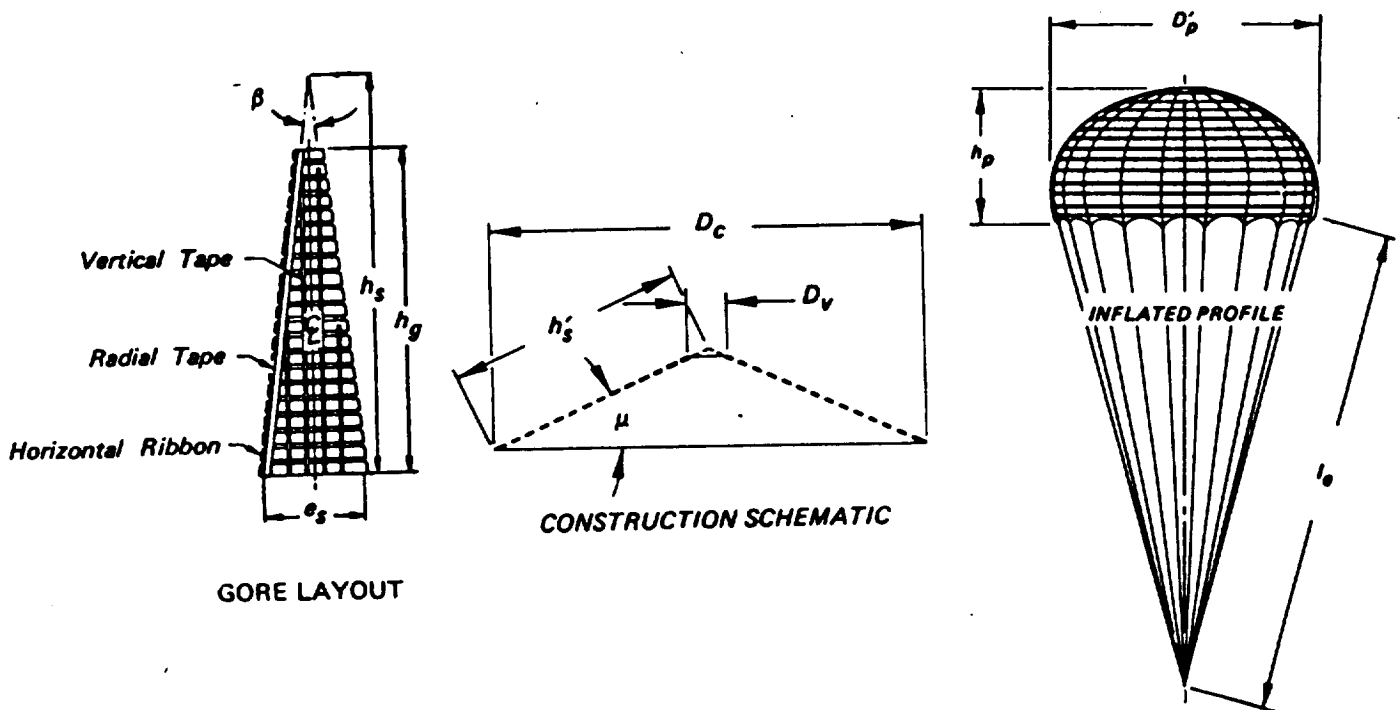


Figure 4.11 Construction of Drogue Parachute

The decelerator is a 60 ft diameter conical ribbon parachute reefed to a diameter of 30 ft would be deployed at 69,000 ft at a velocity of over 1300 ft/s. It would then be disreefed when the loading reached less than 1g. Figure 4.11, (ref. 4.5) shows the conical ribbon parachute and its dimensions, materials and combined weight for each component. The parachute has suspension lines of 60 ft in length and has 41 lines. Because the parachute has 40 gores the parachute is made up of 2 inch wide horizontal ribbons and has a vent diameter of 2 ft.

#### 4.5.4 Drogue Decelerator Performance

The performance of the drogue parachute is shown in the graphs in Figures 4.12 and 4.13 . Figure 4.12 is a graph of altitude vs. velocity, it shows that the velocity goes from over 1300 ft/s at 69,000 ft to a little over 200 ft/s at 10,000 ft. Figure 4.13 is a graph of altitude vs. dynamic pressure, it shows at deployment of the drogue parachute the dynamic pressure is over 160 lb/ft<sup>2</sup> but quickly subsides to under 50 lb/ft<sup>2</sup>.

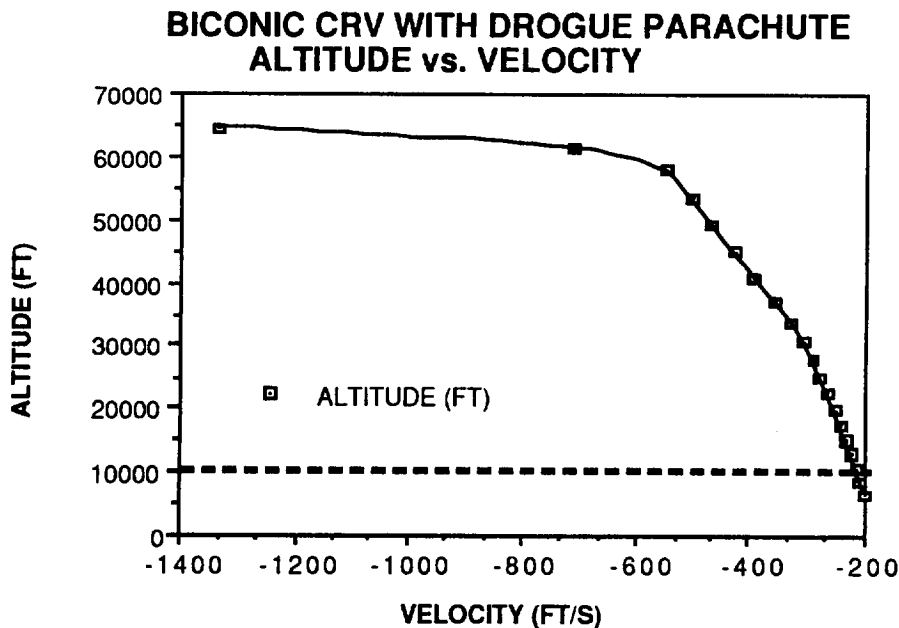


Figure 4.12 Altitude vs. Velocity CRV with Drogue Chute

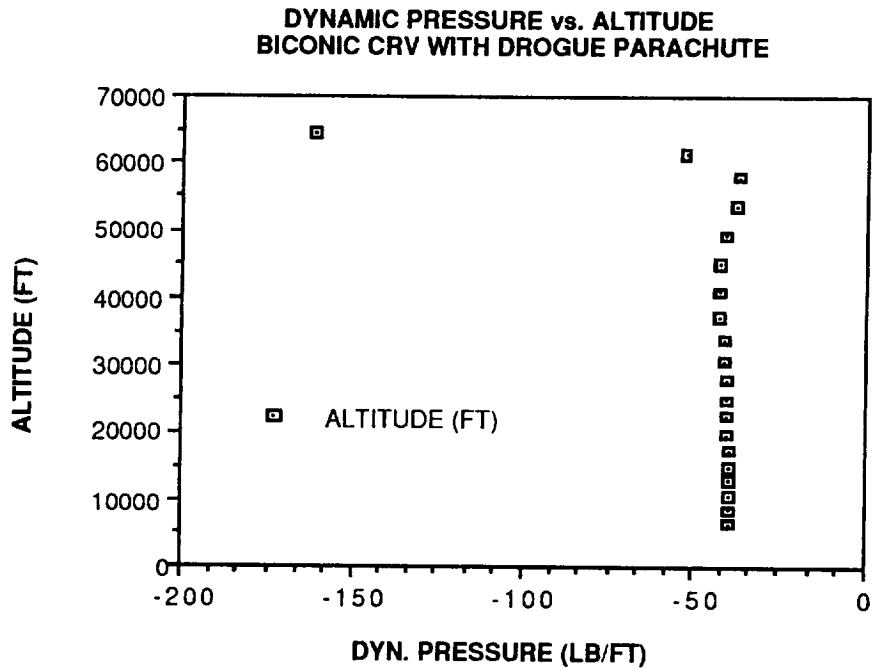


Figure 4.13 Dynamic Pressure vs. Altitude CRV with Drogue Chute

#### 4.5.5 Drogue Decelerator Deployment System

The drogue decelerator is located in a compartment in the rear of the vehicle above the engines with suspension lines that go around the engines to three attachment points. The drogue will need a deployment system to enter the air stream behind the CRV, the possible deployment systems are:

1. Pilot Chute.
2. Motar Deployment.
3. Rocket Extraction.

The pilot chute is a smaller chute that forces out the drogue parachute, the pilot chute would require its own deployment system which could be any of the three possible systems listed above.

The motar deployment system would eject the drogue parachute in its bag out into the air stream by an explosive charge. This system has the disadvantage of putting high loads on the structure.

The rocket extraction system would fire a rocket which would propel the drogue chute out into the air stream behind the vehicle. Rocket extraction has the disadvantage of needing a system to protect the parachute from the rocket exhaust.

The pilot chute system was originally planned as the deployment system, but analysis showed that the pilot chute would have to be 25 ft in diameter to create the deployment force of 1000 lbs to deploy the drogue, and it would need its own deployment system. So a drogue gun was chosen as the deployment system for the drogue parachute. It is similar to the mortar deployment, but instead of propelling the drogue parachute it would propel a slug which would be attached to the drogue parachute which would follow it into the air stream.

#### **4.6 Advanced Recovery Systems**

A trade study was conducted, which narrowed down the choice of an ARS to a rigid structure parawing and a ram-air parafoil (RAP). The rigid structure parawing was highly recommended due to its optimum aerodynamic characteristics and its range capabilities. However, during the preliminary design review, the structures group, which presents its data in Section 10.0, encountered various design difficulties in relation to the rigid structure parawing, the main conflict being between the storage compartment for the parawing and the placement of the cargo bay door. Not being able to find an acceptable compromise between the two, due to the fact that the only reasonable place to store the rigid structure parawing would be along the top of the CRV, and that the cargo bay doors could not be placed underneath the CRV because of aeroheating effects, the structures group recommended focusing all efforts on the design of a RAP as the ARS.

##### **4.6.1 Configuration**

The Ram-Air Parafoil (RAP), when inflated, resembles a low aspect ratio wing. It is entirely constructed from fabric with no rigid members, which allows it to be packed and deployed in a manner similar to a conventional parachute canopy. The wing has upper and lower membrane surfaces at a number of spanwise intervals forming a series of cells. The leading edge

of the wing is open over its entire length so that the ram air pressure maintains the wing shape. The ribs have apertures in them to allow the transmission of pressure from cell to cell during inflation, pressure equalization after inflation and helps prevent end cell tuck.

The basic configuration of the parafoil has a wing planform area of 22250 sq. ft. This wing area was originally designed for a total vehicle weight of 70000 lb, and hence to have a wing loading of 3.146 lb/sq.ft. However, recently the total weight of the CRV has increased by about 5000 lb, but this factor does not cause any major aerodynamic problems or instabilities. The parafoil has an equivalent wingspan of 250 ft and chord length of 89 ft, as shown in Figure 4.14. This is larger than any parafoil ever tested, and so the aerodynamic characteristics of the Ram-Air Parafoil which are presented in this report are only preliminary, and hence represent an approximation of the actual characteristics.

PARAFOIL CONFIGURATION

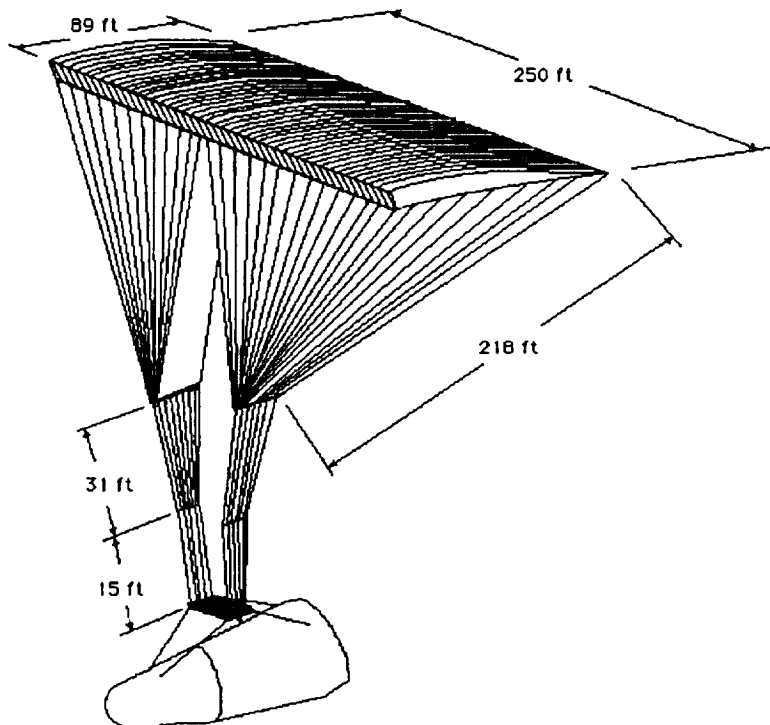


Figure 4.14 Parafoil Configuration

A modified Clarke-Y-17 airfoil section was chosen for the Ram-Air Parafoil. Although it is an inefficient airfoil, this type of section was the most widely used on early ram air parachutes and hence some data was available. The actual dimensions of the airfoil section are shown in Figure 4.15.

### CLARKE-Y-17 AIRFOIL

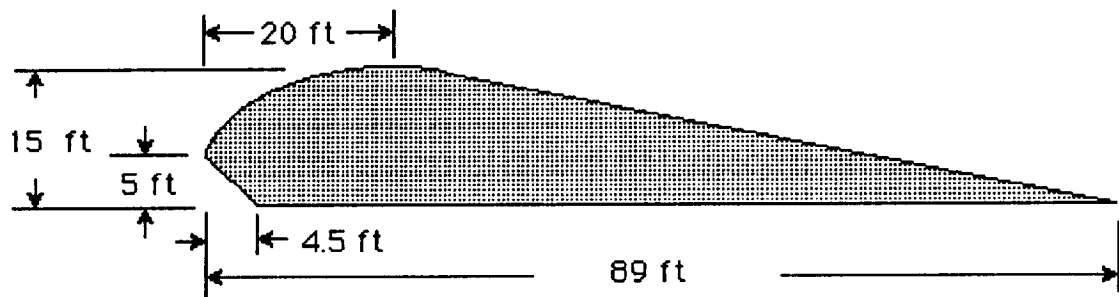
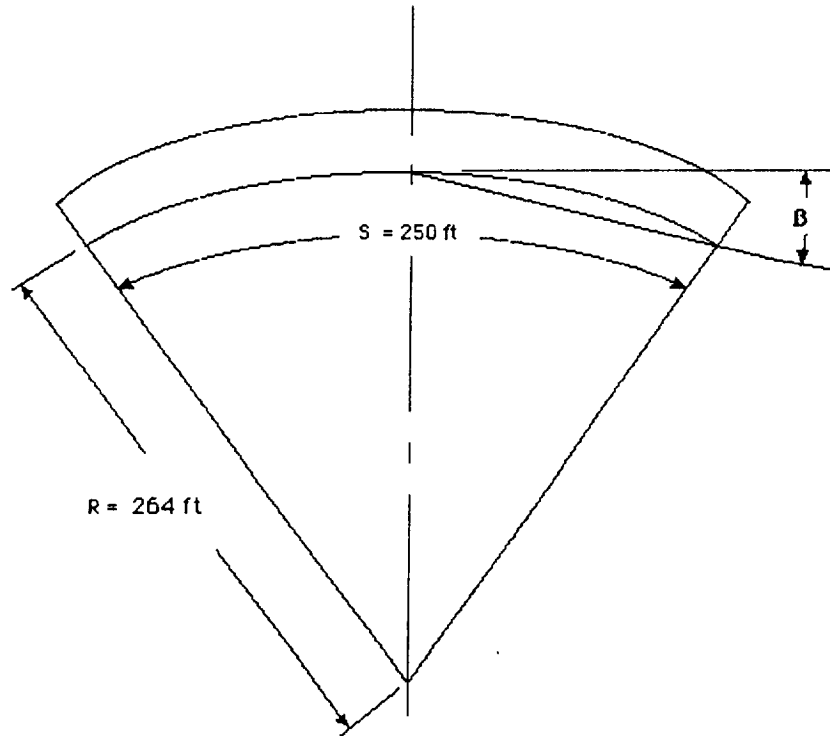


Figure 4.15 Clark-Y-17 Airfoil

The RAP is designed with arc anhedral so as to optimize the directional and lateral stability. Based on experimental data, the anhedral angle was chosen to be  $13.6^\circ$ , and the anhedral ratio designed at 1.06. The anhedral angle for the RAP is shown in Figure 4.16.



ANHEDRAL ANGLE  $\beta = 13.6^\circ$

ANHEDRAL RATIO  $R/S = 1.06$

Figure 4.16 Anhedral

#### 4.6.2 Deployment

The RAP is designed to be deployed and disreefed with 75% flap retraction. The flaps are actually the trailing edge of the parafoil, and they can be retracted to provide additional lift and drag or directional control, as shown in Figure 4.17. For more information on trailing edge deflection, see Section 5.0 on Stability and Control.

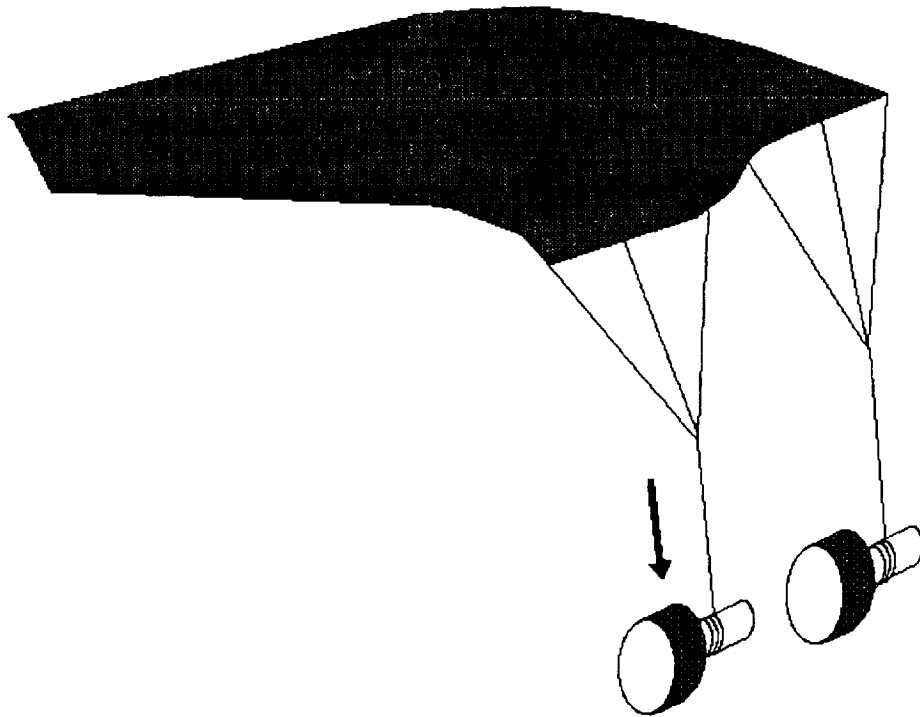


Figure 4.17 Trailing Edge Deflection

The flaps are retracted during deployment and disreefing to reduce the severity of "parafoil pitchover", caused by the sudden increase in lift. As the system decelerates, the individual cells start to fill with air, and the parafoil begins to assume its airfoil shape, creating lift. A component of the lift causes the parafoil to immediately pitch forward to seek the L/D of its current configuration. The flaps are retracted to 75 % to lessen the severity of this pitchover. When the system has stabilized following the final disreef, the flaps are gradually released, decreasing drag and increasing L/D.

The RAP is deployed at 10000 ft, because higher deployment altitudes offer no advantage due to the possibility of higher velocity winds.

#### 4.6.3 Reefing

Conventional reefing, constricting the mouth of the parachute, is not compatible with the geometry of the rectangular parafoil. The selected reefing technique, referred to as mid-span reefing, is illustrated in Figure 4.18. Mid-span reefing is accomplished by folding and stowing a number of cells two

places for each reefing stage. Stowed cells are laced between and completely contained by adjacent inflated cells. At the disreef command, pyrotechnic cutters sever the locking loops releasing the stowed cells and allowing them to inflate

The RAP will go through three main stages as it disreefs. The reefing ratios and resulting parafoil dimensions at each stage are given in Table 4.2. When the parafoil is originally deployed, the eleven center cells will be open, then for stage two, the five outer cells on both ends of the RAP will be disreefed. Finally, during the third stage, the remaining thirty cells will be disreefed.

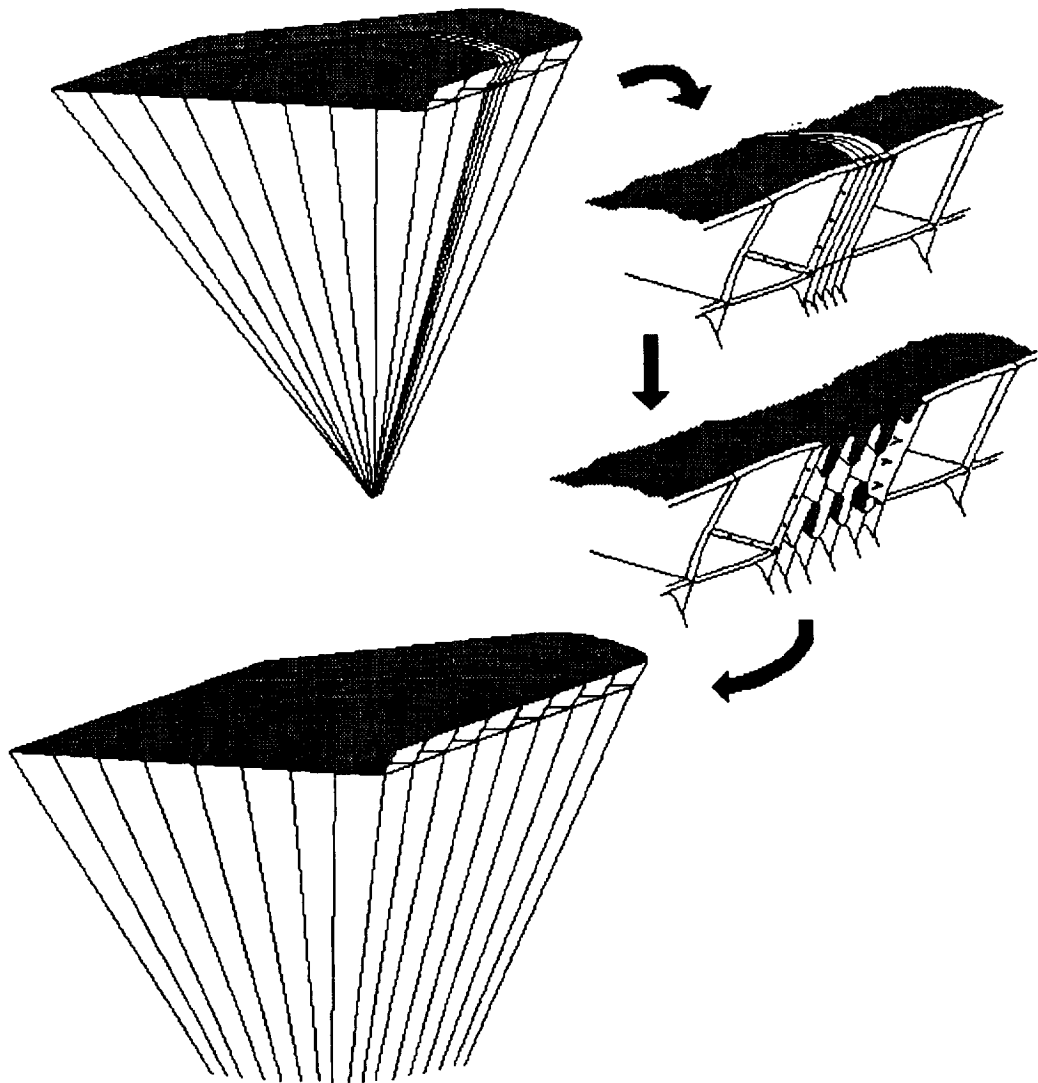


Figure 4.18 Parafoil Mid-Span Reefing

	Deployment Stages			Full Open
	1st	2nd	3rd	
Reefing Ratio %	22	20	100	-
Delta Area (ft <sup>2</sup> )	4799	4363	13088	-
Total Area (ft <sup>2</sup> )	4799	9162	22250	22250
Delta Span (ft)	53.9	49.0	147.1	-
Total Span (ft)	53.9	102.9	250	250
Chord (ft)	89	89	89	89
Aspect Ratio	0.6	1.2	2.8	2.8
Delta Cells	11	10	30	-
Total Cells	11	21	51	51

Table 4.2. Deployment and Reefing Data

#### 4.6.4 Aerodynamic Characteristics

The aerodynamic characteristics of the RAP were predicted by using experimental data from similar parafoils. One fact to bear in mind though, is that all RAPs that have been tested up to the present have been much smaller, and so the aerodynamic coefficients presented in this report should only be taken as preliminary figures that give a general idea of the aerodynamic performance of the RAP. The computer program "Parafoil 30.f" was used to calculate some of the aerodynamic characteristics of the RAP. This computer program is based on data obtained from wind tunnel tests and was obtained from NASA Marshall Space Flight Center.

Some of the aerodynamic characteristics that could be predicted are presented in Table 4.3.

$$\begin{aligned} \alpha (\text{trim}) &= 7^\circ \\ C_l &= 0.84 \\ C_d &= 0.22 \\ C_{m_\alpha} &= -0.005 \\ L/D &= 3.8 \end{aligned}$$

Table 4.3 Aerodynamic Characteristics

For alpha trim = 7° , L/D is a maximum = 3.8, and the coefficient of moment = -0.005 (i.e. stable). Note that the configuration is stable over a wide range of angle of attack (0<alpha<20°).

**4.6.5 Performance**

In order to get some preliminary performance characteristics, the computer program "Trajectory" was modified. The main trajectory points are listed in Table 4.4. The flare maneuver that is listed will be performed by taking advantage of the CRV's potential energy, as illustrated in Figure 4.19.

TRAJECTORY POINTS

EVENT	ELAPSED TIME (sec)	ALTITUDE (ft)	VELOCITY V ft/s	VELOCITY U ft/s
Deploy Parafoil	0.0	10000	239	0
Disreef, 2nd Stage	7.5	9500	104	90
Disreef, 3rd Stage	22.5	8250	83	85
Flap Release	44.0	7060	66	70
Full Glide	50.0	6500	40	90
Flare Maneuver	212.5	60	25	75
Touchdown	216.5	0	8	30

Table 4.4 Trajectory Points

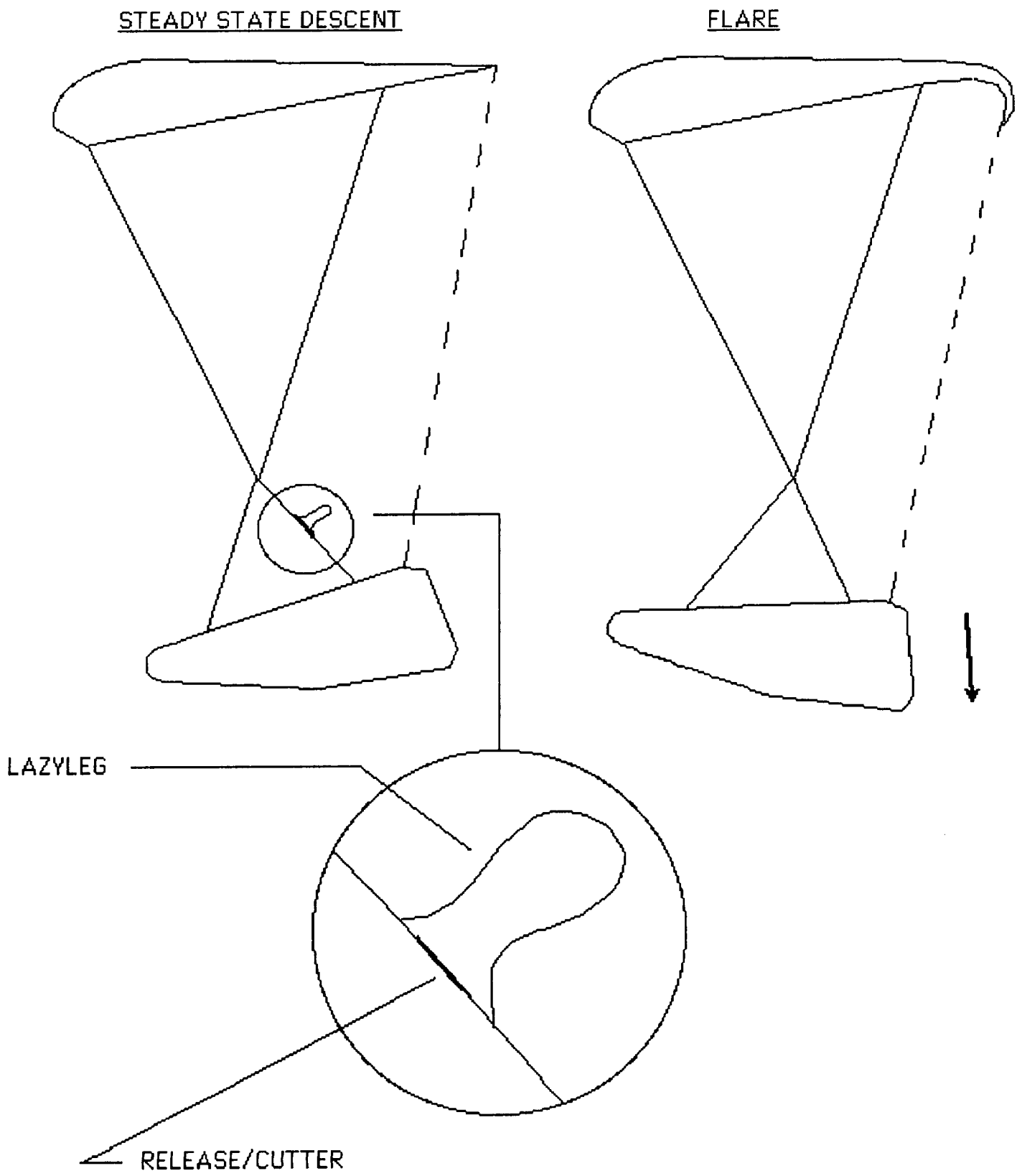


Figure 4.19 Flare

The loads during deployment were calculated by modifying a computer program called "Trajectory Analysis". This program was obtained from the University of Minnesota, and is designed to simulate the trajectory of conventional circular parachutes. The approximate results are graphed in Figure 4.20.

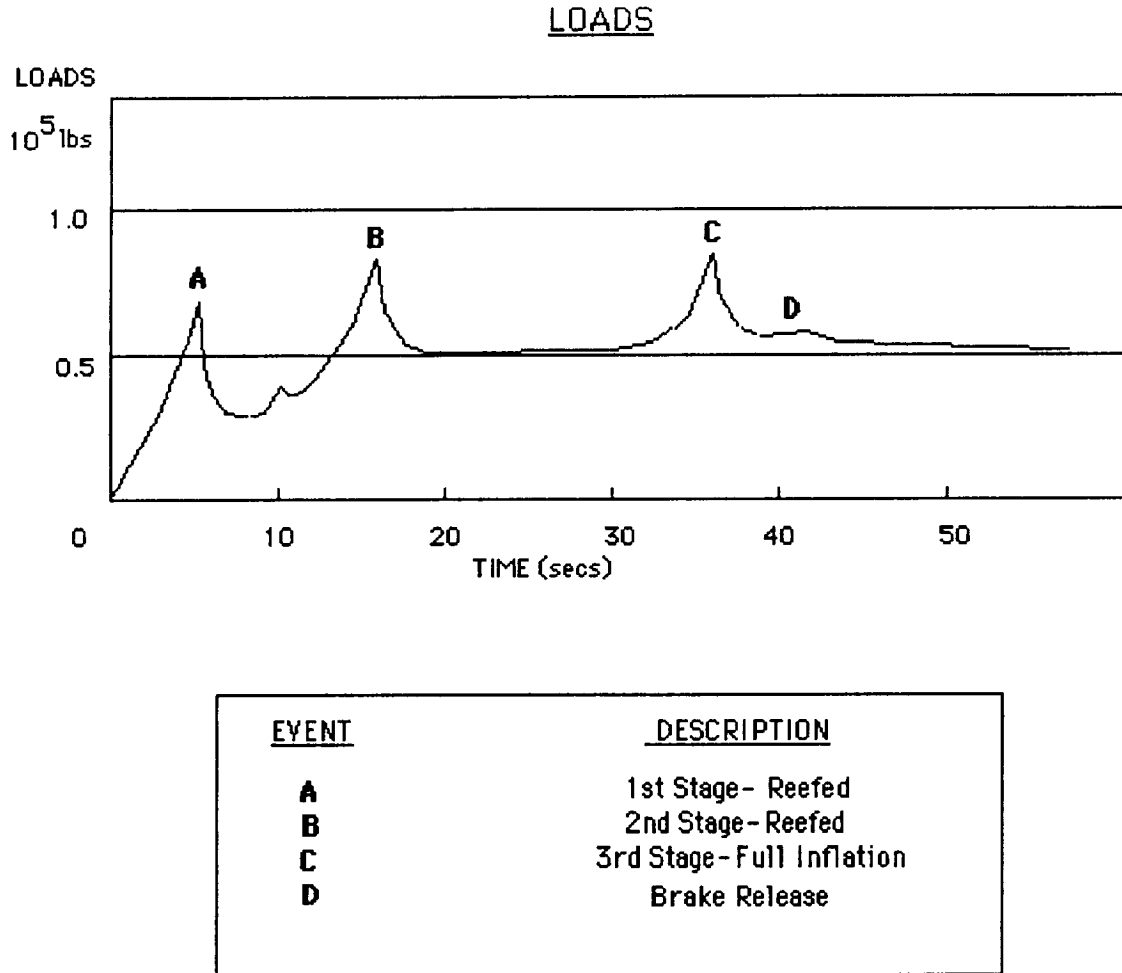


Figure 4.20 Loads

The range of the Ram-Air Parafoil for three different wind conditions are presented in Figure 4.21.

## RANGE OF PARAFOIL

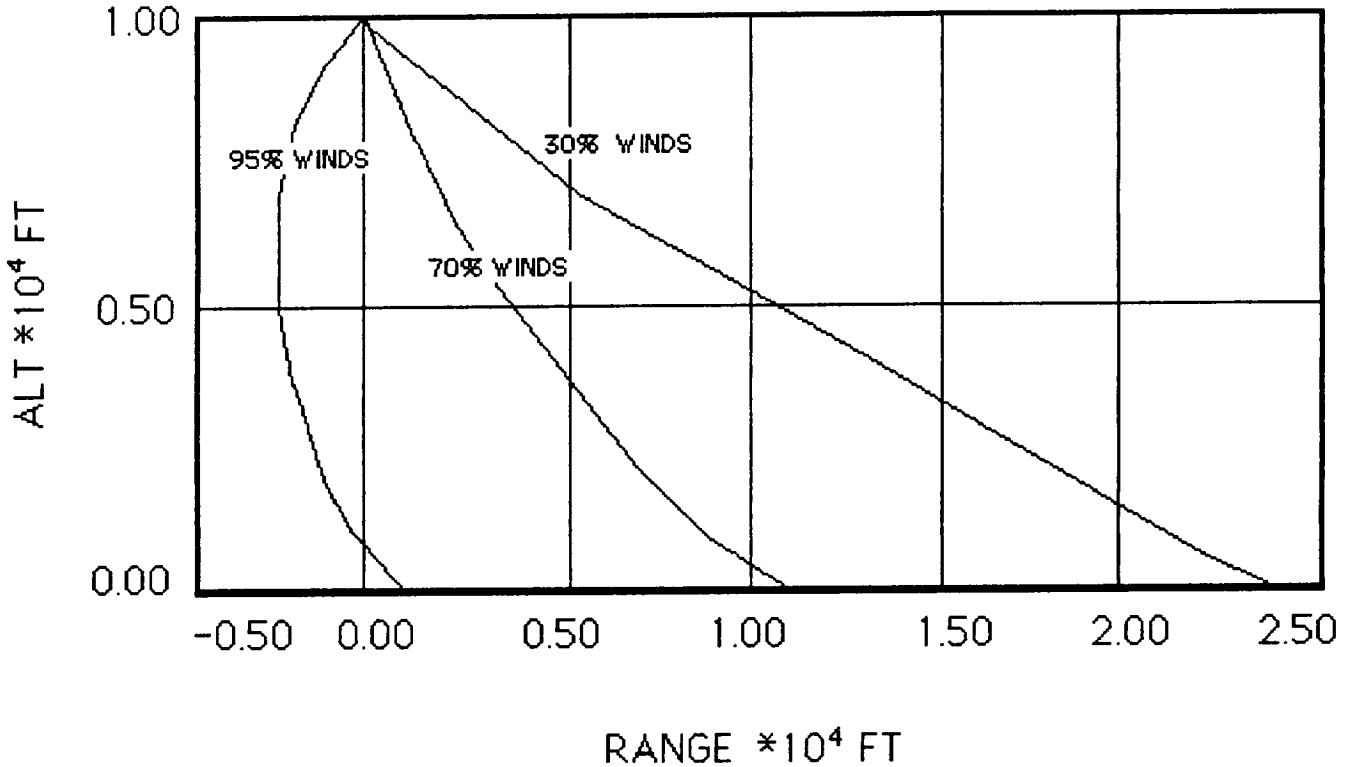


Figure 4.21 Range of Parafoil

The aerodynamic and performance characteristics that are presented in this report are preliminary figures and are based on scaled-up relationships and data. Future wind tunnel tests that will be conducted, will be of vital importance in obtaining a more accurate aerodynamic analysis of the Ram-Air Parafoil.

## **5.0 STABILITY AND CONTROL**

---

### **5.1 Introduction**

The Biconic Stability and Control discipline had three main topics to analyze. The mass distribution analysis, the stability and control analysis of the vehicle, and the Advanced Recovery System (ARS).

The mass distribution analysis consisted of finding the center of gravity (CG) of the vehicle, the percent location of the CG with respect to the total length of the vehicle, and the moments of inertia of the vehicle about all three axis.

The stability and control analysis consisted of determining the static and dynamic stability of the Cargo Return Vehicle (CRV), designing control surfaces to be used upon reentry, and analyzing a orbit control system.

The ARS analysis explored the Ram-air control methods, the deceleration of drogue parachute, and the control and stability characteristics of these devices.

### **5.2 Biconic CRV Control**

The biconic CRV will utilize control surfaces in order to stabilize and control the CRV during its mission. These surfaces will be used only during the time period from reentry until the time the Advanced Recovery System is deployed.

#### **5.2.1 Horizontal Fins**

The two main requirements for the control surfaces are that they must control the pitch of the vehicle and also stabilize the vehicle. Many unique control surface designs were considered to meet these requirements. The most effective design was the horizontal fin configuration shown in Figures 5.1 and 5.2. The horizontal fin control surface design is a simple, yet effective design. The drawings show the two different phases of the horizontal fin. The first phase (Figure 5.1) is the position of the fin for the entire flight of the CRV

except for the time period between reentry and ARS deployment. During this period, the outer third of the fins are turned up (Figure 5.2) and used as rudders to control the vehicle in the yaw direction. This control surface design was chosen because it allowed good pitch control, yaw control, stabilized the vehicle, and did not interfere with other elements of the CRV (ie cargo bay doors). The entire surface of the horizontal fins will be able to deflect a positive or negative 30 degrees. The rear one third of the turned up portion (rudder) of the horizontal fins will also be able to deflect a positive or negative 30 degrees. The fins are very large in order to adequately control the CRV. The dimensions of the fins are shown in Figure 5.3 and 5.4.

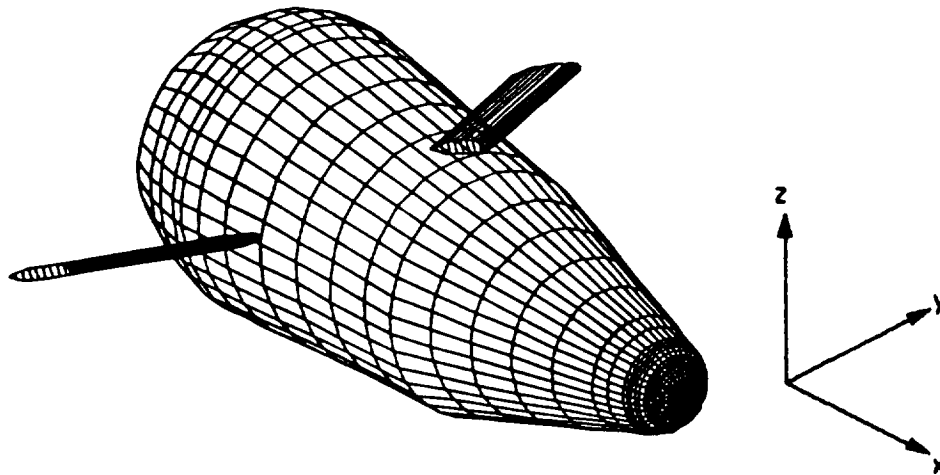


Figure 5.1 - Horizontal Fin

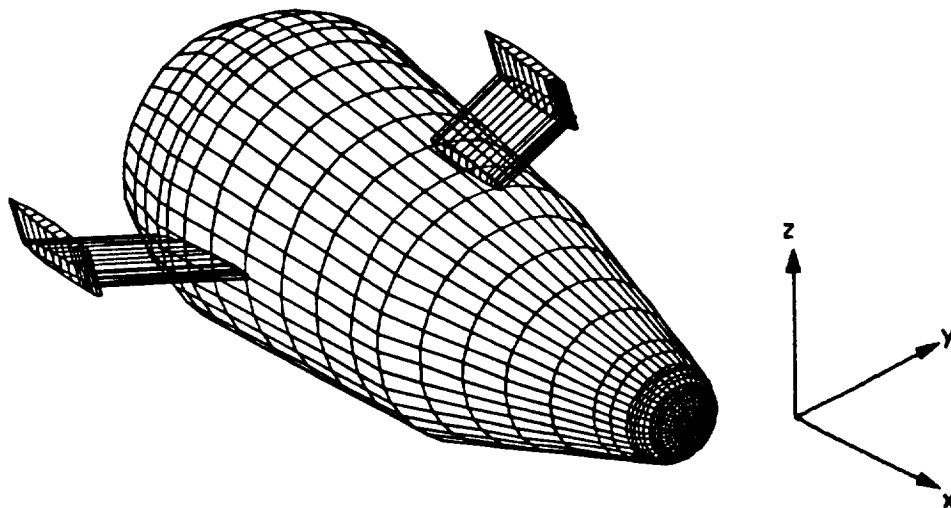


Figure 5.2 - Fin with Rudders Deployed

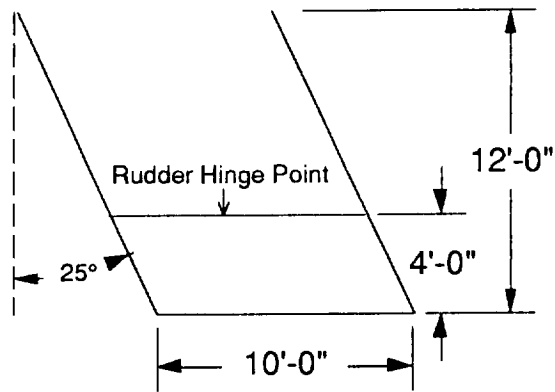


Figure 5.3 - Fin Planform

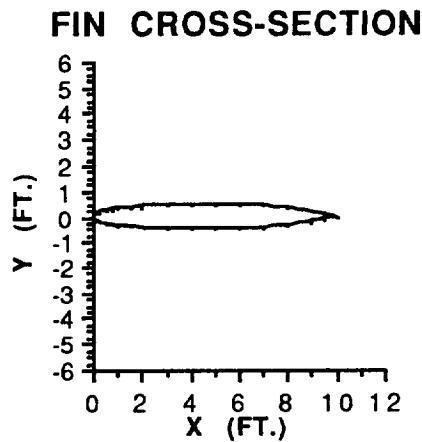


Figure 5.4 NACA 0505

These horizontal fins are very effective in controlling the pitch of the biconic CRV. The CRV can be trimmed at any angle of attack greater than -4 degrees. This is shown in Figure 5.5 for fin deflection of -30 degrees to 30 degrees.

The fins also provide the roll and yaw control needed. This is done by either deflecting one fin up and the other fin down, using the turned up "rudders", or a combination of the two methods.

### 5.2.2 RCS system

The RCS jet subsystem will be used to control the CRV during orbit. The system will be able to control the pitch, yaw, and roll of the vehicle. A complete layout and description of the

RCS subsystem can be found in the Propulsion section 8.0 of this report.

### Elevator Deflection Vs. Trim Angle of Attack

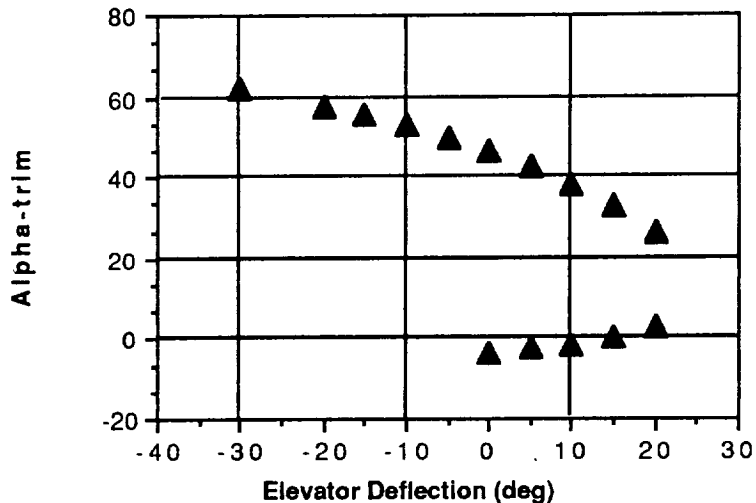


Figure 5.5

## 5.3 Stability Characteristics of the CRV

The stability of the biconic CRV involves both static and dynamic stability. The vehicle is not completely statically or dynamically stable over all possible flight conditions. This does not create a problem. Since there will be no pilot on the CRV, an automatic flight control system will have to be used. The automatic flight control system allows the vehicle to be under control during the periods while it is in an unstable region. This system will utilize sensors, actuators (horizontal fins), compensators, and the dynamics of the CRV to control itself. Details of how and why an automatic flight control system is used can be found in section 5.3.4, Automatic Flight Control System.

### **5.3.1 Static Stability**

The biconic CRV is not completely statically stable. The CRV is stable for all angles of attack greater than 15 degrees. This

is shown in Figure 5.6. For a vehicle to be statically stable, the slope of the  $C_m$  versus  $\alpha$  curve must be negative. This occurs for any  $\alpha$  greater than 15 degrees. The trim angle of attack is also shown in this figure to be 25 degrees.

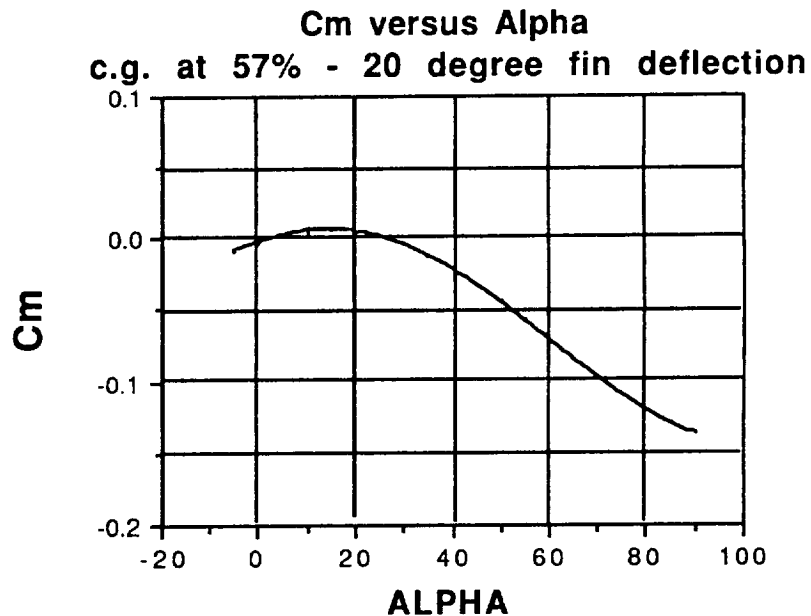


Figure 5.6

The biconic CRV is completely roll stable for any yaw angles. This is shown in Figure 5.7. For the CRV to be completely roll stable, the slope of the  $C_l$  versus  $\beta$  curve must be negative. This occurs for any angle of  $\beta$ .

The greatest instabilities in the biconic CRV occur in yaw stability. This is shown in Figure 5.8. For the vehicle to be stable in the yaw direction, the slope of  $C_n$  versus  $\beta$  must be positive. However the CRV is statically unstable for yaw angles between 10 degrees and 30 degrees. The solution to this problem lies in the use of the automatic flight control system. Details of the use and effectiveness of such a system are found in section 5.3.4, Automatic Flight Control System.

**Cl (rolling) versus Beta**  
**c.g. at 57% - 20 degree fin deflection**

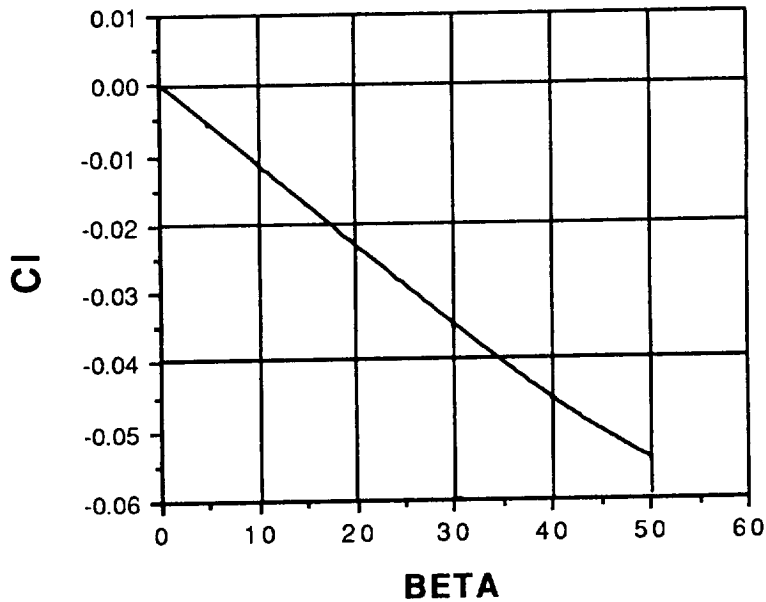


Figure 5.7

**Cn (yaw) versus Beta**  
**c.g. at 57% - 20 degree fin deflection**

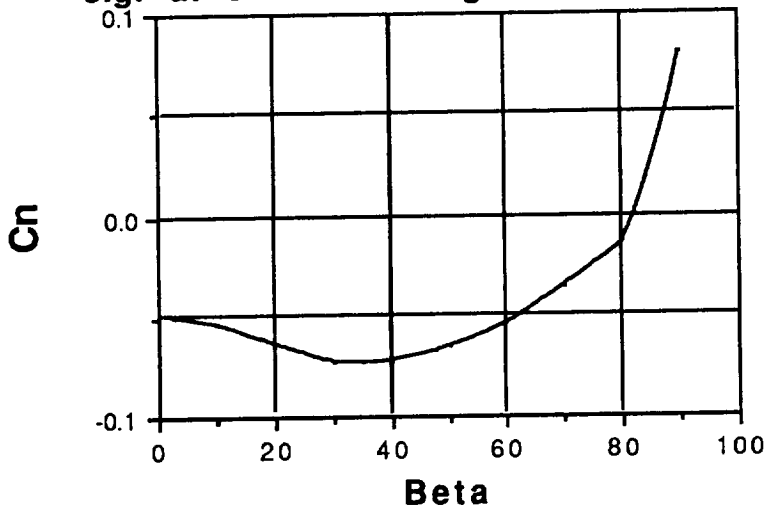


Figure 5.8

### 5.3.2 Longitudinal Analysis

The longitudinal analysis of the biconic CRV involves determining the dynamic stability of the vehicle when it is

subject to angles of attack disturbances. There are two modes that result from these disturbances. They are the phugoid and short period modes. The phugoid mode is characterized by a slow rising and falling of the vehicle, accompanied by change in speed. The period and the time for the amplitude to reach one half its initial value are used to evaluate this mode. Graphs of these characteristics are found in Figures 5.9 and 5.10.

### PHUGOID MODE (Period)

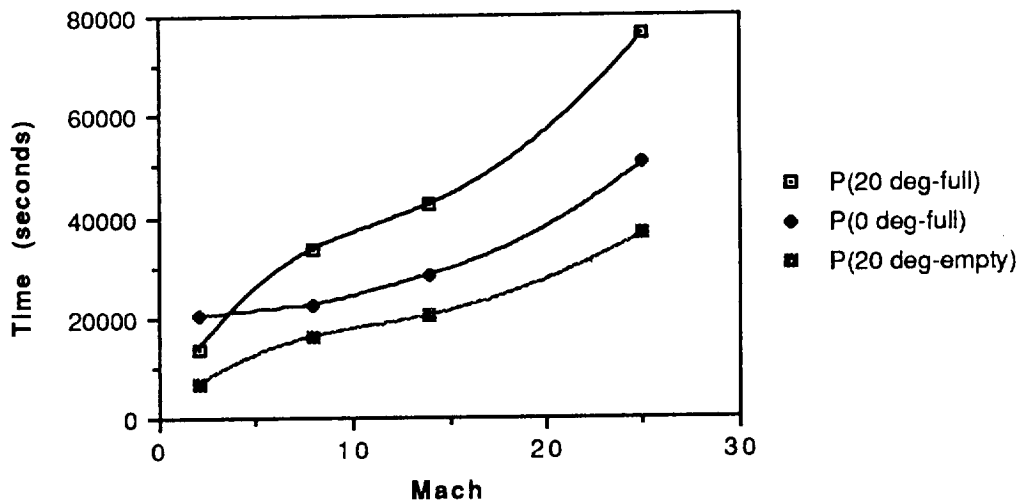


Figure 5.9

### PHUGOID MODE (Time to half)

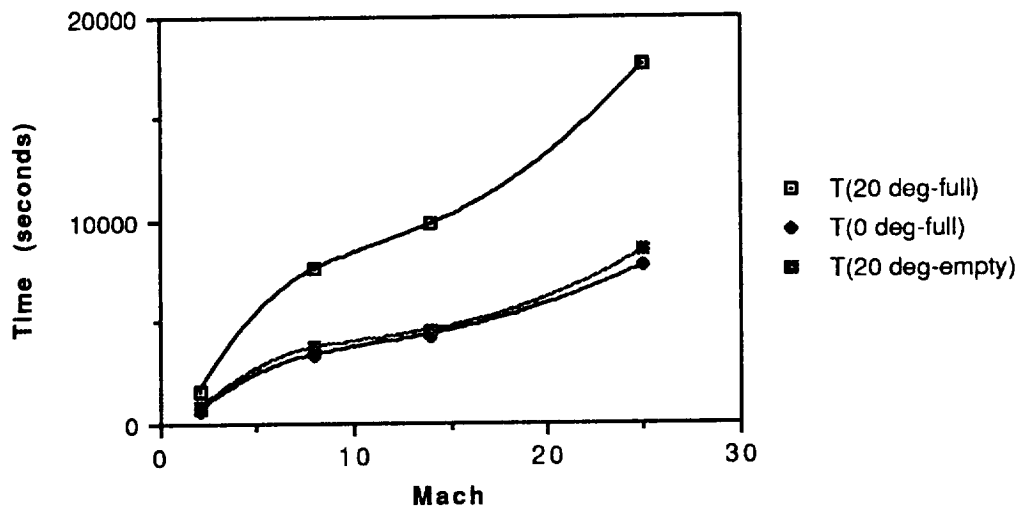


Figure 5.10

These graphs show that this mode is very slow (stable) for the biconic CRV. The slow times of this mode, and any other mode, mean that there is an adequate amount of time for the pilot or auto pilot system to correct the path of the vehicle in time to avoid going into the unstable mode. The short period mode is characterized by a rapid rotation of the vehicle in pitch. The period and time to half are again used to evaluate this mode. The graphs of these are shown in Figures 5.11 and 5.12.

### SHORT PERIOD MODE (Period)

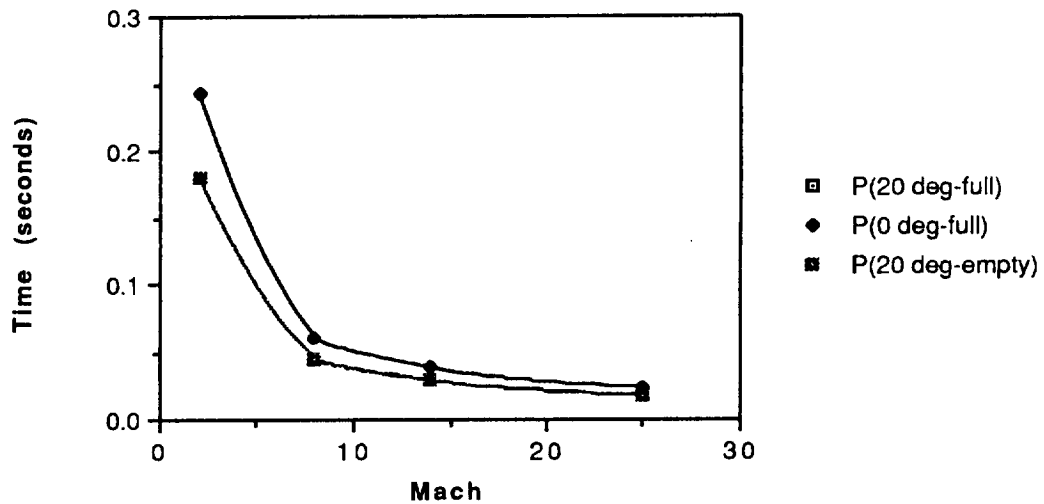


Figure 5.11

### SHORT PERIOD MODE (Time to Half)

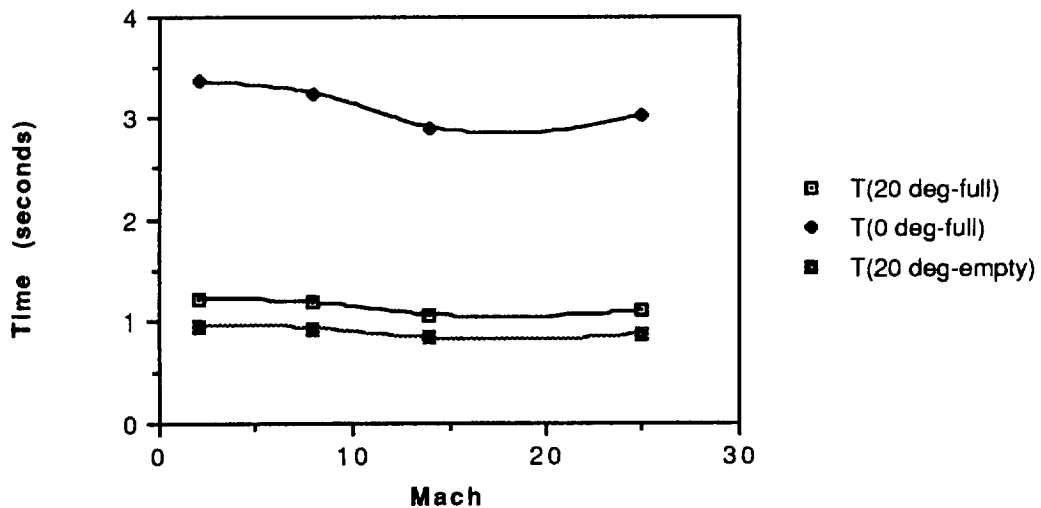


Figure 5.12

The value for the period and time to half are large enough for the control system to prevent the vehicle from going into the unstable short period mode.

### 5.3.3 Lateral Analysis

The lateral analysis of the biconic CRV involves determining the dynamic stability of the vehicle when it is subject to rolling, yawing, and sideslipping disturbances. They are the spiral, rolling, and dutch roll modes. The rolling mode is unstable when the roll angle increases with time instead of decreasing. This mode is characterized by the time it takes for the amplitude to reach one half its initial value (time to half). This is shown in Figure 5.13 for the rolling mode.

The vehicle is very stable in this mode, the times are very slow (stable). This mode also becomes more stable as the mach number is increased. The spiral mode is unstable when the yaw angle increases with time instead of decreasing. The flight of the vehicle in this mode is in a banked turn of ever-decreasing radius. This mode is also evaluated according to the time to half of the mode. This is shown for the spiral mode in Figure 5.14.

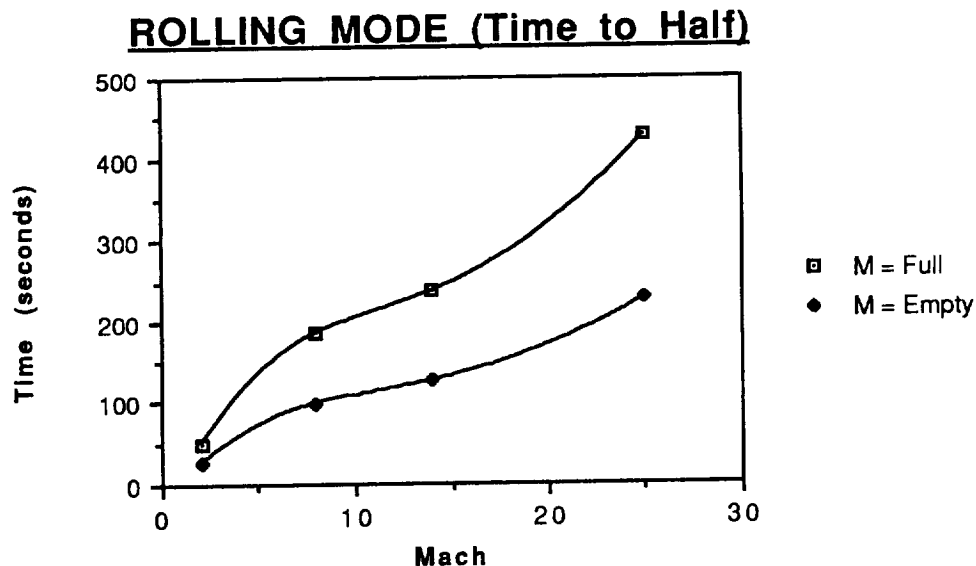


Figure 5.13

### SPIRAL MODE (Time to Half)

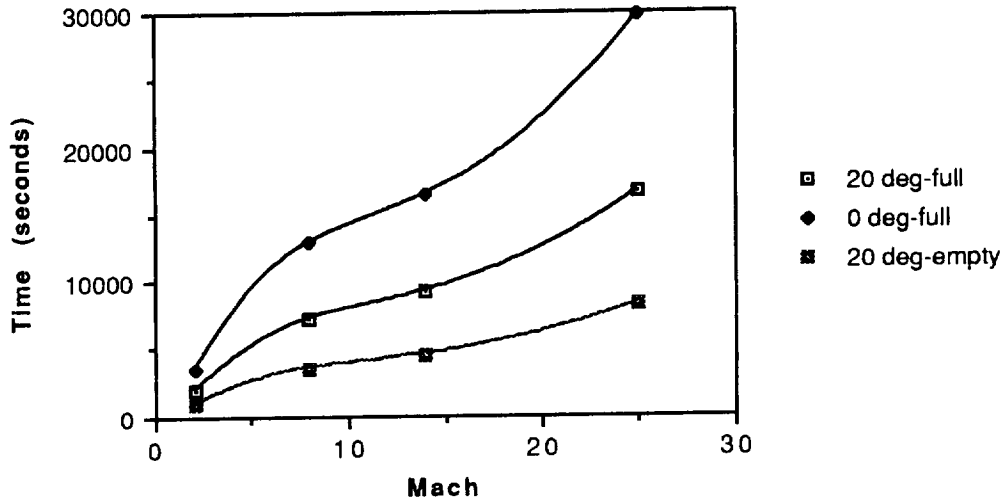


Figure 5.14

This is usually a very weak mode, and it is true for this vehicle. The times are very slow and increase with higher mach numbers. The dutch roll mode is a mode of coupled lateral oscillation between rolling and yawing. This mode is evaluated by its period and time to half, shown in Figure 5.15 and Figure 5.16.

### DUTCH ROLL (Period)

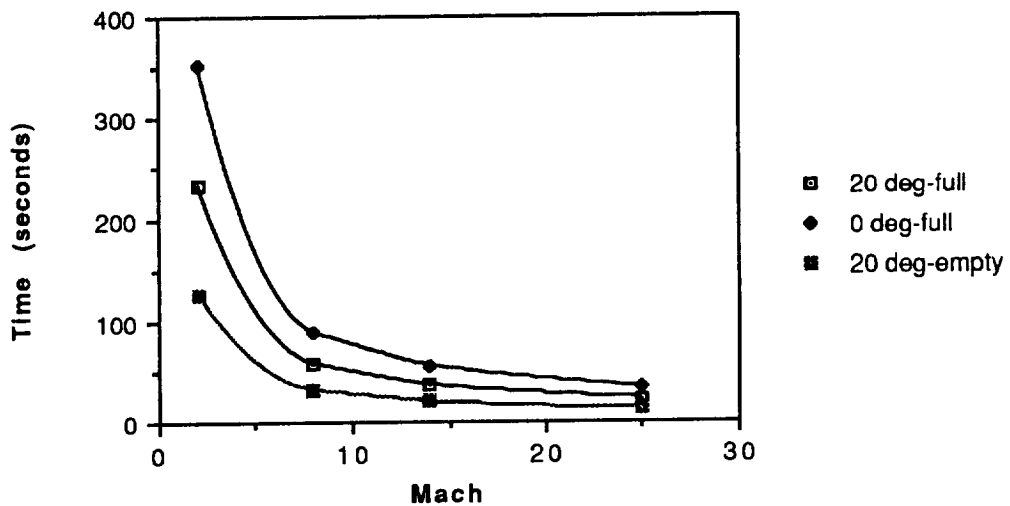


Figure 5.15

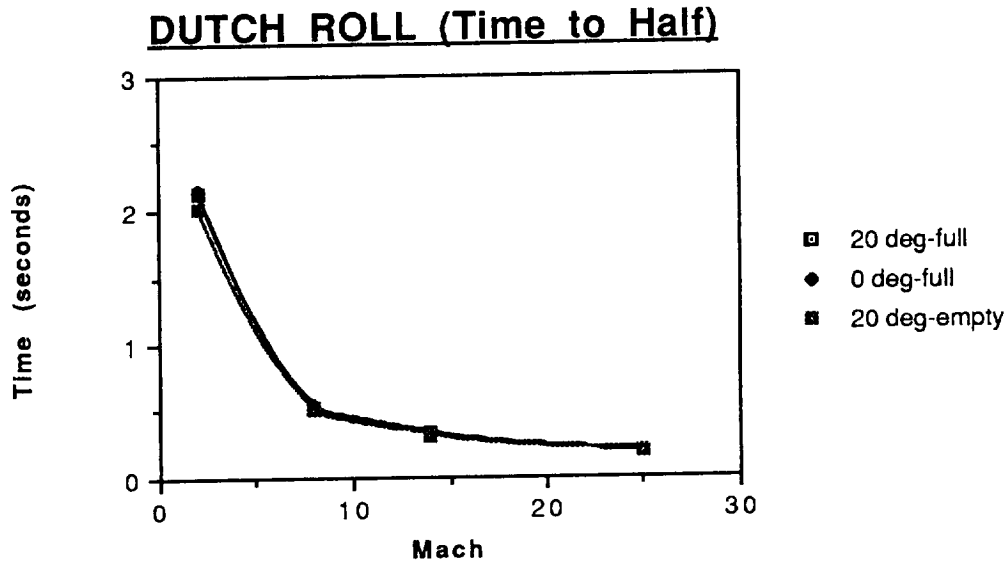


Figure 5.16

The dutch roll mode is slightly unstable for the biconic CRV. This is a result of the roots of this mode being in the right half plane of the root locus. The root locus is shown in Figure A.5.2 of the appendix. The main reason for this mode being unstable is that the CRV is slightly unstable in the yaw direction and the Dutch Roll mode is a coupled oscillation between yaw and roll. The times for this mode are large enough to be controlled by the control system outlined in the next section (5.3.4).

#### **5.3.4 Automatic Flight Control System**

The instabilities that will be handled by the automatic flight control system will be the pitching instability for angles of attack less than 15 degrees and the yaw instability for yaw angles between 10 and 30 degrees. A complete automatic flight control system will not be designed in this section, but the reasons why one can and should be used will be discussed and a general outline of a system will be shown. From reference 5.15 it states that most aircraft/spacecraft with swept bodies or wings have a natural tendency to be slightly unstable or underdamped in the lateral direction. For these vehicles, a control system is designed with natural frequencies less than 1 rad/sec and a damping ratio greater than about 0.5. This is done by using sensors, actuators, dynamics of the system, and feedback control. The sensors

consist of devices to measure the yaw, pitch, and roll rates. The actuators used will be the horizontal-rudder fins. The horizontal part of the fins will be used to mainly control the pitch of the vehicle. But by moving one side up and the other side down some yaw and roll control can be utilized in the control system. The main yaw and roll control will come from the bent up fins (rudders at the ends of the horizontal fins). By having control surfaces in both the horizontal and vertical plane, and automatic flight control system will be able to control the biconic CRV during all flight conditions that it will encounter (ref 5.16). The system outlined below in Figure 5.17 is a yaw damper system. A pitch control system will not be shown because the vehicle is only unstable for angles of attack less than 15 degrees and the flight plans never call for the CRV to be flown at angles of attack less than 15 degrees. An automatic flight control system will be used in the pitch direction in case disturbances force the CRV into angles less than 15 degrees. The main stability problems are in the yaw control, so this system will be shown.

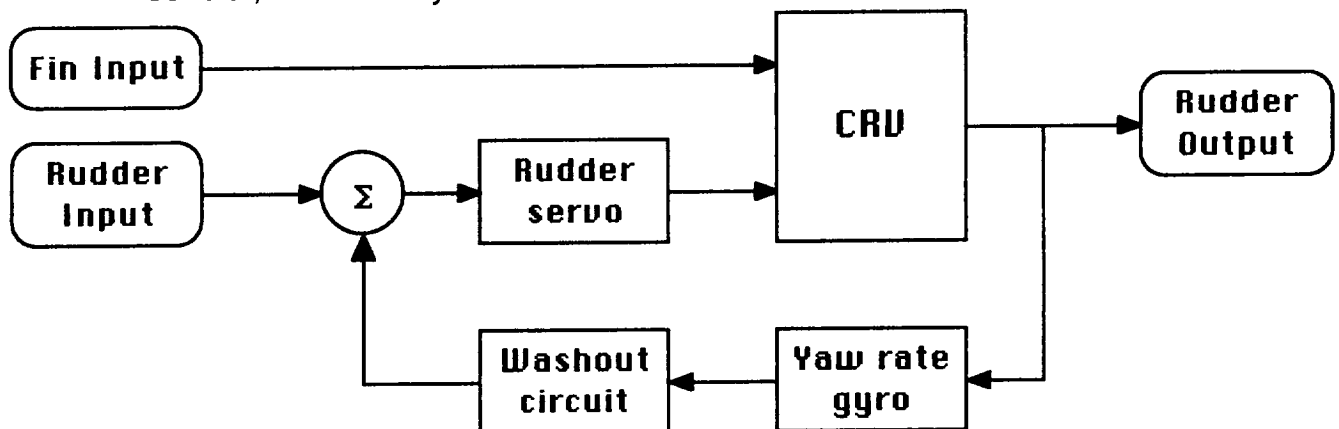


Figure 5.17 Yaw Damper Control System

The system in Figure 5.17 works as follows: a reference fin and rudder displacement are feed into the system, the rudder input proceeds through the rudder servo and both fin and rudder inputs then go through the dynamics of the CRV, the results are then feedback through the yaw rate gyro and a washout circuit, the results are then feed through the system until the correct value is output. The unique feature of this system is the washout circuit. The washout circuit has the feature that it passes only transient inputs and "washes out" steady and low-

frequency inputs. This yaw system and a similar pitch control system can and will be used to control the instabilities in the biconic CRV.

The biconic CRV is stable enough to fly under any flight conditions. The slight instabilities in the static and dynamic characteristics of the vehicle are small enough to be compensated for by an automatic flight control system (described in section 5.3.4).

## **5.4 On-Orbit Control**

The on-orbit stability and control of the biconic CRV is a function of attitude dynamics and attitude control. The vehicle will be stabilized through a combination of "passive" control (dynamics only) and "active" control (sensors, actuators, RCS jets, and control laws).

### **5.4.1 Pitch Control**

The design of an on-orbit automatic pitch control system is straightforward, since the pitch motion is decoupled from other motions. A block diagram for this control is found in Figure 5.18.

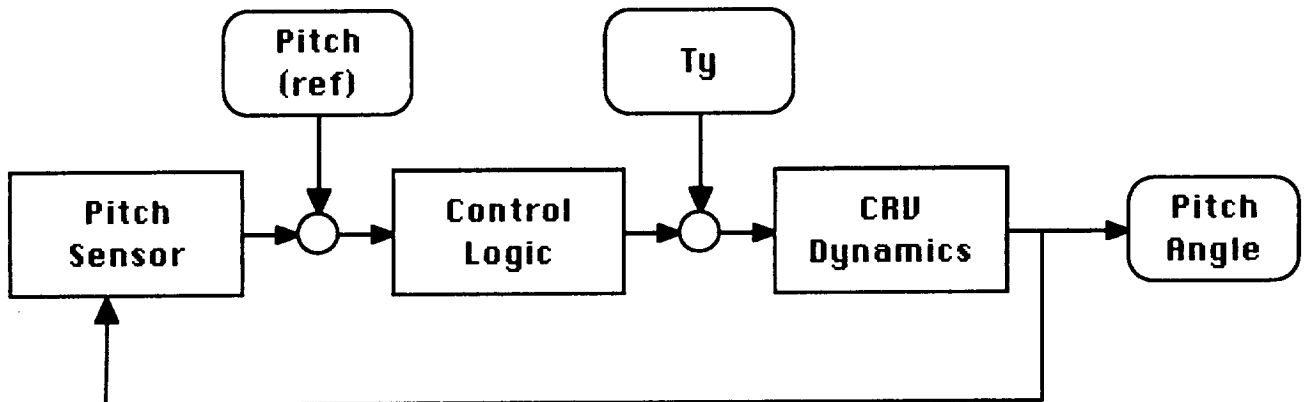


Figure 5.18 Pitch Control Block Diagram

The accuracy for the pitch system will be within 0.05 degrees. This value will allow accurate maneuvering of the CRV when it is near the Space Station Freedom. This will be accomplished by incorporating a lead-lag compensator in the feedback of the system. The system will be designed to be critically damped with a natural frequency of 3 radians per second. With these

design requirements, the pitch autopilot gain equals  $4.0 \text{ lb} - \text{ft}^2(\text{deg}/\text{sec})^2$ . The time constant for the system equals 0.7 seconds. This value is small enough for complete control of the vehicle in the pitch direction. This system results in a steady state error of less than 0.04 degrees, which is less than the design requirements of 0.05 degrees.

#### 5.4.2 Roll/Yaw Control

The design of an automatic roll and yaw system is not as straightforward as the pitch control. The reason for this is that there is a coupling of yaw and roll moments. An attractive feature of this coupling is that accurate yaw control is permitted without a direct yaw sensor. This technique is referred to as gyrocompassing. A block diagram for this system is found in Figure 5.19.

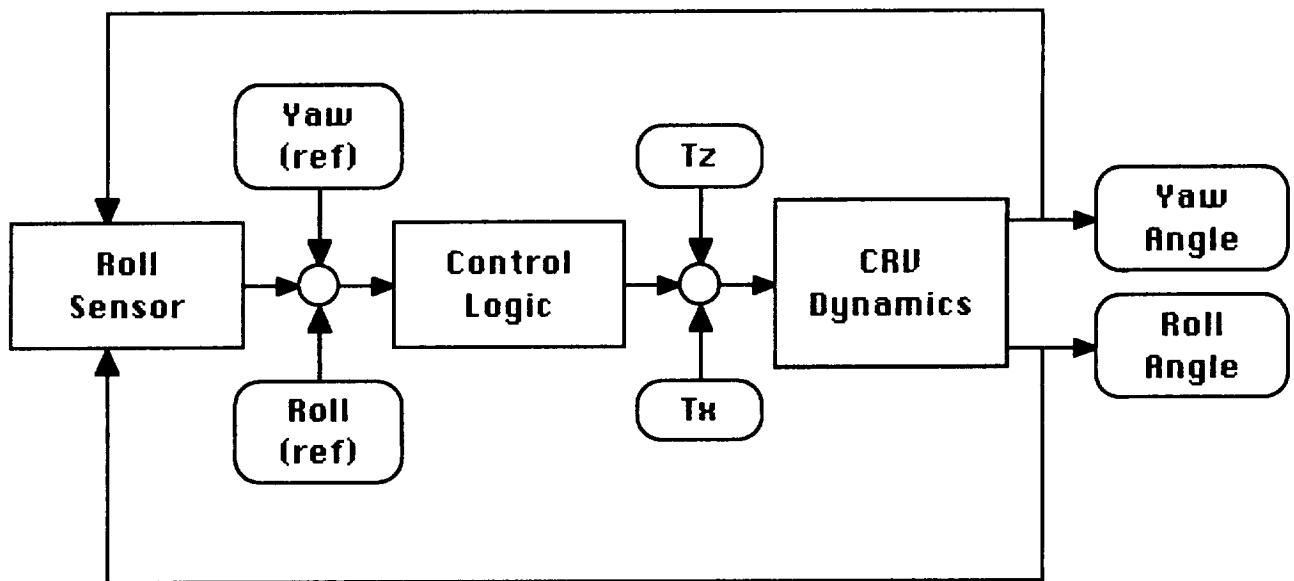


Figure 5.19 Roll/Yaw Control Block Diagram

The accuracy for the roll/yaw system will require that the error in yaw must be less than 0.40 degrees and the roll must be less than 0.05 degrees. These values will again allow accurate control of the CRV near the space station. This again will be accomplished with a lead-lag compensator. The system will be designed with critical damping for both yaw and roll. The design requirements lead to a roll dynamics natural frequency of 2 radians per second, and a yaw dynamics

natural frequency of 0.1 radians per second. The time constant for the system is 1 second. The gain for the roll system is 7500 lb-ft<sup>2</sup>-(deg/sec)<sup>2</sup>, and a yaw gain of 375 lb-ft<sup>2</sup>-(deg/sec)<sup>2</sup>. The steady state errors for both the roll and yaw are below the design accuracy requirements.

The biconic CRV can be controlled in all three directions (pitch, roll, yaw) by two automatic systems. The two systems are accurate enough to position the CRV where ever it is needed.

### **5.5 C.G. and Moment of Inertia**

The center of gravity(C.G.) of the vehicle was calculated for several different vehicle configurations. It was calculated for the three different vehicle designs with the best approximations that were available at the time. For the first vehicle configuration, the vehicle was designed to be a length of 68 feet. The data was very rough since the majority of the weights and C.G. locations of the individual components consisted of intelligent guesses. The design disciplines had not yet had a chance to calculate preliminary data for the C.G. For this 68 foot configuration, the C.G. was located 48.7 feet back from the nose or at 71.6% of the body length.

The aerodynamic discipline then proposed that the length needed to be shortened to 60 feet. The design disciplines were asked to calculate CG locations and weights of the components that they were responsible for. The C.G. for this design was at 36.6 feet or 61%.

Finally, the vehicle was finalized on a length of 59 feet. Data was again gathered from all of the disciplines to determine the final CG location and moments of inertia for the full cargo configuration, Table 5.1. The CG was calculated by using the following equation:

$$X_{cg} = \sum(m_j X_j) / m$$

where  $X_{cg}$  is the distance (ft.) of the CG from the nose of the vehicle,  $m_j$  is the mass (lbm) of an individual component,  $X_j$  is the distance (ft.) of the components CG from the nose of the vehicle, and  $m$  is the total mass of the vehicle.

Stability and control analysis determined from the HABP computer program (ref. 5.6) that the CG percentage of the total length of the vehicle ( $X_{cg}/L$ ) was less than 57% to maintain stability and control of the vehicle. The final data was not able to accommodate that constraint; however, this is not a critical problem since the space shuttle is capable of flying under unstable conditions. The automatic flight control system, section 5.4.3, is capable of adjusting for this condition.

Once the CG location is calculated, the moment of inertias can be calculated. The coordinate convention used for the moment of inertias is shown in Figure 5.20. They are calculated by using the following equations:

$$I_z = \sum [m_i(X^2 + Y^2)_i]$$

$$I_y = \sum [m_i(X^2 + Z^2)_i]$$

$$I_x = \sum [m_i(Y^2 + Z^2)_i]$$

where  $I_x, I_y, I_z$  are the moment of inertias (slug-ft<sup>2</sup>) about their subscripted variables,  $m$  the mass (slugs) of the component, and  $X, Y, Z$  (ft.) are the location of the component with respect to the CG of the total vehicle.

The moments of inertia are important because they determine how much energy is needed to change the velocity of the vehicle. The larger the moments of inertia are, the greater the amount of energy needed to change the velocity and the longer the response time of the vehicle.  $I_x$  is the rotation about the x-axis referred to as rolling,  $I_y$  is the rotation about the y-axis referred to as sideslip, and  $I_z$  is rotation about the z-axis referred to as yawing. If these values get too large, the control systems and propulsion systems will not be able to handle the vehicle. The values that we obtained for the moment of inertias are shown in Table 5.1. The values are very large, but it has been determined that the automatic flight control system can handle it (section 5.4.3 and ref. 5.15).

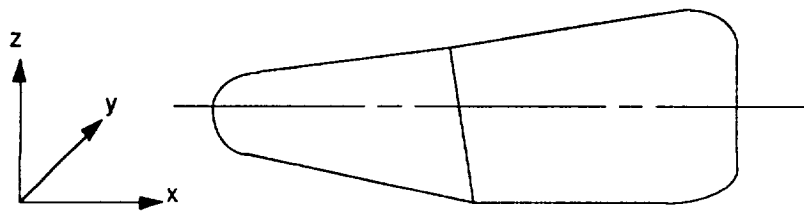


Figure 5.20 - Axes Rotation - Orientation



From the CG calculation, the CG flight envelope can be calculated by loading the vehicle over its full range of mass load configurations. The CG envelope is shown in Figure 5.21. The vehicle must be stable and controllable in this envelope and analysis shows that the vehicle is capable of flying anywhere in this envelope.

**FLIGHT ENVELOPE (TOTAL WEIGHT VS. Xcg/L)**

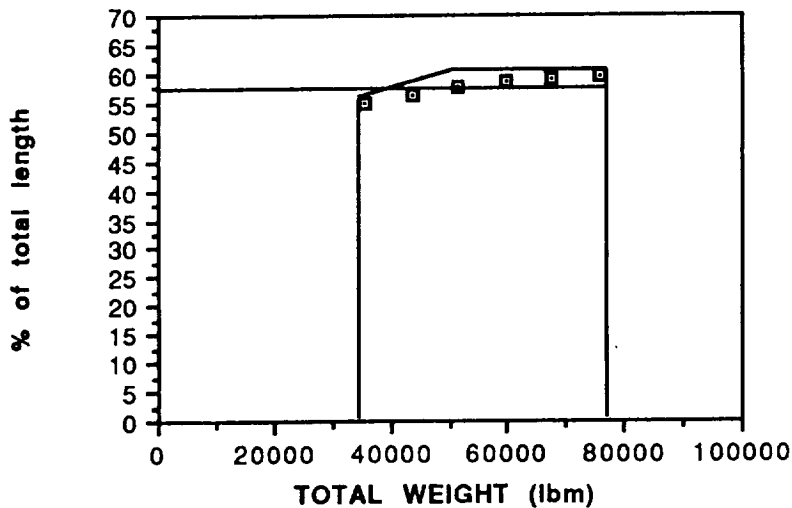


Figure 5.21

## **5.6 Advanced Recovery System**

Several areas of the advanced recovery system were looked at by Stability and Control discipline. The main areas of concern have been the ARS control system and the landing flare system. Drogue chutes and ARS stability was also examined to a lesser degree.

### **5.6.1 Drogue Chute**

A drogue chute is not a necessity for stability, but it is needed to slow the CRV down. The design of this drogue will come from Aerodynamics, and deployment data from Reentry Dynamics; however, it must satisfy these requirements:

- (1) The drogue must be released prior to an altitude of 10,000 ft., as this is the parafoil stage 1 deployment altitude as defined by Aerodynamics.

(2) The dynamic pressure upon parafoil deployment must not exceed 50 psf.

(3) This requires parafoil first stage deployment at 238.66 ft./sec. or Mach 0.2215.

Without the drogue the dynamic pressure exceeds 300 psf at 10,000 ft. The parafoil is also required to be fully deployed in stable gliding flight at 5,000 ft. with the CRV trimmed at 20 degrees angle of attack. This angle of attack corresponds to maximum L/D of the vehicle without the wing deployed.

### **5.6.2 Control System**

The vehicle control system is a trailing edge deflection type. A trailing edge deflection is accomplished by "reeling in" the ARS support cables on the trailing edge of the wing. The cables are reeled in by means of electric motors located in the load bar. The entire trailing edge may be deflected up to an angle of 20 degrees down on either or both sides of the parafoil (see Figure 5.22).

The deflection pivot point is at the quarter chord point from the trailing edge of the wing, or 66.75 feet from the leading edge (see Figure 5.23).

Drawings of the load bar itself are not to any scale, but are rather used as a reference for drawing the steering system motors and components. The trailing edge cable is reeled onto a two inch diameter 1040 steel rod which is 16 inches long. In each revolution of the rod, 0.524 feet of cable are reeled in. This means that for the maximum 20 degree deflection, 14.5 revolutions are completed and 7.61 feet of cable are reeled in. This translates to 0.725 revolutions per degree of deflection. The length of the rod is based on a one inch support cable diameter. This design is easily modified for larger diameter cables. This leaves about a 1.50 inch tolerance (extra rod length). Figure 5.24 shows shaft placement on the load bar reference drawing.

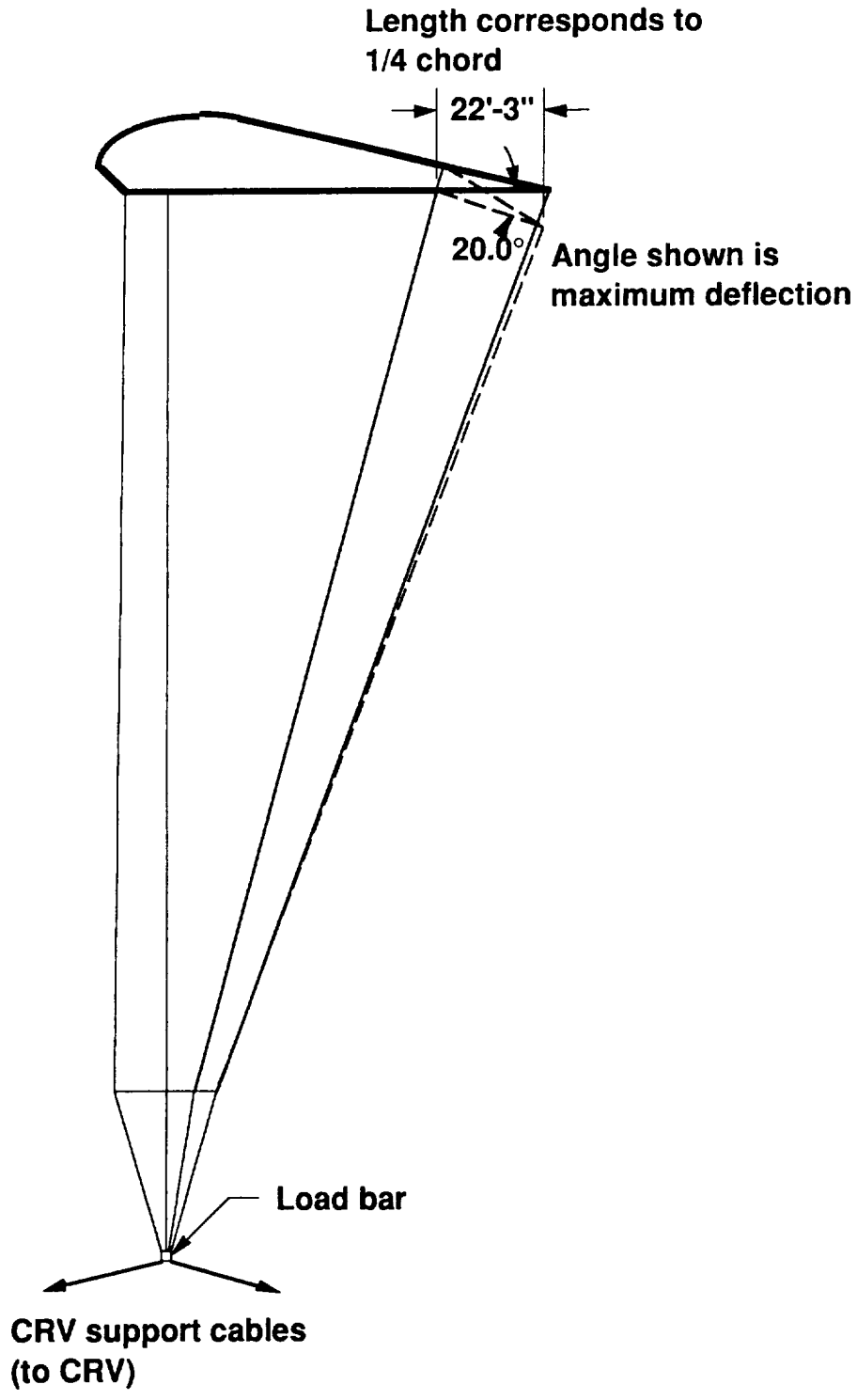


Figure 5.22 - Side View of Control System

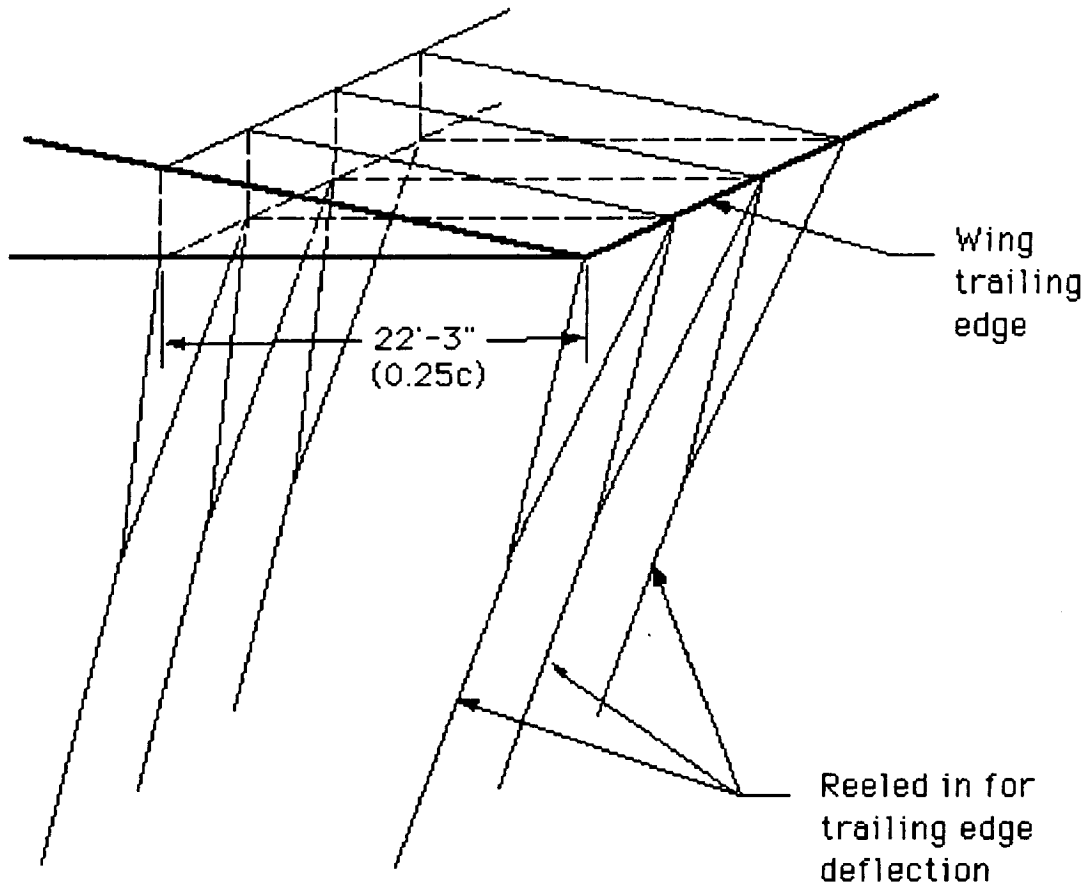


Figure 5.23 - Trailing Edge Detail

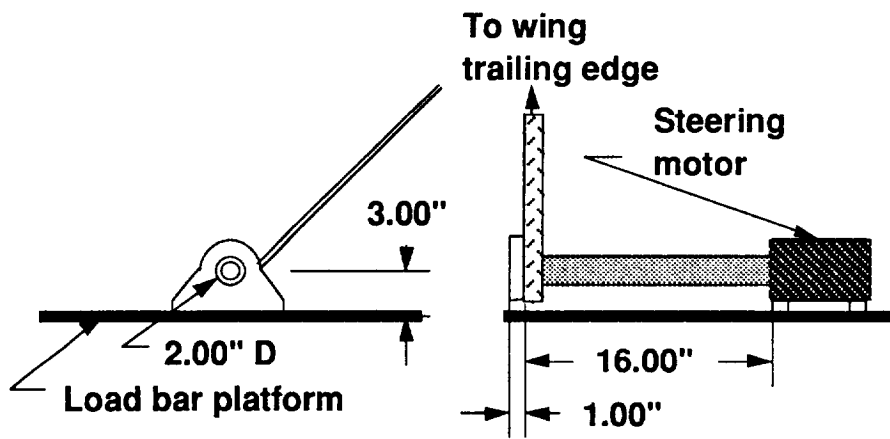


Figure 5.24 - Load Bar Detail

### 5.6.3 ARS Stability

The requirement for static longitudinal stability is that the neutral point must be some distance behind the most aft position of the center of gravity. This distance is usually assumed to be about 10% of the mean aerodynamic chord. For the CRV, the neutral point is taken to be at the aerodynamic center of the ARS, or at the quarter chord point 22.25 feet from the leading edge of the wing. This assumption is based on the fact that the CRV body has little effect on the total vehicle aerodynamic center. Also, the vehicle is assumed tailless because the low tail volume ratio (about 0.004) prohibits its use as an elevator once the ARS is deployed.

As long as the c.g. is ahead of the aerodynamic center the vehicle will be stable; however, assuming a static margin of 10%, the c.g. is then located 8.9 feet ahead of the wing quarter chord point, or 13.35 feet from the leading edge of the wing. Ignoring drag effects and summing the moments about the center of gravity:

$$dM/da = (dC_M/da)_{CRV} C_{CRV} S_{CRV} + dC_L/da S_{para} x_{cg} + (dC_M/da)_{c/4} C_{para} S_{para}$$

C = mean chord

S = reference area

$x_{cg}$  = distance of c.g. from aerodynamic center

a = angle of attack

This yields a value for  $dM/da$  of -11,886/radian, which corresponds to a negative  $C_{Ma}$  (about -0.006) meaning that the vehicle is stable. A more complete  $C_{Ma}$  analysis has been done by aerodynamics on the Sun computer.

Static lateral stability is achieved if the spiral mode (if divergent) has a time to double greater than a specified minimum (usually about 4 seconds). No empirical means of determining control and side force coefficients could be found for this type of configuration. All existing data is determined through the use of a wind tunnel or by drop tests.

## **6.0 AVIONICS AND POWER**

---

### **6.1 Introduction**

#### **6.1.1 Definition of Avionics Systems**

The Avionics Systems can be defined as the systems that perform the following tasks for the CRV:

1. Atmospheric flight control
2. Vehicle Guidance and Navigation
3. Telemetry of command data (uplink) and systems information data (downlink)
4. On-board data management

#### **6.1.2 Definition of Power Sub-Systems**

The power Sub-System can be defined as the systems that perform the following tasks for the CRV:

1. Supply power to the avionics gear in all flight modes
2. Supply power to the Pressurized Logistics Module (P-Log)
3. Supply the cooling needed by the avionics gear and the P-Log

### **6.2 Avionics Equipment List**

The avionics equipment recommended for the CRV is as follows:

<b><u>COMPONENT</u></b>	Laser Internal Navigation System (LINS)	Reaction Jet Driver (RJD)
Source	Honeywell	Honeywell
Weight (lb)	42	33
Units	3	3
Size (in)	16.25 x 11.25 x 5.9	20 x 9 x 6.4
Power (W)	70	38 (avg) / 63 (max)

<u>COMPONENT</u>	General Purpose Computer (GPC)	Multiplexer (MDM)
Source	IBM	Honeywell
Weight (lb)	64	37.4
Units	3	11
Size (in)	19.5 x 10.2 x 7.6	6.6 x 11.6 x 13.25
Power (W)	560	76
<u>COMPONENT</u>	Rate Gyro Assy. (RGA)	Accelerometer Assy. (AA)
Source	Northrop	Honeywell
Weight (lb)	10.1	2.5
Units	3	3
Size (in)	8.25 x 7.6 x 6.25	5 x 5 x 5.43
Power (W)	23.4	2.4
<u>COMPONENT</u>	Data Bus Isolation Amp (DBIA)	Master Event Controller (MEC)
Source	Singer	Autonetics
Weight (lb)	7.5	37
Units	2	2
Size (in)	5 x 5 x 5	7.5 x 11 x 12
Power (W)	22.3	54
<u>COMPONENT</u>	CMMU/PDI	Timer Buffer
Source	Harris	Harris
Weight (lb)	18.5	5
Units	2	1
Size (in)	19 x 8.2 x 3.5	4 x 4 x 4
Power (W)	25.5	31

The listed equipment was taken from the Shuttle-C (Ref. 6.2), with minor additions for the CRV's slightly changed mission profile. This package was designed around the 'single fault tolerance' guidelines used by NASA for unmanned vehicles, meaning the CRV can lose any one avionics or power supply component and still function at full capacity. The redundancy was enhanced with addition of the Global Positioning System and carried through into the systems added for

the recovery phase. It should be noted that the CRV's Avionics package does not have the redundancy a passenger carrying vehicle would require. If the carrying of personnel were desired, the weight of the avionics package would have to be increased by approximately 30-40%.

### **6.3 Storage of Avionics Equipment**

The storage of the avionics gear in the CRV was primarily designed so as to make the cooling system (see Section 7.0, Thermal Analysis) as efficient as possible. The avionics gear was therefore placed in a pressure tight compartment in the forward part of the vehicle (see Figure 6.1). The power cells and their fuel cells will be mounted just aft of the avionics compartment. The cooling system will be located as close as possible to the power cells with two water ejection ports on either side to allow the rejection of water from the flash evaporators during flight.

Figure 6.1 shows how the avionics gear fits into the vehicle as a whole.

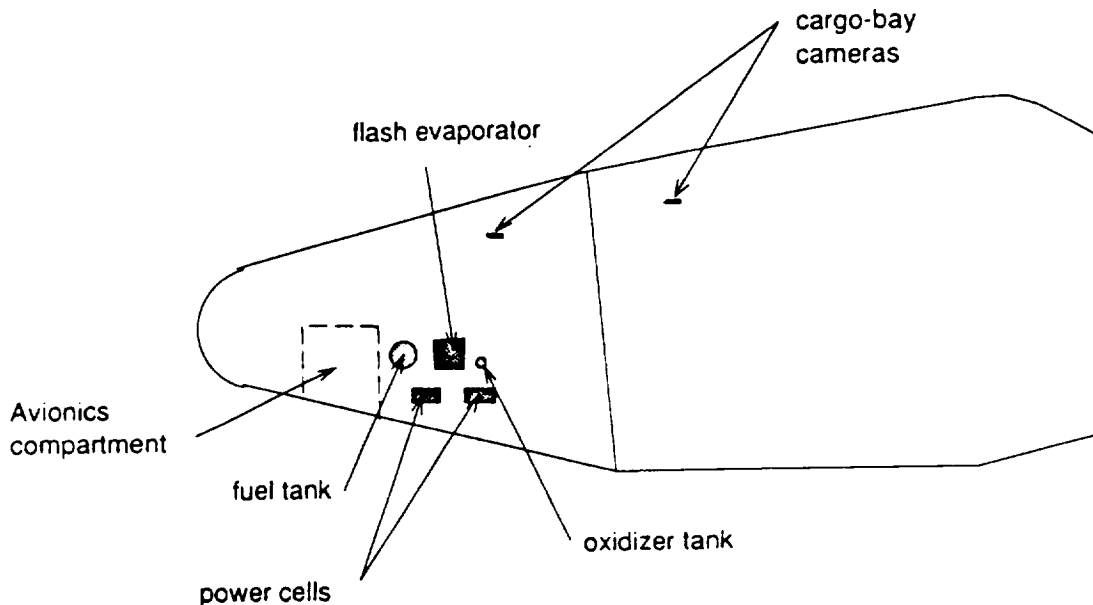


Figure 6.1 Location of Avionics Components

Figure 6.2 shows a cutaway view of the avionics bay from the left profile and rear view.

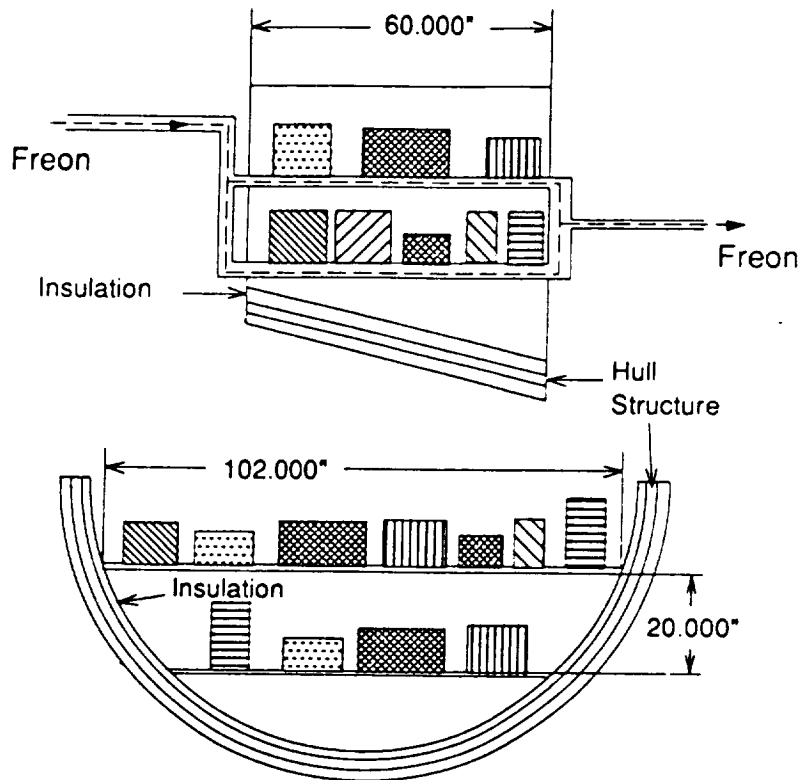


Figure 6.2 Avionics Shelf

The diagrams in Figure 6.3-4 show a first approximation of how the avionics gear might be mounted on the two avionics shelves. It should be noted that such problems as electromagnetic interference are almost impossible to predict in theory and would have to be worked on a full scale working mock up.

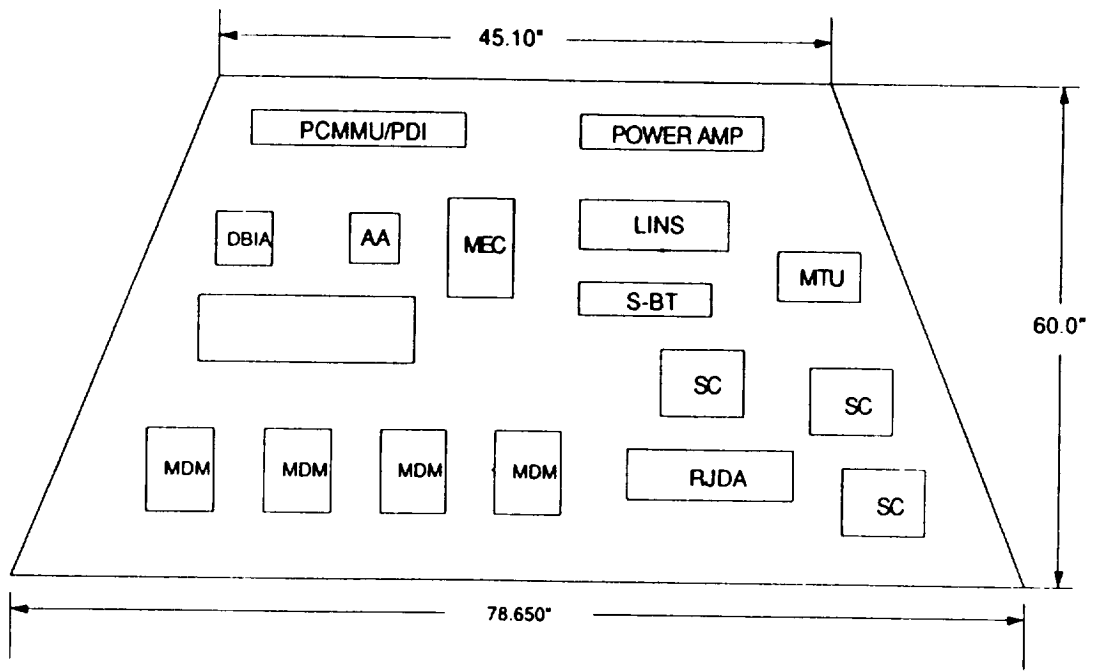


Figure 6.3 Upper Shelf

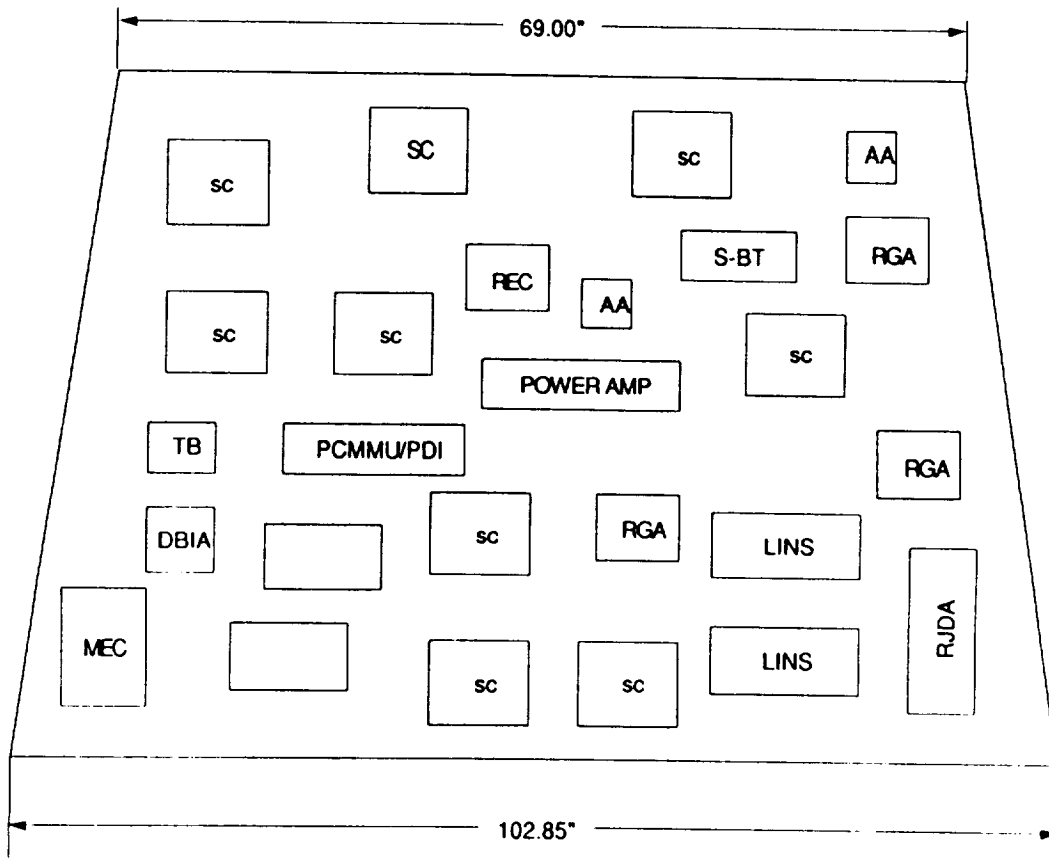


Figure 6.4 Lower Shelf

## **6.4 Choice of Power Supply System**

The chosen power supply system for this vehicle is a liquid fueled power cell which takes in liquid Oxygen and liquid Hydrogen and produces electric power, water and waste heat. The two cells would be smaller versions of those used on the Space Shuttle. Either one would be able supply all of the power needed by the vehicle.

### **6.4.1 Power Supply Cooling System**

Both the liquid fuel power cells and the avionics package produce waste heat that must be rejected from the vehicle in order to maintain a suitable temperature environment for the avionics gear. The cooling system (see Section 7.0 Thermal Protection and Control for more details) consists of radiators, flash evaporators and 20 gal. water tank. With this system the vehicle will have adequate cooling in all flight modes.

## **6.5 Effect of On-Orbit Times on Power Consumption**

The definition of on-orbit power consumption is concerned only with those times that the CRV is in an established orbit and does not pertain to either launch or recovery stages of flight. The launch and recovery flight stages are covered in detail in the boost stage power supply and recovery stage power supply sections of this report.

Using an average value of the calculated power consumption, the approximation of 1.1 lbs of hydrogen and oxygen per kilowatt hour of power produced (Ref. 3) and the desire for a 48 hr mission time plus a 24 hr reserve, the total Hydrogen and Oxygen needed will be about 500 lbs. As a first approximation, the fuel was divided into three sets of tanks, drawn to scale in Figure 6.1. Also it should be noted that when docked to the Space Station Freedom (SSF), the CRV can draw all needed power and cooling from SSF, this gives the CRV an indefinite 'lay over' period in the event of bad weather at the landing

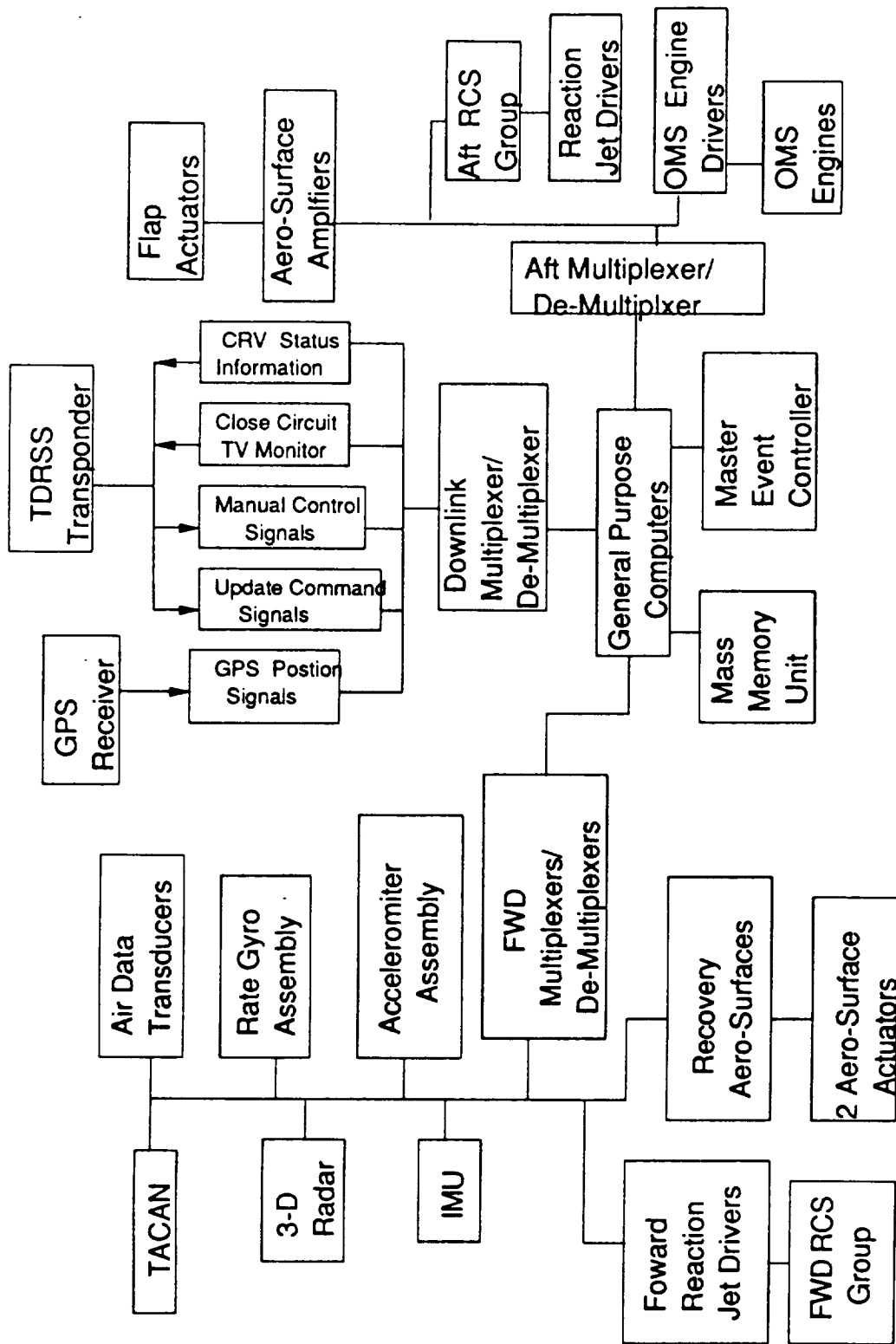


Figure 6.5 Arrangement of Components on Control Buses

site. Furthermore, the power usage chart (Figure 6.5) was calculated for a mission that required the supplying of 1.5 Kw to the Pressurized Logistics Module. In the event that the cargo being carried has no power or cooling requirements, the supply of fuel will last 25% longer.

## **6.6 In Atmosphere Power Supply**

The flash evaporators that cool the avionics gear are dependent on the pressure differential between the evaporator and the vacuum of space. This differential is greatly reduced in the atmosphere thus reducing the efficiency of the flash evaporators. This problem becomes significant at altitudes below 100,000 ft., during the boost and recovery stages.

### **6.6.1 Boost Stage Power Supply**

During the boost phase power demands are at or very near maximum. Meanwhile, the fuel cells which are dependent on the flash evaporators are not at full capacity. In addition to internal power requirements, there is also the strong possibility of supplying power to the main boost engines (see Section 8.0, Propulsion for details). To assist in cooling, heat will be dumped into a 20 gal. water tank. Also in the event that the power supply becomes strained, the Pressurized Logistics Module can be disconnected from the power supply (it can be self powered for up to six hours) for the short boost period.

## **7.0 THERMAL ANALYSIS AND CONTROL**

---

### **7.1 Introduction**

The Thermal Protection System (TPS) protects the Cargo Return Vehicle (CRV) structure from excessive heat loads experienced during reentry. Since some structure heating is unavoidable, passive protection (insulation) must be provided where possible to components internal to the structure. These components could include but are not limited to: Avionics gear, fuel lines and tanks, hydraulic lines, and the cargo (PLOG/UNPLOG). In addition, active cooling must be provided to the avionics gear during the mission and protection from space debris must be allowed for to ensure the TPS is functional to protect the CRV during reentry. Most of these concerns were addressed in previous trade studies. The intent of this study was to scrutinize and refine the design in these and other subject areas. The subjects addressed were:

- Avionics cooling design.
- Cargo bay heating loads and protection.
- Trajectory heating analysis using the NASA/Remtech computer program MINIVER.
- Control surface heating loads.
- Materials and Weights.
- Attachment methods.
- Structure type (hot, warm, or cold).
- Seals at all access points to CRV.
- Space debris protection.
- Costs and repairs.

### **7.2 Avionics Cooling Design**

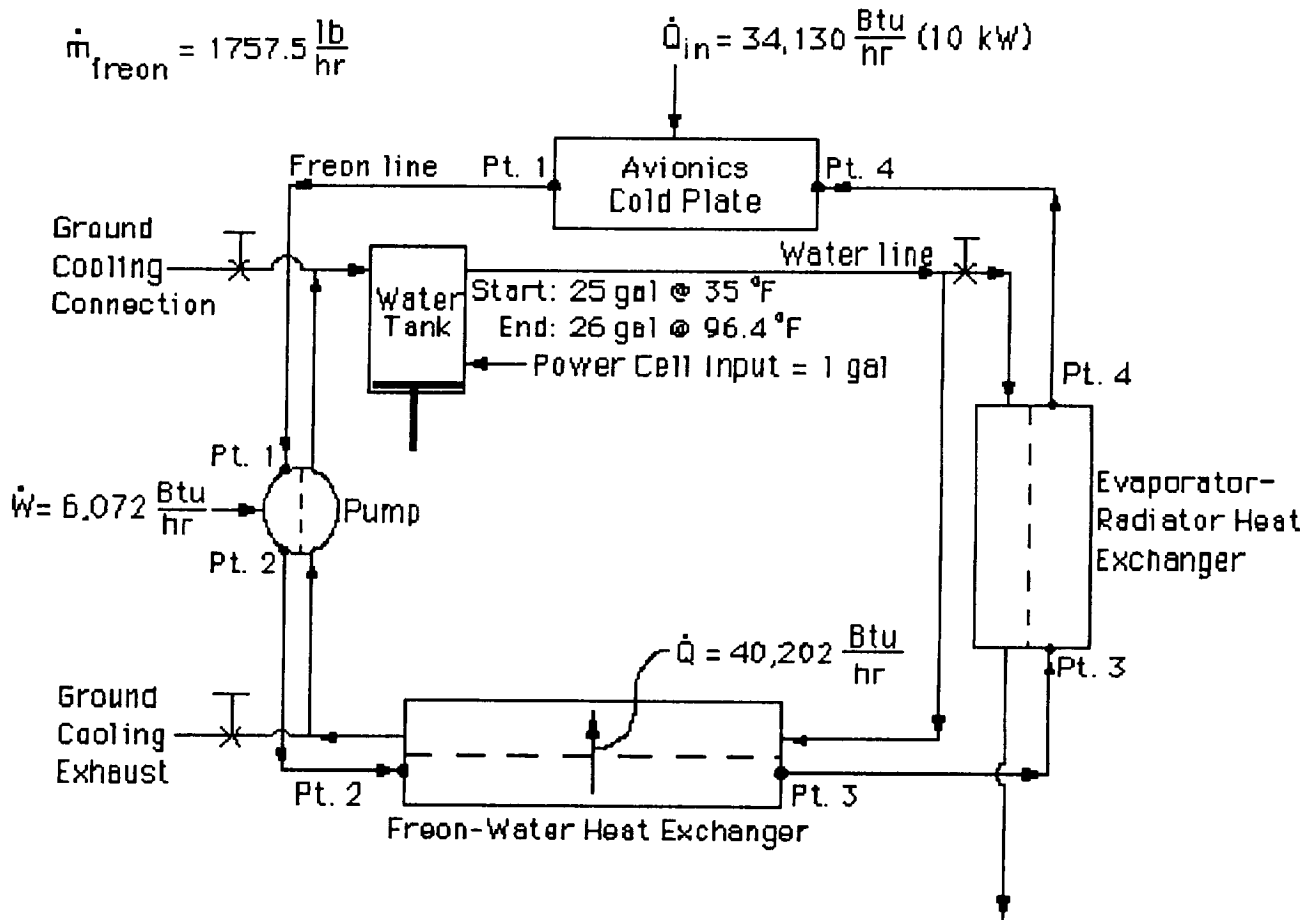
The Avionics and Power Group is using components that are pressure rated. The cooling design will place all these components on freon cooled cold plates inside a pressurized (air) container. The freon will be pumped thru a radiator with approximately 117 sq. ft. of area that is placed on the inside of the cargo bay doors. This will provide direct cooling to the avionics.

In tandem with the radiator system will be an evaporative system designed to provide direct cooling to the freon system, indirectly cooling the avionics. This heat transfer will occur between the radiator and an evaporative heat exchanger. This mode of cooling will occur shortly after lift-off until the cargo bay doors are opened and from the time the cargo bay doors are closed until shortly before landing.

Lastly, cooling must be allowed for in the lower atmosphere, where evaporative or radiative cooling cannot take place. By circulating the freon and water through another heat exchanger, a certain amount of heat can be absorbed by the water, raising its temperature approximately 61 deg F during ascent and descent. Additional water will be available as a by product from the avionic power cells which produce about 1.1 lbs of water per hour per kilowatt of power used.

The cooling system has been designed to provide about 34,000 Btu/hr (10 kW) of cooling during the first and last two hours of the mission, and 14,000 Btu/hr (4 kW) of cooling during the on-orbit phase when the cargo bay doors are open. A possible cooling scenario during a 24 hour mission might look like this:

- 0 to 20 minutes into mission  
The water-freon heat transfer system will be operating, raising the water temperature about 61 deg F. (See Figure 7.1)
- 20 minutes to 2 hours into mission  
Water will be evaporated at a rate of about 5.1 gal/hr with 19.6 gal of water remaining. (See Figure 7.2)
- 2 hours to 22 hours into mission  
The cargo bay doors are open with the radiators working. During this phase, approximately 10.3 gal of water will be restored to the water system from the power cells. (See Figure 7.3)
- 22 hours to 23 hours 40 minutes into mission  
The evaporator system will be operating, ejecting about 7.1 gal of water. (See Figure 7.4)
- 23 hours 40 minutes to touchdown  
The water-freon system will be absorbing heat, raising the waters temperature to 97 deg F. (See Figure 7.5)
- Shortly after touchdown, cooling will be provided by ground operations.



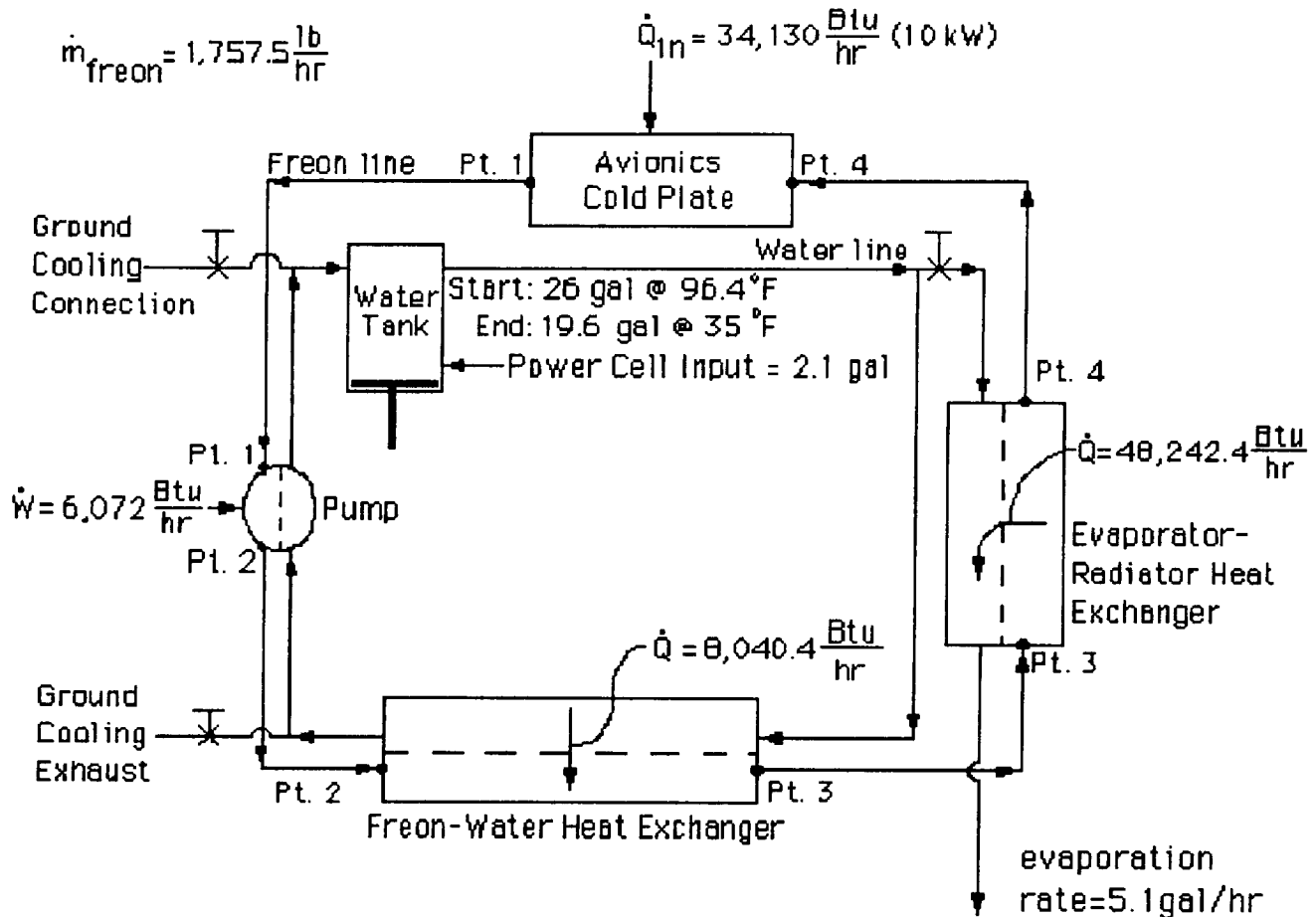
Point 1	Point 2	Point 3	Point 4
$p = 10 \text{ psi}$	$p = 200 \text{ psi}$	$p = 50 \text{ psi}$	$p = 15 \text{ psi}$
$T = 160.0^\circ \text{F}$	$T = 208.0^\circ \text{F}$	$T = 38.1^\circ \text{F}$	$T = 23.8^\circ \text{F}$
$h = 100.67 \frac{\text{Btu}}{\text{lb}}$	$h = 104.12 \frac{\text{Btu}}{\text{lb}}$	$h = 81.25 \frac{\text{Btu}}{\text{lb}}$	$h = 81.25 \frac{\text{Btu}}{\text{lb}}$

### Sample Calculations

$$\Delta T = \frac{(40,202 \frac{\text{Btu}}{\text{hr}})(\frac{12 \text{ in}}{\text{ft}})^3(\frac{1}{3} \text{ hr})}{(25.5 \text{ gal})(1 \frac{\text{Btu}}{\text{lb}^\circ \text{F}})(64 \frac{\text{lb}}{\text{ft}^3})(231 \frac{\text{in}^3}{\text{gal}})} = 61.4^\circ \text{F}$$

$$T_{\text{final}} = 35^\circ \text{F} + 61.4^\circ \text{F} = 96.4^\circ \text{F}$$

Figure 7.1 Avionics Cooling, 0- 20 minutes into 24 hr Mission



Point 1	Point 2	Point 3	Point 4
$p = 10 \text{ psi}$	$p = 200 \text{ psi}$	$p = 50 \text{ psi}$	$p = 15 \text{ psi}$
$T = 160.0^\circ\text{F}$	$T = 208.0^\circ\text{F}$	$T = 210.6^\circ\text{F}$	$T = 23.8^\circ\text{F}$
$h = 100.67 \frac{\text{Btu}}{\text{lb}}$	$h = 104.12 \frac{\text{Btu}}{\text{lb}}$	$h = 108.69 \frac{\text{Btu}}{\text{lb}}$	$h = 81.25 \frac{\text{Btu}}{\text{lb}}$

Sample Calculations

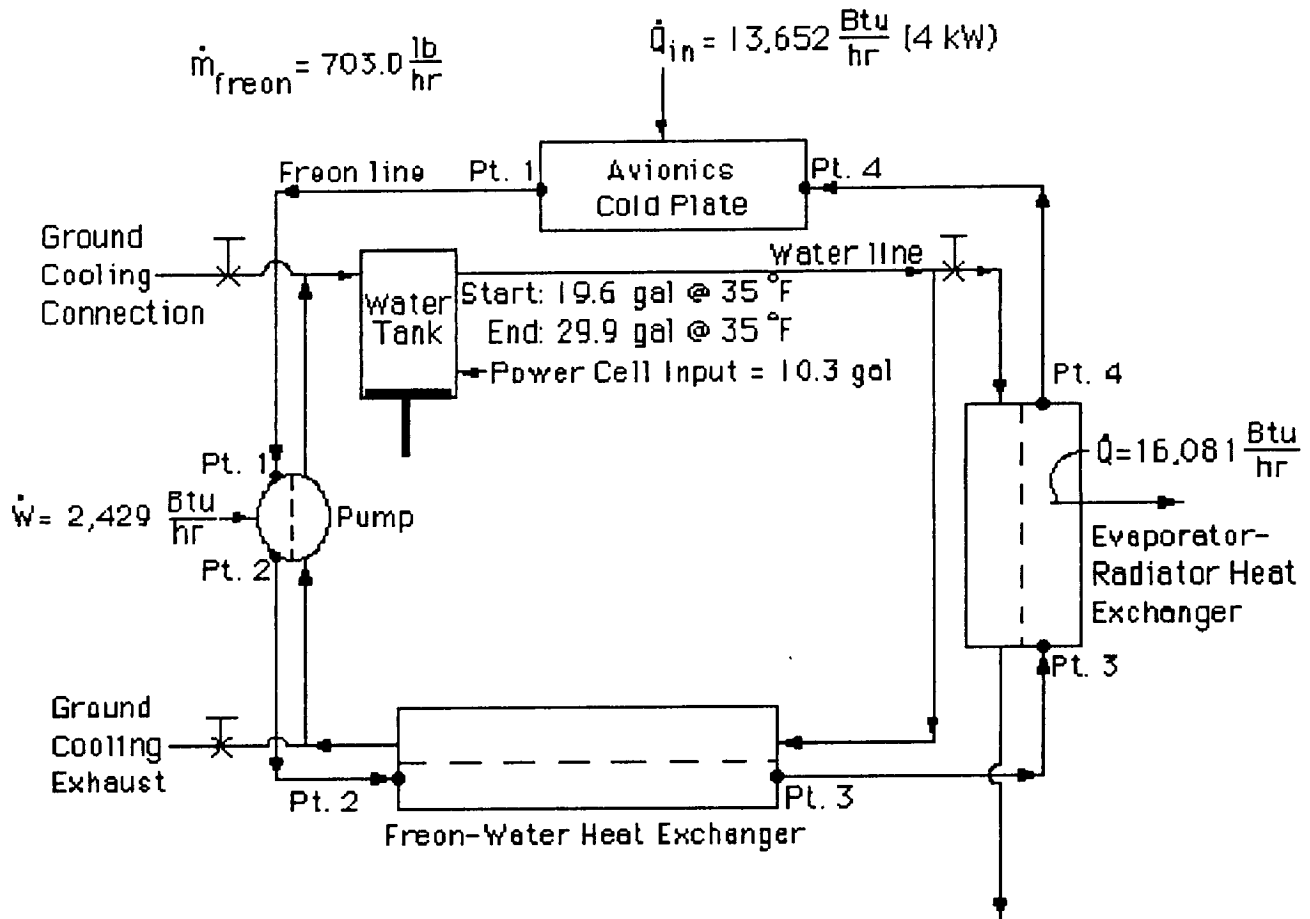
$$\text{evaporation rate} = \frac{(48,242.4 \frac{\text{Btu}}{\text{hr}})(12 \frac{\text{in}}{\text{ft}})^3}{(231 \frac{\text{in}^3}{\text{gal}})(1100 \frac{\text{Btu}}{\text{lb}})(64 \frac{\text{lb}}{\text{ft}^3})} = 5.1 \frac{\text{gal}}{\text{hr}}$$

$$\text{total water evaporated} = (5.1 \frac{\text{gal}}{\text{hr}})(1 \frac{2}{3} \text{ hr}) = 8.5 \text{ gal}$$

Energy rate required to return water temperature to 350°F

$$= \frac{(40,202 \frac{\text{Btu}}{\text{hr}})(\frac{1}{3} \text{ hr})}{(1 \frac{2}{3} \text{ hr})} = 8040.4 \frac{\text{Btu}}{\text{hr}}$$

Figure 7.2 Avionics Cooling, 20 min-2 hours into 24 hour Mission



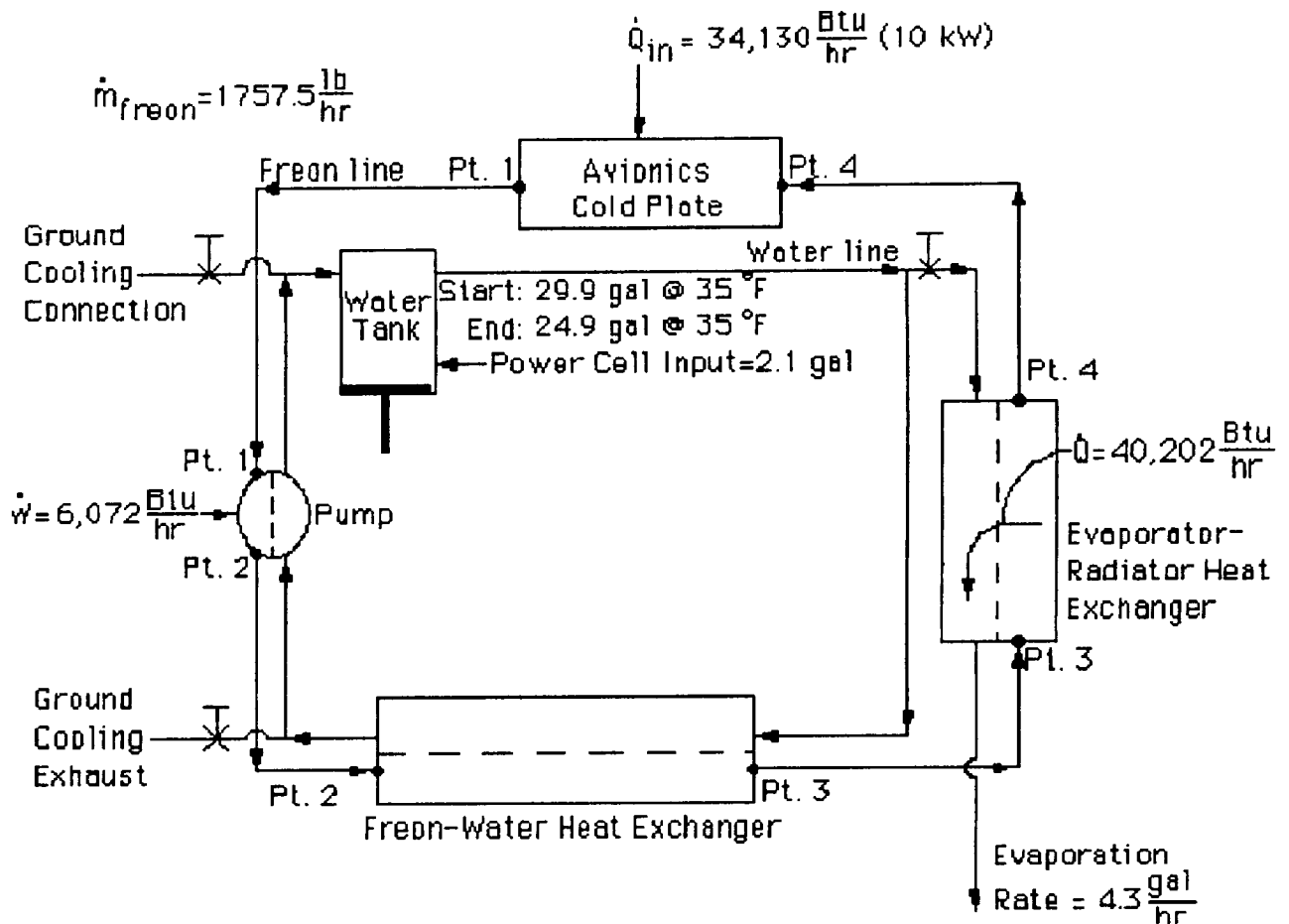
Point 1	Point 2	Point 3	Point 4
$p = 10 \text{ psi}$	$p = 200 \text{ psi}$	$p = 50 \text{ psi}$	$p = 15 \text{ psi}$
$T = 160.0^\circ \text{F}$	$T = 208.0^\circ \text{F}$	$T = 182.5^\circ \text{F}$	$T = 23.8^\circ \text{F}$
$h = 100.67 \frac{\text{Btu}}{\text{lb}}$	$h = 104.12 \frac{\text{Btu}}{\text{lb}}$	$h = 104.12 \frac{\text{Btu}}{\text{lb}}$	$h = 81.25 \frac{\text{Btu}}{\text{lb}}$

### Sample Calculations

$$\text{Radiator Area} = \frac{(16,081 \frac{\text{Btu}}{\text{hr}})}{(4.76\text{E-}13 \frac{\text{Btu}}{\text{ft}^2 \text{ s}^\circ \text{F}^4})(.8)(\frac{182.5+23.8+920}{2}^\circ \text{F})^4(3600 \frac{\text{sec}}{\text{hr}})} = 116.6 \text{ ft}^2$$

$$\text{Power Cell Input} = (1.1 \frac{\text{lb}}{\text{kW hr}})(4 \text{ kW})(20 \text{ hrs})(\frac{\text{ft}^3}{64 \text{ lb}})(\frac{12 \text{ in}^3}{\text{ft}^3})(\frac{\text{gal}}{231 \text{ in}^3}) = 10.3 \text{ gal}$$

Figure 7.3 Avionics Cooling, 2 hr-22 hours into 24 hr Mission



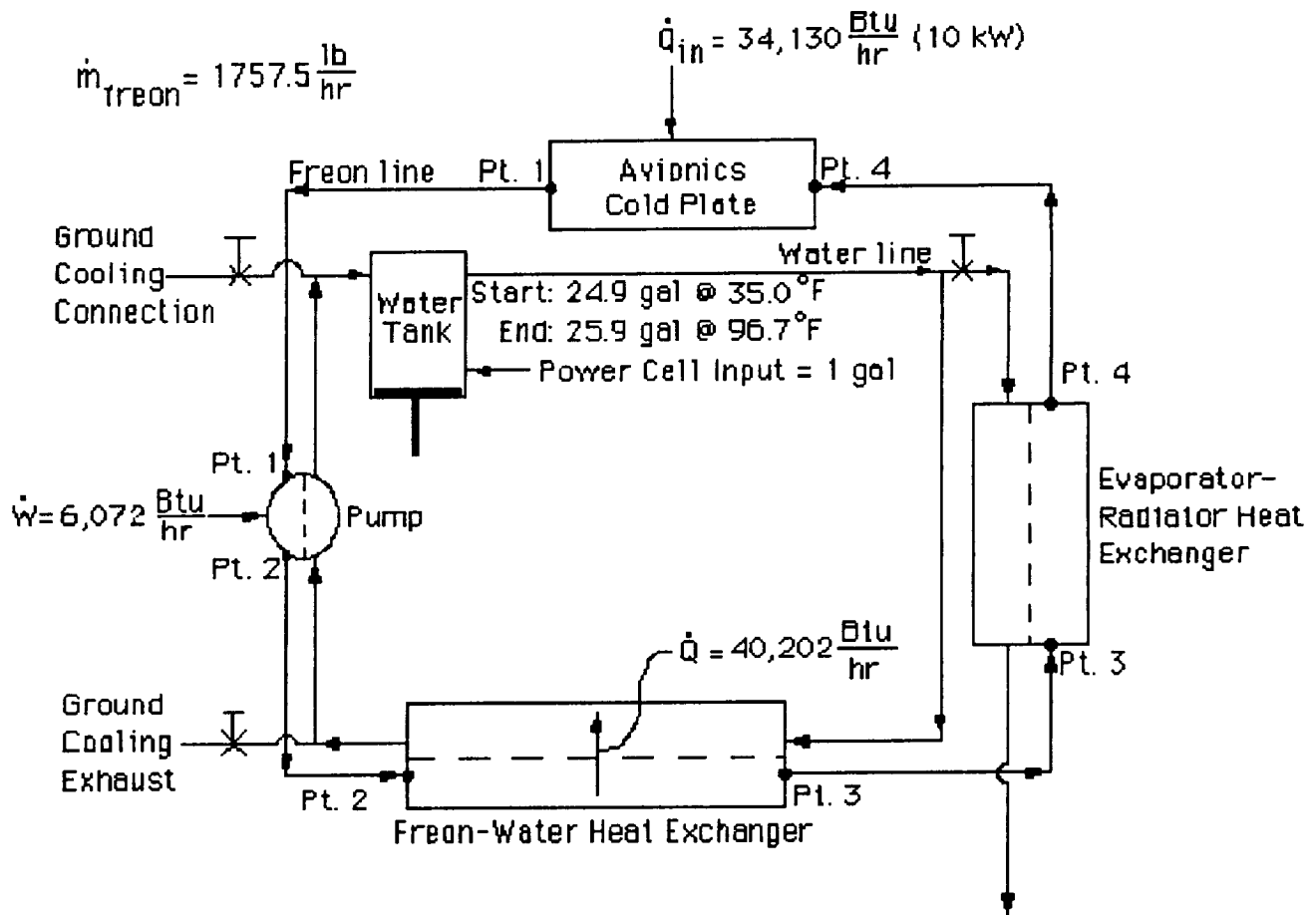
Point 1	Point 2	Point 3	Point 4
$p = 10 \text{ psi}$	$p = 200 \text{ psi}$	$p = 50 \text{ psi}$	$p = 15 \text{ psi}$
$T = 160.0^\circ \text{F}$	$T = 208.0^\circ \text{F}$	$T = 182.5^\circ \text{F}$	$T = 23.8^\circ \text{F}$
$h = 100.67 \frac{\text{Btu}}{\text{lb}}$	$h = 104.12 \frac{\text{Btu}}{\text{lb}}$	$h = 104.12 \frac{\text{Btu}}{\text{lb}}$	$h = 81.25 \frac{\text{Btu}}{\text{lb}}$

### Sample Calculations

$$\text{evaporation rate} = \frac{(40,202 \frac{\text{Btu}}{\text{hr}})(12 \frac{\text{in}}{\text{ft}})^3}{(231 \frac{\text{in}^3}{\text{gal}})(1100 \frac{\text{Btu}}{\text{lb}})(64 \frac{\text{lb}}{\text{ft}^3})} = 4.3 \frac{\text{gal}}{\text{hr}}$$

$$\text{total water evaporated} = (4.3 \frac{\text{gal}}{\text{hr}})(1 \frac{2}{3} \text{ hr}) = 7.1 \text{ gal}$$

Figure 7.4 Avionics Cooling, 22 hr-23 hours 40 minutes into 24 hr Mission



Point 1	Point 2	Point 3	Point 4
$p = 10 \text{ psi}$	$p = 200 \text{ psi}$	$p = 50 \text{ psi}$	$p = 15 \text{ psi}$
$T = 160.0^\circ \text{F}$	$T = 208.0^\circ \text{F}$	$T = 38.1^\circ \text{F}$	$T = 23.8^\circ \text{F}$
$h = 100.67 \frac{\text{Btu}}{\text{lb}}$	$h = 104.12 \frac{\text{Btu}}{\text{lb}}$	$h = 81.25 \frac{\text{Btu}}{\text{lb}}$	$h = 81.25 \frac{\text{Btu}}{\text{lb}}$

### Sample Calculations

$$\Delta T = \frac{(40,202 \frac{\text{Btu}}{\text{hr}})(12 \frac{\text{in}}{\text{ft}})^3 (\frac{1}{3} \text{ hr})}{(25.4 \text{ gal})(1 \frac{\text{Btu}}{\text{lb}^\circ \text{F}})(64 \frac{\text{lb}}{\text{ft}^3})(231 \frac{\text{in}^3}{\text{gal}})} = 61.7^\circ \text{F}$$

$$T_{\text{final}} = 35^\circ \text{F} + 61.7^\circ \text{F} = 96.7^\circ \text{F}$$

Figure 7.5 Avionics Cooling, 23 hr 40 min-touchdown for 24 hr Mission

During a 48 hour mission, the avionic power cells would provide an additional 12.3 gal of water with a final water temperature of 77 deg F after touchdown.

### **7.3 Cargo Bay Heating Loads and Protection**

A major change from the previous Biconic study was the decision to use a warm structure. This means that the maximum temperature that the structure experiences will be 550 deg F approximately 1 hour after the launch/deorbit phase. This has affected virtually all subject areas of thermal design. Because of this, thermal protection must be provided to the structure to protect the cargo and internal components from excessive heat loads. Since the PLOG/UNPLOG is the primary cargo, this was used to set the maximum heat loads that the cargo could tolerate. The PLOG/UNPLOG should be designed to withstand, at a minimum, the heating loads experienced from the sun (about 440 Btu/hr/sq. ft). This value was chosen as the maximum heat load that would exist in the cargo bay. Little information was found about the PLOG/UNPLOG insulation, with the exception of 4.50 inches of unknown material around the periphery. For this analysis, the material was assumed to have properties similar to Advanced Fibrous Refractory Strain Insulation (AFRSI). This analysis was analytical in nature with the following additional assumptions:

- Conductive and convective heat transfer between the CRV insulation and the PLOG/UNPLOG insulation was negligible(See Figure 7.6)(ref 7.3,7.5).
- PLOG/UNPLOG insulation is heated uniformly with no thermal gradient.
- Conductive and radiative heat transfer occurs between flat planes.

Based on these assumptions, a computer program was written to solve for the temperatures and heat loads that the cargo bay/PLOG/UNPLOG experienced. (See Figure 7.7) Several materials were evaluated, with a .375 inch thick Q-fiber insulation chosen for its low weight. This resulted in 125 lbs of insulation for the cargo bay (ref 7.4).

Due to the unique analysis involved and the time required to program and calculate insulation thicknesses for each individual component,

For low-density conductive heat transfer

$$\begin{aligned} \frac{\dot{Q}}{A} &= k \frac{(T_1 - T_2)}{L} \\ &= (.00534) \frac{(470)}{(1)} \\ &= 2.5 \frac{\text{Btu}}{\text{hr ft}^2} \end{aligned}$$

where k = Thermal conductivity for air  
 $= .00534 \frac{\text{Btu}}{\text{hr ft}^\circ\text{F}}$

$T_1$  = Structural temp. = 550°F  
 $T_2$  = Minimum PLOG/UNPLOG surface temp  
 $= 80^\circ\text{F}$   
L = Gap between structure and PLOG/UNPLOG  
 $= 1 \text{ ft}$

For radiative heat transfer

$$\frac{\dot{Q}}{A} = \sigma E (T_1^4 - T_2^4)$$

where  $\sigma$  = Stefan-Boltzman constant  
 $= 4.76\text{E-}13 \frac{\text{Btu}}{\text{ft}^2 \text{ s}^\circ\text{R}^4}$   
 $E = .8$

$$\begin{aligned} \frac{\dot{Q}}{A} &= (4.76\text{E-}13)(.8)(1010^4 - 540^4)(3600) \\ &= 1310 \frac{\text{Btu}}{\text{hr ft}^2} \end{aligned}$$

For convective heat transfer

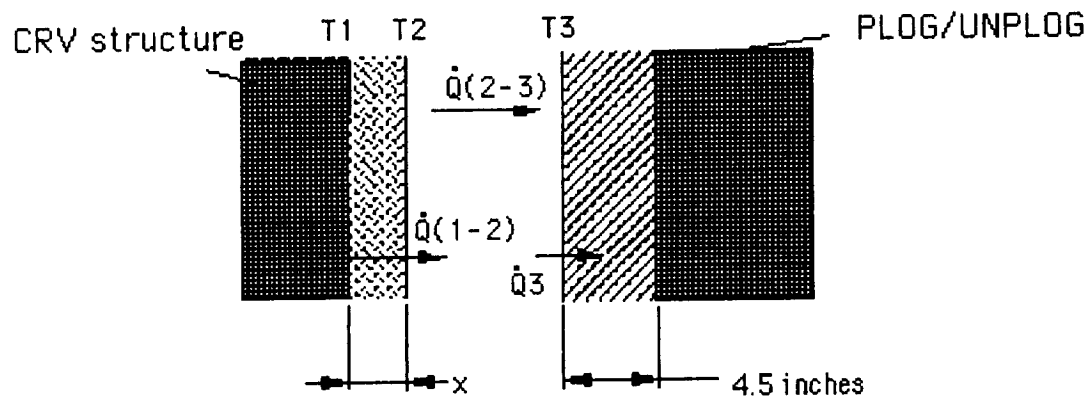
$$\begin{aligned} \frac{\dot{Q}}{A} &= h(T_1 - T_{aw}) \\ &= 0 \end{aligned}$$

where h = enthalpy  
 $= (\rho)(c_p)(u)(St)$   
 $= 0 (u = 0)$

So of the three forms of heat transfer, radiation is dominant.

Figure 7.6 Negligible Heat Transfer Assumptions

an assumption was made that an additional 300 lbs of insulation would be sufficient to protect all other internal components.



From heat transfer (radiation)  $\frac{\dot{Q}_{2-3}}{A} = \epsilon E (T_2^4 - T_3^4)$

From heat transfer (conduction)

$$\frac{\dot{Q}_{1-2}}{A} \approx k \frac{(T_1 - T_2)}{x}$$

From thermodynamics of incompressible substances

$$\frac{\partial u}{\partial t} = mc \frac{\partial T}{\partial t} = \dot{Q}_3$$

$$\frac{\dot{Q}_{1-2}}{A} = \frac{\dot{Q}_{2-3}}{A} = \frac{\dot{Q}_3}{A}$$

$$\implies k \frac{(T_1 - T_2)}{x} = \epsilon E (T_2^4 - T_3^4) = \frac{mc}{A} \dot{T}_3$$

since  $m_{\text{PLOG/UNPLOG}} = (\text{area})(\text{skin thickness})(\text{density})$

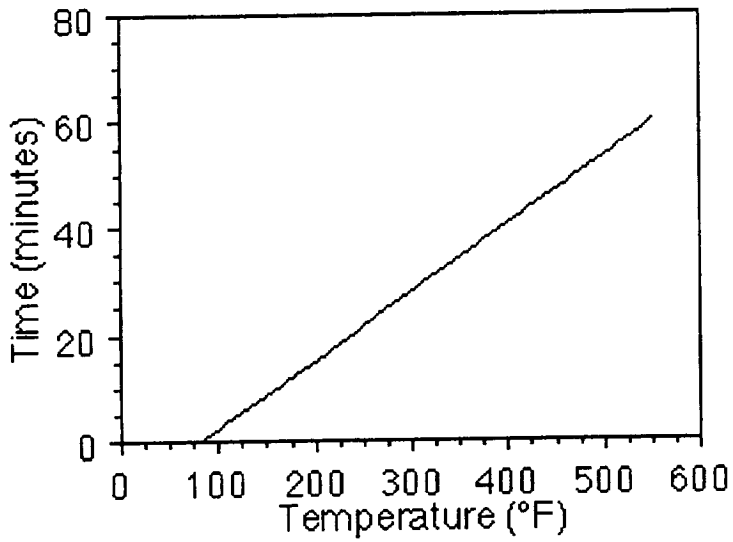
$$\implies k \frac{(T_1 - T_2)}{x} = \epsilon E (T_2^4 - T_3^4) = (\text{density})(\text{thickness})(c)\dot{T}_3$$

Structure temperature was assumed to increase from 80°F to 550°F in 1 hour. Density not known for this analysis so AFRSI material properties were assumed. Several materials were evaluated for total weight. Q-fiber (density=.0017 lbs/in<sup>2</sup>) was selected.

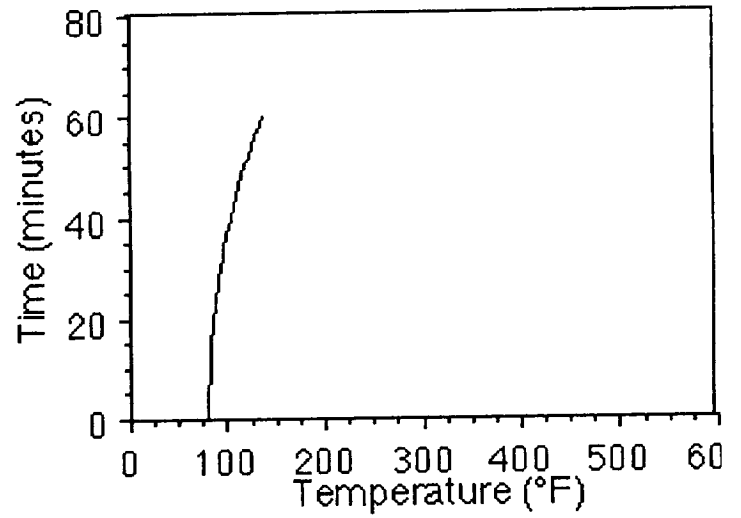
Figure 7.7 PLOG/UNPLOG Heating Rates

- where  $\dot{Q}$  = Heating Rate ( $\frac{\text{Btu}}{\text{s}}$ )  
 $A$  = Area (ft<sup>2</sup>)  
 $\epsilon$  = Stefan-Boltzman constant  
 $= 4.76 \times 10^{-13} \frac{\text{Btu}}{\text{ft}^2 \cdot \text{s} \cdot \text{R}^4}$   
 $E$  = Emissivity = .8  
 $T$  = Temperature °R  
 $k$  = Material thermal transfer coefficient  
 $x$  = Insulation thickness  
 $m$  = Mass  
 $t$  = Time  
 $c$  = Material specific heat  
 $u$  = Internal energy

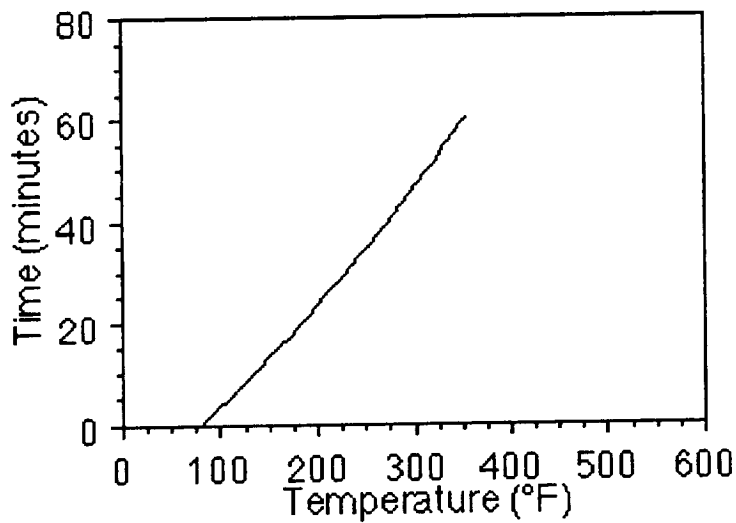
T1 vs Time



T3 vs Time



T2 vs Time



dQ/Dt vs Time

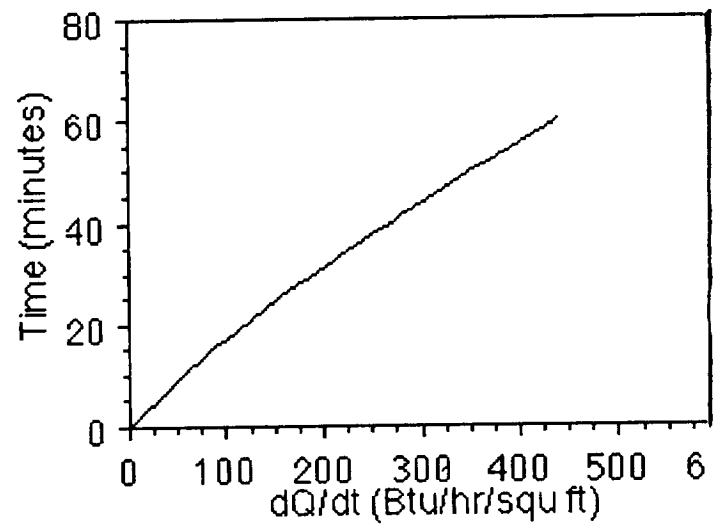


Figure 7.7 (continued)

## **7.4 Trajectory Heating Analysis**

The trajectory to be used during descent is one that was generated by the Reentry Dynamics group by using a NASA/Martin Marietta program called IMP. Then using a conversion program, the output trajectory file from IMP was transformed into a form that MINIVER could use, which was a NASA/Remtech computer program and was the heart of the heating analysis. This program required the user to model the vehicle as one of the choices given in the program (wedge, cone, etc.) and allowed the user to enter particular TPS (LI-2200, FRCI, etc.) to be used. The program would then find the point on the model that became the hottest during the given trajectory and find all relevant data about that point such as: maximum temperatures, heat rates, heat loads, etc. Then with the given information, the user could see if a particular TPS entered would be safe or if it would have to be scaled up or down. Once the TPS was shown to be adequate, a relatively accurate analysis could be made on materials, thicknesses, weights, and attachment methods to be used every where else on the vehicle. Since the MINIVER program is extremely complicated, the full potential of the program was not explored as time became a problem. However, excellent-relevant data was generated and that information was the basis for the final analysis.

## **7.5 Control Surface Heating**

During reentry, the vehicle tends to incur the greatest heating on areas where there is a small leading edge radius (Ref. 7.2). Therefore, the largest heat rates occur on the nose and leading edges of the control surfaces of the BICONIC CRV. As a result, these were the two areas modeled in MINIVER and the data generated was used to find the materials, thicknesses, and attachment methods required for these two areas.

According to MINIVER, it was found that the maximum heating occurs roughly mid way through the reentry trajectory.

A graph of Time VS. Temperature for the BICONIC CRV can be seen in Figure 7.8, which shows this occurrence. In addition to the high temperature at this time, the vehicle experiences a Mach number of 22.03, heat rate of 42.24 BTU/SFT-S, heat load of 3597 BTU/SFT,

and pressure of 115.8 lb/SFT. This is a critical time for the TPS since it has to withstand so many extrema and still protect the vehicle. Therefore, this point during reentry was critical in TPS design.

### Time VS. Temperature

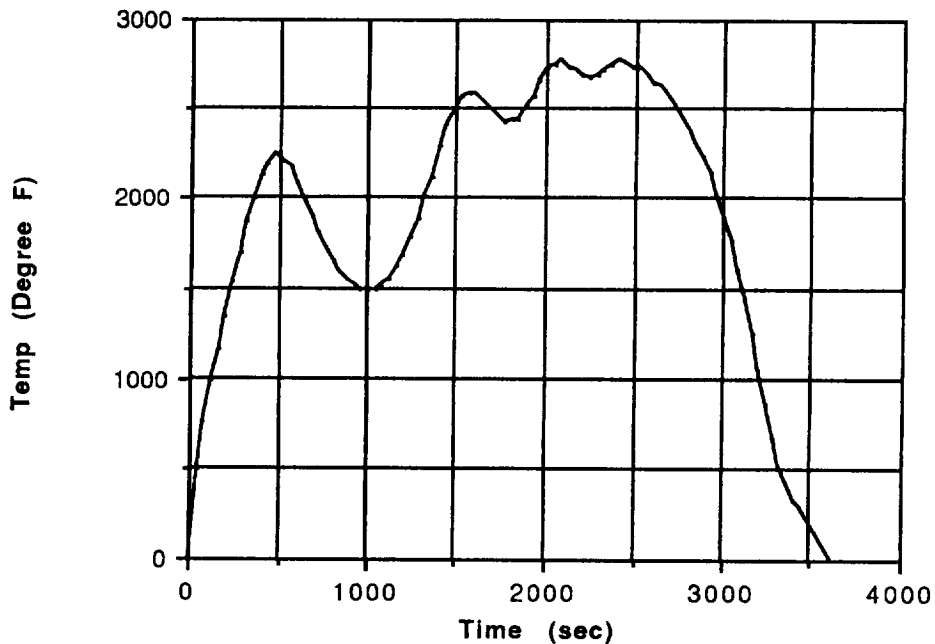


Figure 7.8 Time vs Temperature Plot

With the maximum temperatures of the nose and control surface leading edge known, the TPS was designed and entered into MINIVER to see if it would hold up under the given conditions. Then once it was found to be adequate, the material and thickness were known for these areas. The TPS was then designed for the rest of the vehicle by approximating the temperature decrease as one moves toward the rear of the vehicle and scaling the materials and thicknesses accordingly. A complete list of materials and thicknesses can be seen in Section 7.6.

## 7.6 Materials and Weights

There were a number of different materials considered for use, but only three were ultimately chosen. These materials were chosen according to three categories: weight, temperature resistiveness, and cost. MINIVER found the maximum temperature to be 2775

degrees Fahrenheit, which is within the maximum temperature of the best material selected. Then, once this was known, a precise layering of materials was designed for use in the nose (where heating is greatest) using the EXITS subroutine of MINIVER. Since MINIVER would only calculate information for the point on the vehicle that was the hottest, an approximation method was developed to design the TPS for the rest of the vehicle. The following description is a detailed summary of the TPS, excluding the weights and total square footage (see Figure 7.9):

-LI-2200(Lockheed Insulation): This material is to be used in the nose cap and control surface leading edges. The tiles will be basically 6 square inches in area, but trapezoidal in shape. They will be inclined at 18 degrees to the airflow. The thickness will vary from 2.5 inches in the flow stagnation area to 2.0 inches at the LI-2200/FRCI interface along the bottom surface. At the upper surface it will vary from 2.5 inches at the stagnation point to 1.5 inches at the LI-2200/TABI interface.

-FRCI(Fibrous Refractory Composite Insulation): This material will extend from the nose cap to first BICONIC bend on the underside of the vehicle. It will also cover the remaining area on the control surfaces. The tiles will be 6 inches by 6 inches square at 18 degrees to the airflow. The thickness will vary from approximately 2.0 inches at the LI-2200/FRCI interface to 1.5 inches at the FRCI/TABI interface.

-TABI(Tailorable Advanced Blanket Insulation): This material will cover the remaining vehicle area. The tiles will be approximately 2 foot by 2 foot square, and will be inclined at 18 degrees to the airflow. The thickness along the upper and lower surfaces will vary from approximately 1.5 inches at the LI-2200-FRCI/TABI interfaces to a minimum of .75 inches.

The tiles will vary in thickness as determined by local temperatures, which will require tapering the tiles. In addition, a Strain Isolator Pad (SIP) will be used between two layers of RTV-560 adhesive to allow some tile movement due to thermal expansion. As result of designing a complete list of materials, thicknesses, and designated areas, a total TPS weight break down was achieved. Both a table of Material Properties and weight can be found in Table 7.1.

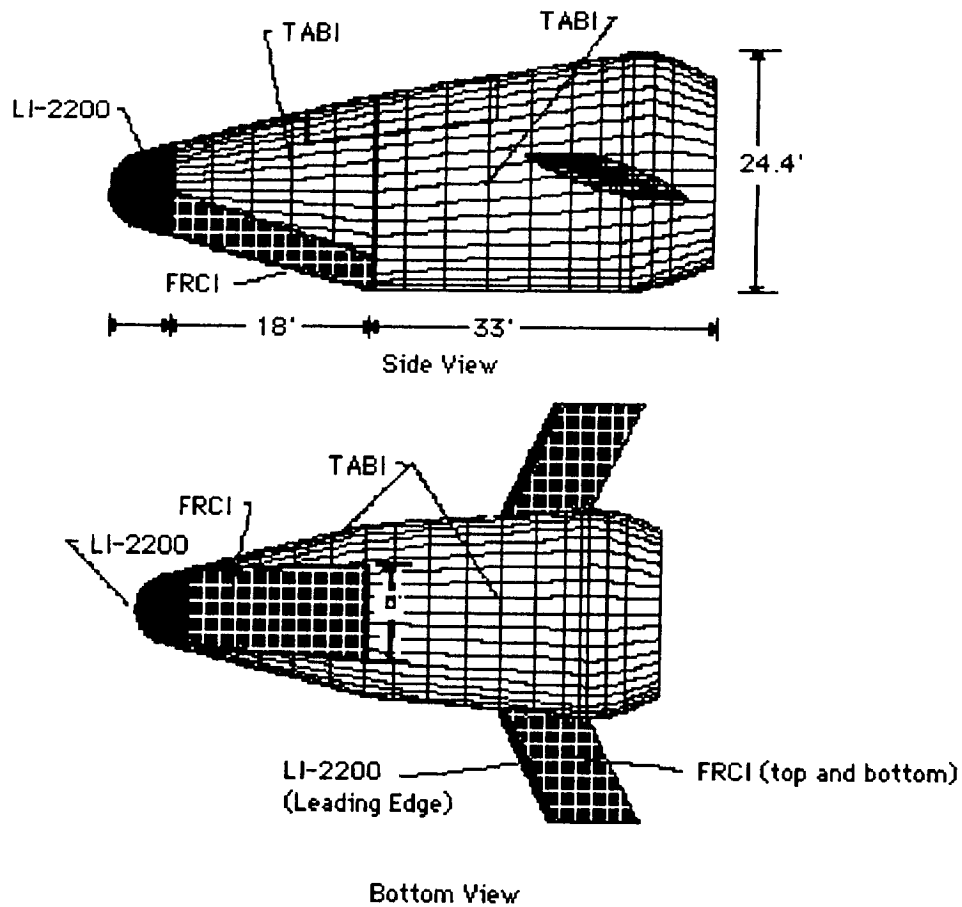


Figure 7.9 Material Placement

Density (lb/ft <sup>3</sup> )	Thickness (in)	Area (ft <sup>2</sup> )	Material	Weight (lbs)
22	2.5	100.5	Nose LI-2200	461
22	2.5	89	C.S. LI-2200	409
11	2.5	176	Body FRCI	403
7.3	2.0	456	C.S. FRCI	836
7.3	1.5	2028	1st Cone TABI	1851
7.3	.75	4644	2nd Cone TABI	2119
5.2	1.0	468	Tail TABI	284
5.2	.5	100.5	Nomex Nose	22
5.2	.5	176	Nomex Body FRCI	36
5.2	.5	89	Nomex L.E. C.S.	19
5.2	.5	456	Nomex C.S. FRCI	100
				Total 6666 lbs

Table 7.1 Material Properties and Weights

In addition to the materials mentioned earlier, there were also two materials which were designed to fill the gaps between tiles. These materials were the Ames Gap Filler and the Pillow Gap Filler, and each of these were to be used in only specified interfaces of tiles. The Ames Gap Filler was to be used only in the LI-2200/FRCI interface and the Pillow Gap Filler in the LI-2200/TABI and FRCI/TABI interfaces. The reasoning for this stems from the fact that TABI is so pliable that the Ames Gap Filler doesn't seem to fill in the "cracks" as well as the Pillow Gap Filler. Furthermore, the Pillow Gap filler cannot withstand the heat at the LI-2200/FRCI interface. A pictorial representation of these two gap fillers can be seen in Figure 7.10.

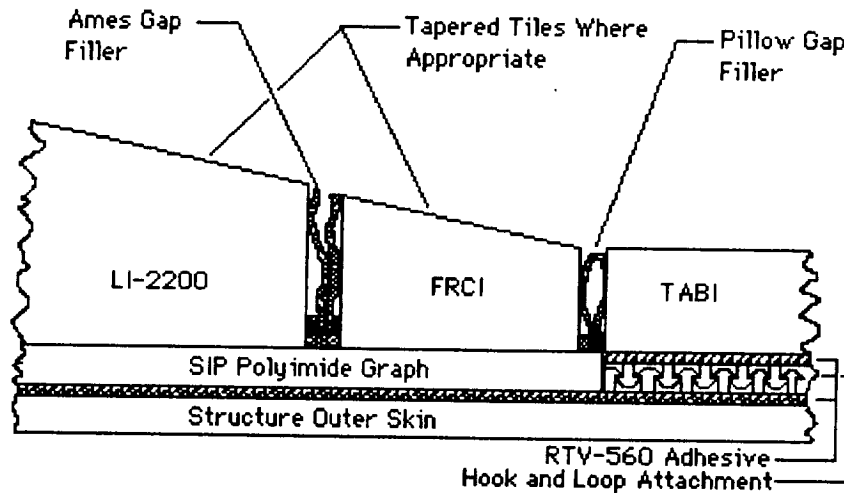


Figure 7.10 Materials and Attachments

In addition to designing the TPS, a protection system had to be found for the Advanced Recovery System (ARS) cables since they will be mounted on the outside of the vehicle (where heating is greatest). In order to compensate for this, the cables are recessed a little inside the TPS and protected all around by the various TPS materials. The cable is held in place (prior to deployment of ARS) by high temperature metal clasps and they themselves are held by a high temperature bolt. As a visual aid, Figures 7.11, 7.12, and 7.13 show three different views of the system.

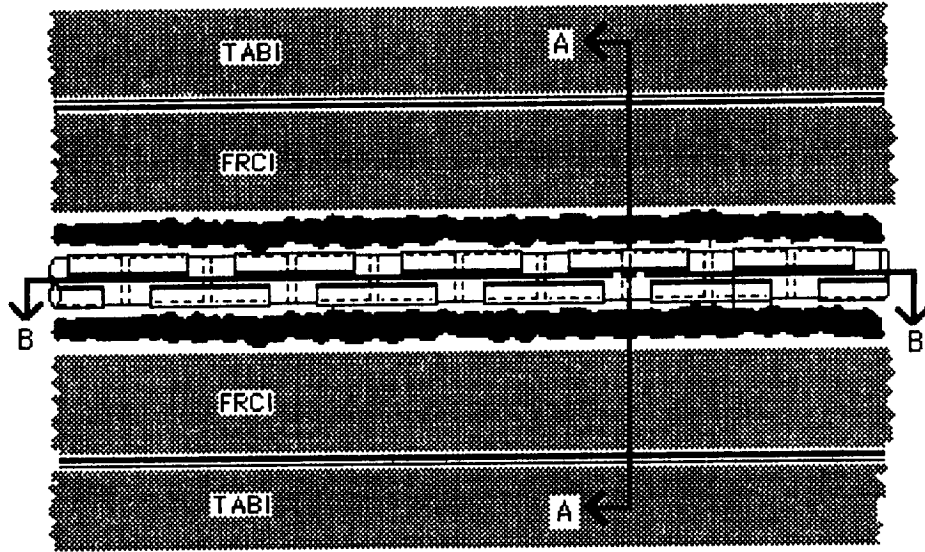


Figure 7.11 ARS Cable Attachment

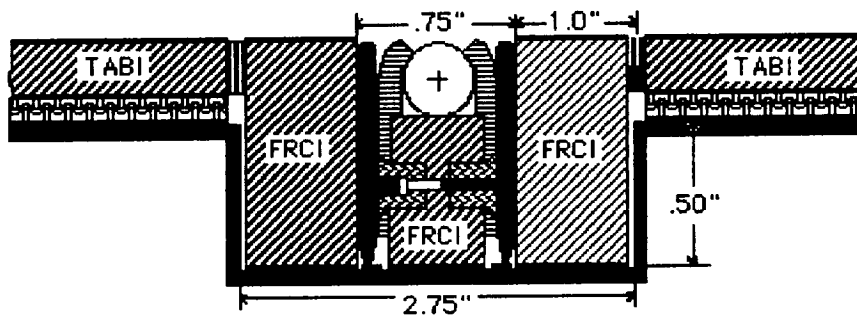


Figure 7.12 Section A-A

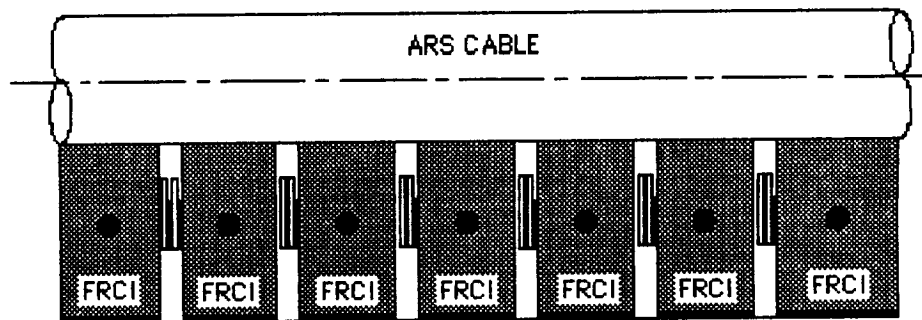


Figure 7.13 Section B-B

## **7.7 Attachment Methods**

During the study a number of attachment methods have been discussed and their respective advantages and disadvantages shown. These methods ranged from adhesives to mechanical fasteners. After viewing the given information, two types have been chosen for their strength, reusability, and cost effectiveness. Both of the methods will be used on a specified portion of the vehicle as determined by their strength, and temperature resistiveness as follows:

-RTV-560: This adhesive will be used on the nose cap and control surfaces due to their high heat loads. RTV-560 performs well under this high temperature and is very cost effective. In addition, RTV-560 will also be used in the cargo bay for the attachment of insulation around the P-log and Avionics. Although insulation replacement is more difficult with this type of attachment method, its low cost makes it a good choice.

-Hook and Loop: This will be used on the remaining surface of the vehicle where both temperature and stresses are low. Specifically, this method will only be used under the TABI insulation and RTV-560 will bond the Hook and Loop to TABI and vehicle skin. The advantage of this material is that it allows for very easy removal and reattachment of TPS blankets and tiles while maintaining a fairly good strength rating. However, some development must be done to improve its material properties, but does not pose a problem at this time. (Diagrams of both attachment methods can be seen in Figure 7.10)

When the vehicle returns from orbit, there will be the chance that some TPS tiles may be lost (as is the case with the shuttle) or that they might have to be removed for maintenance reasons.

Furthermore, since the tiles will vary in material, thickness, and attachment method, replacing tiles will be difficult and time consuming. To reduce this problem, a grid system will be used (similar to that used on the shuttle) which allows replacement of a

damaged or lost tiles easily. The user will only be required to know the number of the tile and all information necessary for replacement will be known. An additional time saving benefit that will result from the use of the grid system is that the tile dimensions will only have to be checked by their ability to fit in the required tile-to-tile gaps rather than checking each tile individually. This will save both time and money prior to launch time. A graphical representation of this system can be seen clearly in Figure 7.14. As a further protection against tile loss, the tiles will be aligned at 18 degrees to the airflow. By positioning the tiles in this manner, the airflow cannot get into the seems and possibly lift the tiles off. A pictorial representation of this alignment can be seen in Figures 7.14 and 15.

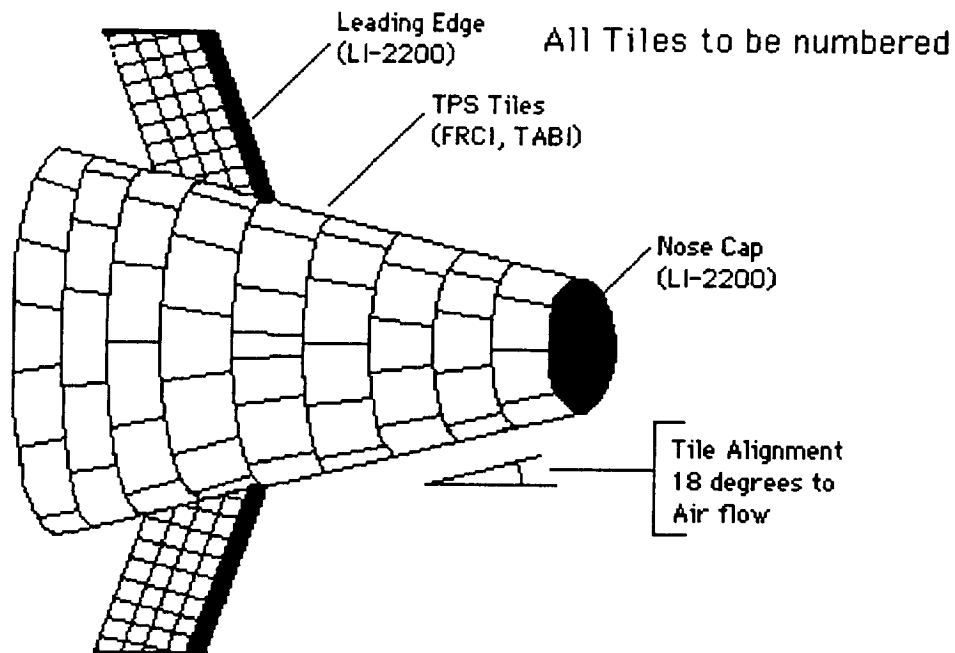


Figure 7.14 TPS Grid System of Attachment

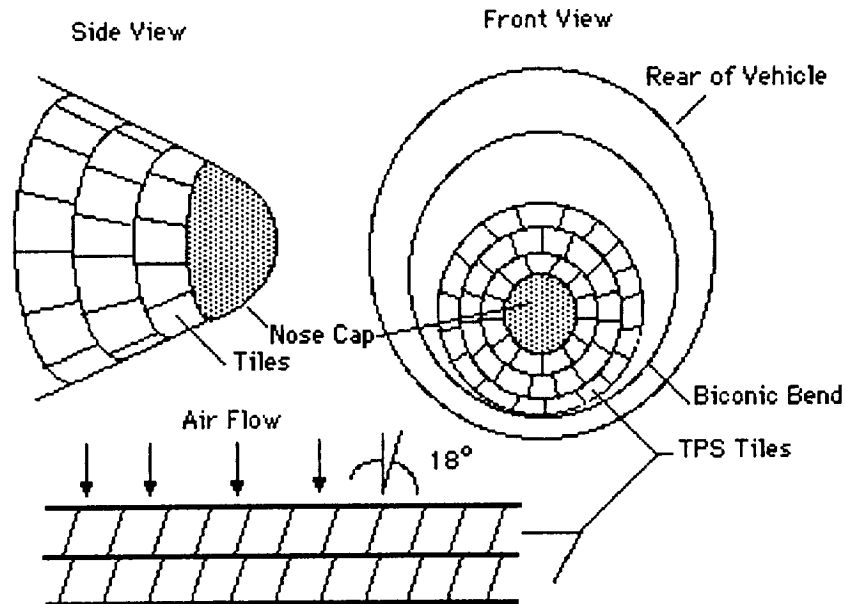


Figure 7.15 Tile Gap Placement and Proximity with Respect to Flow

## **7.8 Structure Type**

### **7.8.1 Hot Structure**

At the beginning of this study, NASA expressed an interest in the utilization of a hot structure for the Cargo Return Vehicle. Hot structure, unlike cold structure, requires no external insulation to protect the structure. The structure itself must be fashioned out of a material with a high enough heat capacity to absorb the entire thermal load encountered during ascent/descent.

The Thermal Control Group eliminated hot structure from the possible material selections for the following reasons :

- Increased cost due to the use of composite structures
- A lack of information on hot structures, due to the classified status of hot structure research
- Increased heating of internal components will be realized.
- Thermal gradients which exist at the outer metallic surface may produce warping, which may increase localized heating,

and may adversely effect the aerodynamic, control, and stability qualities of the CRV (ref 7.14).

### **7.8.2 Warm Structure**

Research into the use of hot structures led to the selection of a warm structure, a compromise between hot and cold structure. Unlike cold structure, a maximum temperature limit of 550°F is set for the primary structure (cold structure maximum temperature =350°F). External insulation is still required to keep the structure to this temperature limit. This temperature limit of 550°F increases the weight savings of the CRV, due to the lesser amount of insulation required, and the use of lighter weight composites for the primary structure.

## **7.9 Seals**

Because the CRV uses a warm structure with a maximum structure temperature of 550°F, some of the seals which exist for cold structure have been redesigned to meet the new criteria.

### **7.9.1 Landing Gear Door Seals**

High temperature seals are required for the landing gear doors, which are located along the bottom of the CRV (Figure 7.16). The maximum temperature which will be encountered by these doors occurs at the nose landing gear door, where the surface temperature is approximately 1400°F. With gap heating, the temperature which will be encountered by the seal will be around 1800°F (ref 7.1).

The seals which will be installed on the landing gear doors are a simple metallic type, similar to that used to prevent leaking through gaps between the split rudder and speed brake on the Space Shuttle (Figure 7.17).

When the landing gear doors are retracted, the door will move towards the structure surface, and the U-shaped seal will be compressed, providing a thermal barrier good up to 1900°F, well above the estimated temperatures of 1400°F.

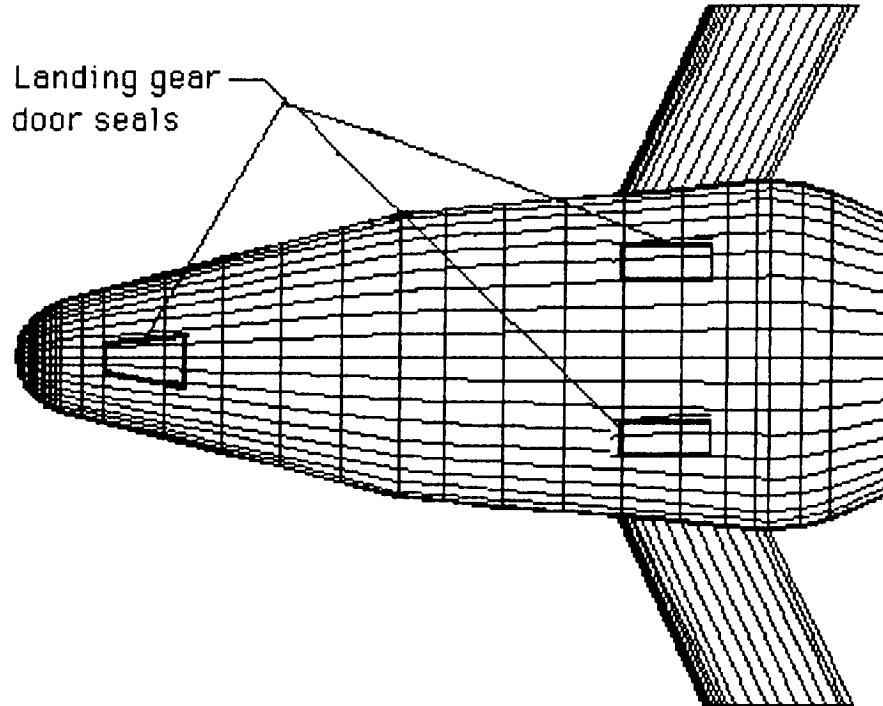


Figure 7.16 Landing gear door seals

The barrier consists of a series of U-shaped Inconel strips which are electroplated with silver to increase the sealing properties at high pressures and in vacuum. The strips are installed along the entire perimeter of the landing gear door. Each strip is secured by bolts to the landing gear door. High temperature insulation lining (glass-fiber) will be installed on both the door and the structure to prevent gas from leaking into the landing gear cavity. Each section of the seal is fastened to the next by a tab, which is spot welded to the next. The upper contact point of the seal consists of a Inconel honeycomb panel with Q-fiber internal insulation. This panel protects the primary structure from hot vapors which may leak past the seal on the outer side (ref 7.2).

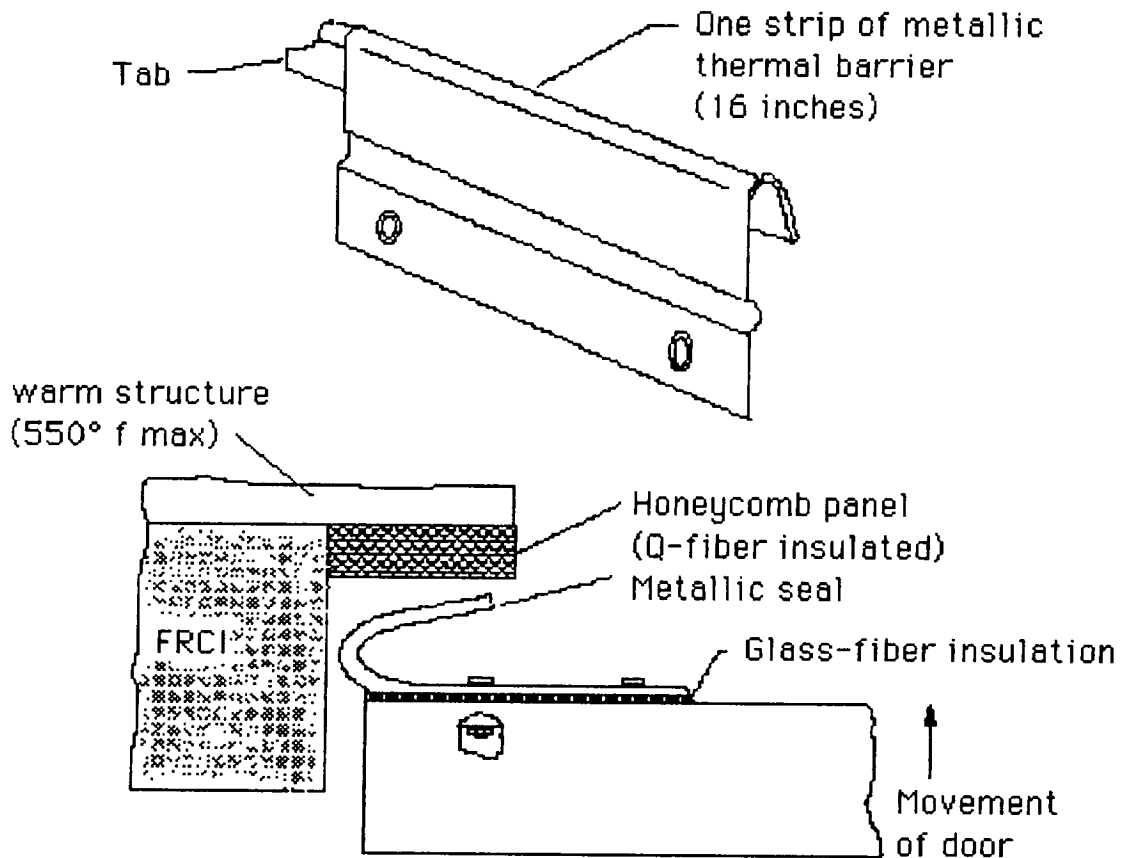


Figure 7.17 Landing gear door seal

### **7.9.2 Cargo Bay Door/Docking Ring Door Seals**

A flexible pile thermal barrier will be used to insulate the both the cargo bay door/cargo bay interface area and the docking ring bay/door interface area (Figures 7.18, 7.19). This brush-like material is made with fiberglass strands set into a base of ceramic fiber. The unique feature of this seal is its ability to insulate large gaps required for the movement of the cargo bay doors during PLOG/UNPLOG loading and unloading. Gaps of up to 1.0 inch can be safely sealed using this design (ref 7.2).

Because the docking ring door must be opened for docking maneuvers, this seal will also be utilized in the docking ring

bay/door area. With safe sealing of up to 1 inch gaps, larger tolerances are allowable, and the need for inspection of the seals while in space is unnecessary.

The maximum temperature which will be encountered in these areas of the CRV during ascent/descent will be approximately 800°F. This seal has a maximum temperature limit of 900°F, well above the encountered temperatures (ref 1).

### **7.9.3 ARS Bay Doors**

A flexible seal will be used to insulate the ARS bay door/bay interface (Figure 7.18). Because the ARS bay doors will not be opened in space, a flexible thermal pile barrier like that used in the cargo bay doors will not be used. Instead, a flexible heat seal will be used (Figure 7.20).

Because the ARS bay sits forward of the cargo bay and docking ring bay, larger heating rates will be encountered (ref 7.1). The flexible seal can withstand temperatures of 1950°F on one side while maintaining the temperature on its cool side at less than 350°F. These insulating qualities will be suitable for the ARS bay, where a maximum temperature of 1400°F is

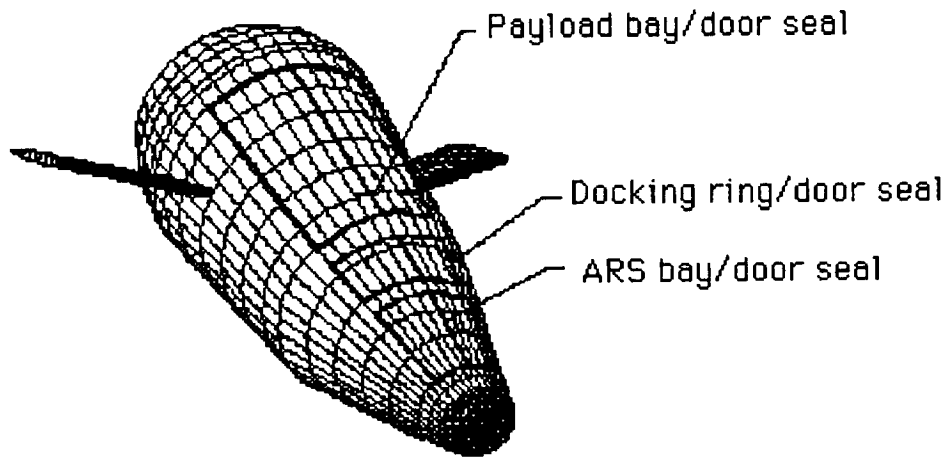


Figure 7.18 Payload bay/Docking Ring bay/ARS bay seals

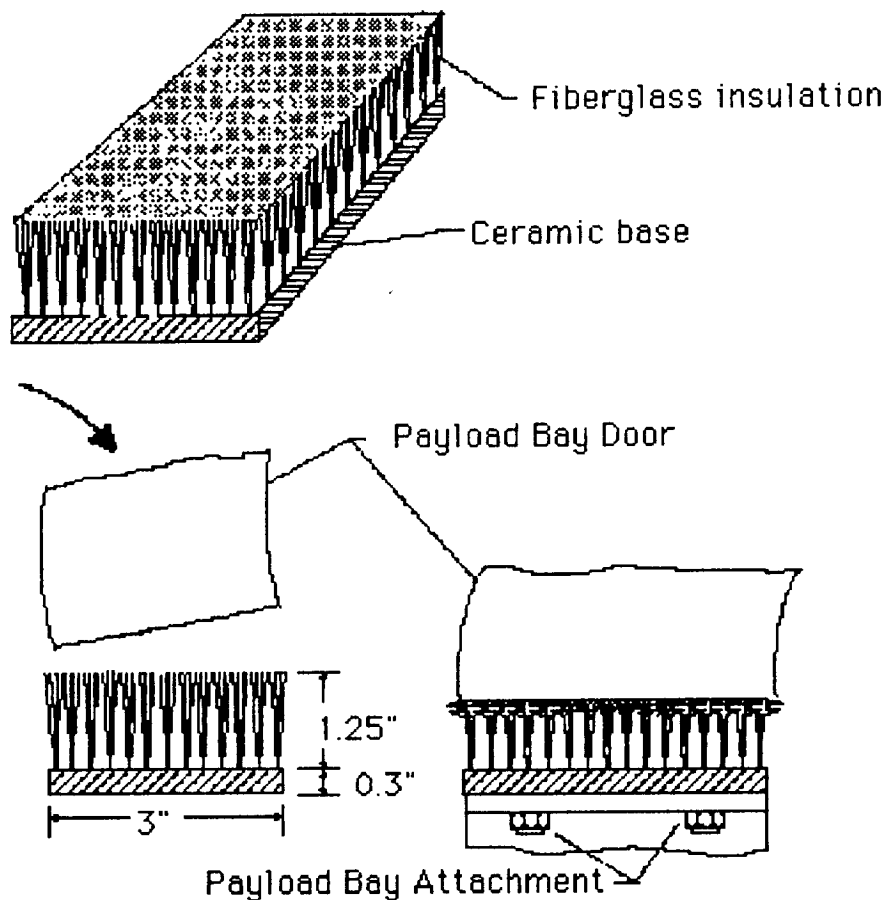


Figure 7.19 Cargo bay/Docking Ring bay seals

encountered. Because the seal also can maintain a temperature of 350°F on the inner side, protection will be provided for both a kevlar recovery system and a nylon system.

The core of the tube is filled with alumina/silica batting for heat insulation. The batting is held in a sheath of knit iron/nickel-alloy wire, which gives the necessary strength, flexibility, and resilience. A ceramic-fiber sleeve is braided snugly around the wire sheath for further insulation, and the sleeve is enclosed in a glass-fiber cover coated on the outside with a layer of silicone (ref 7.2).

The tube is held in place by a ceramic retaining strip on both the ARS door and ARS bay sides. The seal nests between the ceramic strips with the end flaps of the outer covering held in place by the tensioning rod. This seal allows movement of the doors, because the seal will deform with relative motion of either surface.

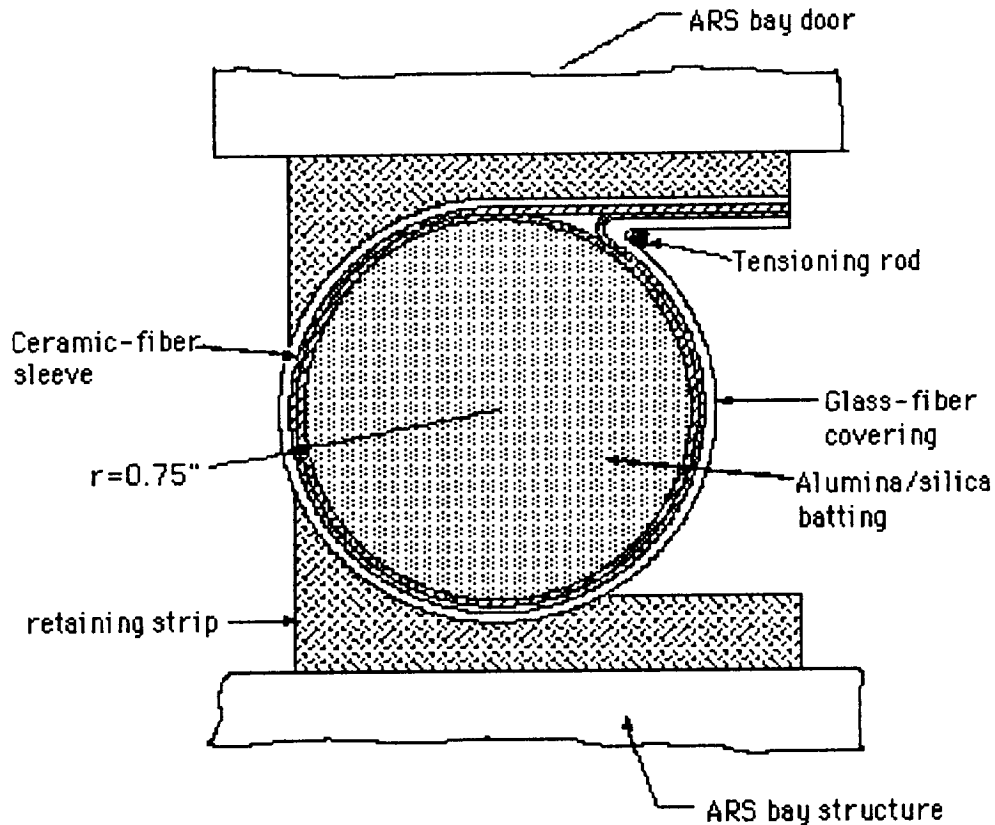


Figure 7.20 ARS seal

At ARS deployment, the seals will be broken at the retaining strip/ seal interface. Because the seal and bottom retaining strip are fastened to the ARS bay structure, the upper retaining strip, fastened to the ARS door, creates a snug-fitting friction fit with the upper side of the seal. Upon deployment, the retaining strip moves away from the seal, with the ARS door.

## **7.10 Space Debris**

The space debris environment is made up of different size, velocity, and material particles generated by collisions and explosions of satellites, rocket motor casings, etc. The number of space debris particles in orbit is directly related to the number of launches into space. Because the world launch rate is increasing, the amount of space debris is also increasing, becoming an important factor in the design of space vehicles.

### **7.10.1 Meteoroid Analysis**

The largest threat to spacecraft is from the more numerous cometary meteoroids which may be considered as loosely packed ice, having a density of .5 ounces per cubic inch, and an average impact velocity of 10 miles per second. The average flux is given by the equation :

$$\text{Log } F = -6.20 - 3.66 \text{Log } (D/.3937)$$

where D is the diameter of the impact particle (in). This relation is shown in Figure 7.21. Assuming a minimum particle diameter of .004 inches, the number of CRV impacts is:

$$\text{Impacts}(\text{total}) = .0019 \text{ impacts/operational life (1 in 500 flights)}$$

There is less than a 0.19% chance of space debris penetration of the CRV during its lifetime, assuming a minimum particle diameter of 0.004 inches (ref 7.12).

### **7.10.2 Space Debris Shielding**

For space debris protection, the best theory for protection to date is that of a 'bumper,' or protection shield (see Figure 7.22). The shield vaporizes the incident meteoroid as shown in the drawing. Typically, several centimeters behind bumper is the main shield which must absorb the resultant blasts. Due to the ability of this two wall system to spread out the damage over a wide area on the wall, the areal density of the bumper system is much less than a single wall system which will defeat the same particle. Experiments indicate that an aluminum bumper should be from .1 to .25 times the thickness of an incident aluminum particle. Bumpers of other materials

may be used but should have approximately the same areal density (ref 7.12).

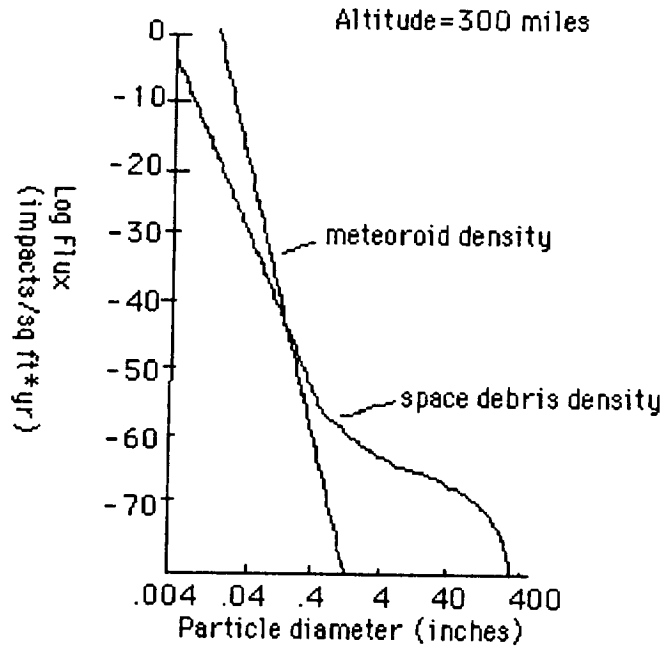


Figure 7.21 Space debris density

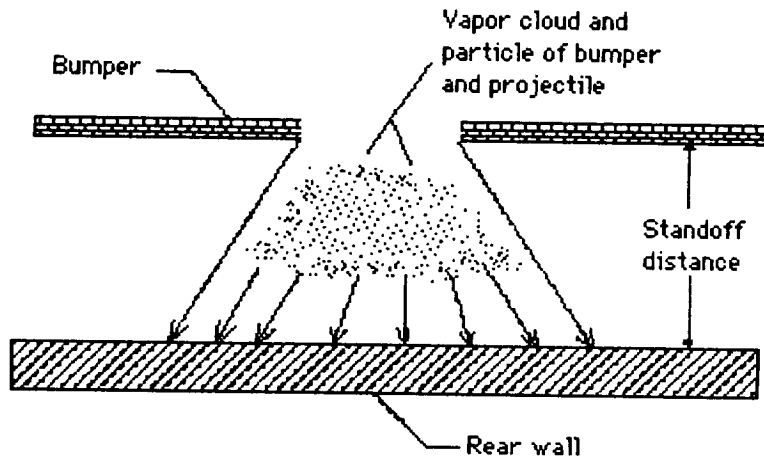


Figure 7.22 Space Debris 'Bumper'

### **7.10.3 Recommendation**

Previous Reports indicate that utilizing an outer layer of metal over the outer skin of the thermal protection system is impractical. Because the densities of the insulation are less than 5% the density of aluminum, the TPS will not act as an outer shield to vaporize and scatter the incident particles. It is unnecessary to include further details on barriers, because it is not a Thermal Control concern, for the following reasons :

- Space Debris Protection System (SDPS) would require an outer layer of metal to act as a 'bumper'. This type of hot structure has been eliminated from further design considerations.
- Probability of space debris impact is minimal (0.19%, 1 in 500).
- Titanium outer shell will absorb more of the particle impact than aluminum.
- Unmanned missions make space debris impact less of a concern.

### **7.11 Costs and Repairs**

Based on costs of \$16,000/ square foot for LI 2200, \$16,000/ square foot for FRCI, and \$3,100/ square foot for TABI, total material costs are approximately 14 to 18 million dollars. Assuming that the Biconic Design will lose half as many tiles per landing as the Shuttle does (approximately 20), costs based on complete replacement of damaged tiles are approximately \$50,000 per flight. Estimated time to fabricate and replace these tiles is approximately 2 weeks (ref 7.15).

## **8.0 PROPULSION**

---

### **8.1 Introduction**

This report documents the biconic Cargo Return vehicle's propulsion systems. It covers the CRV's launch, on-orbit, and reentry systems, and it addresses such issues as launch configuration and space station proximity operations.

The Cargo Return Vehicle begins its mission top mounted on a liquid rocket booster launch system. The LRB boosters lift the CRV into a 50 n.mi. x 110 n.mi. x 28.5° orbit. At that point, the LRB's separate from the CRV and fall back to the earth, burning up in the atmosphere. The CRV continues its journey to the space station using its own propulsion system of three OMS engines and twenty RCS jets. Once inside the Command Control Zone (CCZ), the CRV uses its fourteen cold-gas RCS jets to complete its maneuvers and dock to the station. The process is reversed for deorbit and reentry.

The details of the propulsion systems employed by the CRV are outlined in the report below.

### **8.2 Launch Configuration**

The CRV is top mounted on a dual booster/single core liquid rocket booster (LRB) system as shown in Figure 8.1. Liquid hydrogen (LH2) and liquid oxygen (LO2) are burned by ten space transportation main engines (STME's) to place the CRV in a 50 n.mi. X 110 n.mi. X 28.5° orbit. After main engine cut-off (MECO) the SRB's are ejected and the CRV initiates a series of orbital plane transfers using its own propulsion system (to be discussed later). The LRB's are burned up upon reentry.

A picture of this launch sequence can be found in Figure 8.2. The following sub-sections discuss the details of the LRB launch system.

**\*\*Note: Launch system analysis did not involve developing new systems; only choosing among existing systems.**

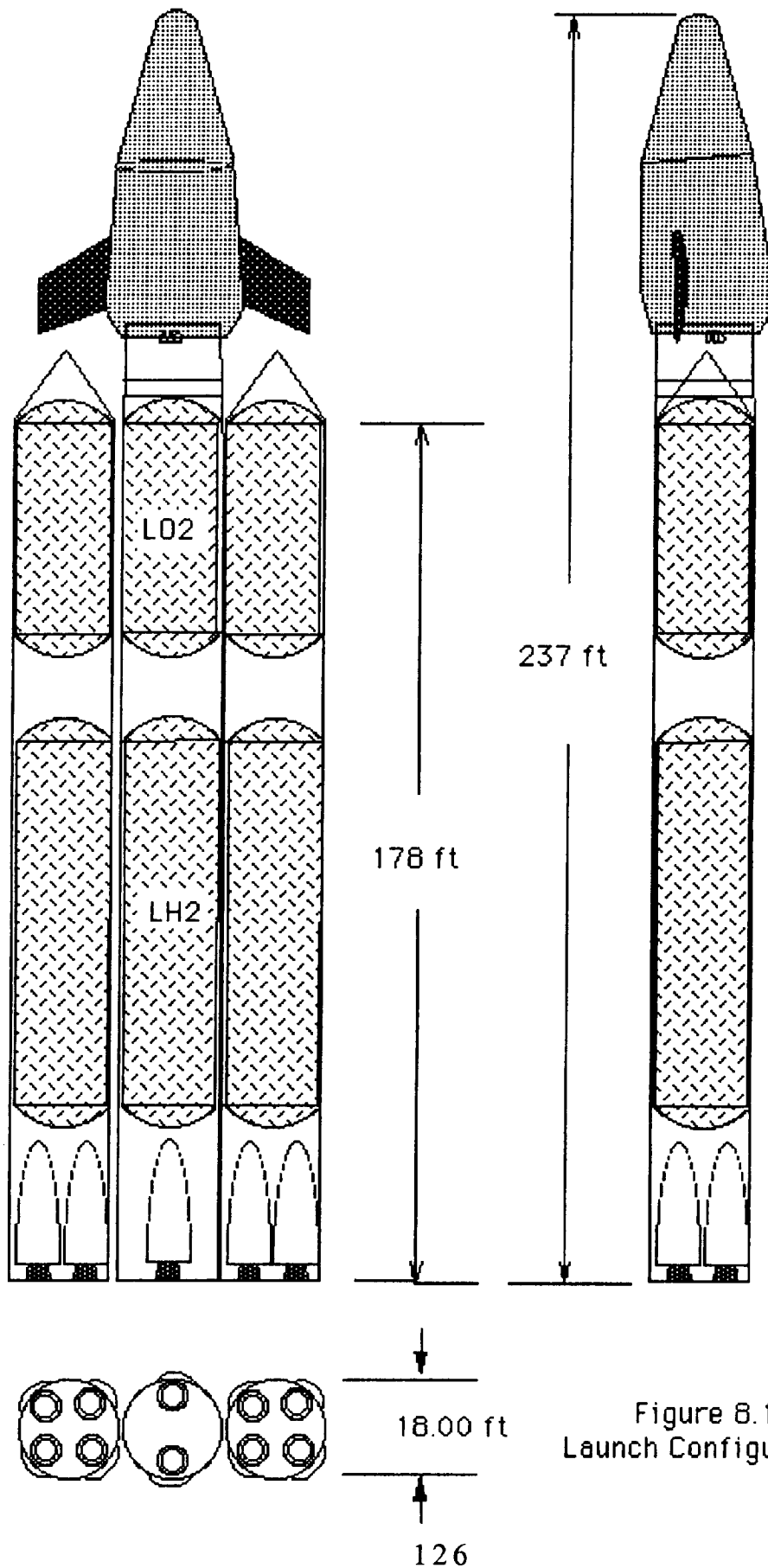
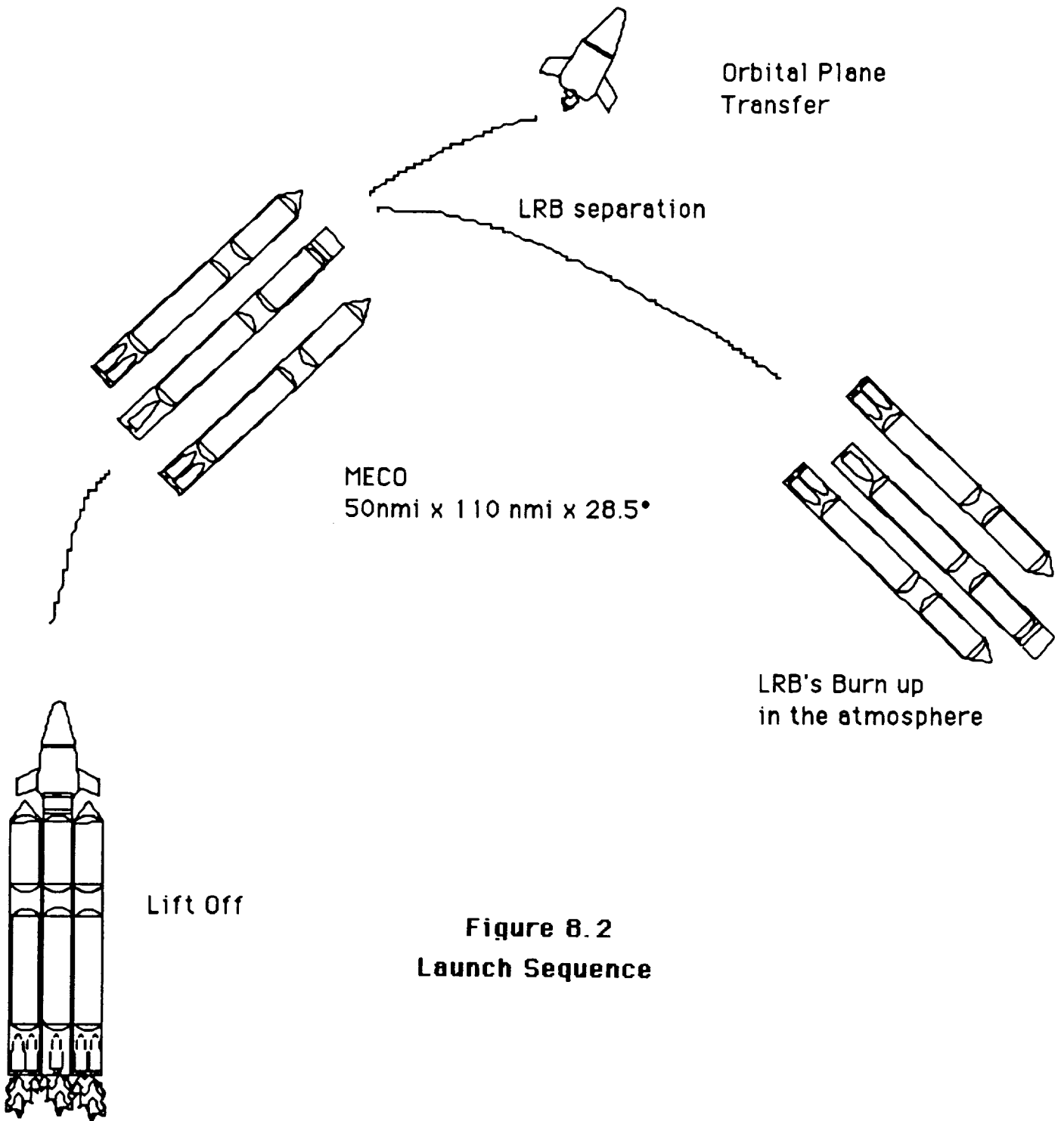
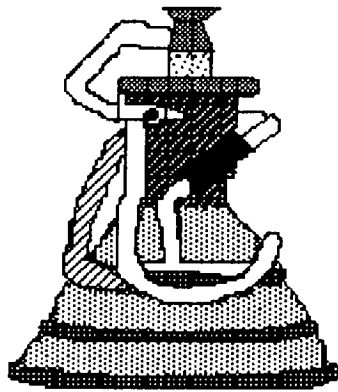


Figure 8.1  
Launch Configuration



**Figure 8.2**  
**Launch Sequence**



**Propellant: LH2/L02**  
**Pc: 2250 psia**  
**Mixture Ratio: 6.0**  
**Expansion Ratio: 20**  
**Isp,vac: 548.9 klbs**  
**Length: 110 in**  
**Diameter: 63 in**  
**Weight: 6746 lbs**

Figure 8.3 Space Transportation Main Engine Specifics

STME Performance  
(STME 20:1)

	Core Out	Booster Out
Payload Capability	91.1 k	85.2 k
q,max	813 psf	849 psf
Max Acceleration	4.00 g's	4.00 g's

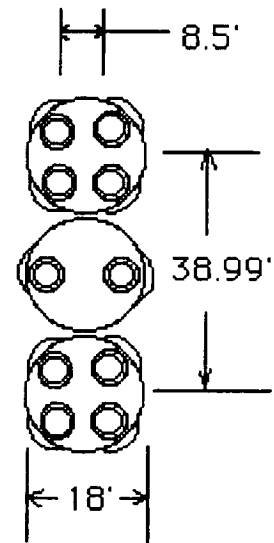


Figure 8.4 STME Performance

### **8.3 The Orbital Maneuvering System (OMS)**

Once the CRV is delivered to a 50 n.mi. x 110 n.mi. x 28.5° orbit (a low earth orbit--LEO), it separates from the LRB's and initiates a series of orbital plane transfer burns using its three OMS engines. The OMS engines produce large  $\Delta V$ 's to take the CRV from LEO to its 220 x 220 x 28.5° final orbit. The details of the orbit transfers can be found in section 2.0 of this report.

The CRV orbital maneuvering system consists of three OMS engines, two LH2 (fuel) tanks, and one LO2 (oxidizer) tank. It shares a helium pressurant tank with the aft RCS systems. The details of the OMS system follow.

#### **8.3.1 The OMS Engine**

The CRV has three OMS engines with engine-out capability. The engines use cryogenic LH2/LO2 to produce high specific impulses (high performance) . Liquid hydrogen from the fuel tanks is routed through the engine bells prior to ignition to prevent the bells from cracking. This hydrogen is then injected into the combustion chamber and is ignited. Hydrogen continues to cool the bells during firing.

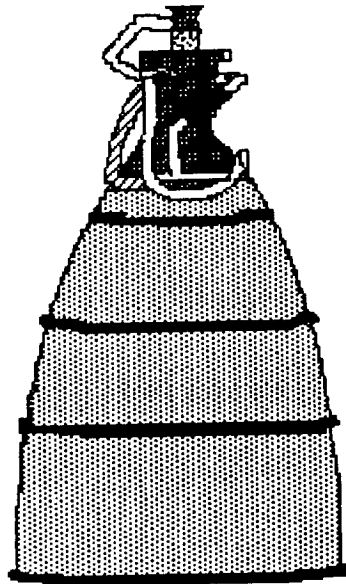
The engines are located on the back of the vehicle in a triangle formation (see Systems Layout). The triangle formation helps prevent spinning during engine out situations. OMS engine specifics are outlined in Figure 8.5.

As noted, the OMS system runs on cryogenic LH2/LO2. Although the engine described above does not presently exist, the technology to build such an engine does exist. By the time the CRV is funded and built, it safe to assume that such an engine will exist.

#### **8.3.2 The OMS Propellant Tanks**

The propellant for the OMS system is stored in three tanks: two fuel and one oxidizer. The amount of propellant needed is based on the mass of the vehicle, the total  $\Delta V$ 's, the specific impulse of the engine, and the on-orbit mission time (for boil off).The masses given in Figure 8.6 include residual

mass, boil-off mass, cool-down mass (vital to a cryogenic system), and a 20% reserve mass.



Propellant: LH2/ L02  
 Pc: 400 psia  
 C\*: 7646 ft/sec  
 Isp,vac: 414.4 sec  
 De: 15.28 in  
 Dt: 1.71 in  
 Lnozzle: 213 in  
 Lhead: 8.54 in  
 Ltotal: 28.68 in  
 Mass: 86.65 \* ea.  
 T,vac: 1600 lbf

Figure 8.5 The OMS Engine

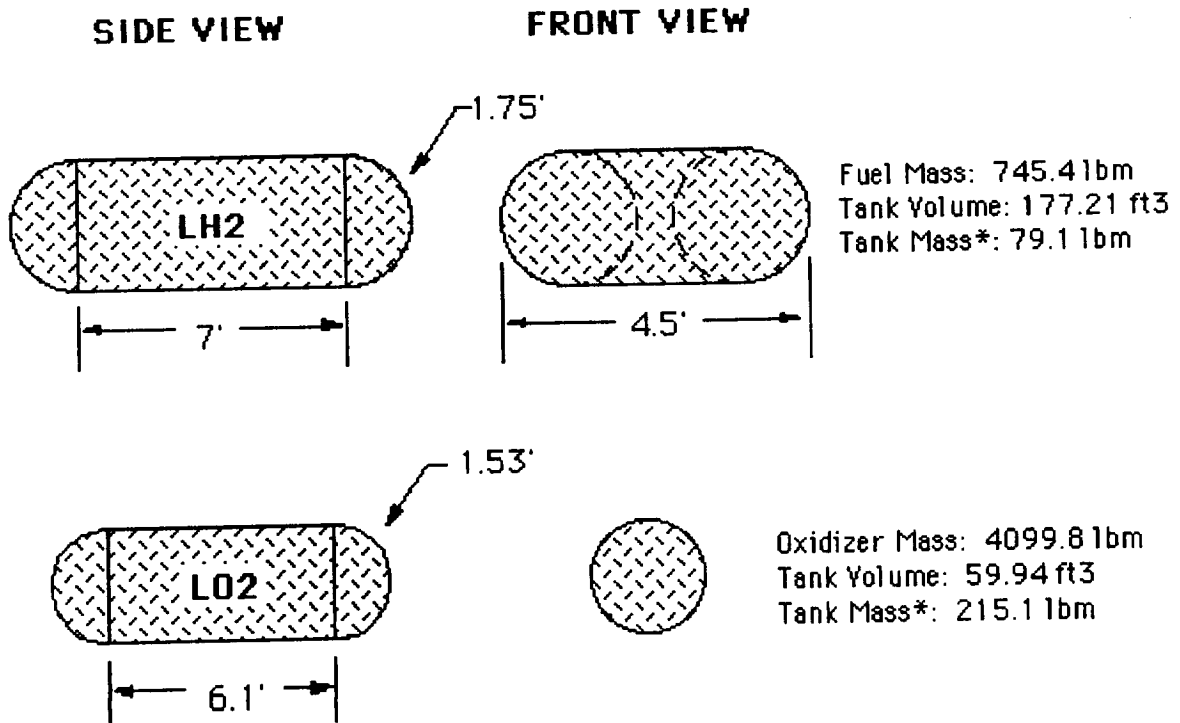


Figure 8.6 OMS Propellant Tank Data

### 8.3.3 OMS Pressurant

See Pressurant Data, Section 8.5.

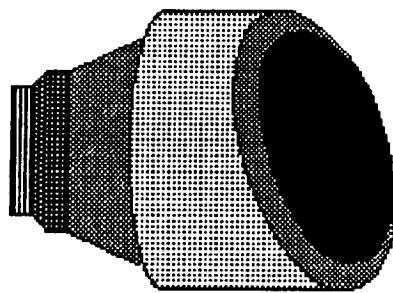
## 8.4 The Reaction Control System (RCS)

The purpose of the CRV RCS system is to assist in orbital plane transfers and to perform small on-orbit attitude changes. It also must complete space station docking maneuvers. Because the CRV will operate within the Command Control Zone (CCZ), it must possess cold-gas engines to avoid toxic residues (see Section 2.0, Mission Operations). After analytical fuel and tank mass values yielded unacceptably high results, it was decided to employ two separate RCS systems: one to operate within the CCZ zone and one to operate outside of the CCZ zone. Also, to ensure rotation about the center of mass, each RCS system possesses forward jets and aft jets. Graphical RCS jet and tank placement can be found in the Systems Layout (3.0) section of the report.

### 8.4.1 The Non-Command Control Zone RCS System

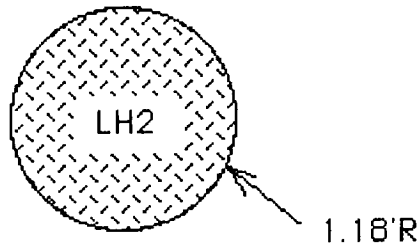
This system consists of 14 cryogenic LH2/LO2 RCS jets: 6 forward and 8 aft. The forward jets possess their own propellant tanks and share a pressurant tank with the CCZ RCS jets. The aft jets use propellant from the OMS tanks and share a pressurant tank with the OMS and the aft CCZ system. All jets are coupled, ensuring maneuvering capability during RCS engine out situations.

The jet shown in Figure 8.7 is manufactured by Rocketdyne. Figure 8.8 details the Non-CCZ propellant tank.

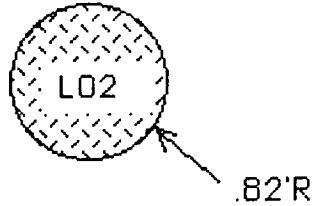


Propellant: LH2/LO2  
Pc: 400 psia  
Isp,vac: 390 sec  
Length: 16.2 in  
Diameter: 5.4 in  
Mass: 7.5 \* ea.  
T,vac: 25 lbf

Figure 8.7 The Non-CCZ RCS Engine



Fuel Mass: 28.83 lbm  
 Tank Mass\*: 1.25 lbm  
 Tank Volume: 6.84 ft<sup>3</sup>



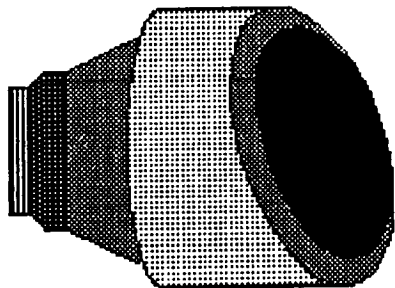
Oxidizer Mass: 158.58 lbm  
 Tank Mass\*: .42 lbm  
 Tank Volume: 2.32 ft<sup>3</sup>

\*Tanks made from Aluminum

Figure 8.8 Non-CCZ Propellant Data (tanks made from aluminum)

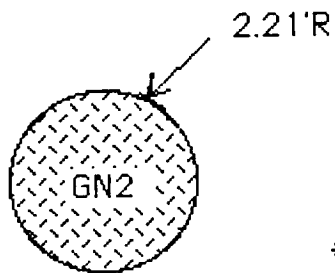
#### 8.4.2 The Command Control Zone RCS System

The CCZ RCS system consists of 6 forward engines and 14 aft engines, and, with the exception of contingency cases, operates only within the CCZ zone. Because of the delicacy of space station proximity operations, each CCZ engine, except the two rearward pointing jets, has a redundant twin. The specifics of the CCZ RCS engines and tanks are outlined in Figures 8.9, 8.10 and 8.11.



Propellant: GN2  
 Pc: 100 psia  
 Isp,vac: 68 sec  
 Lengine: 4.0 in  
 Dt: .5 in  
 Mass: 2.5 \*ea.  
 T,vac: 30 lbf

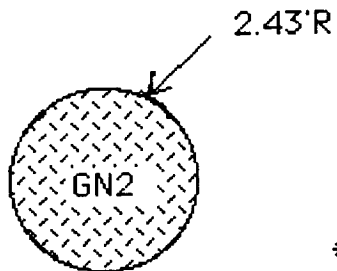
Figure 8.9 CCZ RCS Engine



Propellant: GN2 (Cold Gas)  
 Propellant Mass: 875.88 lbm  
 Tank mass: 39.47 lbm  
 Tank Volume: 45.32 ft<sup>3</sup>

\* Tank made from titanium

Figure 8.10 CCZ RCS Forward Propellant Tank



Propellant: GN2 (Cold Gas)  
 Propellant Mass: 1166.89 lbm  
 Tank mass: 52.65 lbm  
 Tank Volume: 60.46 ft<sup>3</sup>

\* Tank made from titanium

Figure 8.11 CCZ RCS Aft Tank

### 8.5 CRV Pressurant Systems (Forward and Aft)

The purpose of the pressurant system is to maintain tank pressures as propellant is expelled. For all CRV propulsion systems, high pressure helium (stored @ 4500 psia) is used. There are two separate helium tanks : one for the forward systems and one for the aft systems. The helium tanks are made from titanium and the specifics of each system is shown in Figure 8.5.1

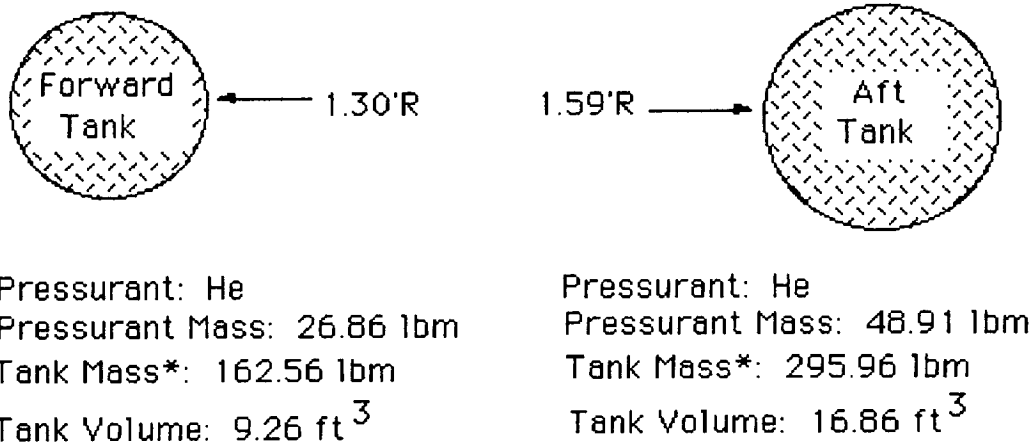


Figure 8.12 The CRV Pressurant System

## **9.0 REENTRY GUIDANCE**

---

### **9.1 Introduction**

There were three main tasks to be completed by the reentry guidance and dynamics section.

The first task was to determine the footprint of the CRV. This task constituted an analytical analysis of the reentry procedure to find possible landing sites relative to the atmospheric reentry point. A computer program was eventually developed to do this task.

The second task was to develop a reentry profile for the CRV. This task constituted using a computer program to solve the reentry problem. Different control variable combinations were entered into the computer program so that an optimal reentry profile was attained. This was the main task of the reentry guidance and dynamics section.

The final task was to determine guidance methods used throughout the entire CRV mission. This involved research into the available guidance methods and a determination of the best one to use for each phase of flight.

### **9.2 Footprint Determination**

The footprint of a reentry vehicle is defined as all of the possible ground locations that a vehicle can land at for a given entry position. By banking the craft, or by changing its trim angle of attack, the vehicle can maneuver to different landing sites. The footprint is then the plot of the outer limits of these landing sites.

A typical footprint has width because most vehicles can change their bank angle during reentry and thus, maneuver either left or right of the ground track. The distance perpendicular from the ground track that the vehicle lands at is called the crossrange. A typical footprint also has length because most vehicles can change their L/D characteristics. Flying the whole reentry procedure at the minimum L/D causes the vehicle to land in a very short distance which is called the minimum downrange. Flying the whole reentry at

the maximum L/D extends the glide, and the vehicle lands at a much further distance which is called the maximum downrange.

### 9.2.1 Crossrange Requirements

Each of NASA's landing facilities is at a certain perpendicular distance away from a given ground track. The ground track will shift to the west for each revolution of the vehicle around the Earth as a result of the Earth's rotation to the east. Because of this shifting of the ground track, different orbits (orbit 1 being the first orbit after launch) have different crossrange requirements at each landing site. Figure 9.1 shows the locations of all of NASA's landing facilities, and Table 9.1 lists the crossrange requirements for each of the landing sites.

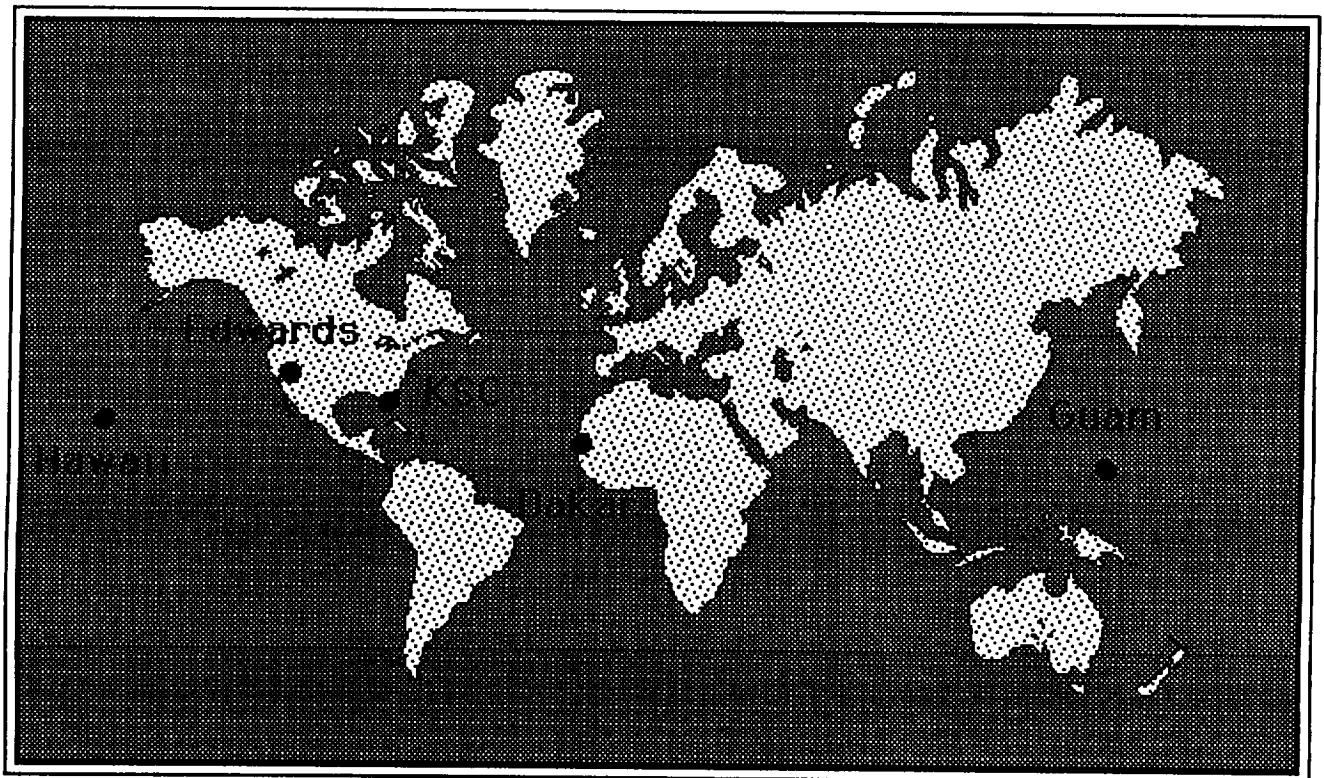


Figure 9.1 Landing Sites

<b>Orbit</b>	<b>Landing</b>	<b>Site</b>	<b>Crossrange (nmi)</b>
1		KSC	170
1		Edwards	412
<b>2</b>		<b>KSC</b>	<b>572</b>
2		Edwards	417
<b>3</b>		<b>Edwards</b>	<b>682</b>
4		Hawaii	309
5		Hawaii	53
6		Hawaii	623
7		Guam	595
8		Guam	68
9		Guam	596
10		Dakar	11
11		Dakar	509
12		Dakar	792
<b>13</b>		<b>KSC</b>	<b>585</b>
14		KSC	177
15		KSC	8
<b>16</b>		<b>Edwards</b>	<b>662</b>

**Table 9.1 Crossrange Requirements (Ref.1)**

Table 9.1 gives the crossrange requirement for each CRV landing site. The minimum crossrange needed is 682 nautical miles. Primary landing sites are shown in bold. The largest crossrange on the list is 792 nmi, but this is only for one orbit and an alternate landing site. Since the vehicle is unmanned, this alternate landing site can be left out.

### **9.2.2 Footprint Equations**

Several equations were used in the analysis of the CRV's footprint. One equation was used to determine the crossrange, a second was used to determine the downrange and a third was used to determine the heating rate. The heating rate equation is needed because it tells whether or not the downrange and crossrange values found in the first two equations are over the heating limits specified by the TPS system.

$$\text{Crossrange} = \text{Re} \frac{(L/D)^2 \pi^2 \sin^2 \theta}{48} + \left[ 1 - \frac{3(L/D)^2 \cos^2 \theta}{2\pi^2} \sum_{n=1} \frac{1}{n^2(n^2 + \frac{1}{4}((L/D)\cos\theta)^2)} \right]$$

$$\text{Downrange} = \frac{1}{2} \text{Re} \frac{L}{D} \ln \left[ \frac{1}{1 - \left( \frac{V_e^2}{g\text{Re}} \right)} \right]$$

$$dQ_{\text{mx}} = K \sqrt{\frac{8 B}{27(R_n)\rho_s(g)\text{Re}(L/D\cos\theta)}}$$

**Table 9.2 Footprint Equations (Ref. 6)**

R <sub>n</sub>	:	Nose Radius
ρ <sub>s</sub>	:	Air density at sea level
Re	:	Earth's Radius
g	:	Gravitational acceleration
θ	:	Bank angle
B	:	Ballistic coefficient
K	:	Heating rate constant
V <sub>e</sub>	:	Entry velocity

**Table 9.3 Symbol Definitions**

These equations are quite accurate for small entry flight path angles and moderate to high lift over drag values. The CRV's entry flight path angle is only -1° and the lift over drag is about 1.0 so these equations are appropriate.

A program Footprint was developed by Andrew A. Johnson to determine a footprint using the equations above. This program took in as inputs all the specifications of the vehicle needed by the equations above. The program then used a loop to look at several L/D values from the minimum trim L/D to the maximum trim L/D. At each L/D value, the program then used

another loop to look at several different bank angles from 0° to 90°.

At each combination of  $\theta$  and L/D, the program computed the crossrange, downrange and heating rate. If the heating rate was below the maximum heating rate as specified in the input, the downrange and crossrange values were entered into an array. Also, the maximum crossrange and downrange was traced throughout both loops.

When all of the calculations were completed, each acceptable combination of downrange and crossrange was plotted. This gave an accurate picture of the footprint.

### 9.2.3 Final Footprint

The program Footprint was used to specify the final footprint of the CRV (Figure 9.2). The input values for the program are listed in Table 9.4 as the output ones are in Table 9.5.

Maximum Trim L/D	:	1.044
Minimum Trim L/D	:	0.455
Cd at Max L/D	:	0.429
Cd at Min L/D	:	1.154
Nose Radius	:	4.0 ft
V entry	:	25,800 ft/sec
Weight	:	63,336 lb
Reference Area	:	507.5 ft <sup>2</sup>

**Table 9.4 Vehicle Model for Footprint**

Maximum Crossrange	:	711 nmi
$\theta$ at Max Crossrange	:	46°
L/D at Max Crossrange	:	1.00
Maximum Downrange	:	8,335 nmi
Minimum Downrange	:	2,135 nmi

**Table 9.5 Footprint Characteristics**

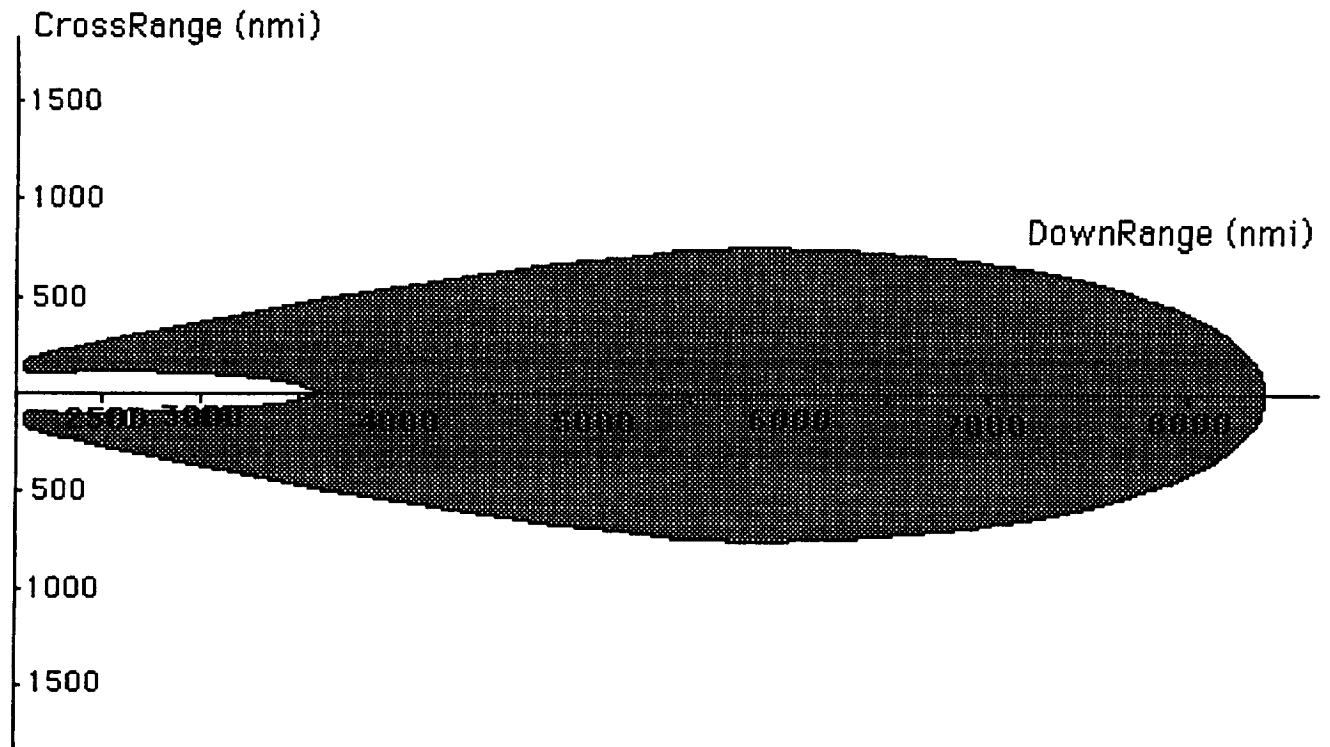


**Figure 9.2 CRV Footprint**

### **9.3 Reentry Profiles**

The reentry profile of the CRV is very important. Extreme forces and heating rates occur during the reentry procedure, and they must be managed such that none exceed the limits of the CRV. Also, a reentry profile might skip-out of the atmosphere which is very undesirable.

The vehicle can control several aspects of the reentry procedure. First, the vehicle could enter the atmosphere at a desired angle. A steep entry angle will cause steep oscillations and high structural loads since the vehicle will still have relatively high velocity when it encounters dense air. A shallow entry angle would increase the likelihood of skipping-out of the atmosphere.

Second, the vehicle could determine what angle of attack to fly at throughout the reentry procedure. The vehicle could change its angle of attack and thus, its effective L/D by the use of fins. Flying at low L/D will cause a steady drop, but will result in little of the crossrange needed to reach a landing site. Flying at high L/D will

cause higher crossrange values, but could also cause steep oscillations and increase the chances of skipping-out of the atmosphere. Many steep oscillations also make control of the vehicle difficult. The vehicle could change its L/D throughout the flight to try to minimize the undesirable effects (oscillations, high heating rates, high structural loads and no crossrange).

The varying of the control parameters stated above to find a combination with acceptable results was one of the main objectives for the Reentry Dynamics group.

### **9.3.1 Integrated Mission Program**

The Integrated Mission Program (IMP, Ref 9.3) was used to analyze the reentry profiles. IMP allows the user to input all of the control variables stated earlier, and then determines the entire reentry profile from on-orbit phase to touchdown. Also, specifications about the craft (aerodynamic data, weight and thrust) and desired landing site coordinates must be entered into the program.

The reentry profile output by IMP is quite complex. It gives many variables for each time interval during reentry. Some of the variables IMP gives for each time interval are velocity, flight path angle, altitude, angle of attack, density, heating rate, dynamic pressure, acceleration and ground coordinates. It also gives the orbital parameters and event times for each phase of flight from before the deorbit burn to reentry point including the delta V needed to initiate reentry. The output file can also be used to generate plots of any of the variables just stated.

## **9.4 Final Trajectory**

The computer program IMP was used to determine the trajectory of the CRV from the deorbit burn to ground. The primary objectives for the final computer trajectory modeling were;

- Reduce the entry altitude oscillations.
- To cover the greatest range.

- Keep within structural restraints.
- Model a drogue parachute opening.
- Provide entry information for other disciplines.

The final computer run went as follows, the CRV was orbiting at 220 nmi above the Earth at a velocity of 25147 feet per second. The CRV performed its deorbit burn with a delta V of 317.3 ft per second. It entered the atmosphere with a flight path angle of -1.00 degrees and a velocity of 25933 ft/s. At this point in the mission, the undesired altitude oscillations occur (see Figure 9.3). These altitude oscillations are undesirable because they introduce the possibility of skipping out of the atmosphere if they are not controlled.

The first oscillation is the only one that presented any concern with skipping out of the atmosphere. To alleviate this problem several things are done. From past experience the CRV tends to plunge deep into the atmosphere and then rebound up to nearly the altitude of reentry. To remedy this problem the CRV was programmed to enter the atmosphere at its highest stable lift over drag angle of attack 26.5 degrees (see Figure 9.4). This was done to prevent the deep plummet into the atmosphere.

When the CRV reached the lowest point in its initial plunge into the atmosphere (at a time of 500 seconds) the lift over drag was decreased by means of a step function to its lowest stable lift over drag. The step decrease in lift over drag was done to prevent the uncontrolled rebound away from the Earth. The jump up in altitude is desired up to a point however. The range of the CRV increases when the CRV glides from a higher altitude. The step function controlled the increase in altitude to an acceptable safe level.

Slightly before the CRV reached the highest point in its initial rebound (time equal to 800 seconds) the lift over drag was increased to its highest value (angle of attack of 26.5 degrees) by means of a ramp function. This ramp increase took place over a time period of 300 seconds.

This was done to slow the oscillation drop in altitude that occurs at this time. The lift over drag was left at this maximum value (angle

of attack of 26.5 degrees) until the drogue parachute was deployed at 3400 seconds. This was done because after the initial rebound is over, there is little danger of leaving the atmosphere and the maximum lift over drag is necessary to cover the greatest cross range. Figure 9.3 shows a small convex extension of the curve at an altitude of about 10 nautical miles and a time of 3400 seconds. This is where the parachute was programmed to deploy.

The drogue parachute modeling was performed by programming the computer to default to a value of lift over drag that corresponded to the value of lift over drag of the CRV/parachute combination. This angle of attack is represented on Figure 9.4 as 81.7 degrees. Figures 9.13 and 9.14 compare the values of acceleration with and without the drogue chute.

To model the opening of the parachute an opening time of 5 seconds was used. The opening time would actually be much faster however. Determining the opening force was not the reason for the modeling. The parachute would be reefed in several stages to reduce opening forces. The modeling was performed to get an estimate of the descent characteristics and to determine if the drogue chute would decelerate the CRV to a velocity that could accommodate the deployment of the recovery system. The spike in Figure 9.5 is the opening of the drogue chute. Figures 9.7 and 9.8 represent the velocity versus altitude for the CRV with and without the drogue chute. The decrease in velocity is small but noticeable when the drogue chute is deployed (at 10 nautical miles).

The entry oscillations can also be observed from the figures. Figures 9.5 and 9.6 show rebound away from Earth (between 300 and 800 seconds) and then shows the gradual increase in g loading as the CRV enters the atmosphere. Figures 9.7 and 9.8 show the change in velocity that correspond to the altitude oscillations.

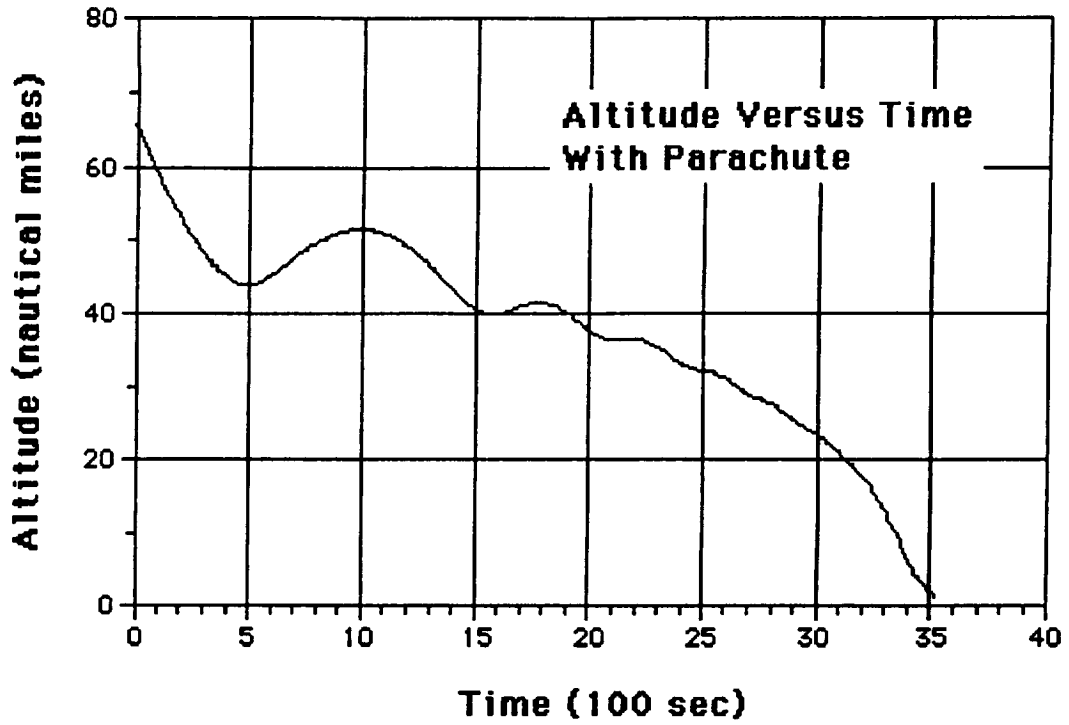


Figure 9.3 Altitude vs Time for Final Trajectory

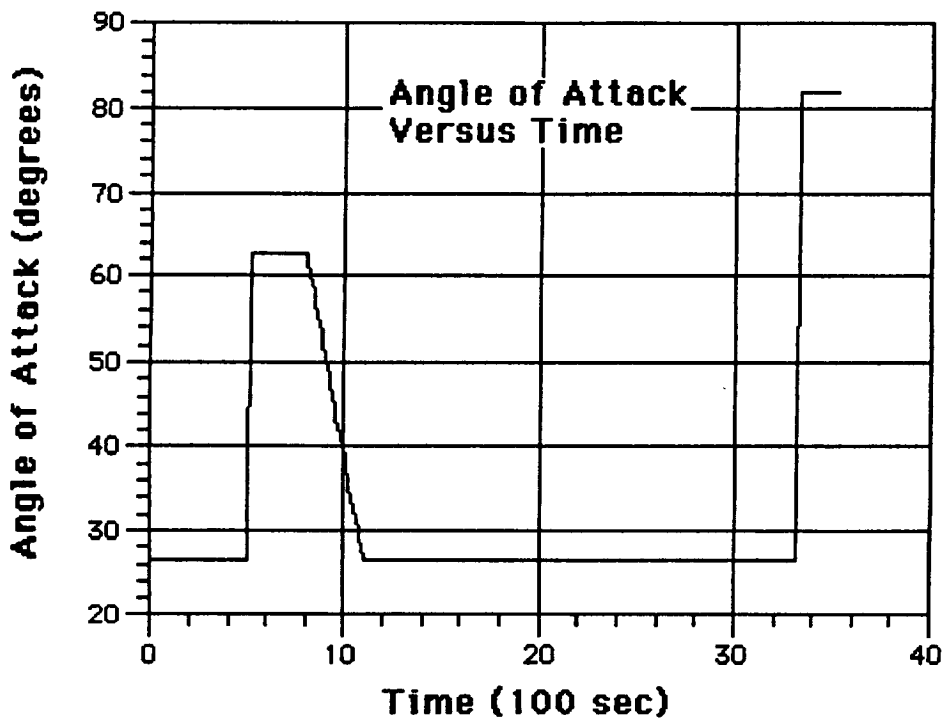


Figure 9.4 Angle of Attack Versus Time For Final Trajectory

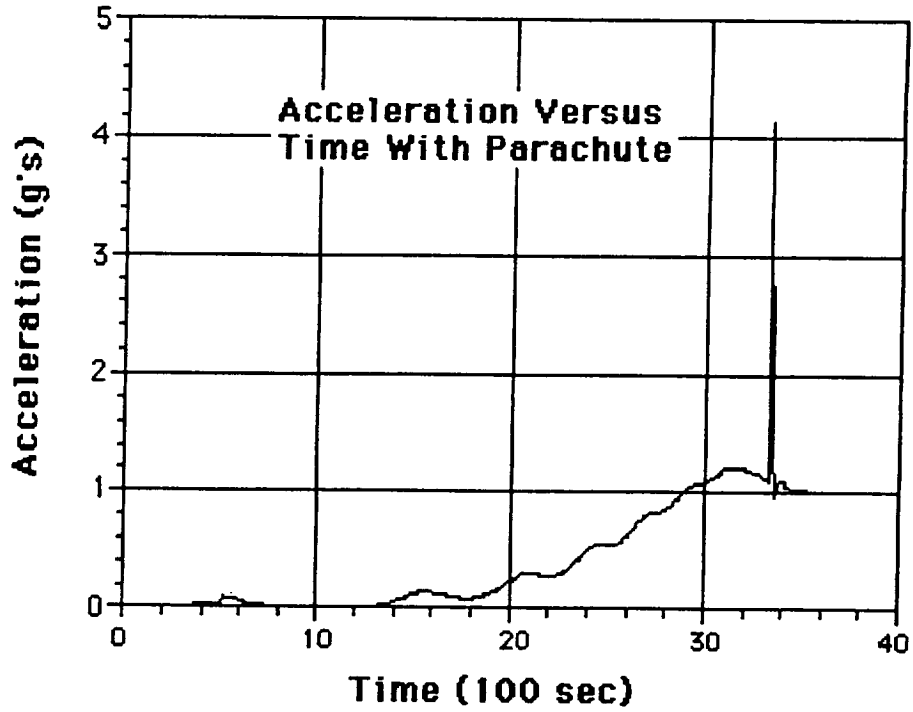


Figure 9.5 Acceleration vs Time with Drogue Parachute

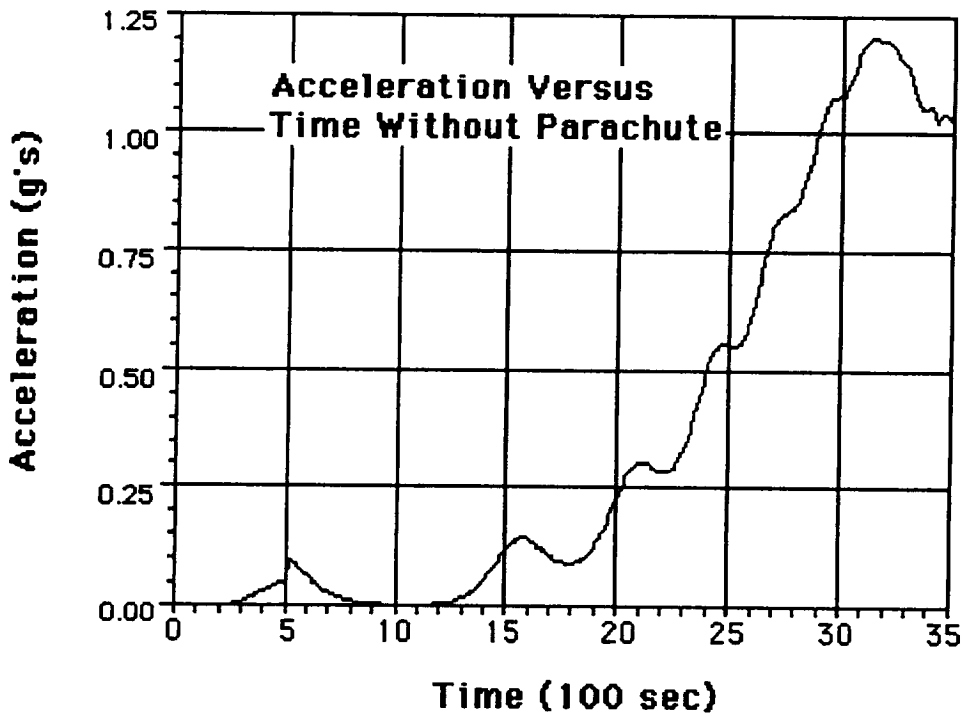


Figure 9.6 Acceleration Versus Time Without Drogue Chute

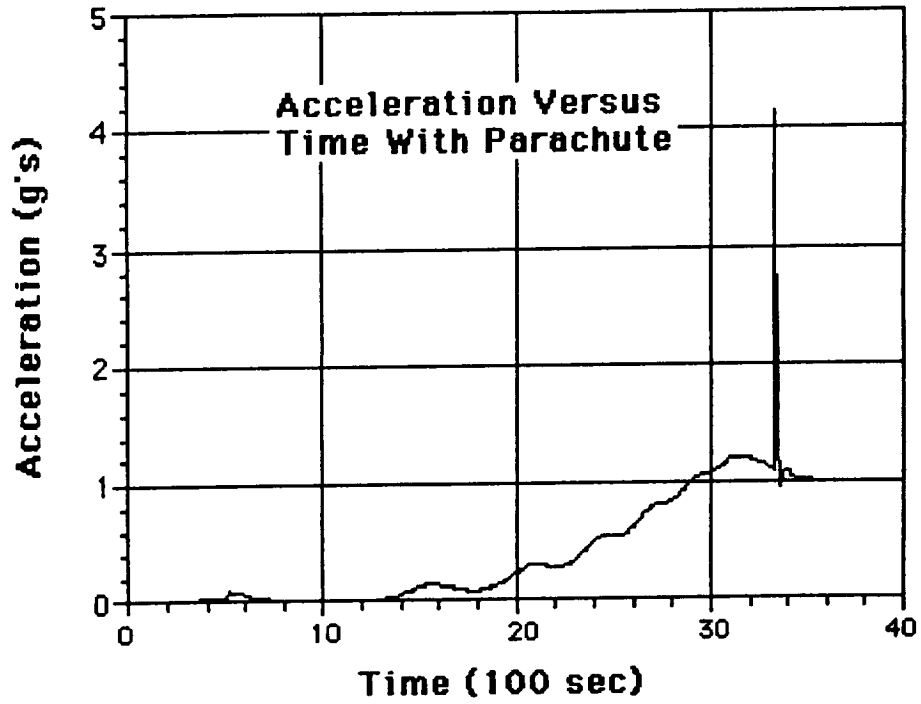


Figure 9.7 Velocity vs Altitude with Drogue Parachute

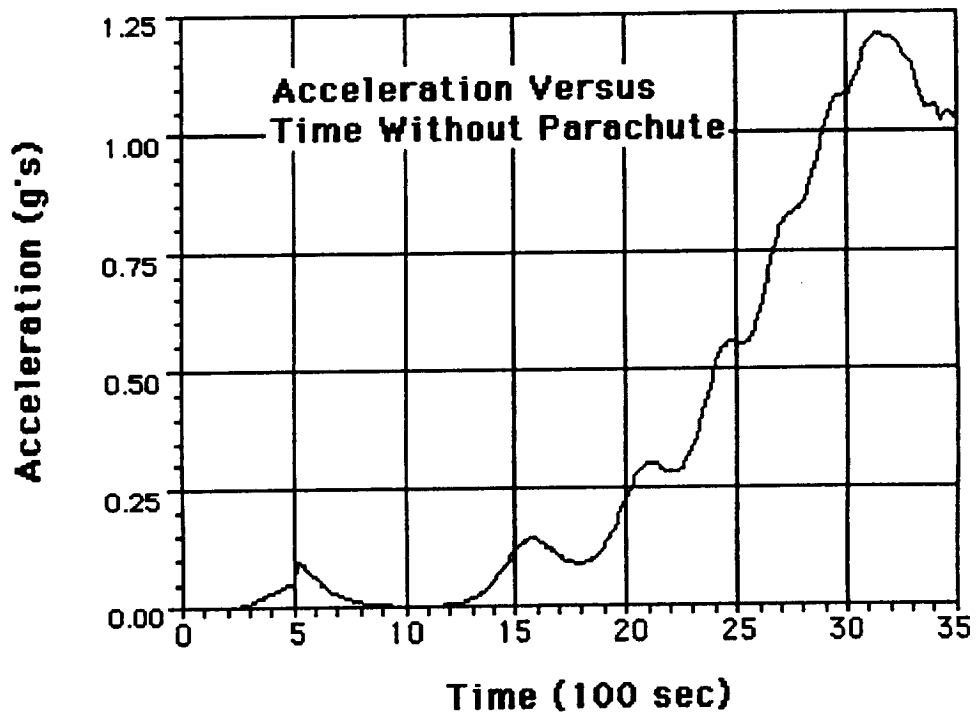


Figure 9.6 Acceleration Versus Time Without Drogue Chute

## 9.5 Guidance System

The guidance system used for this mission is very similar to the guidance system used on the Space Shuttle. The basic construction of the system is divided into seven main subsystems (see Figure 9.9);

- Aft controls.
- Booster controls.
- Main computer.
- Communications.
- Forward controls.
- Attitude and position.
- Landing.

The dashed lines in Figure 9.9 enclose a subsystem listed above. The aft control block (upper right corner of Figure 9.9) is made up of the CRV's Orbital Maneuvering System (OMS), rear Reaction Control System (RCS), and the control surfaces. The primary function of this block is control and thrust for the CRV. This block receives commands from the main computer via the aft multiplexer. A multiplexer is a circuit that interleaves or transmits two or more messages on a single channel. The block immediately to the left of the aft control block, in Figure 9.9, is the communications block. This block is comprised of the Tracking and Data Relay System, two outgoing signals, and two incoming signals. The outgoing CRV status signals are used by the SSF and ground crew to determine the location, orientation, and general status of the CRV. The closed circuit TV monitor is used when visual contact with some area in or around the CRV is necessary. The incoming manual control signals control all aspects of the CRV by manual remote control. Manual control of the CRV is required inside of a twenty mile co-orbit distance in front and behind the SSF. Manual controls can be used at any time during the mission if necessary. The last of the four signal blocks is the incoming update commands. If the mission profile is changed in any way, the new updated mission is stored in the update command block.

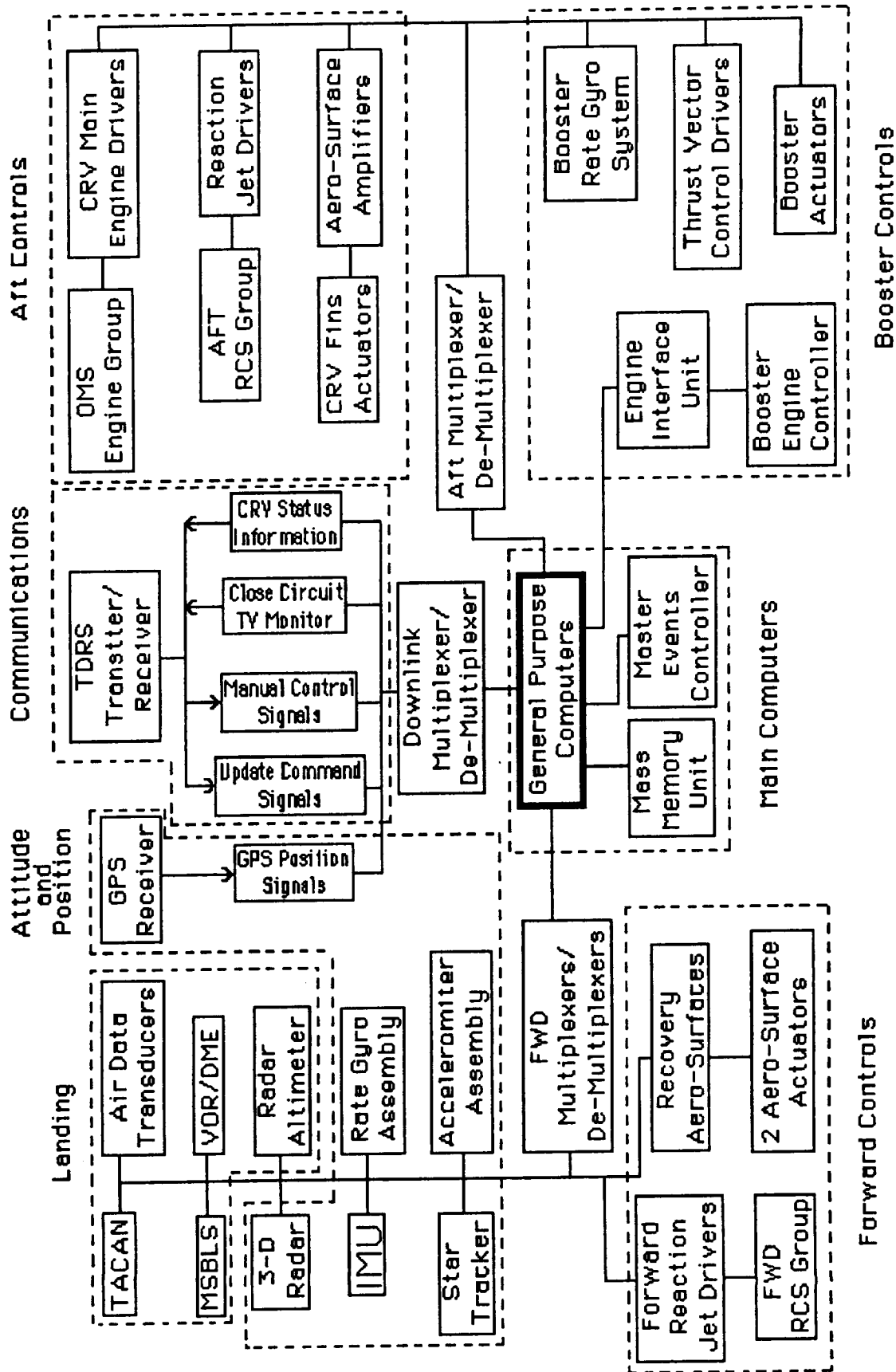


Figure 9.9 Biconic CRV Functional Diagram

To the left of the communications block (Figure 9.9) is the Attitude and Position block. The primary function of this block is to determine the orientation and position of the CRV at all phases of the mission. The attitude and position are determined different ways at different stages of the mission (Section 9.6). One way of determining position is by making use of the Global Positioning System (GPS). The GPS is a series of tracking satellites placed in orbit around the Earth. These satellites determine position by triangulating the location of the CRV and sending the results to the CRV. Accelerometers are another way of determining position. By placing 3 accelerometers in each of the three coordinate axes, the accelerations in each direction can be integrated twice to give distances in each of the coordinate directions. The 3-D radar can be used to determine position if the region of interest is within the range of the radar. To determine the orientation of the CRV relative to some reference (Earth) the gyros in the Inertial Measuring Unit (IMU) and Star Tracker can be used. Star Tracker determines orientation of the CRV by sighting a known star and computing the angles between the axes of the CRV and the sighting line with the star. This requires that the CRV hold a steady flight path so that the star can be sighted.

The section above the Attitude and Position block is the Landing block. This section is dedicated to guiding the CRV in to land. The VOR/DME sends out signals for the CRV to track and also determines distances. Tactical Air Navigation (TACAN) is ground based and is used after the CRV comes out of the zone of ionization to determine range and bearing. The MSBLS is a ground based microwave scanning beam landing system that can be incorporated if the CRV is below 18000 feet. The MSBLS determines the distance to the destination and the angle between the desired trajectory and the actual course. The radar altimeter gives the distance between the ground and the CRV, a critical function during landing.

In the bottom left corner of Figure 9.9 is the Forward Controls Block. This primary function of this section is control of the CRV by the front Reaction Control System (RCS) and control of the CRV by use of the aerosurface actuators on the recovery system. To the right of the Forward Controls block is the main computer. This is the control center for the entire operation. All commands to the CRV originate or pass through this area. The results of the

position and orientation determinations are transmitted to the main computer and it generates the commands necessary to complete the mission.

The last of the seven subsections is the Booster Controls block. The booster system that lifts the CRV to its initial 110 nmi orbit has its own rate gyro system for guidance. The necessary maneuvers to reach orbit are performed by the thrust vector control drivers.

## **9.6 Guidance Mission Profile**

The Biconic Cargo Return Vehicle (CRV) mission can be broken down into 10 separate submissions (see Figure 9.10). Each of these submissions requires that the vehicle know its position and orientation relative to some reference (Earth) at all times. The devised guidance and control scheme discussed in the previous section will complete this endeavor to the degree of accuracy necessary for a successful mission. The method for determining the CRV's position and orientation for each of the 10 submissions will follow.

The first stage of the mission (Stage 1 in Figure 9.10) is the launch of the CRV to the initial 110 nautical mile orbit. The CRV will be attached to a separate launch vehicle until the desired orbit is reached and then will disconnect from the launch vehicle. To determine the vehicles position during this portion of the mission, the CRV will have ground tracking, integration of accelerometers, and the Global Positioning System (GPS). To determine the CRV's orientation, it can use the gyros in the Inertial Measuring Unit (IMU).

The next four stages (Stages 2,3,4,and 5 on Figure 9.10) all use the same methods for determining the CRV position and orientation. The position can be determined by the GPS and integration of the accelerometers while the orientation can be determined by use of the gyros in the IMU. To insure accuracy of the readings from the gyros, the Star Tracker can be used during the phasing stages of the mission (Stages 2 and 3 of Figure 9.10) to calibrate the IMU. By performing the calibrations during these stages, this will leave little time for the readings from the IMU to deviate and cause errors in the mission. It should be noted that in Figure 9.10, the transfers from one orbit to another are only graphical representations of an

orbit change and do not portray the actual orbit transfer. Actually, the CRV would begin the initial thrust to change orbits at a time that would allow it to rendezvous with its desired target exactly 180 degrees from the location of its initial thrust.

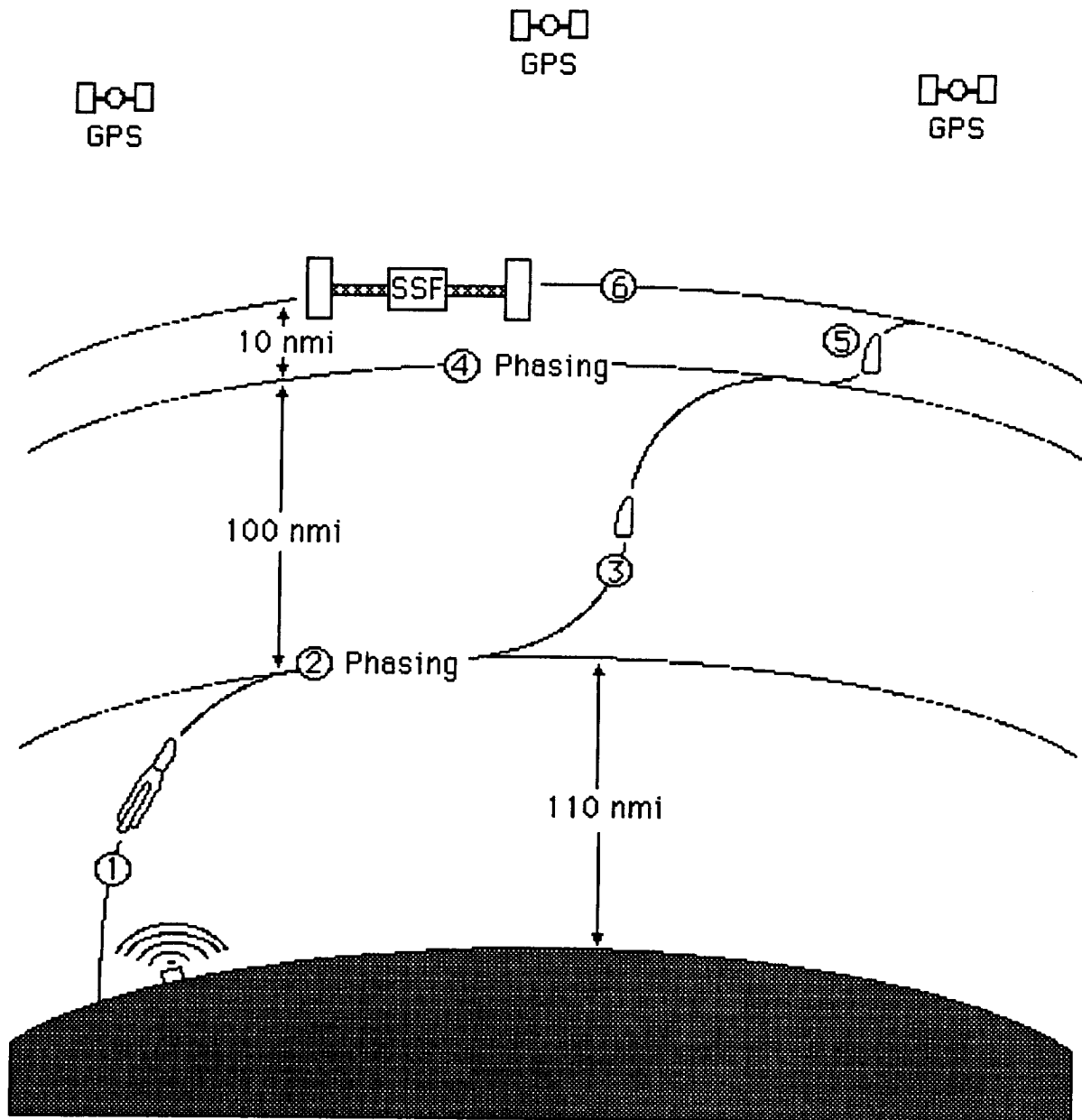


Figure 9.10 Mission Profile from Launch to SSF Docking

The time that the CRV is waiting to perform its initial thrust provides an opportune time to use Star Tracker to calibrate the IMU's. As will be recalled from section 9.5, Star Tracker uses a distant star to determine the orientation the vehicle, as a result a level flight path is required to site the star. The next stage of the mission (Stage 6 on Figure 9.10) is docking to the Space Station Freedom (SSF). The location of the CRV can be determined by the GPS, integration of accelerometers, and by 3-D radar between the SSF and the CRV. The orientation of the CRV can be determined by the IMU and Star Tracker. The CRV will be manually remote controlled by SSF personnel when the CRV is within a 20 mile co-orbit distance behind the SSF.

The final four stages of the mission comprise reentry of the CRV (see Figure 9.11). The first of these stages is detaching from the SSF and moving to the required twenty mile co-orbit distance in front of the SSF. To determine the position of the CRV, the GPS, integration of accelerometers, and 3-D radar can be used. The orientation of the CRV can be determined by the IMU and Star Tracker units. During this phase, Star Tracker should be used to calibrate the readings from the IMU. The Star Tracker unit cannot be used after this point because the CRV will not be in a controlled position to site a star. The CRV will have to depend on the IMU to determine its orientation for the remainder of the mission.

The next stage is the deorbit burn and glide to the "Zone of Ionization" (Stage 8 on Figure 9.11). The CRV's position can be determined by the GPS and integration of accelerometers. The orientation of the CRV can be determined only by the IMU. The CRV then enters the "Zone of Ionization" (Stage 9 on Figure 9.11). The Zone of Ionization is a region where the temperature of the CRV surpasses the ionization temperature of air. When the air becomes ionized it acts as a block to all signals to or from the CRV. This signal block lasts approximately 10 minutes. The position of the CRV during this phase can be determined only by integration of accelerometers. The orientation can be determined only by the IMU. The Zone of Ionization ends when the CRV decelerates to a velocity that produces a temperature less than the ionization temperature of the air.

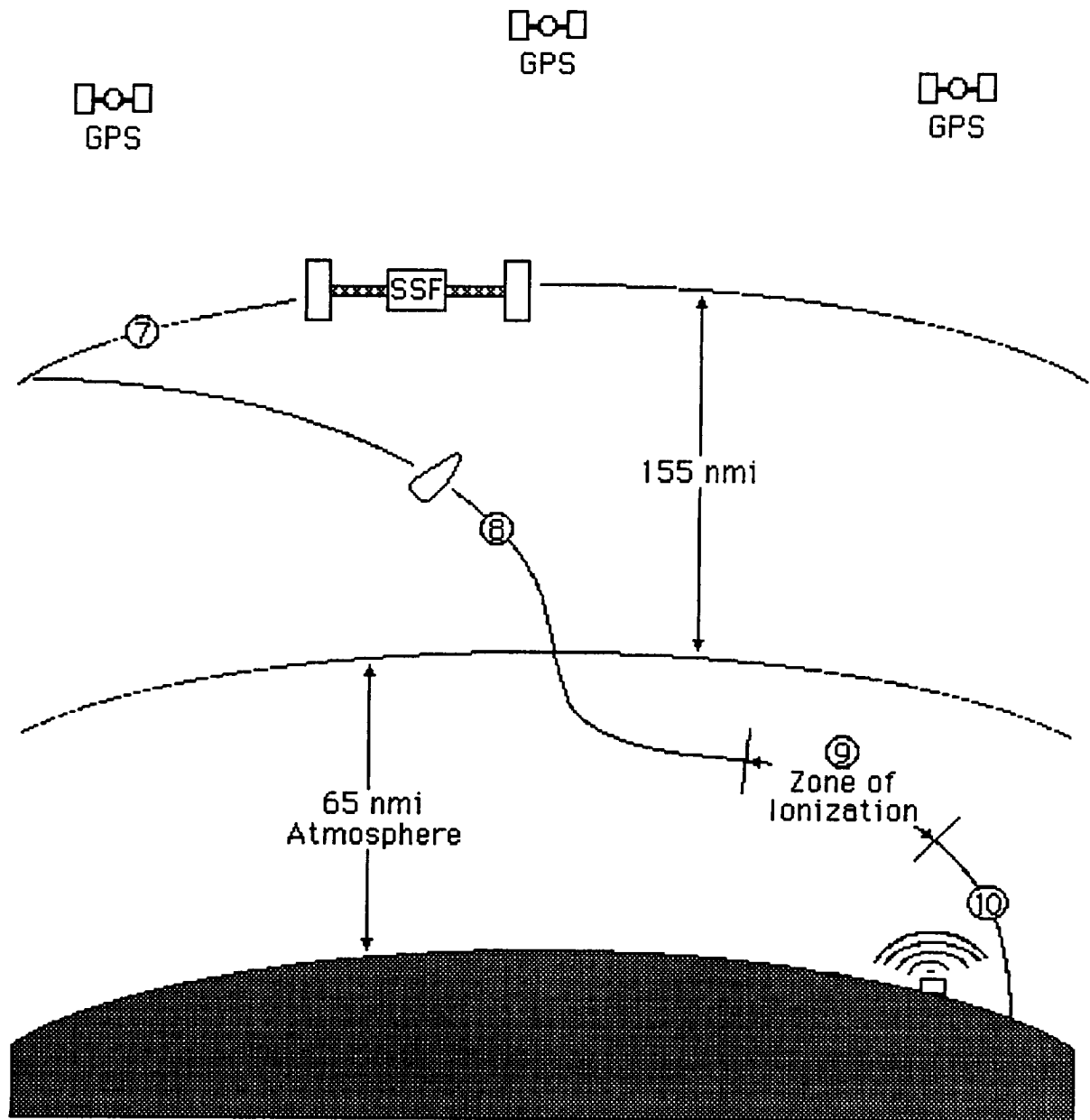


Figure 9.11 Reentry Mission Profile

The final stage of the mission is from the exit of the Ionization Zone to landing (Stage 10 on Figure 9.11). After exiting the Zone of Ionization the CRV can use the GPS, integration of accelerometers, and the ground based Tactical Air Navigation System (TACAN) to determine its position. When the CRV reaches an altitude of 18,000

feet its position can also be determined by the microwave landing system. After 9000 feet the radar altimeter can also be used to determine position. During the entire landing sequence the IMU is used to determine the CRV's orientation. The VOR and DME units are used at this time to guide the CRV to its destination.

## **10.0 STRUCTURAL ANALYSIS**

---

### **10.0 Introduction**

The Structural Design and Analysis Group was given the challenge of developing a preliminary structural design of the biconic CRV and its subsystems. During the design process, basic structural analysis techniques were utilized to estimate cross sectional moments of inertia, thickness and shape of structural members, and material types.

Preliminary designs for the underlying fuselage substructure, cargo bay support structure, skin cross section and panel sizing, landing gear system, OMS engine support structure and attachment method, drogue parachute and parafoil compartment bays, parafoil cable attachment system, and the ram-air parafoil advanced recovery system were developed. This group will also be conducting the structural analysis phase of the project using NASTRAN finite element modeling with the predicted flight loads.

### **10.1 CRV Fuselage Support Structure Layout**

After determining that the best and really only practical method of supporting the fuselage would be a system of ring frames and stringers, the design of the structure took place in three phases.

First, a layout skeleton was developed which indicated the spacings between the rings as well as the stringers at every point along the CRV. These spacings were calculated by considering the fully loaded weight of the vehicle, the diameter of the vehicle, and the requirement to minimize the mass of the structure.

It was determined that the maximum allowable spacing was 24 inches for the rings and just over 12 inches for the stringers. The majority of the rings on the CRV are 22 inches apart with the exception of those in the very rear of the vehicle and those located at the position where the conic sections change. There is a total of 32 ring frames used to support the fuselage. In the forward conic section, these rings are circular, while in the rear section they are elliptical due to the fact that the rings must lie in parallel planes

and the two conic sections do not lie on the same axis. The stringers are spaced slightly over 12 inches apart at the largest diameter of the CRV and then gradually converge as the diameter of the vehicle decreases.

There are 74 stringers surrounding and supporting every ring frame except for the first six which only require 37. At the sixth ring, half of the stringers can be eliminated because the diameter of the CRV at this point is small enough to produce spacings of under 12 inches with the reduced number. Therefore, at the seventh frame, alternating stringer supports stop while the rest travel on to the front of the vehicle. Rings 15 - 28 are used to support the payload bay and are thus cut off somewhat at the top in a manner in which they will fit flush with the bay doors. Rings 3,4 and 5 are also cut off a very small amount at their top in order to allow the insertion of the ARS compartment. This compartment fits in the vehicle such that stringers are used to connect and support it. Refer to Figure 10.1 and Table 10.1 for complete information on the structural skeleton.

Phase two consisted of determining the shapes to be used for the rings and stringers. Choices for the stringers included U-shaped, Y-shaped, Z-shaped, and a truss type, while those for the ring frames were a Y-section and a box section. The best type of stringer, and thus the one selected for the CRV, was the Z-shaped. It was chosen because it has just as much bending strength as the other configurations, is very efficient with respect to weight, and allows for the easiest connections between both the skin and the ring frames. The stringer supports are welded to the outside edge of the frames so there must be adequate enough area connecting the two pieces to get a good bond. Box-section rings were more favorable than Y-section ones because of their greater bending stiffness and the relative ease with which they can be manufactured, so the frames in the CRV are box-sections. Refer to Figure 10.2 for a detailed view of the ring and stringer system.

The third and final phase in the design of the fuselage support structure was determining the exact dimensions - lengths, widths, and thicknesses of the rings and stringers. This was accomplished by examining the pressures on the fuselage at various points, the diameter of the vehicle, and by looking at the dimensions of other

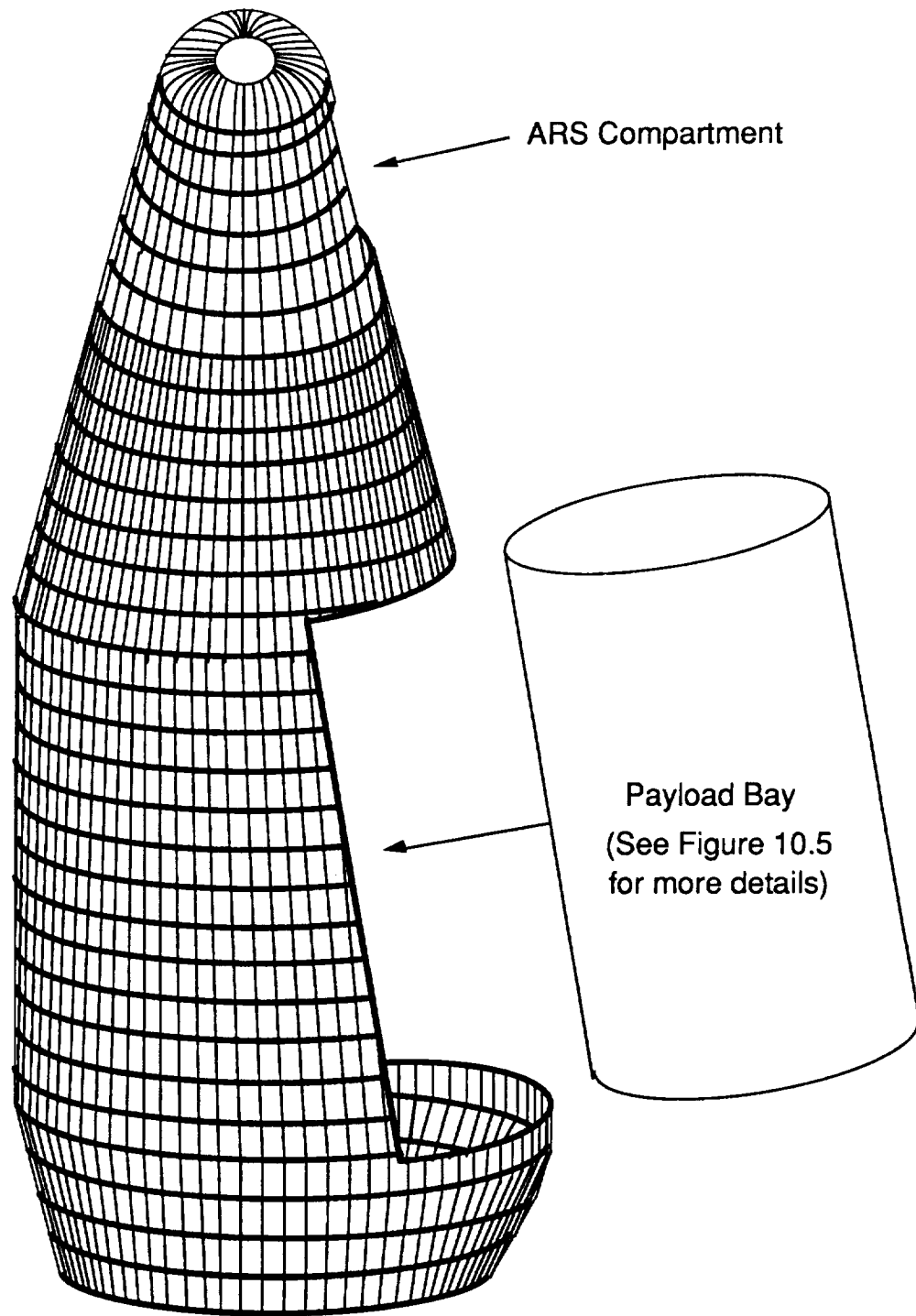


Figure 10.1 Support Structure Skeleton

<b>Ring #</b>	<b>Location (in.)</b>	<b>O.D. (in.)</b>	<b>Major Axis (in)</b>	<b>Minor Axis (in)</b>	<b>Spacing (in.)</b>
1	35.5	81.69			6.94
2	47.5	88.11			7.48
3	69.5	99.91			8.48
4	91.5	111.70			9.48
5	113.5	124.49			10.57
6	135.5	136.28			11.57
7	157.5	148.07			6.29
8	179.5	159.86			6.79
9	201.5	171.65			7.29
10	223.5	183.44			7.79
11	245.5	195.23			8.29
12	267.5	207.02			8.79
13	289.5	218.81			9.29
14	311.5	230.60			9.79
15	332.5		234.69	231.92	9.96
16	354.5		238.57	235.65	10.13
17	376.5		242.45	239.38	10.29
18	398.5		246.33	243.12	10.46
19	420.5		250.21	246.85	10.62
20	442.5		254.09	250.59	10.79
21	464.5		257.96	254.32	10.95
22	486.5		261.84	258.05	11.12
23	508.5		265.72	261.79	11.28
24	530.5		269.60	265.52	11.45
25	552.5		273.48	269.25	11.61
26	574.5		277.36	272.99	11.77
27	596.5		281.24	276.72	11.94
28	611.5		283.88	280.36	12.05
29	635.5		277.37	271.15	11.77
30	659.5		264.51		11.23
31	683.5		248.77	242.20	10.56
32	707.5		233.04		9.89

**\*\*Note:** For location, point 0.0 is at the tip of the nose.  
All stringers are 4 inches deep for their entire length.

Table 10.1 Structural Layout Data

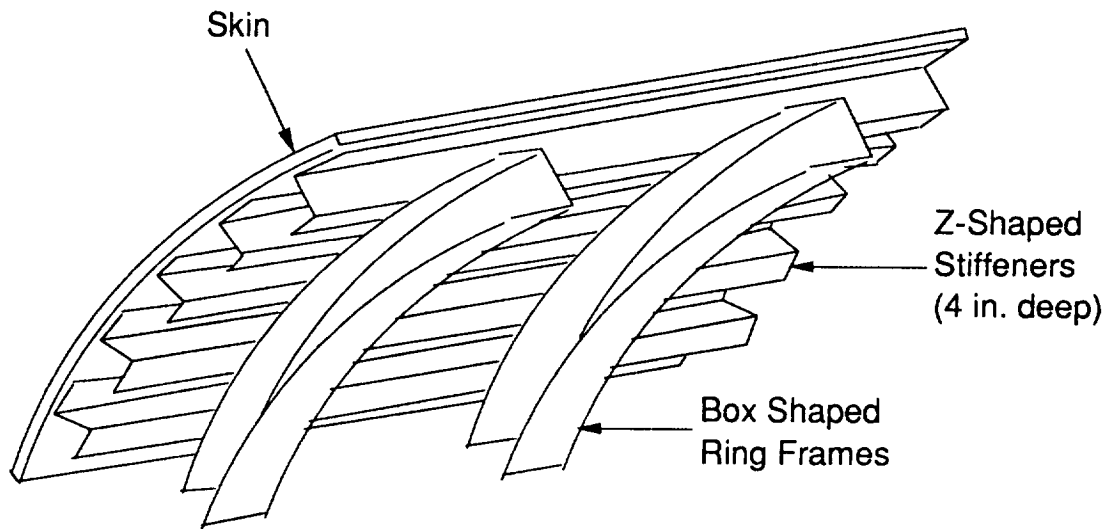
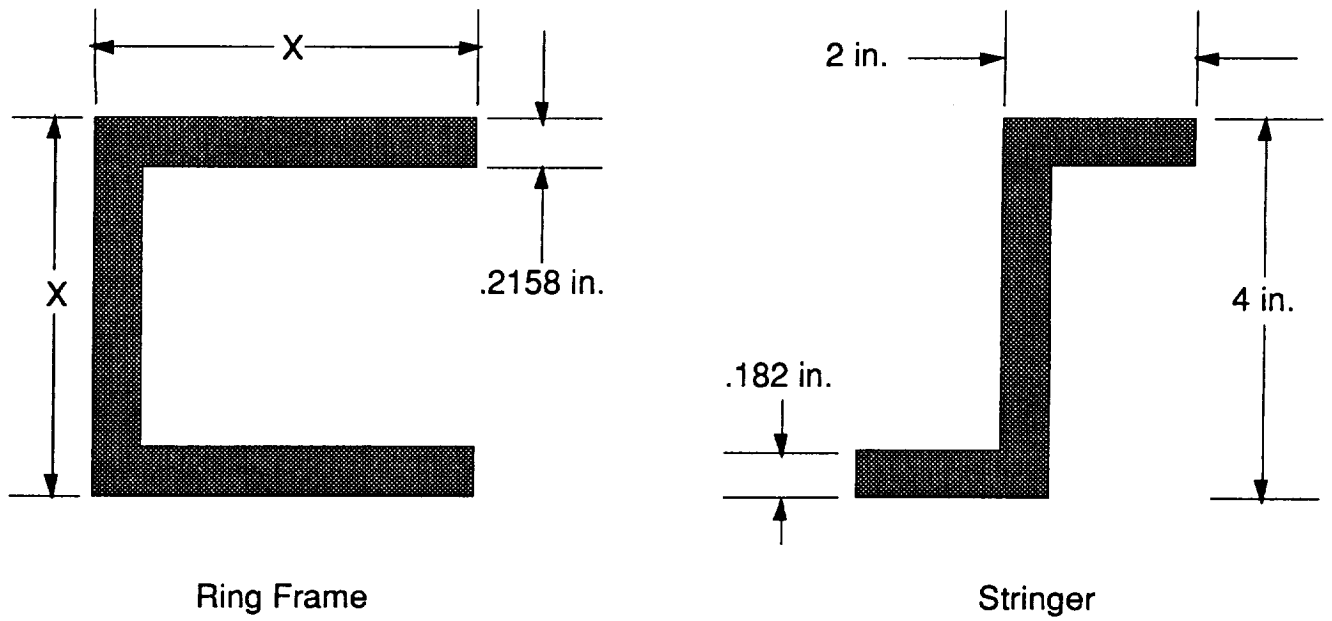


Figure 10.2  
Structural Detail

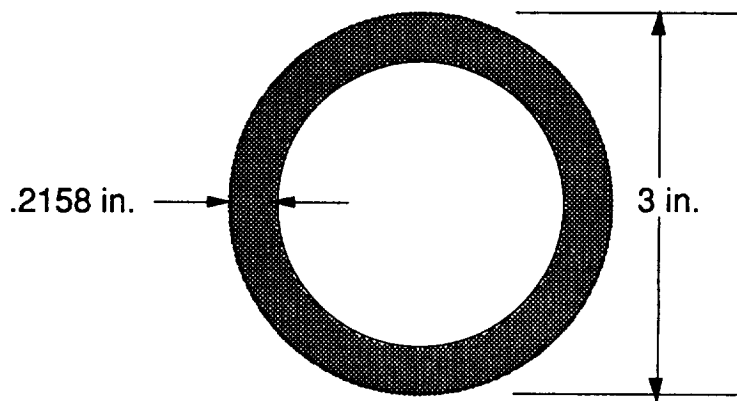
ring and stringer systems used to accommodate similar stresses and strains.

Every stringer support is 4 inches deep for its entire length so that at ring number 7, when half of the stringers stop, the supports that continue on do not change shape. The frames, on the other hand, vary in depth from 2 inches to 4 inches. Rings 1 - 6 are 2 inches deep, 7 - 14 are 3 inches deep, and 15 - 32 are 4 inches deep. This is due to the fact that the entire structure has to be thicker at the positions where the fuselage has larger diameters.

The thickness of the stringers is .182 inches, and that of the rings is .2158 inches, regardless of the particular depth. For drawings of the structural cross-sections and complete dimensional information, refer to Figure 10.3 and Table 10.1. The entire fuselage support structure will be made out of aluminum 2219 because it is able to handle the temperatures and stresses that will be encountered and it is cheaper as well as lighter than titanium. The weight of the fuselage support structure, including the payload bay support system, will be 11,400 pounds.



Refer to layout data for value of  $X$  in each particular ring.



Tubular Truss Member

Figure 10.3 Structural Members Cross Sections

## **10.2 Fin Structure**

Two fins are used to give the cargo return vehicle additional stability. The fins protrude 12 feet out from each side of the fuselage at its midpoint and have a constant chord of 10 feet. They are symmetric airfoils and therefore have zero camber. Refer to Figure 10.4 for different views of the fins. The support structure for the two identical fins is a general system of ribs and stringers with a honeycomb skin, as used on the fuselage. However the mechanics of these fins are anything but conventional. The design allows the outer third of the fin (4 ft.) to be mechanically rotated upward 90° in a similar manner as a flap is positioned. This operation would be performed at the desired time during descent in order to give the vehicle a vertical control surface, which was determined to be a necessity by the stability and control group. These fins were chosen as an alternative to a vertical tail, which could not be implemented into the design of the biconic CRV. The fins are directly attached to the fuselage by fastening stringers to the truss frames, thus creating a single unit.

## **10.3 Payload Bay**

The primary requirement of the payload bay is that it is able to hold a pressurized logistics module or two unpressurized logistics modules. Refer to section 2.5 on mission operations for further details on the logistics modules and payload bay. The payload bay is 25 feet long with a diameter of 15 feet. Sill longerons are placed along the bay door/fuselage junction and serve as a mounting point for the payload bay door hinges. These longerons, constructed of aluminum 2219, will be two inches thick and run the entire length of the payload bay. Each of the two bay doors also span the entire length of the payload bay and have a radius that varies as the diameter of the vehicle but which is approximately 10 feet. The structure of the doors will consist of a graphite/epoxy sheet permanently bonded to a frame of graphite/epoxy stringers. The stringers will run transversely from the upper to lower edge of the door and will be spaced 2 feet apart at the rear of the bay and converge slightly as they move forward, with a uniform rectangular cross-section of 0.5 inches by 0.25 inches. The payload bay door hinges will be made out of the composite Inconel which is also used on the space shuttle hinges. Composite materials were chosen for the doors and hinges because of their low coefficients of thermal

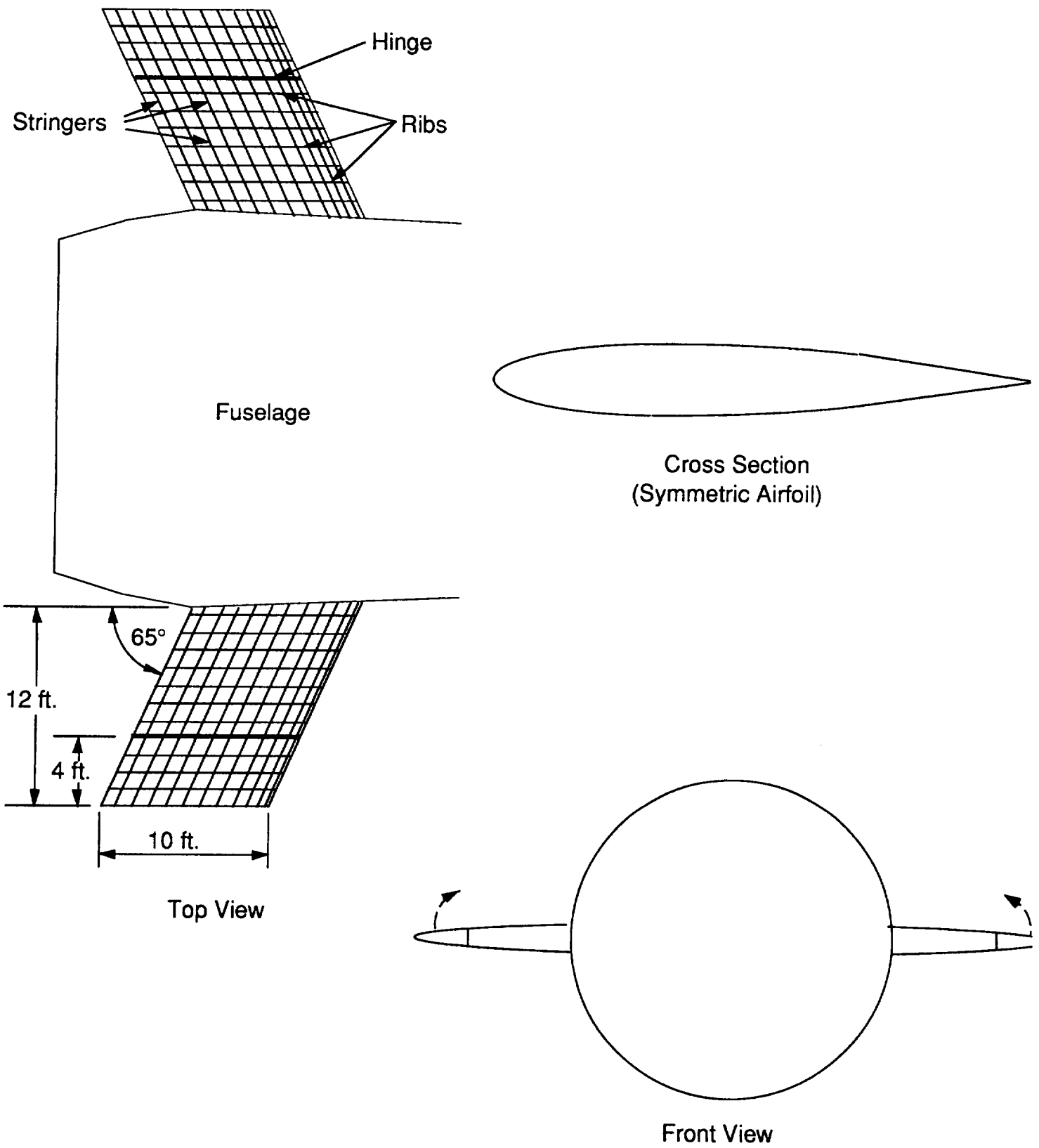


Figure 10.4 Fin Structure

expansion as compared to metals. This promotes good sealing characteristics as extreme temperature differences are encountered. The floor of the payload bay must be able to withstand the loadings from the payload and must also carry structural loads from the fuselage. The floor will be attached directly to the semi-circular inner ring frames described in the next section. This floor will be an aluminum honeycomb design with a thickness of 0.5 inches. Refer to Figure 10.5 for a front view of the payload bay.

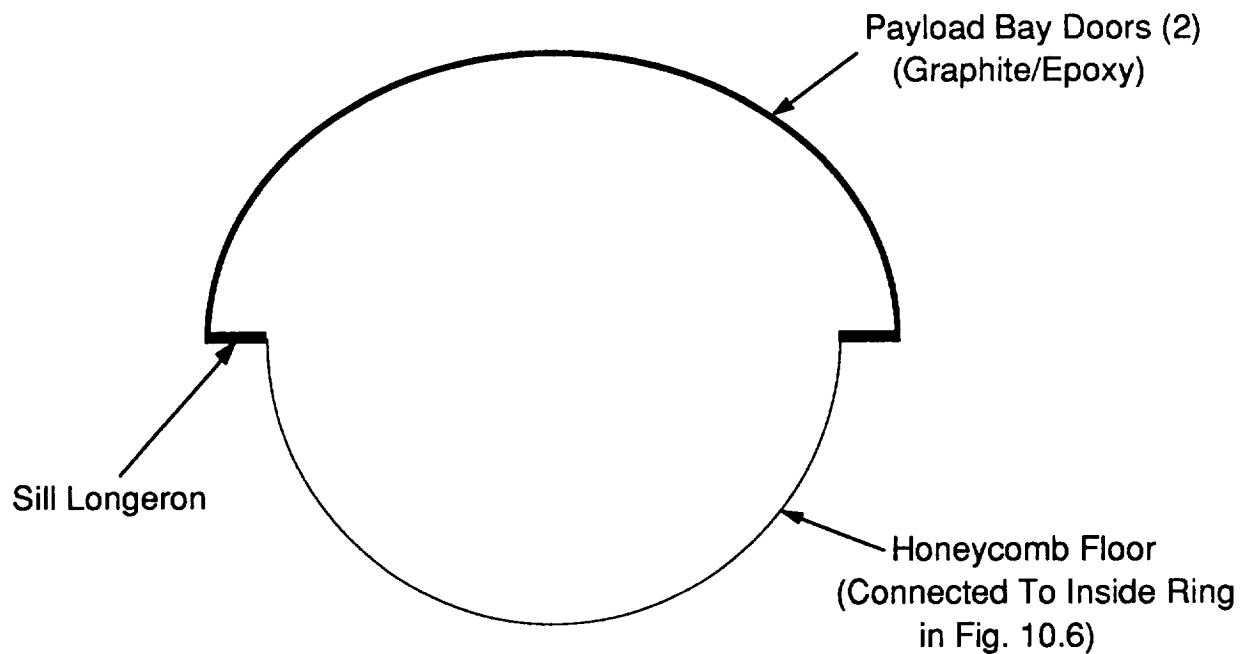


Figure 10.5 Payload Bay (Front View)

#### **10.4 Payload Bay Support Structure**

The structure that will be used to support and hold the payload bay is a series of half rings which have an inside diameter of just over 15 ft. There are 14 of these half rings and they are coplanar with the outside rings, numbers 15-28, so they are also spaced 22 in apart.

The inside ring frames will all be box shaped with a depth of 4 inches and a thickness of .2158 inches. These rings will give support to the bay along its entire length. The inner half frames are connected to and supported by the outer rings through the use of a truss assembly. Inner frames are connected to the outer ones in the same plane as shown in the front view of the payload bay support structure in Figure 10.6.

Alternating inner and outer rings are also connected to give the bay some longitudinal support as shown in the side view of the payload bay support structure in Figure 10.7. Note that this figure shows only 5 of the 14 rings used to support the payload bay. Since tubular beams provide the greatest compressive strength per unit cross-sectional area, it was decided that all of the truss members would be tubular.

The truss members will be 3 inches in diameter with a uniform thickness of .2158 inches, the same thickness as in the ring frames. A detailed view of the cross-section of one of the tubular truss members can be seen in Figure 10.3. Every truss member is constructed from aluminum 2219 because of its outstanding thermal and mass properties as well as its relatively high level of strength.

## **10.5 Materials**

The Biconic CRV will be using the warm structure concept in its design. With this concept, the thermal protection system (TPS) is designed to keep the structure at a predetermined temperature. The TPS discipline has determined that the structure must withstand temperatures up to 550° F. Using this as a lower temperature limit, the options available for materials that can be used are limited. Since the structure will be at these higher temperatures for a short amount of time, Aluminum 2219 has been chosen as the primary structural material. Aluminum 2219 is an aluminum alloy that is recommended for higher temperature applications. Al 2219 is capable of retaining fairly good tensile properties and it has a high resistance to creep at the elevated temperatures. Table 10.2 shows some of the properties of Aluminum 2219.

Figures 10.8 (a) & (b) show the effects of elevated temperatures on the Tensile Yield and Tensile Ultimate strengths for Al. 2219 in the sheet and plate form.

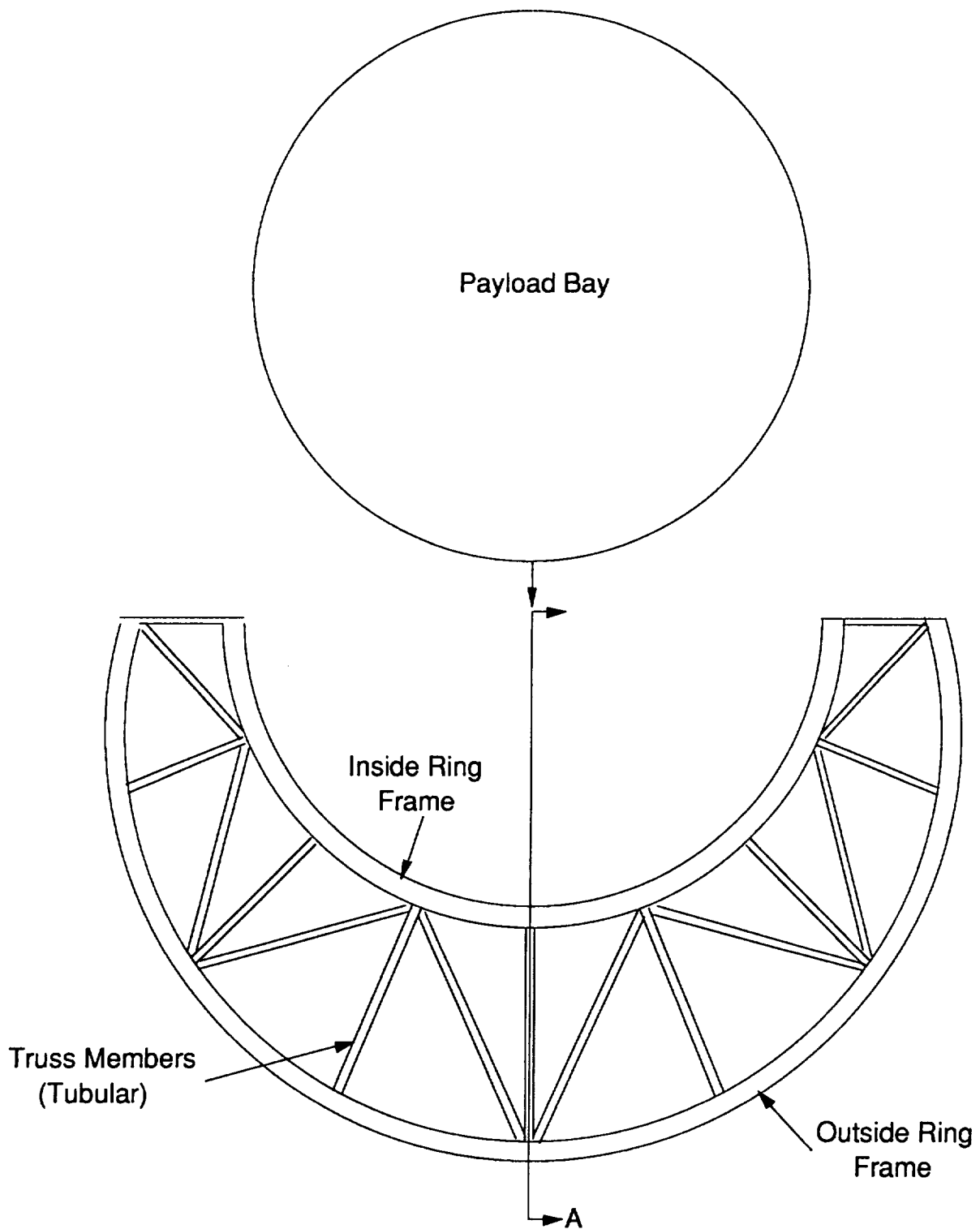
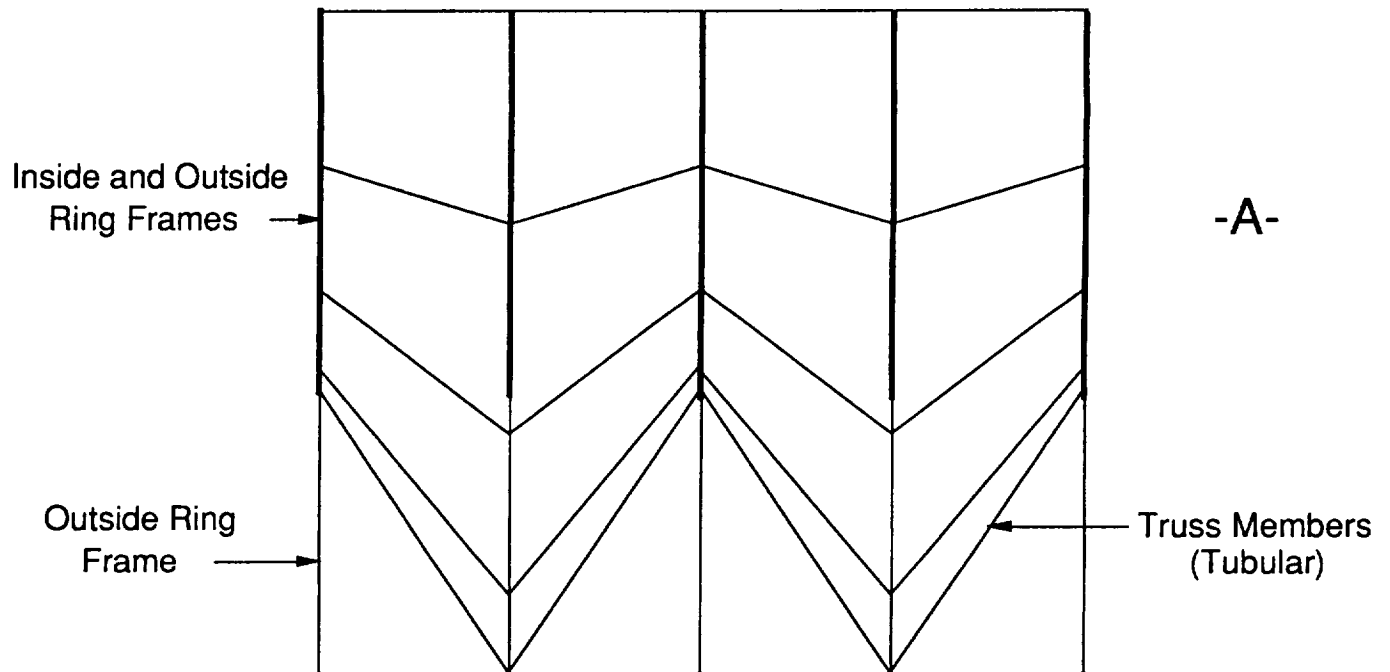


Figure 10.6 Front View of Payload Bay Support Structure



Note: These truss members connect alternating inner and outer rings.  
 This figure shows only 5 of the 14 rings used to support the bay.

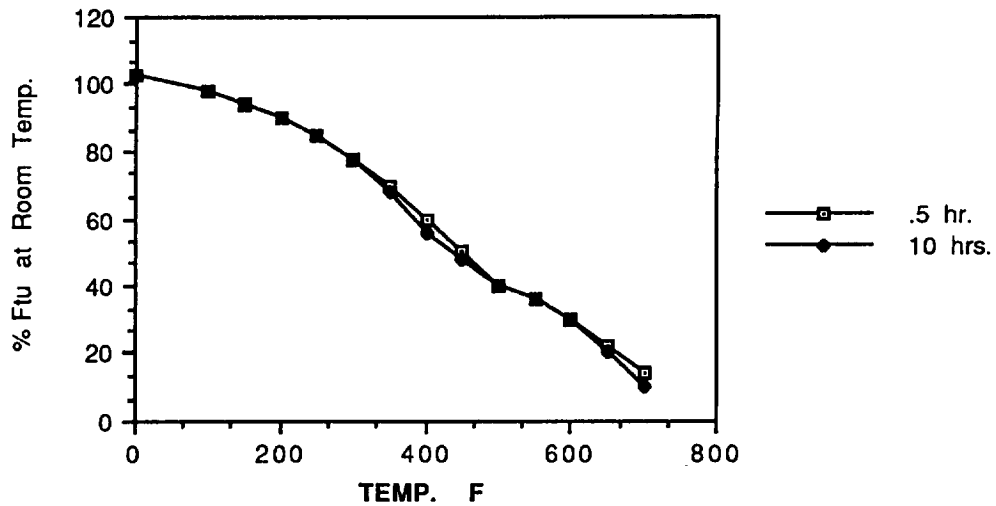
Figure 10.7 Sidew View of Payload Bay Support Structure  
 (-A- View in Figure 10.6)

Physical Constants:

Density	lb./cu.in.	102
Specific Gravity		2.82
Thermal Conductivity	Btu/ft <sup>2</sup> /in./s./°F	0.25
Mod. of Elasticity	psi x 10 <sup>6</sup>	10.6
Therm. coef. expans.	in./in./°F x 10 <sup>-6</sup>	13.0
	68-392 °F	

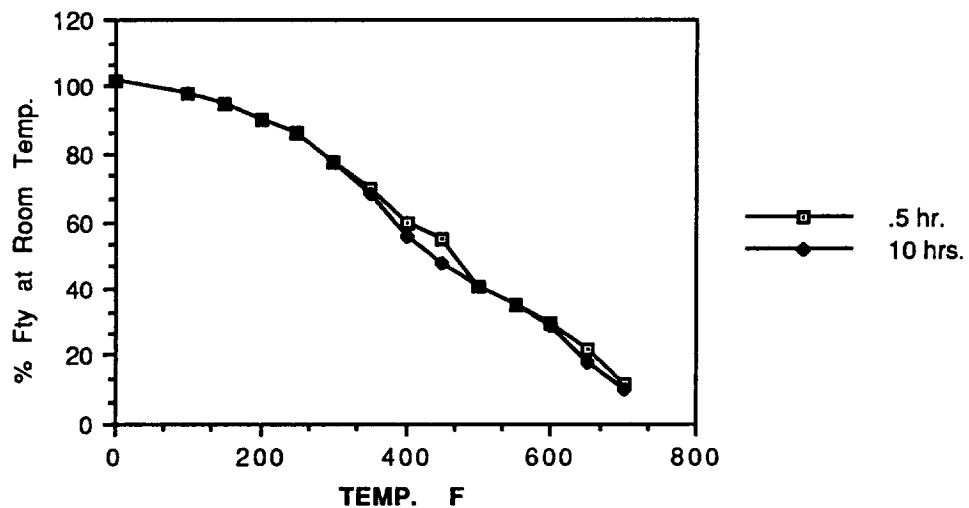
Table 10.2 Properties of Aluminum 2219 (Ref. 10.1)

Effects of Temperature on Tensile Ultimate for Aluminum 2219 in sheet and plate form.



(a)

Effect of Temperature on Tensile Yield for Aluminum 2219 in sheet and plate form



(b)

Figure 10.8 ( Ref. 10.2 )

In areas where the loads will be very high, such as in the thrust structure area, stronger materials will need to be used. The space shuttle used a diffusion bonded titanium in this area, which would also work very well in the Biconic CRV. Titanium is a much stronger

alloy than aluminum and also has a much higher temperature limit. In the areas of the main structure that experience critical loads, a boron/aluminum material can be used. Some of these structural hardpoints would include the points of attachment for transportation, the connection points of the Advanced Recovery System, and the attachment points of the horizontal fins. The outer skin of the CRV will be comprised of a honeycomb material sandwiched in two layers of aluminum 2219 facing material that can withstand the high temperatures and the loads that it will experience.

With a preliminary design analysis that was done, it was determined that the structure should meet the design requirements that are set by NASA for a unmanned metallic structure. (Ref. 10.3) In a simple analysis, the CRV will experience a maximum dynamic pressure of 400 lb./ft.<sup>2</sup> and have a maximum pressure coefficient of .96065. These numbers were obtained from the HABP program, which the aerodynamics group (section 4.0) used. These numbers lead to a maximum force applied to the vehicle of 15.16 klb./in.<sup>2</sup>. A detailed structural analysis was done using a program from NASA called NASTRAN. This program analyzes a structure that is input by a method of finite elements. The results of this analysis can be found in Volume 3, Structural Analysis.

## **10.6 Outer Skin**

The outer skin of the CRV will be made of HRH-327 honeycomb with Aluminum 2219 facing material on each side. The reasons for going with a honeycomb skin are that it is most efficient for getting the maximum strength with the least amount of weight.

A honeycomb panel consists of five layers of materials. Figure 10.9 shows the five layers and their placement. These layers are then put together to form a sandwich which makes a strong panel. Figure 10.10 shows two views of a fabricated honeycomb panel section. Table 10.3 shows how the thickness of a honeycomb panel compares in stiffness, strength, and weight to a panel made of one solid material.

The material selected for use as the honeycomb is HRH-327, made by the HEXEL Corporation. HRH-327 is a glass fabric, polyimide node adhesive, bias weave reinforced plastic honeycomb dipped in a

## HONEYCOMB SANDWICH CONSTRUCTION

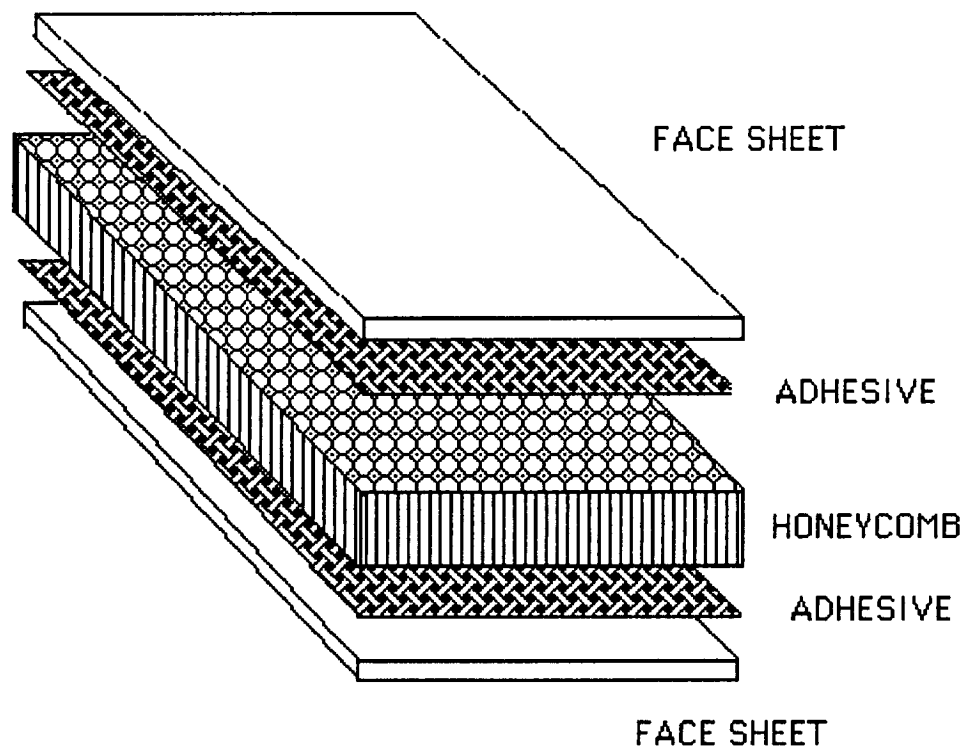


Figure 10.9 Structure Face Sheet

polyimide resin to achieve the final density. This specific material has been designed for temperatures up to 500°F with short range capabilities to 700°F (Ref. 10.5). With these high service temperatures it is well suited for use in the warm structure. The Biconic CRV will use HRH-327 with a cell size of 3/8" and a density of 4 lb./ft.<sup>3</sup> for the honeycomb material. The material properties of HRH-327 are highlighted in Table 10.4.

FABRICATED  
HONEYCOMB  
SANDWICH  
PANELS

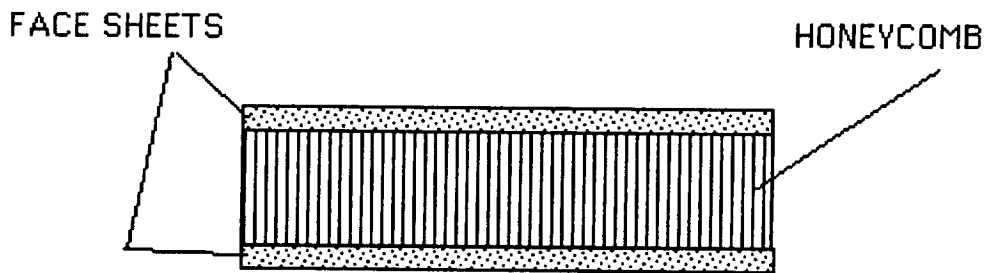
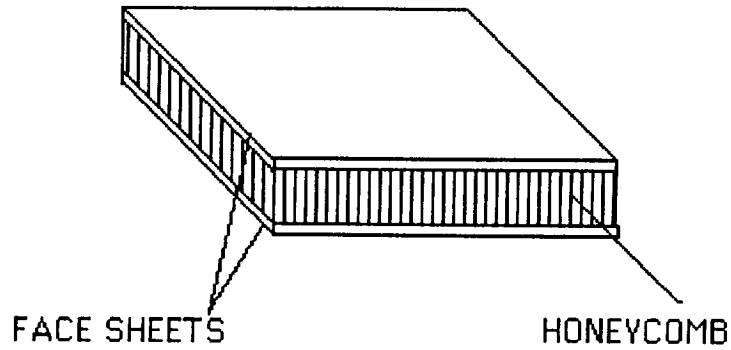
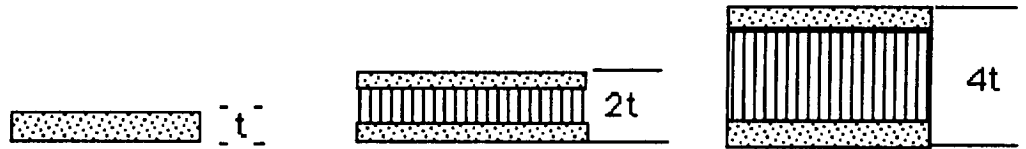


Figure 10.10 Fabricated Honeycomb Sandwich Panels

Non-metallic honeycomb material has some thermal resistance which may aid in keeping the temperature of the structure lower. If necessary, the honeycomb can also be filled with a insulating

## HONEYCOMB VS. SINGLE PLY



RELATIVE STIFFNESS	100	700	3700
RELATIVE STRENGTH	100	350	925
RELATIVE WEIGHT	100	103	106

Table 10.3 Honeycomb vs. Single Ply( Ref. 10.4 )

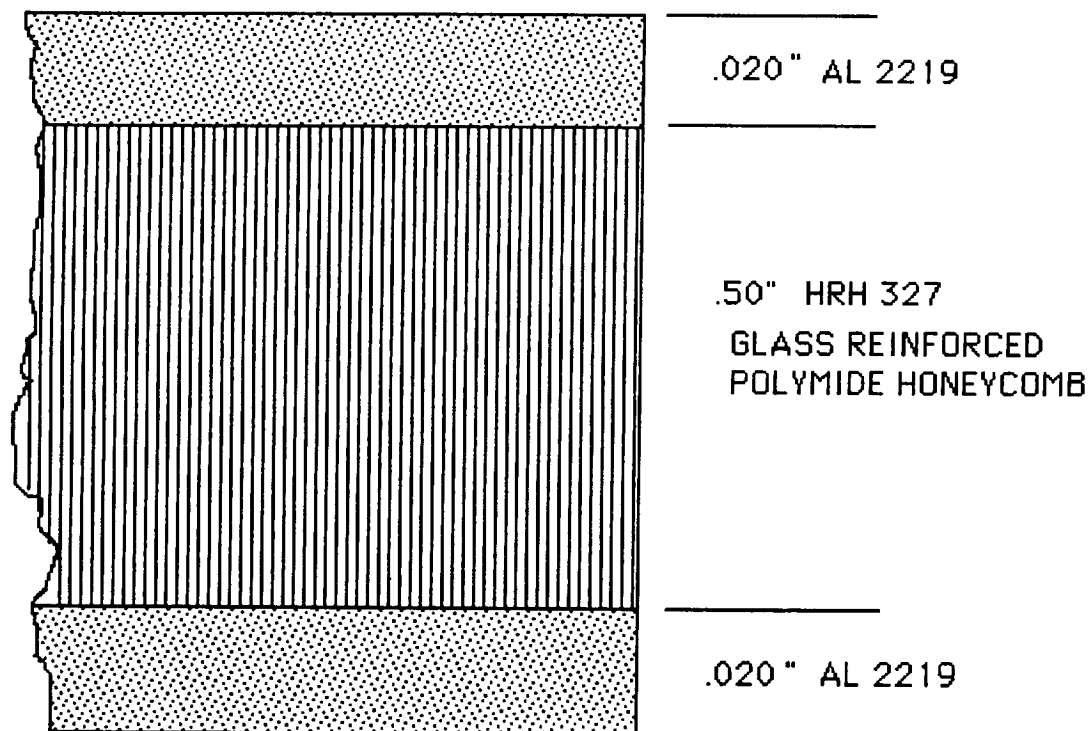
	STRENGTH		MODULUS Ksi min.
	psi typ.	psi min.	
COMPRESSION	440	325	50
PLATE SHEAR (L - direction)	280	195	29
PLATE SHEAR (W - direction)	150	100	12

Table 10.4 Properties of 3/8" HRH-327 (Density 4)

material so as to increase the thermal resistance of the skin. HRH-327 is also a fair material to use in the area of impact resistance.

Space debris is an increasing problem in space travel and a honeycomb material will aid in the event of debris collision.

Figure 10.11 shows a cross section of the outer skin. It shows the two layers of Aluminum 2219 at 0.020" thickness and the HRH-327 honeycomb material at 0.50" thick. The combination produces a total skin thickness of 0.540 inches. With this skin thickness a total weight of the outer skin will be 1412.14 lbs.



Total Thickness = .540 in.

Figure 10.11 Outer Skin

The advanced recovery system (ARS) group has had a problem with the attachments for its cables. As a part of the solution, a notch will have to be put into the skin of the CRV to house the cables and the appropriate thermal protection. This notch will have to be 0.50 inches deep and 2.75 inches wide. Figure 10.12 shows a detail of the skin for this requirement.

## NOTCH IN SHELL FOR ARS CABLES

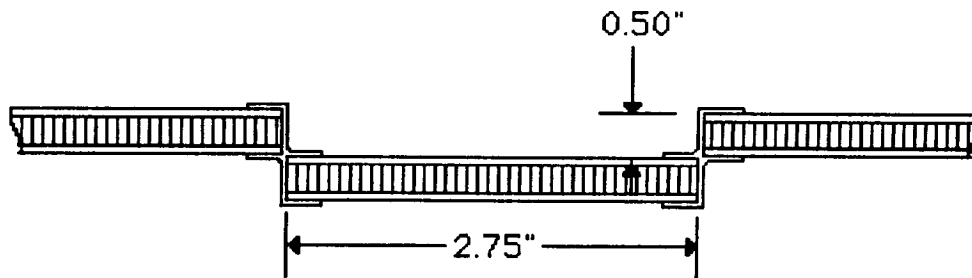


Figure 10.12 Notch for ARS Cables

The sizing of the panels for the outer skin are a study of compromise. The panels need to be small enough so that they can be removed and handled easily, made in dimensions so that they can be easily attached to the stringers. The panels also cannot be made so small that the number of them adds too much weight in the form of closeouts and attachment of separate panels.

The Z-shaped stiffeners are positioned twelve inches apart which would make attachment points for the ends of the panels as well as the middle of the panels. Figure 10.13 shows an example of one of the panels from each cone section of the CRV.

The panels will be attached with the use of bolts. These bolts will go through the outer skin panel and bolt to the Z-shaped stiffeners. The honeycomb panels will have to be fabricated so that there is a reinforced area in the panel where the bolts will have to go through. This will have to be done during the manufacturing of the panels. Figure 10.14 shows a cutaway view of what this will look like and more detail of how the attachment works.

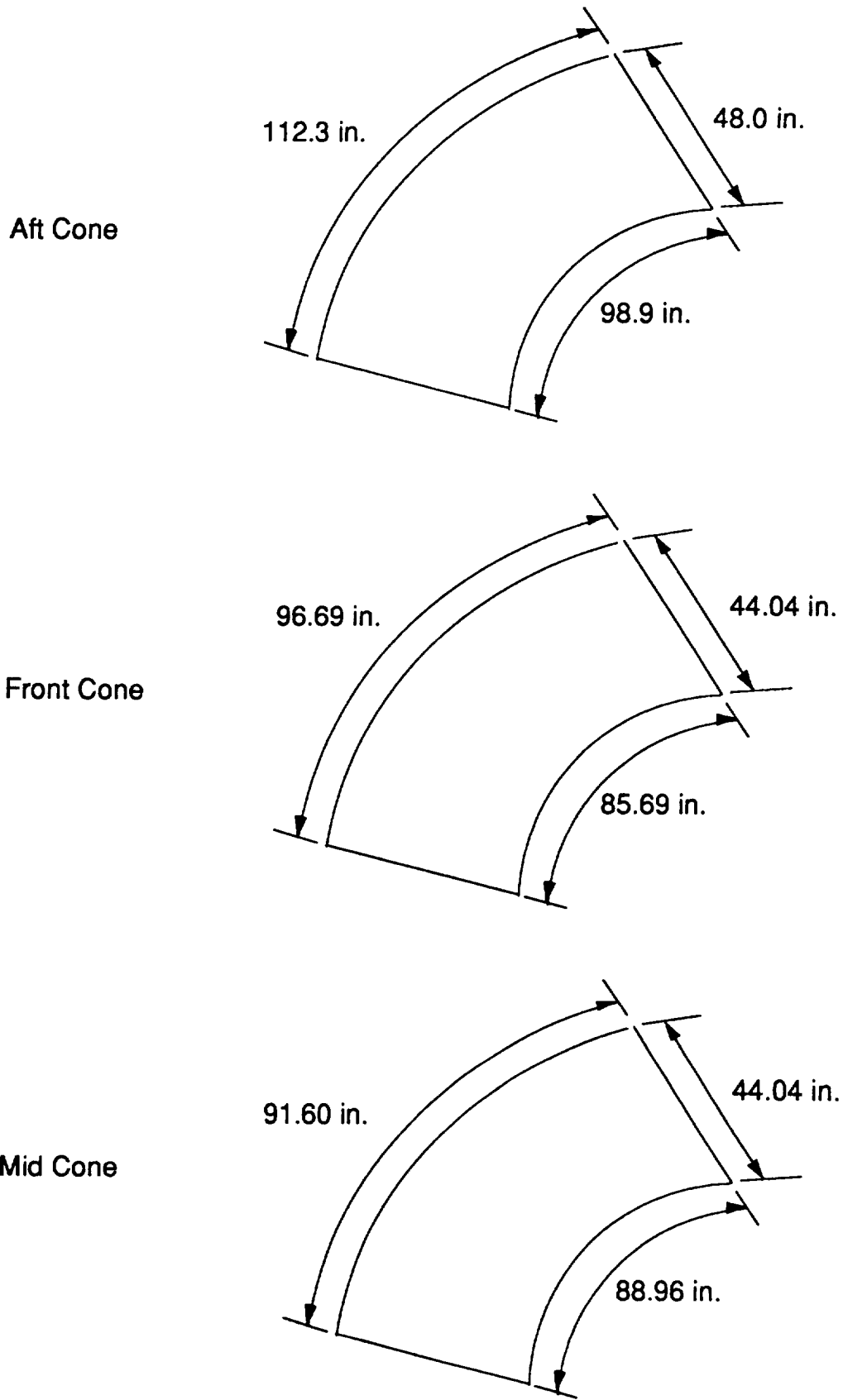


Figure 10.13 Example Panels for Front, Mid, and Aft Cones

## PANEL ATTACHMENT METHODS

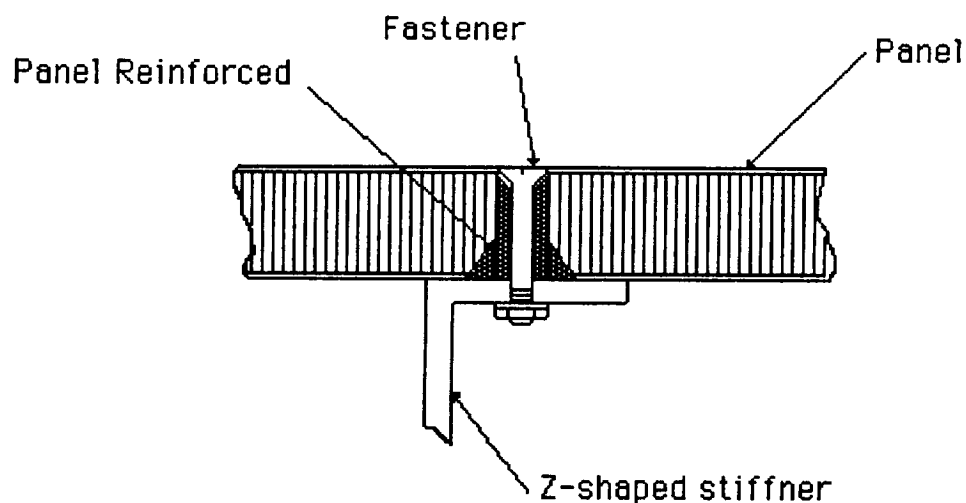


Figure 10.14

### **10.7 Landing Gear System**

The hardline requirements for the Biconic CRV's landing gear system are a dryland recovery and ability to land on a 10,000 foot runway. An arrangement of the system will be a "tricycle" gear, with two main wheels aft of the center of gravity(c.g.) and an auxiliary wheel forward of the c.g. This provides the CRV with more stability and a

larger landing angle of attack. The following are the constraints in the design of the landing gear.

Landing weight	70000 lbs	
CRV's velocities before touch down		
Horizontal velocity	80 ft/sec	
Vertical velocity	5 ft/sec	
Center of Gravity (c.g.)	AFT	FWD
From the nose of CRV(x)	36.2 ft	33.4 ft
From the geometric center(y)	0 ft	0 ft
From the bottom of CRV(z)	11.9 ft	8.56 ft

- \* The y-axis is a lateral distance starting at the geometric center of the CRV.

In designing this landing gear system, a minimum safety factor(SF) of 7% to 25% has been added. Finally, the landing gear system with a total weight of 4058 lbs is designed to fit the hardline requirements. The CRV will use an advanced recovery system (ARS) in order to maneuver and slow the vehicle down for a soft dry land recovery. Otherwise, a sudden increase in vertical landing velocity of the vehicle can damage the landing gear system.

### 10.7.1 Landing Gear Location

The actual length of the main gear will be 6.0 ft instead of 5.575 ft. Figure 10.15 shows the turnover angle of the CRV, 59°.

Nose Gear Location (x, y, z) (9.9, 0, 2.09) ft

Main Landing gear Location (x , y, z) (39.4, 2.77, 5.575) ft  
(39.4, -2.77, 5.575) ft

The actual length of the nose gear will be 2.5 ft instead of 2.09 ft. The main concern in designing the landing gear system was the length of nose gear. Because the Biconic CRV has an airfoil shape, the middle section of the vehicle is now 1 ft above the ground at static position (Figure 10.16).

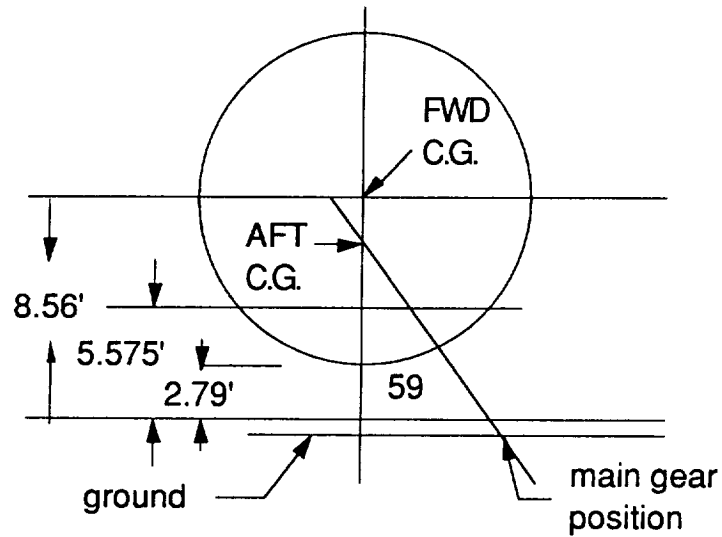


Figure 10.15 Frontal Cut Out View of Two Main Gears

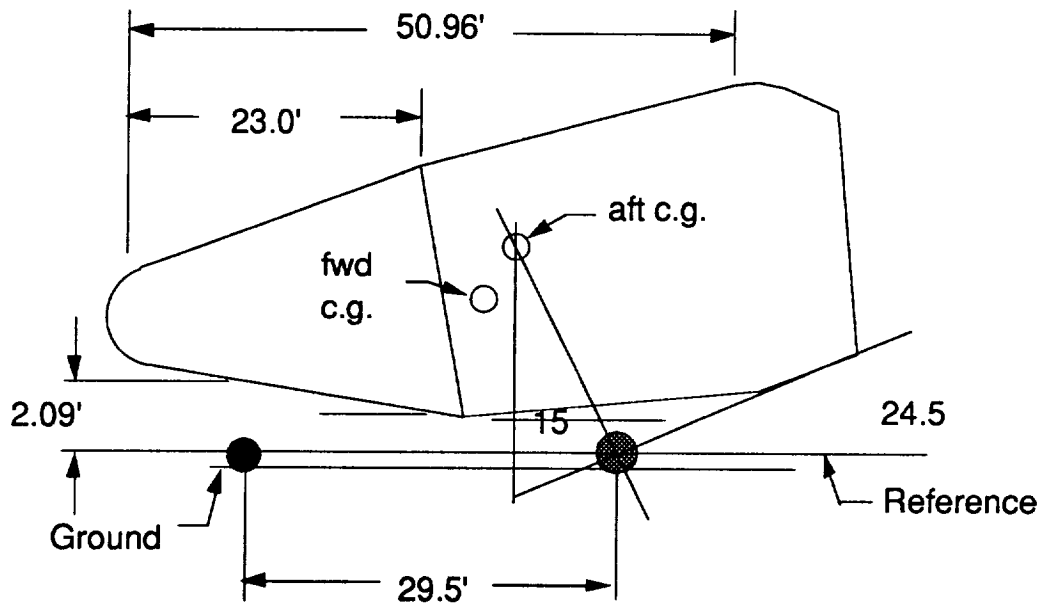


Figure 10.16 Side View of CRV with Landing Gear.

## 10.7.2 Landing Geometry and Load Distributions

The CRV is recommended to land with the nose up, while its landing angle or angle of attack must be lower than 24.5 degrees. This is given from the geometrical figure of the CRV (Figure 10.15). The ARS of the vehicle will be released after the main gear touches down on the ground.

### Load Distributions:

Maximum static main gear load per strut	30135.6 lbs
Maximum static nose gear	16372.9 lbs
Minimum static nose gear	9728.8 lbs
Maximum braking nose gear load	20529.1 lbs

In order to calculate the maximum braking nose gear load, the deceleration of the CRV must be known. From hardline requirements, the stopping distance of the vehicle must be under 10000 feet. However, if this vehicle stops at that distance, the deceleration is only .32 ft/sec/sec. This is negligibly small which means that is hard to find a brake system with that kind of precision. So, the deceleration has been chosen to 5 ft/sec/sec which allows the CRV to stop 640 ft after touch down on the ground.

Tire Selections:	Load on each tire	Safety factor (25%)
Main Gear	15067.8 lbs	18840 lbs
Nose Gear	8186.45 lbs	10240 lbs

The tires' size, pressures, and maximum loads have been chosen with a 25% safety factor.

	Size	Pressure	Max Load
Main Gear	29 x 10	210 psi	19500 lbs
Nose Gear	24 x 5.5	355 psi	11500 lbs

The main gear will have two wheels per strut and there will be two struts. The nose gear will have two wheels with only one strut.

### Landing Gear Weight Estimate:

The total landing gear's weight is 4058 lbs.

	% Tot. Weight	Weight (lbs)
Main Gear	80	3246.4
Nose Gear	20	811.6

Shock Absorbers (Oleo-Pneumatic Shock):

The Oleo-Pneumatic shock absorber has been chosen because it is lighter than any other shock with one of the highest efficiency, 0.8 - 0.9.

1. Kinetic Energy

Vertical	27173.9 ft-lbs
Horizontal	6956521.7 ft-lbs

2. Distance of Shock

	Minimum	Actual
Main Gear	6.94 inch	9.0 inch
Nose Gear	5.12 inch	7.1 inch

- \* Each shock absorber has been lengthen for safety reasons. An additional length increase of 2 inches will allow the shock's pressurized fluid, in this case 1800 psi, to be less than its maximum at touch down. The minimum distance of the shock should be added to the minimum length of each landing gear. For example, if the main gear requires 5.575 feet of length but needs to install a 9 inch shock, the total extension of the gear will be 6.325 feet. The previous estimation of 6 feet length, however, is not wrong because the whole gear will not be attached to the outermost shell of the vehicle. There will be some internal distance which will be structurally joined with the main frame of the CRV.

3. Area of Shock (inch ^2)

	Minimum	Actual
Main Gear	16.742	18.08
Nose Gear	9.096	9.82

- \* The installed shock absorbers are larger than minimum required shocks for safety reasons (8% SF).

## 10.8 Engine Mount Design

The structural design of the engine mount must meet several requirements. The most important requirement is the location of the engine in the CRV. This location must allow the engine to operate efficiently and effectively.

Another important task in this design is to allow easy access for maintenance of the engine. A flange type ring attached on the top of the nozzle will allow this easy access. More importantly, this improves the nozzle attachment to the main engine compartment by decreasing the time needed to remove the nozzle.

This "Removable Ring" will be made out of the FS-85 Cd. alloy to overcome the stress and strain of the engines' full thrust. This is the same material used to make nozzle. The heat generated from the engine will not be an important factor for this ring, but a heat shield will cover the important part of the engine for precautions. The following are the constraints for the engine mount design.

OMS engine	Full Thrust(lbs)	Total mass(lbs)	Total length(inch)
	166.67	64.19	23.87

- \* The engine must gimbal 7 to 10 degree. The exit area of the nozzle is 127.03 sq. in. and its diameter is 12.72 inches. The diameter of the nozzle's neck, which is the entrance of the fuel before burning, is 1.74 inches.

### **10.8.1 OMS Engine Attachment**

The main criteria in the attachment of OMS engines is structural stability through out its entire operation. As the Figure 10.17 shows, the main structure of the rear portion of the vehicle will be spider web shape. This shape will evenly distribute the stress and strain of both internal and external force and moment.

The empty and full c.g. must lie within the triangular shape region described by three OMS engines. When the engines are in operation, each firing point is on a different side of the c.g. to control the moment of CRV. Since the OMS may also operate in

both empty and full weight of the CRV, that triangle must include both center of gravities.

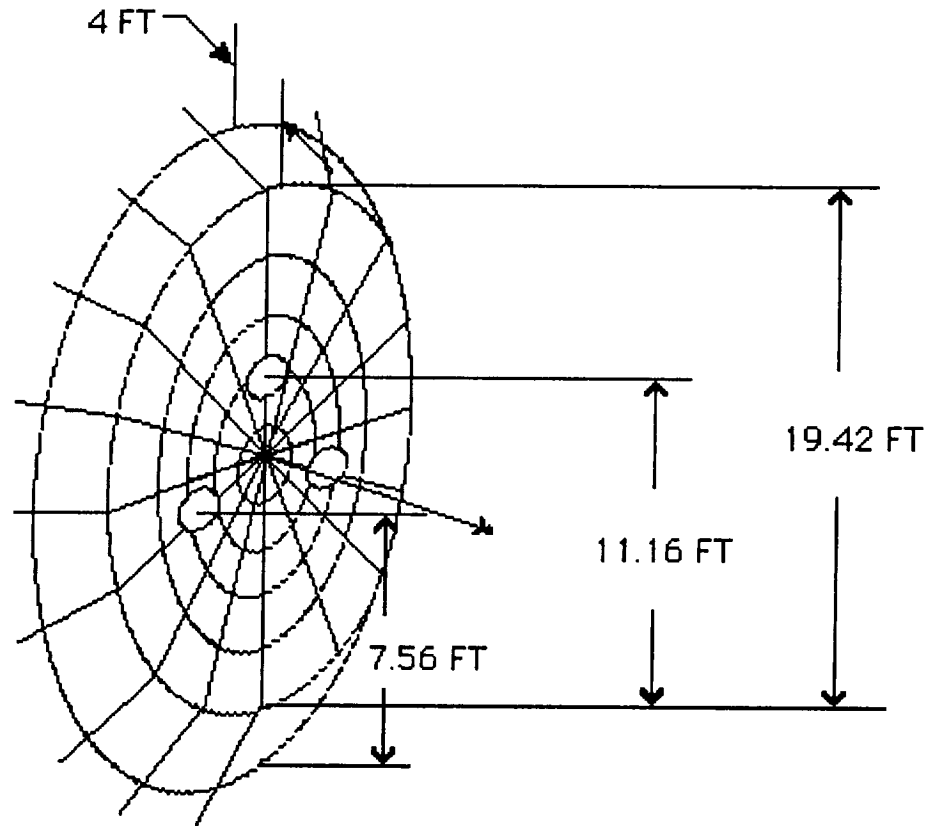


Figure 10.17 Structural View From Rear of CRV.

There will be eight tension bars connecting each engine to the main structure of the vehicle (Figure 10.18). Another four tension bars are also used in holding the nozzle. During the operation of the engine, the nozzle will expand itself. This expansion is accommodated by tension bars that are allowed to expand with the nozzle without causing any problems of fracture.

Finally, each engine is attached on the circular shape of main frame. The rear view of the CRV has a main structure that will distribute the load evenly over all of the frames. Therefore, this frame is shaped in a spider's web.

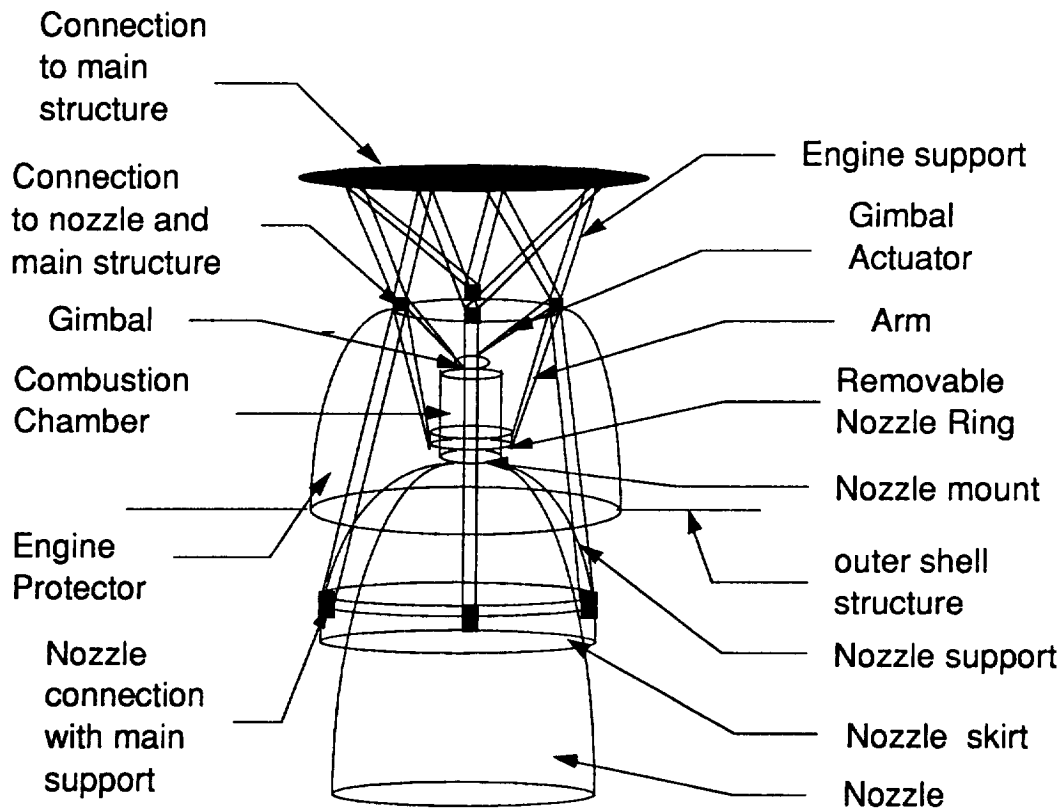


Figure 10.18 OMS Engine Attachment

### 10.8.2 "Removable Nozzle Ring"

The "Removable Nozzle Ring" will be attached on top of the nozzle. The location of the ring relative to the engine is shown in Figure 10.18. Figure 10.19 shows the precise dimensions of the ring.

This ring is in a shape which will allow the nozzle to gimbal almost 10 degree in any direction. This is achieved by two T-shape flanges (Figure 10.20) which operate like two arms that hold both engine and nozzle.

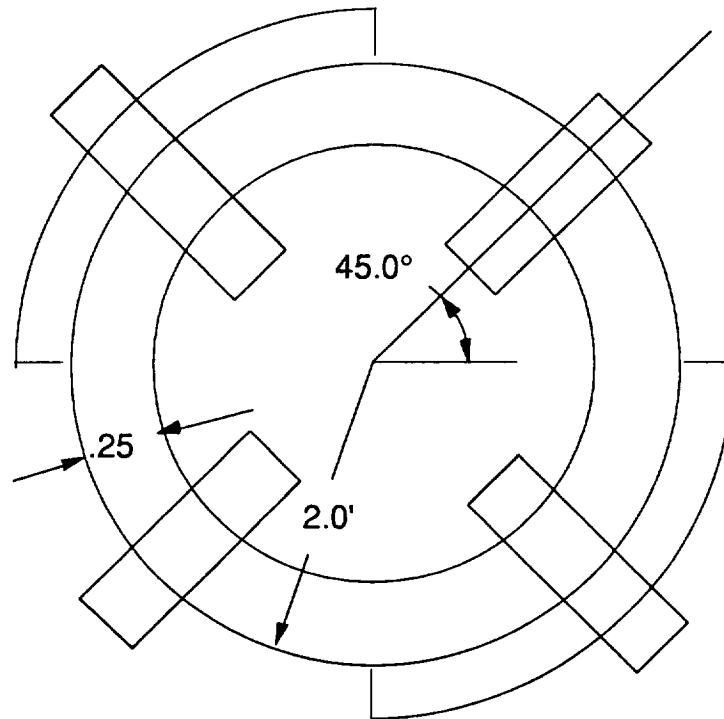


Figure 10.19 "Removable Nozzle Ring"

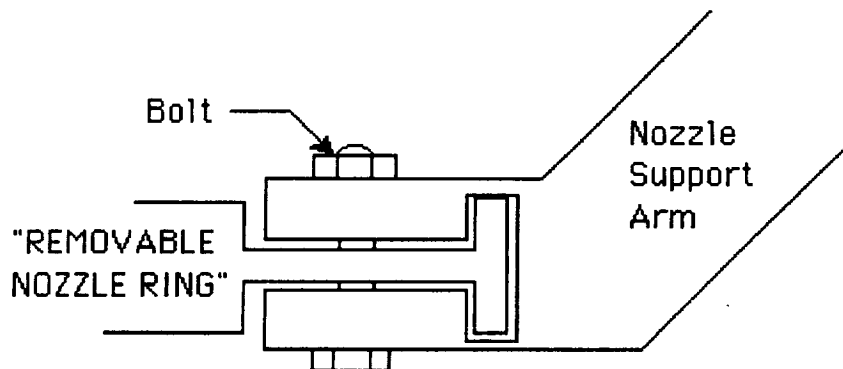


Figure 10.20 Side View of the Ring and Support Arm

This flange allows the engine to gimbal the nozzle and it provides a solid mount for the nozzle to the engine. The heat shield will cover this part so that the engine will be protected from atmosphere.

## **10.9 Advanced Recovery System**

The trade study conducted at the beginning of the biconic CRV design project narrowed the choices for the advanced recovery system to two: a ram-air inflated parafoil, and a rigid structure parawing. During initial preliminary design, the decision was made to concentrate primarily on the ram-air inflated parafoil design. This decision was made because of the interference that an externally, top-mounted parawing would have with the cargo bay doors and with the docking mechanisms. In contrast, the ram-air parafoil is capable of internal storage, and thus, is more easily integrated into the overall design.

The preliminary design of the advanced recovery system consists of a 51 cell ram-air inflated parafoil constructed of Kevlar. The canopy is supported by a combination of Kevlar and nylon shroud lines that converge at the cable attachment platform. This platform will support the trailing edge deflection motors, as well as the camera for remote control. Four main cables attach the platform to the CRV. (See Figure 10.21 for an overall view of the advanced recovery system configuration.)

A drogue decelerator parachute will be deployed to reduce the dynamic pressure to 50 PSF at 10,000 ft altitude. At this point, the ram-air parafoil will deploy from its compartment and a two stage reefing process will take place. Initially, 11 parafoil cells are allowed to open. Once equilibrium is reached, an additional 10 cells are reefed open by use of pyrotechnic cutters. Finally, the remaining 30 cells are reefed open, and the ram-air parafoil is in full glide. A preliminary design of the advanced recovery system and its storage is explained throughout Section 10.9.

### **10.9.1 Drogue Parachute Compartment**

A drogue parachute packing volume of approximately 8 cubic feet was determined by the Aerodynamics Group. Including room for a deployment mechanism and a 50% margin for error

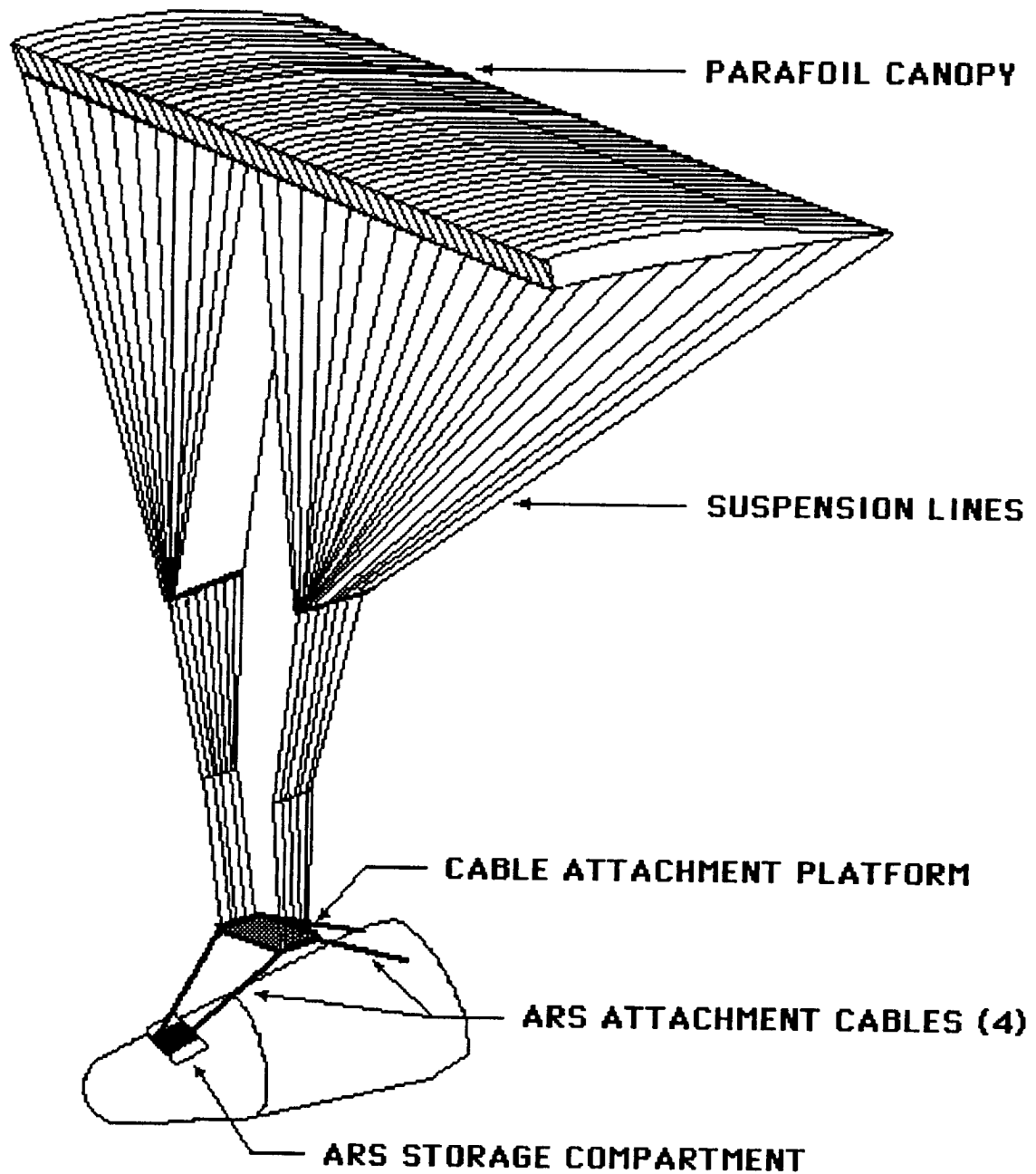


Figure 10.21 Advanced Recovery System Configuration

on the packing volume, a total drogue parachute compartment volume of 15 cubic feet was specified. The Systems Layout Group (Section 9.0) provided space for the drogue parachute

compartment near the top of the aft end of the CRV so that the compartment can be easily attached to the underlying ring structure of the CRV.

The drogue parachute is attached to the CRV with two main cables that are sunk into the thermal protection system (TPS), and are pulled out of the TPS when deployment occurs. (See Figure 10.22 for details).

An isometric drawing of the drogue parachute compartment is shown in Figure 10.23. The compartment door is fastened to the aft of the CRV with six exploding bolts. To avoid damage to the CRV during opening, the door will be discarded and need to be replaced for each mission.

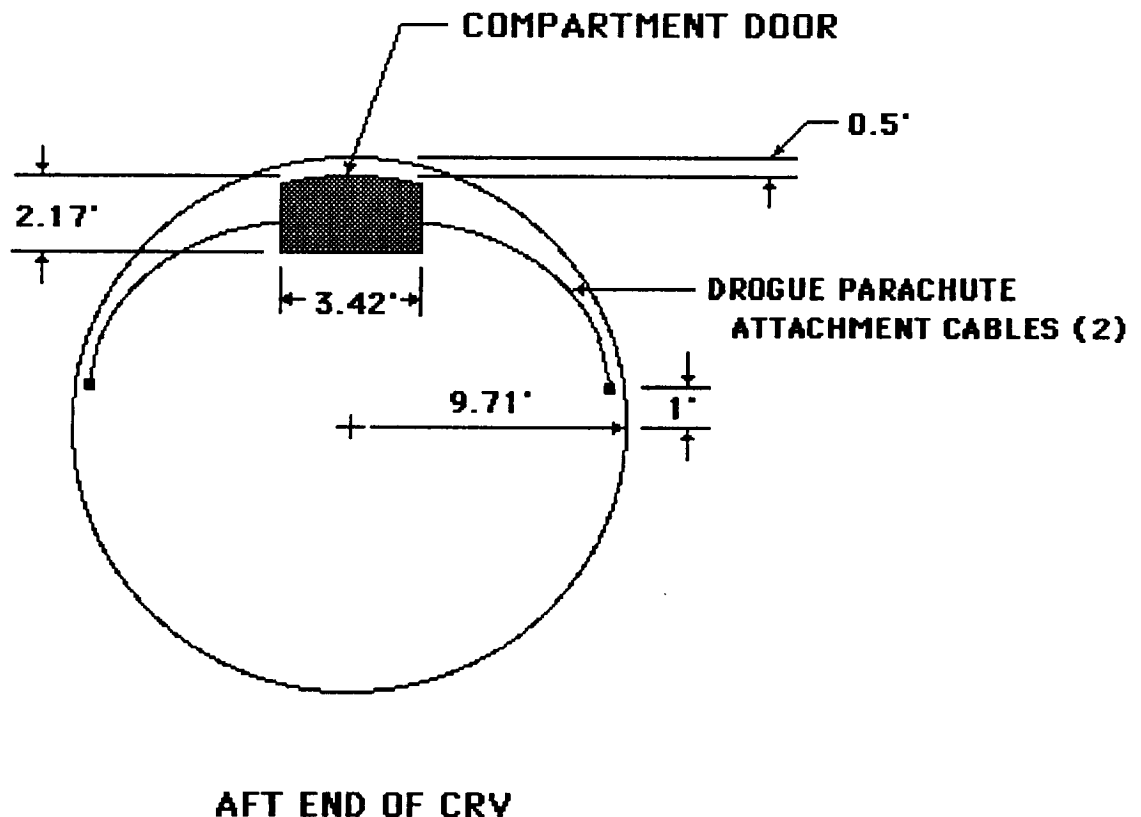


Figure 10.22 Drogue Chute Compartment Placement

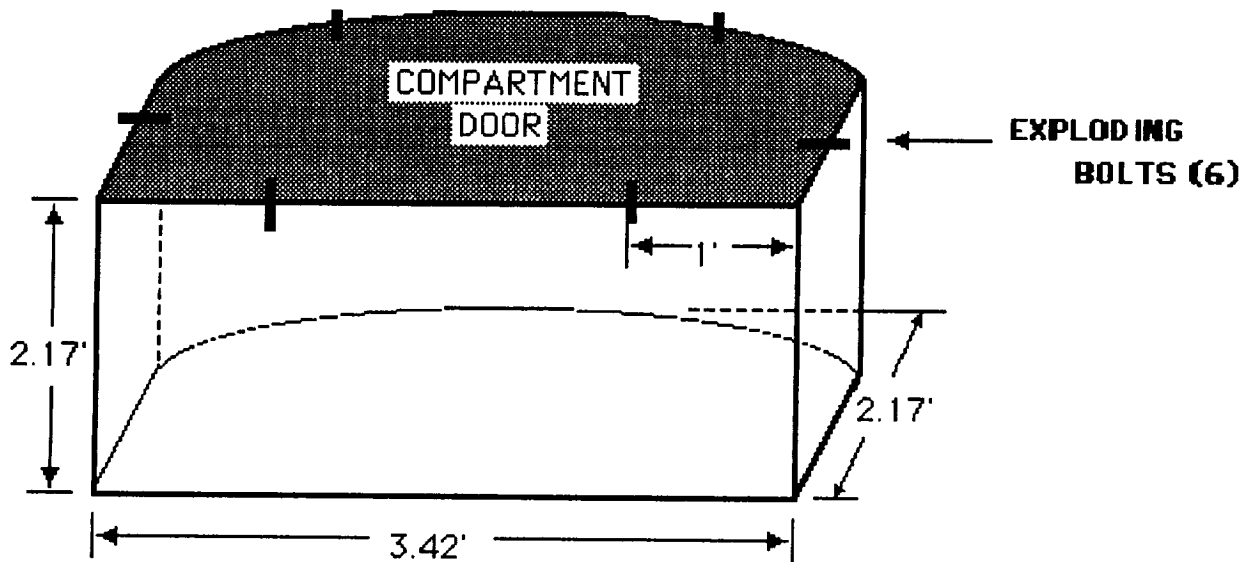


Figure 10.23 Dimensions of Drogue Chute Compartment

### 10.9.2 Ram Air Parafoil Storage Compartment

A minimum parafoil packing volume of 69.05 cubic feet was determined by the Aerodynamics Group (Section 4.0). This value was multiplied by 1.25 to provide some margin for error, and a volume of 10 cubic feet was added to provide space for the deployment parachute. Thus, a value for the total enclosed volume of the ARS storage compartment of 96.3 cubic feet was obtained. The location of the compartment on the CRV is shown in Figure 10.24.

The design of the shape of the compartment consists of a rectangular box with a ramp at the aft end. This is to allow the ARS to slide easily out of the compartment during deployment. The overall compartment dimensions and placement of the compartment doors are illustrated in Figure 10.25. The compartment doors will be spring loaded at the hinges, and exploding latches will release the doors and allow them to swing open.

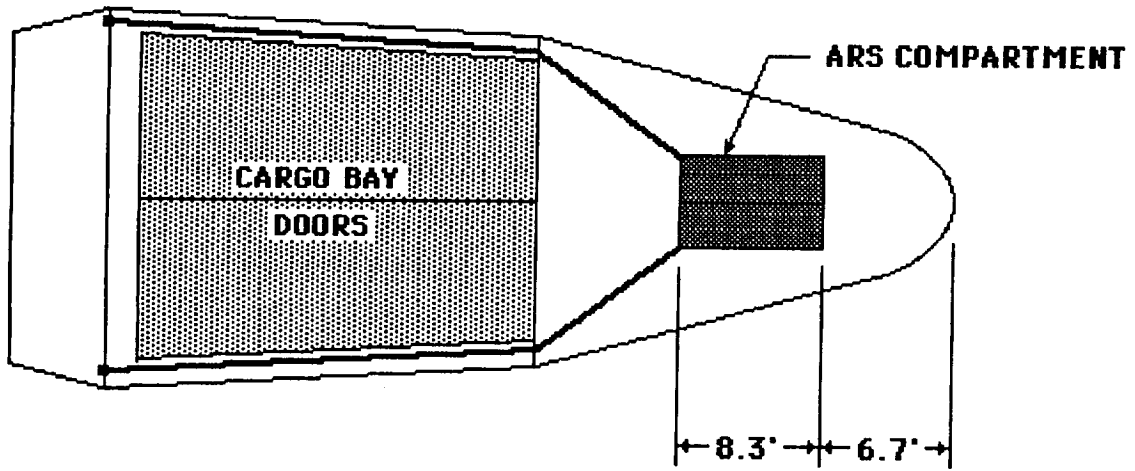


Figure 10.24 Placement of ARS Compartment

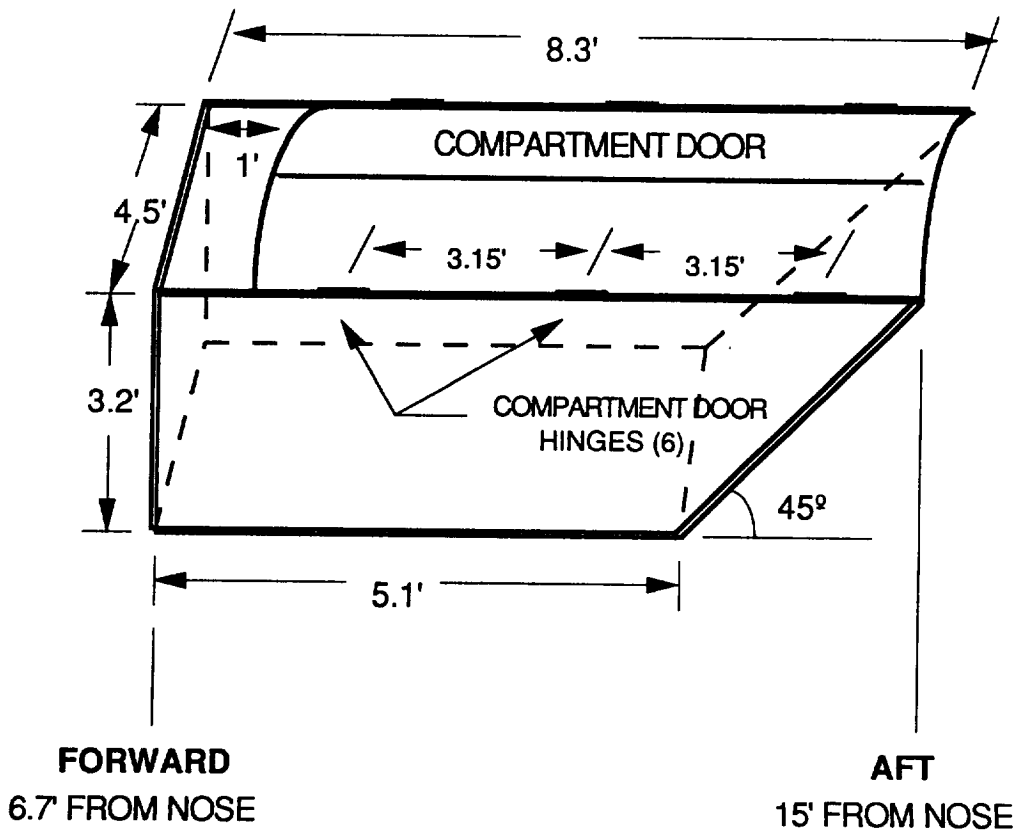


Figure 10.25 Dimensions of ARS Compartment

### 10.9.3 ARS Attachment Cables

The ARS will be attached to the CRV with four main cables; two attached to the fuselage support structure ring at the front end of the ARS compartment bay, and the other two at the aft of the vehicle (see Figure 10.26).

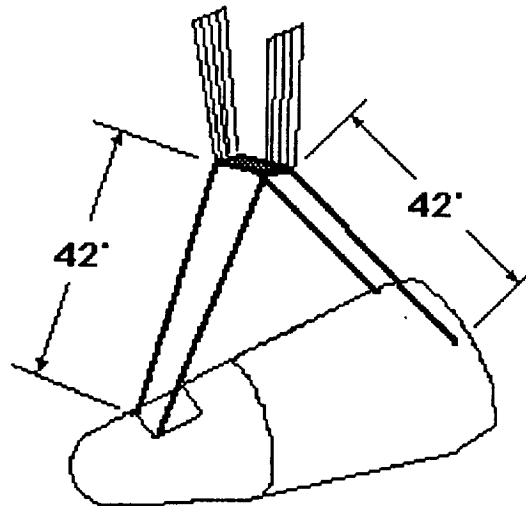


Figure 10.26 ARS Cable Configuration After Deployment

This presents the unique problem of needing to run the two aft cables along the CRV body and around the cargo bay doors. Two, 3/4 inch steel alloy cables will attach to the cable attachment platform inside the ARS compartment and run to the aft of the CRV as shown in Figure 10.27. The cables are sunk into the TPS system and held taught with clips that allow the cables to release during deployment. A design of the TPS around the attachment cables is provided by the Thermal Protection System Group (Refer to section 7.6 for more a detailed design). Steel alloy cables are used because of their high temperature limits of approximately 1000 degrees Fahrenheit. This matches well with maximum reentry temperatures of approximately 800 degrees experienced at the cable locations. An attachment method for the rear ARS cables is shown in Figure 10.28.

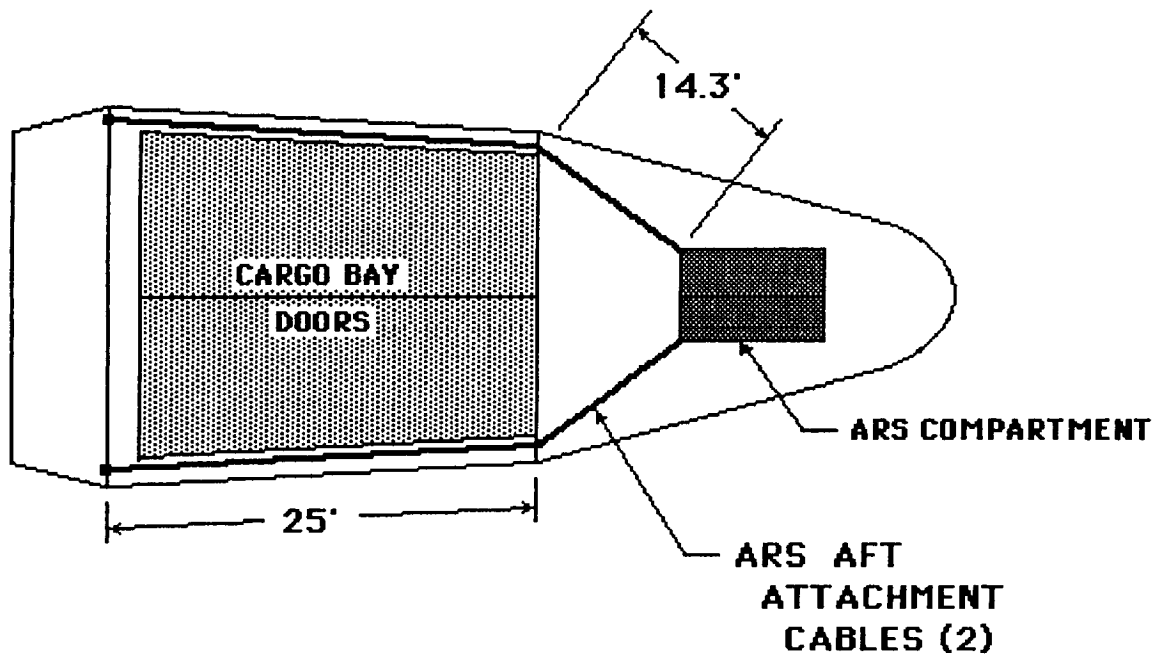


Figure 10.27 Placement of ARS Attachment Cables

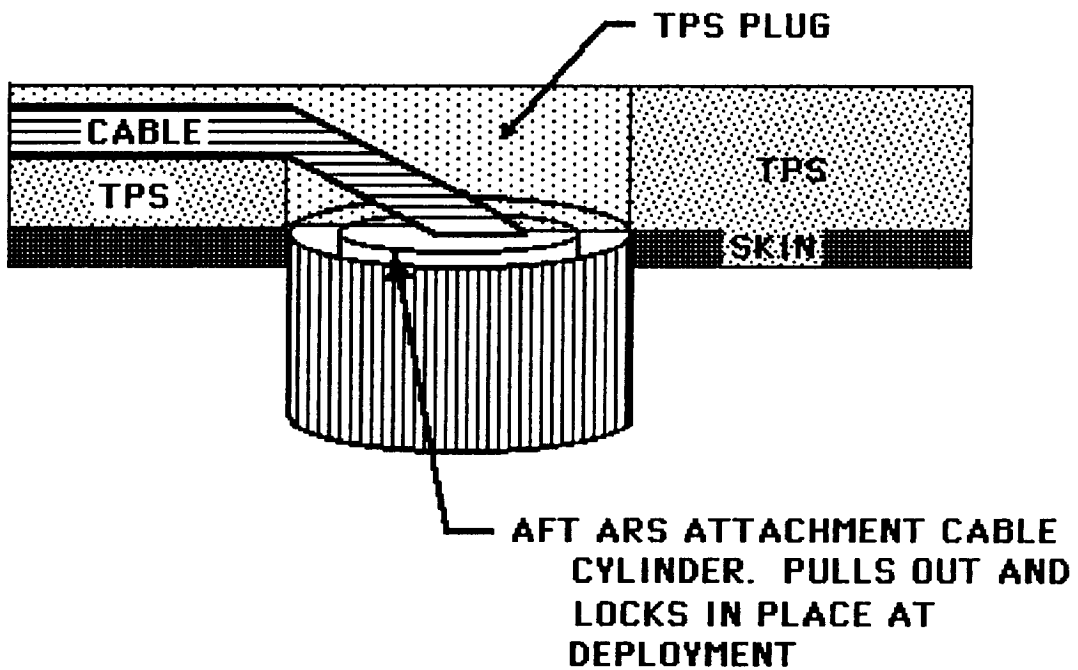


Figure 10.28 Aft Cable Attachment

The four main attachment cables attach to the platform shown in Figure 10.29. The parafoil shroud lines also converge at the platform. This platform will support the motors necessary for trailing edge deflection control, as well as serving as a mount for the camera used for remote control.

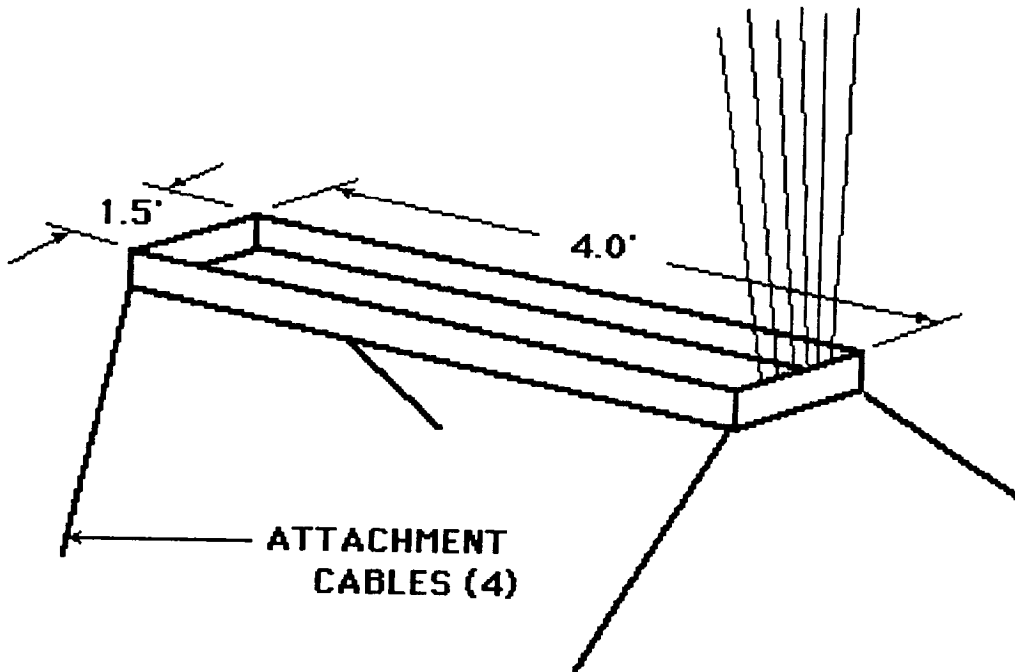


Figure 10.29 Attachment Cable Platform

#### 10.9.4 Parafoil and Attachment Lines

Fabrics used for the recovery system of the CRV must be extremely light to keep the vehicle weight at a minimum, and at the same time provide sufficient strength and thermal properties to withstand the opening and flight loads of recovery. The known fabrics that best meet these requirements are Kevlar and nylon. Table 10.5 illustrates some of the properties of each material.

<u>Material</u>	<u>% Elongation</u>	<u>Specific Gravity</u>	<u>Ultimate Tensile lbs/ft<sup>2</sup></u>	<u>Relative Strength-to-Weight Ratio</u>
Kevlar 29	4 - 5	1.44	400,000	2.70
Nylon 66	16 - 28	1.14	117,000	1.00

Table 10.5 Properties of Nylon and Kevlar Cable

It is clear from this comparison that Kevlar has a much higher strength-to-weight ratio than nylon. Therefore, from a weight standpoint it would be advantageous to construct an all Kevlar recovery system. However, the amount of stretch that Kevlar can withstand before failure is much lower than that of nylon. The limited amount of stretch that Kevlar experiences would produce a high snatch load during initial deployment, and subsequent high loads on the CRV and logistics modules. In addition to high snatch loads, all-Kevlar parachutes have experienced deployment problems in previous drop tests. Therefore, the fabric and lines of the advanced recovery system will be constructed out of a combination of Kevlar and nylon. This will take advantage of the high strength-to-weight ratio of Kevlar, and the stretch and deployment properties of nylon.

Assuming a total vehicle landing weight of 70,000 lbs, a rectangular parafoil with a planform area of approximately 22,000 square feet is necessary to provide the CRV with enough lift for a horizontal landing. A planform span of 250 feet and chord of 89 feet place the planform area at 22,250 ft<sup>2</sup>. This configuration has an aspect ratio of 2.81 and an approximate L/D of 3. The dimensions of the parafoil and attachment lines are shown in Figure 10.30.

The parafoil is divided into 51 cells open at the leading edge. Initially, only 11 cells will be allowed to open. This is done to limit the area and resulting load at the highest level of aerodynamic pressure. These 11 cells are constructed of 2.0 oz/ft<sup>2</sup> Kevlar. Using cables and pyrotechnic cutters, 10 additional cells will be opened. These cells are constructed of

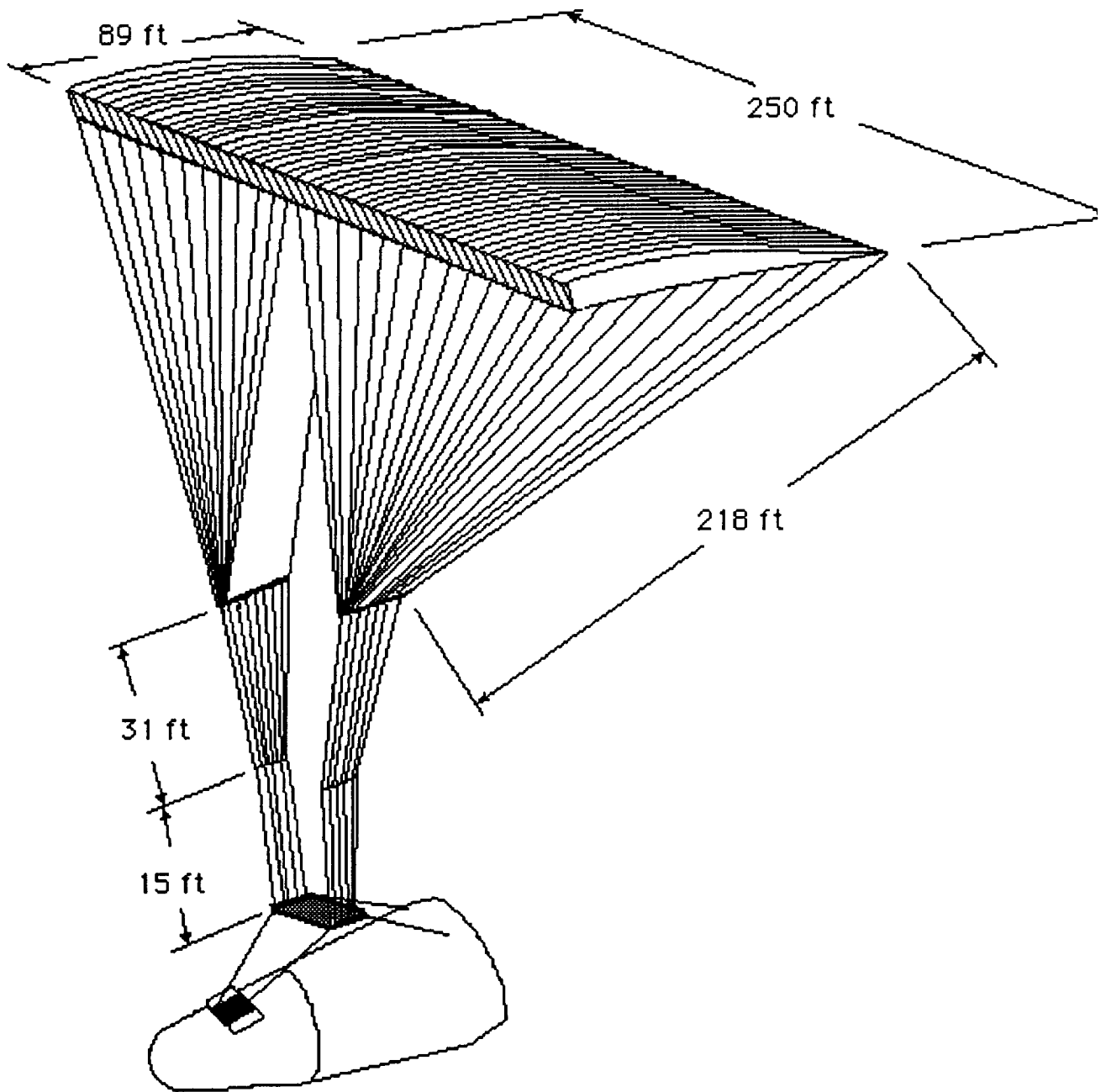


Figure 10.30 ARS layout and Dimensions

1.5 oz/ft<sup>2</sup> Kevlar, which is less than the first stage because of lower dynamic pressure at opening. Finally, the remaining 30 cells will be opened and the ARS will be fully deployed. The

third stage cells are constructed of 1.0 oz/ft<sup>2</sup> Kevlar. See Figure 10.31 for a diagram illustrating the location of the reefed sections on the parafoil. The canopy and attachment line materials and strengths for each stage, based on maximum opening loads, are shown in Figures 10.32, 10.33, and 10.34.

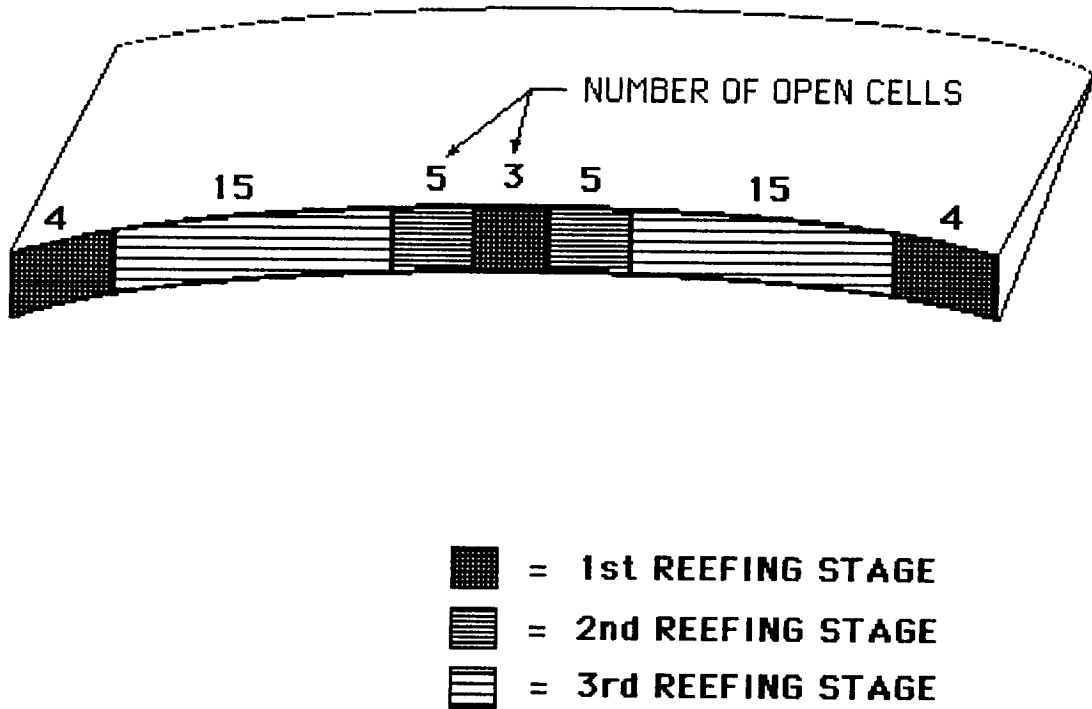


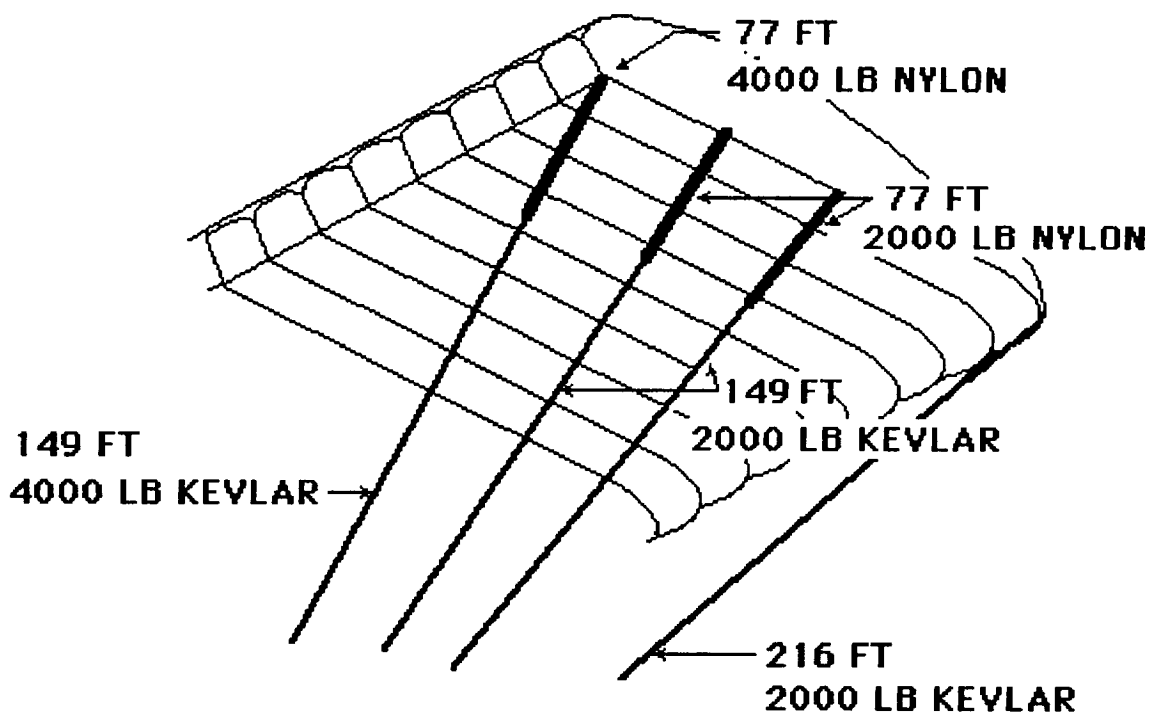
Figure 10.31 Parafoil Reefing Stages

The approximate weight of the parafoil and attachment lines is 2,800 lbs. This figure was obtained by adding the weight of each stage and corresponding attachment lines, plus an additional 100 lbs for the deployment bag and other miscellaneous items. The approximate weight of the deployment parachute is 150 lbs.

Because of high altitude winds, and to reduce the catastrophic failure footprint, 10,000 ft has been chosen as the altitude of main ARS deployment. Based on drop test data from Pioneer, a dynamic pressure of less than 50 PSF is necessary at this altitude to keep the ARS from being destroyed during deployment. A flare maneuver caused by lengthening of the

# LINE STRENGTHS - REEFING STAGE 1

11 CELLS OPEN

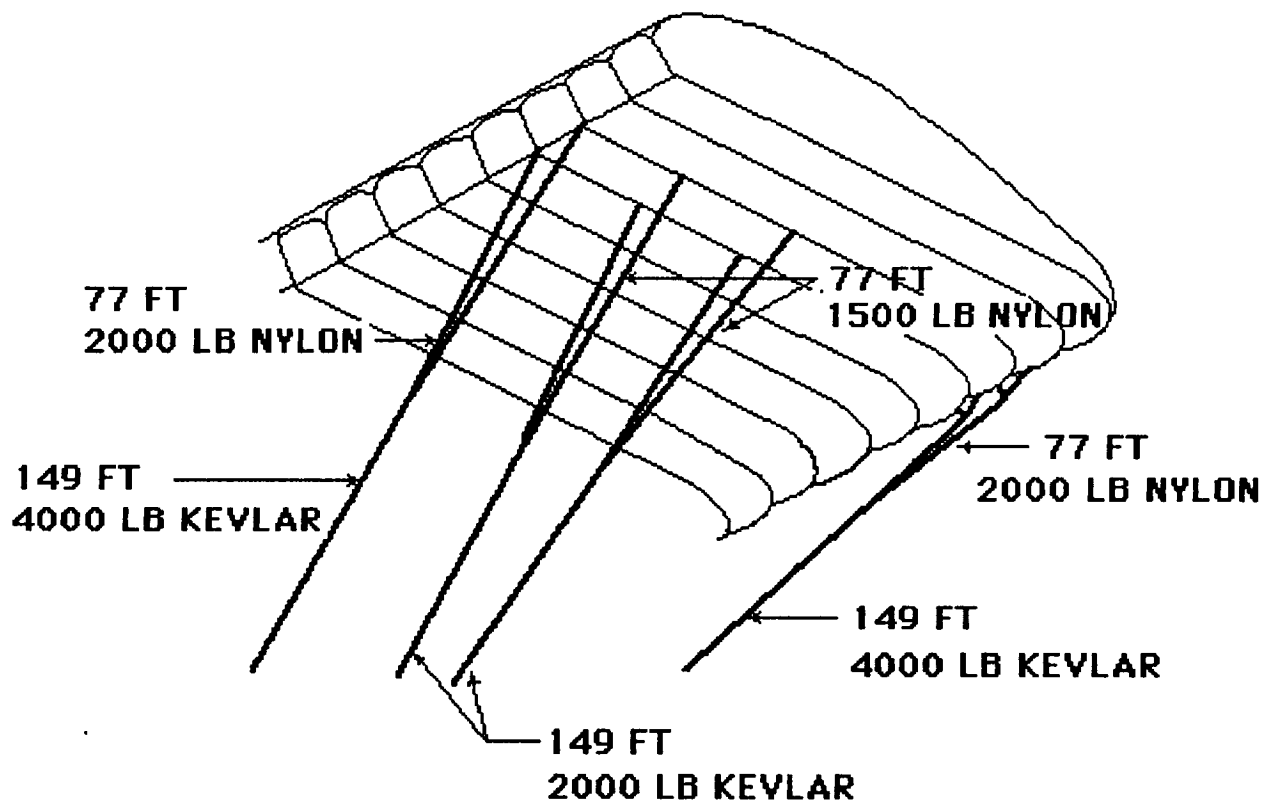


**CANOPY MATERIAL: 2.0 OZ/FT<sup>2</sup> KEVLAR**  
**TOTAL FIRST STAGE LINE STRENGTH = 120,000 LB**

Figure 10.32 First Stage of Reefing (11 Cells Open)

## LINE STRENGTHS - REEFING STAGE 2

10 ADDITIONAL CELLS OPEN - 21 TOTAL



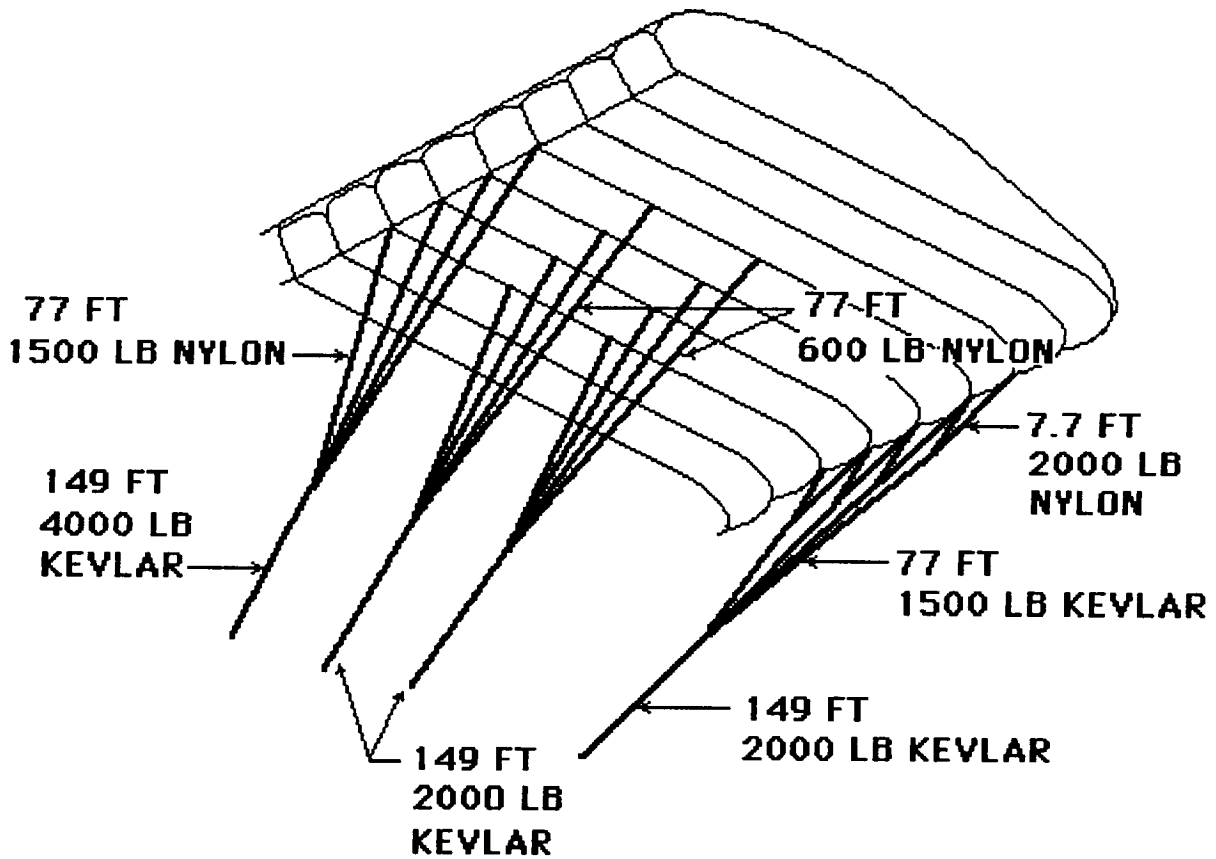
**CANOPY MATERIAL: 1.5 OZ/FT<sup>2</sup> KEVLAR**

**SECOND STAGE LINE STRENGTH = 60,000 LB**

Figure 10.33 Second Stage of Reefing (10 Additional Cells Open)

# LINE STRENGTHS - REEFING STAGE 3

30 ADDITIONAL CELLS OPEN - 51 TOTAL



CANOPY MATERIAL: 1.0 OZ/FT<sup>2</sup> KEVLAR

THIRD STAGE LINE STRENGTH = 100,000 LB  
**TOTAL LINE STRENGTH = 280,000 LB**

Figure 10.34 Third Stage of Reefing (30 Additional Cells Open)

leading edge attachment lines will be performed at 60 feet, and the CRV will land with a horizontal velocity of approximately 55 ft/sec.

Figures 10.32 to 10.34 show the line strengths and canopy material of each of the three reefed stages. These material strengths were calculated from predicted opening loads and previous Pioneer drop tests. Kevlar is used as the primary material because of its excellent strength-to weight ratio, and some nylon is integrated into the system to take advantage of its shock absorbing properties. The lines shown in the figures are the parafoil suspension lines pointed out in Figure 10.21. These lines are bound together at two bridling points and are then attached to the cable attachment platform.

## **11.0 OPTIMIZATION AND COSTS**

---

### **11.1 Introduction**

Optimization and cost analysis can be considered as a final check of a design but it is a necessary element in the design process of any structure. Optimization models, at their simplest, involve showing how design variables change with respect to one another in order to find the best (realistic) plan to make a design as efficient as is possible in the performance of a task. The designed efficiency depends of course on what part of the overall plan is to be minimized or maximized.

The optimization and costs group worked toward three objectives for the start of optimization and cost study. The first and most important objective was to learn about the field of optimization. Approximately seven weeks were spent learning optimization methods with Professor Warner. The culmination of the learning process was solving two original, simple problems. The second objective was to study ground operations in order to decide the best way the cargo return vehicle should be made ready for launches. Costing of the CRV was delayed until information from contractors could be found.

### **11.2 Optimization of Ground Facilities**

One of the most expensive costs of CRV integration belongs to the ground facilities. The current facilities are capable of handling the needs of fourteen flights per year. In the years to come, there may be an increase in flights, thus requiring new facilities. Because these facilities will be expensive, it is essential to optimize them by looking at the long term effects.

#### **11.2.1 Number of Missions Per Year**

The number of space shuttle missions to supply the space station is five per year. The number of flights of the CRV, in order to fulfill the remainder of the space station requirements, is three. Because the use of the space shuttle is not limited to transporting cargo, the number of missions it makes to supply the space station cannot always be depended on. Therefore, the number of projected flights

of the CRV should account for this. A higher number of flights of the CRV will however increase ground operation costs.

### **11.2.2 Use of Current Versus New Facilities**

Present shuttle facilities can sustain 14 flights per year. Three of these flights are scheduled for Shuttle-C. If the CRV should share facilities with the space shuttle, only three flights will be available for missions not involving the space station. This would severely limit future use of both the space shuttle and CRV for other projects. The advantage of using present facilities is a much lower investment cost.

Another option is the construction of new launch facilities with the CRV sharing the horizontal payload processing facility. The cost of this would be \$1.3 billion in 1991 dollars. The facility would cost about \$350 million to operate a year. One advantage of this option is the new facility would be capable of servicing 16 launches per year. This would make future expansion possible, which is a major concern of option 1. The main disadvantages are the high investment and yearly costs.

A third option is a combination of present and new facilities. Mainly, this combination consists of new processing facilities and current shuttle launch pads. Because the present launch facilities will be able to handle up to 22 flights by 1997, only new processing facilities need be built. The cost of building processing facilities alone is \$750 million, a reduction of 42% over building totally new facilities. This option also has the capability of expansion. The disadvantage is a high investment cost.

### **11.2.3 Transportation From Landing Site**

There are two main methods for transportation of the CRV to its processing facilities. The first option is by barge or boat, which would be used in the event the CRV needed to use an emergency landing site. This method is less costly, but it is slow and somewhat risky due to corrosion from salt water. Another disadvantage is the investment cost of developing a secure method of transport.

The other method is airlift. It is the method currently used on the space shuttle and this has a proven reliability. Also, another advantage is transportation time is short.

After review of the ground operations, the Optimization and Cost discipline have made the following recommendations. New facilities, excluding launch pads, should be built without too much delay. New launch pads should be delayed until a later time when the need arrives. The main transportation of the CRV from Edwards Air Force Base to Kennedy Space Center should be by airlift similar to that of the space shuttle.

### **11.3 Future Optimization Tasks**

#### **11.3.1 Amount of Cargo**

The payload has a specific weight and volume limit. The variables involved are length, width, and height of cargo bay. Parameters include volume (length, width, and height) of pressurized and unpressurized logistics modules, weight of cargo, and size of CRV allotted to cargo bay. It may be the case that the cost of designing, building, and maintaining a CRV to take up two unpressurized logistics modules instead of one as the current design suggests, might be more economical for the long term. This might result because the cost of preparing and maintaining a CRV that carries only one logistics module would cost more due to the greater number of scheduled missions and ground operations costs. As of now, it has not been determined whether the CRV is economically feasible. This is one possible reason why the research of an increased payload limit may prove to be very important.

#### **11.3.2 Fleet Size**

Right now, the sizing of the fleet will only take into account servicing needs of the space station. The decision whether to expand the fleet size to account for other missions such as servicing a lunar base (reference two) will be looked into later. The number of CRV's chosen will need to be able to meet the yearly needs of the space station. Some factors affecting the fleet size are: 1) turn around time of the CRV's, 2) configuration of vehicle, 3) amount of total cargo needed to be boosted per year, as well as individual liftoff cargo size, 4) cost of CRV, 5) capacity of ground operation facilities, and 6) amount of funds available.

### **11.3.3 Cost of a CRV**

Research in the cost of a single Biconic CRV has begun with an estimate expected for the following quarter. Through a preliminary cost analysis, it was realized it will be difficult to use analytical methods by NASA to find a good cost estimate. Information will have to be found from existing documents and from contractors.

## 12.0 CONCLUSION

---

### 12.1 General

This volume presents the results of a preliminary design of a biconic CRV. All of the requirements that were asked of the CRV have been met. The biconic Cargo Return Vehicle is capable of meeting all the SSF resupply requirements.

Worthy of mention is the absence of a backup recovery system to the ARS. A design for such a system was actually carried out, but it was decided not to include it as part of the design for several reasons. Firstly, the extra weight would necessitate down scaling of the max. payload, this is undesirable. Further, volume constraints in the backup system bay are such that the size of the secondary chute would have to have limits; given these limits, the touchdown velocity of the CRV, in case of main system failure, would have to be greater than desired, causing some systems to be damaged on impact. Thirdly, the high reliability of the ream-air ARS does not warrant the penalty weight of a back up system.

### 12.2 Summary

- Bent axis biconic with a ram air inflated parafoil ARS
  - Δ  $(L/D)_{\text{Hyper}} = 1.5$
  - Δ  $(L/D)_{\text{Subsonic}} = 3.8$  -ARS
  - Δ Weight Unloaded = 34,061lbs
  - Δ Cargo Cap. = 40 Klb
  - Δ Crossrange  $\approx$  700 n.mi.
  
- The Advanced Recovery System
  - Δ Planform Area = 22,250 ft<sup>2</sup> (250 ft X 89 ft)
  - Δ Deployed at 10,000 ft altitude
  - Δ Midspan reefing in three stages
  
- Vehicle dimensions
  - Δ Length = 59 ft

- Δ Radius<sub>nose</sub> = 7.7 ft
  - Δ Diameter<sub>max</sub> = 19.5 ft
- Supersonic reentry control via tail mounted adjustable deflection fins, with folding winglets
- The CRV will be capable of docking directly to the SSF as well as being OMV compatible
  - Δ Mission time with OMV = 19.85-76.85 hrs
  - Δ Mission time non-OMV = 18.35-75.35 hrs
- Propulsion
  - Δ Top mounted launch on dual booster/single core LRBs
  - Δ Orbit insertion at 50 n.mi. X 100 n.mi. @ 28.5°
  - Δ Three OMS engines
    - √ LH<sub>2</sub>/LO<sub>2</sub> propellant and oxidizer
    - √ Weight = 86.65 lbs (each)
    - √ I<sub>sp, vac.</sub> = 414.4 sec
    - √ Thrust<sub>vac.</sub> = 1600 lbf
  - Δ The RCS system uses LH<sub>2</sub>/LO<sub>2</sub> outside of the CCZ and GN<sub>2</sub> inside, as specified by SSF requirements
- Transportation of the CRV back to KSC will be via the Boeing Super Guppy
- CRV turnaround time is 66 days

## **13.0 REFERENCES**

---

### **Mission Operations**

- 2.1 G D, "CRV Ground Operations," General Dynamics Division
- 2.2 Jane's All the World's Aircraft, Sampson Low, 1972-1973
- 2.3 NASA, "Information Summaries-Countdown!" PMS 018 (KSC), March 1987
- 2.4 Shuttle Operator's Manual
- 2.5 Scott, L.P., "PLS-Launch Site Integration," Lockheed Space Operations Company, November 1, 1989
- 2.6 MacKnight, Nigel; Shuttle 2, Motor Books International, Osceola, WI, 1988
- 2.7 Brown, W.R., MFSC, PD34, "CRV Requirements for Docking at SSF", Nov. 1, 1989
- 2.8 Shuttle-C User's Guide, May 1989, Martin Marietta Manned Space Systems
- 2.9 Space Shuttle System Payload Accommodations, Revision 10.
- 2.10 Space Shuttle Integration Hardware, Appendix 10
- 2.11 Space Shuttle Payload Deployment and Retrieval System, Appendix 8, Revision J, May 2, 1988
- 2.12 SSP Def. and Req. Section 3: Space Station Systems Requirements, NASA SSP 3000.
- 2.13 Space Station Operations, NASA JSC 30201.
- 2.14 Sachdev, Savi, MSS Technical Summary, SPAR Aerospace Ltd., Jan 23, 1990, Weston, Ontario.

- 2.15 Foley, Theresa M., "Space Station Back on Track After Year of Policy Disarray," Aviation Week and Space Technology, June 15, 1987, p. 277.
- 2.16 Logistics Elements Fact Book, Draft 1, Boeing Aerospace, Huntsville, Alabama.
- 2.17 Brown, W.R., MSFC, PD34, "CRV Requirements for Docking at SSF," Nov 1, 1989, p. 2,3.
- 2.18 Bates, Fundamentals of Astrodynamics, Air Force Academy
- 2.19 Breakwell, John; Space Mechanics, Stanford University
- 2.20 "Abort Capability of the Langley Star Vehicle", NASA
- 2.21 Design and Analysis of Hypervelocity Vehicles: Vol. 4- Trajectory and Aeroheating

### **Reentry Aerodynamics**

- 4.1 Miller, C. G., Gnoffo, P. A., "Control Effectiveness for Biconic Geometry Vehicles," AIAA Paper 83- .
- 4.2 Anderson, J. D., "Hypersonic and High Temperature Gas Dynamics", McGraw Hill Inc., 1989.
- 4.3 Hayes, W. D., Probstein, R. F., "Hypersonic Flow Theory", Academic Press, 1958.
- 4.4 Gentry, A. E., Douglas, D. N., Oliver, W. R., "The Mark IV Supersonic/Hypersonic Arbitrary-Body Program Volume 1- User's Manual," Technical Report AFFDLTR-73-159, November 1973.
- 4.5 Ewing, E. G., Bixby, H. W., Knackle, T. W., "Recovery Systems Design Guide," Technical Report AFFDL-TR-78-151, December 1978.
- 4.6 Trajectory Analysis Program.
- 4.7 IMP., Reentry Vehicle Trajectory Program.

## **Stability and Control**

- 5.1 Spacecraft Attitude and Dynamics, Hughes
- 5.2 Modern Spacecraft Dynamics and Control, Kaplan
- 5.3 Biconic Recovery Systems-Parawing Configurations, Peter Thompson, 10/22/89
- 5.4 Status Report: Recovery Systems Group, Check, Raschke, Thompson, 11/15/89
- 5.5 DYNAMICS OF FLIGHT Stability and Control, Bernard Etkin
- 5.6 HABP Manuals and handouts
- 5.7 Fundamentals of Aircraft Design, Nicolai
- 5.8 Biconic CRV Final Report - ARS, section 3.12
- 5.9 Wind Tunnel Studies ..., United Technologies Report Design Library Document 42
- 5.10 Pioneer Systems Report, Design Library Document 34
- 5.11 ARS Phase 2 Eighth Quarter Review, Pioneer Aerospace Corp., November, 1989
- 5.12 Dynamics of Atmospheric Flight, Bernard Etkin, 1972
- 5.13 Aerodynamics, Aeronautics, and Flight Mechanics, Barnes W. McCormick, 1979
- 5.14 Summary of Methods for Calculating Lateral Stability and Response and for Estimating Lateral Stability Derivatives, J. P. Cambell and M.O. McKinney, NACA Report #1098
- 5.15 Feedback Control of Dynamical Systems, G. F. Franklin, 1986

5.16 Professor C.A. Harvey, University of Minnesota

### **Avionics & Power**

- 6.1 Orbiter and Subsystems, Rockwell Inc.
- 6.2 Shuttle-C Avionics: In House Study, MSFC Report
- 6.3 Space Shuttle Electrical Power and Avionics, JSC Report
- 6.4 Electrical Power Systems in the Us Manned and Some of the Unmanned Spacecraft, NASA (R-174809)
- 6.5 Aeroassist Flight Experiment Preliminary Design Document, (NASA) Marshall Space Flight Center
- 6.6 Advanced Thermal Components for Efficient Cooling of Avionics Systems, W. J. Schwarzoot, Dornier system GBMH, W. Germany
- 6.7 Orbiter and Subsystems, Rockwell Inc.
- 6.8 Cold Plate Specifications, ESA Report
- 6.9 CRV Avionics. Power and Thermal Control, General Dynamics

### **Thermal Analysis & Control**

- 7.1 Harvey, Curtis, Status Reports 1-6, University of Minnesota, Fall 1989.
- 7.2 Cleveland, John J., and Iannetti, F., "Thermal Protection System of the Space Shuttle," NASA Contractor Report 4277, June 1989.
- 7.3 Holman, J.P., "Heat Transfer," McGraw-Hill, 1981.
- 7.4 Wark, Kenneth, "Thermodynamics," McGraw-Hill, 1983.
- 7.5 Gailey, J.W., and Kotker, D.J., "Conceptual Design and Analysis of Hypervelocity Aerospace Vehicles Volume 4 - Trajectory and Aeroheating," Boeing Aerospace Company, February 1988.

- 7.6 Program Development Preliminary Design Office, "Shuttle-C Avionics In-House Study," NASA, 1976.
- 7.7 "Materials Engineering - Materials Selector 1989," Penton Publications, December 1988.
- 7.8 Stewart, J.D., and Bloom, H.L., "Refurbishable Thermal Shields for Lifting Entry Vehicles," 1966.
- 7.9 Rittenhouse, John, and Singletary, John. "Space Materials Handbook," NASA SP-3051, Third Edition.
- 7.10 Kourtides, D.A., "Ceramic Insulation/ Multifoil Composite for Thermal Protection of Reentry Spacecraft," AIAA 24th Thermophysics Conference, Buffalo, New York, June 1989.
- 7.11 Calamito, Dominic P., "Development of Tailorable Advanced Blanket Insulation for Advanced Space Transportation Systems," NASA Contractor Report 177444, April 1987.
- 7.12 Elfer, N., and Kovacevic, G. "Design for Space Debris Protection," 3rd Annual AIAA Symposium, November 1985.
- 7.13 Lecy, Scott M. Project Engineer, Automotive Systems/ 3M Division Engineering. Phone conversation, February 21, 1990. 'Content was to obtain permission to use 3M Dual-Lock® in presentation.'
- 7.14 Hays, D. "An Assessment of Alternate Thermal Protection Systems for the Space Shuttle Orbiter, NASA CR 3548, 1981.
- 7.15 AEM 5329/ NASA Marshall Research Center Teleconference, October 1989.

## **Propulsion**

- 8.1 **Rocket Propellant and Pressurization Systems**, Elliot Ring, Prentice-Hall, INC., Englewood Cliffs, N.J., 1964
- 8.2 **Solid Rocket Technology**, Morton Shorr and Alfred J. Zaehring, John Wiley and Sons, Inc., New York, 1967

- 8.3 **Solid-Fuel Rocket Propulsion**, J.E. Daboo, Temple Press Books, London, 1962
- 8.4 **Launch System Data Folder**, Aerospace Design Library, Packet 185
- 8.5 **Conceptual Design and Analysis of Hypervelocity Aerospace Vehicles, Volume 3 - Propulsion**, Aerospace Design Library, Packet 109
- 8.6 Informal talk with Beth R. Jensen, Quality Engineer, Thiokol Corporation, January 30, 1990.
- 8.7 Phone conversation with Lindy Shambough, Pratt & Whitney, February 5, 1990 [407-796-5784].
- 8.8 Phone conversation with Bob Marable, Pratt & Whitney, February 6, 1990 [407-796-3047].
- 8.9 Phone conversation with James Brown, Pratt & Whitney, Rocket Systems Engineering, February 6, 1990, [407-796-7770].
- 8.10 **Propulsion Systems Data Book-Vol 1**, Aerospace Design Library, Packet 187.
- 8.11 **Launch Vehicles for PLS/CRV**, Marshall Space Flight Center document, Aerospace Design Library

### **Reenty Guidance**

- 9.1 Brauer G.L., Cornick D.E., Olson D.W., Peterson F.M., and Stevenson R., Six-Degree-of-Freedom Program to Optimize Simulated Trajectories POST-6D, Martin Marietta Corporation, September 1987.
- 9.2 Brown B., Seminar on Inertial Navigation, Guidance, and Control, R. G. Brown Associates Inc., December 1989.
- 9.3 Dauro, V. A., Integrated Mission Program, Users Manual Volume I, Northrop Services, Inc., July 1989.

- 9.4 Gailey J. W. and Kotker D. J., Conceptual Design and Analysis of Hypervelocity Aerospace Vehicles. Volume IV, Boeing Aerospace Company, February 1988.
- 9.5 Joels K., Kennedy G., and Larkin D., The Space Shuttle Operator's Manual, Ballantine Books, 1988.
- 9.6 Martin, John J., Atmospheric Reentry. an Introduction to its Science and Engineering, Prentice-Hall, Inc., 1966.

### **Structural Design**

- 10.1 Alloy Digest, Engineering Alloys Digest Inc., October 1960.
- 10.2 Military Handbook, Metallic Materials and Elements for Aerospace Vehicle Structures, 1 May 1986.
- 10.3 Structural Strength Program Requirements, MSFC-HDBK-505, Revision A, January 1981.
- 10.4 The Basics of Bonded Sandwich Construction, TSB 124, Hexcel Corporation, Fall 1986 Revision.
- 10.5 Mechanical Properties of Hexcel Honeycomb Materials, TSB-120, Hexcel Corporation, 1987.
- 10.6 Currey, N. S. Aircraft Landing Gear Design: Principles and Practices AIAA Education Series, 1988
- 10.7 de Veubeke, B. F. Matrix Methods of Structural Analysis. The MacMillan Company, 1964.
- 10.8 Jenkins, Jerald M. The Effect of Thermal Stresses on the Integrity of Three Built-Up Aircraft Structures NASA TM-81352, 1980.
- 10.9 Jenkins, Jerald M. Thermal Stresses in a Laboratory Heated Built-Up Structure.

- 10.10 Nicolai, Leland M. Fundamentals of Aircraft Design METS, Inc. San Jose, California, 1984.
- 10.11 Pioneer Aerospace Corp. ARS Phase 2 Eighth Quarter Review Melbourne, Florida, November 1989.
- 10.12 Raymer, Daniel P. Aircraft Design: A Conceptual Approach AIAA Educational Series.

### **Optimization and Cost**

- 11.1. "Applied Optimal Design", by Haug and Arora
- 11.2. "Globally Optimal Design", by Wilde
- 11.3. Ground Operations from the CRV Biconic Report of Fall Quarter
- 11.4. Haug and Arora, "Applied Optimal Design"
- 11.5. Wilde, "Globally Optimal Design"
- 11.6. Ground Operations from the CRV Biconic Report of Fall Quarter
- 11.7. Scott, L.P., "Personnel Launch System (PLS) - Launch Site Integration", Lockheed - Space Operations Company, November 1, 1989.

